

UNCLASSIFIED

AD 283 758

*Reproduced
by the*

**ARMED SERVICES TECHNICAL INFORMATION AGENCY
ARLINGTON HALL STATION
ARLINGTON 12, VIRGINIA**



UNCLASSIFIED

NOTICE: When government or other drawings, specifications or other data are used for any purpose other than in connection with a definitely related government procurement operation, the U. S. Government thereby incurs no responsibility, nor any obligation whatsoever; and the fact that the Government may have formulated, furnished, or in any way supplied the said drawings, specifications, or other data is not to be regarded by implication or otherwise as in any manner licensing the holder or any other person or corporation, or conveying any rights or permission to manufacture, use or sell any patented invention that may in any way be related thereto.

283 758

62-4-6

U. S. A R M Y
TRANSPORTATION RESEARCH COMMAND
FORT EUSTIS, VIRGINIA

TCREC TECHNICAL REPORT 62-66

RECIRCULATION PRINCIPLE FOR GROUND EFFECT MACHINE
TWO-DIMENSIONAL TESTS

Task 9R99-01-005-04

Contract DA 44-177-TG-710

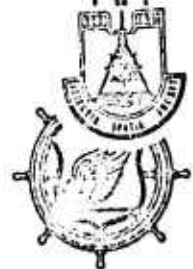
June 1962

283 758
ASTIA
CATALOGED BY
AS AD INC

prepared by:

MARTIN COMPANY
Orlando Division
Orlando, Florida

ASTIA
RECEIVED
SEP 14 1962
RECEIVED
ASTIA C



DISCLAIMER NOTICE

When Government drawings, specifications, or other data are used for any purpose other than in connection with a definitely related Government procurement operation, the United States Government thereby incurs no responsibility nor any obligation whatsoever; and the fact that the Government may have formulated, furnished, or in any way supplied the said drawings, specifications, or other data is not to be regarded by implication or otherwise as in any manner licensing the holder or any other person or corporation, or conveying any rights or permission, to manufacture, use, or sell any patented invention that may in any way be related thereto.

ASTIA AVAILABILITY NOTICE

Qualified requesters may obtain copies of this report from

Armed Services Technical Information Agency
Arlington Hall Station
Arlington 12, Virginia

This report has been released to the Office of Technical Services, U. S. Department of Commerce, Washington 25, D. C., for sale to the general public.

The information contained herein will not be used for advertising purposes.

The findings and recommendations contained in this report are those of the contractor and do not necessarily reflect the views of the Chief of Transportation or the Department of the Army.


HEADQUARTERS
U. S. ARMY TRANSPORTATION RESEARCH COMMAND
Fort Eustis, Virginia

This report presents the results of a theoretical and experimental investigation of the recirculation principle as a source of lift for ground effect machines. The recirculation principle is of considerable interest to the U. S. Army in its program of basic research on GEM, since theoretically the power required for a given lift can be substantially reduced. In addition, there are benefits such as reduced drag in forward flight, reduced dust and spray problems, and reduced structural weight which may potentially be of more importance than the lift efficiency.

The present report is restricted to a two-dimensional analysis and experimental investigation of the concept using ejectors as the means of inducing flow. A basic data report, OR 2496, dated January 1962, is available on loan from the USATRECOM Library.

Additional investigations of the principle in hover and forward flight using a small-scale three-dimensional model and a large-scale manned test vehicle are in progress, and the results will be reported in the near future.

FOR THE COMMANDER:


JOHN H. PARRY, JR.
1st Lt., TC
Adjutant

APPROVED BY:


W. D. Hinshaw
Project Engineer

CONTRACT DA 44-177-TG-710

JANUARY 1962

RECIRCULATION PRINCIPLE FOR GROUND EFFECT MACHINE
TWO-DIMENSIONAL TESTS

OR 2073

Prepared by:

MARTIN MARIETTA CORPORATION
ORLANDO AEROSPACE DIVISION

for

U. S. ARMY TRANSPORTATION RESEARCH COMMAND
FORT EUSTIS, VIRGINIA

FOREWORD

This interim report is submitted in full compliance with the requirements of Paragraph 1, Modification 3, Contract DA 44-177-TC-710. It contains the theoretical considerations of the recirculating ejector concept and analysis of test results. This work was conducted in the one year period between January 1961 and January 1962.

The basic notation used in this report is defined in the List of Symbols and any special notation is defined in the section of the text in which it is used.

Mr. A. Ortell has been the principal investigator for this effort. Significant contributions were made by Messrs. J. Butsko, C. Casteleiro, G. Martin, and C. Middlebrooks. This report has been reviewed and approved by Mr. Keith Cossairt, GEM Project Engineer.

CONTENTS

	<u>Page</u>
List of Illustrations	iv
List of Tables	ix
List of Symbols	x
1.0 Summary	1-1
2.0 Conclusions	2-1
3.0 Recommendations	3-1
4.0 Introduction	4-1
5.0 General Recirculation Methods	5-1
5.1 Diffuser Recirculation Concept	5-1
5.2 Labyrinth Seals	5-2
5.3 Annular Jet Recirculation Systems	5-3
6.0 Martin-Marietta Recirculation Concept	6-1
7.0 Analytical Studies	7.1-1
7.1 Straight Ejector	7.1-1
7.2 Ejectijet Concept	7.2-1
7.3 Hovering	7.3-1
7.4 Forward Flight	7.4-1
8.0 Ejectijet GEM Performance	8.1-1
8.1 Tabulation of Basic Performance Equations	8.1-1
8.2 Component Efficiency	8.2-1
8.3 Recirculating Ejector Parametric Study	8.3-1
8.4 Propulsion	8.4-1
8.5 Performance Estimates	8.5-1
8.6 Operational and Environmental Considerations	8.6-1
9.0 Experimental Program	9.1-1
9.1 Straight Ejector Tests	9.1-1
9.2 Recirculating Ejector Tests	9.2-1
10.0 Comparison of Theory with Experiment	10-1
10.1 Straight Ejector	10-1
10.2 Recirculating Ejector	10-8
11.0 References	11-1
12.0 Distribution	12.1-1

LIST OF ILLUSTRATIONS

<u>Figure</u>		<u>Page</u>
5-1	Diffuser - Recirculation Concept	5-5
5-2	Labyrinth - Seal Concept	5-5
5-3	Annular Jet Recirculation Concept	5-6
5-4	Central Fan Installation for Annular Jet Recirculation System	5-6
6-1	Recirculating Ejector Lift System	6-1
7.1-1	Conventional Straight Ejector	7.1-1
7.1-2	Graphical Solution of Compressible Bernoulli Equation	7.1-11
7.1-3	Prandtl-Schlichting Incompressible Flat Plate Turbulent Skin Friction Coefficient	7.1-12
7.2-1	Mass Augmentation of a Recirculating Constant Pressure Ejector	7.2-2
7.2-2	Efficiency of a Recirculating Constant Pressure Ejector	7.2-3
7.2-3	Two Flow Regions in Recirculation	7.2-6
7.2-4	Momentum Geometry	7.2-7
7.3-1	Comparison of Predicted Total Load with Experiment	7.3-14
7.3-2	Two-Dimensional Ejectorjet Cross-Flow in Pitch (Roll)	7.3-15
7.3-3	Flow Pattern under Pitched Ejectorjet	7.3-16
7.3-4	Effect of Height on Momentum Thrust	7.3-17
7.3-5	Effect of Pitch Angle on Cavity Pressure	7.3-18
7.3-6	Effect of Height on Cavity Pressure and Jet Momentum	7.3-19
7.3-7	Base Pressure Versus Height	7.3-20
7.3-8	Jet Thrust Versus Pitch Angle	7.3-21
7.3-9	Lift Versus Height	7.3-22
7.3-10	Analog Computer Schematic	7.3-23
7.3-11	Pitch Motion for the Wind Tunnel Model	7.3-24
7.3-12	Heave Motion for the Wind Tunnel Model	7.3-24
7.3-13	Internal Geometry	7.3-26
7.3-14	Force Vector Diagram	7.3-27
7.3-15	Comparison of Theoretical Vertical Ejector Force with Experiment	7.3-29
7.3-16	Plan View of Ejector Assemblies for Control	7.3-30

LIST OF ILLUSTRATIONS (Cont'd)

<u>Figure</u>		<u>Page</u>
7.3-17	Ejector Tilting Procedure	7.3-31
7.3-18	Cancellation of Ejector Side Force by Rotation of the Lift Vector	7.3-33
7.3-19	Translation of Lift Curve Due to Ejector Rotation	7.3-34
7.3-20	Double Ejector Control Model	7.3-38
7.4-1	Forward Flight Lift of 1/4 Scale Recirculation GEM Model	7.4-6
7.4-2	Forward Flight Drag of 1/4 Scale Recirculation GEM Model	7.4-7
8.2-1	Hover Efficiency	8.2-2
8.3-1	Theoretical Recirculating Ejector Efficiency - $V_4 = 200$ fps	8.3-3
8.3-2	Theoretical Recirculating Ejector Efficiency - $V_4 = 256$ fps	8.3-4
8.3-3	Theoretical Recirculating Ejector Efficiency - $V_4 = 328$ fps	8.3-5
8.3-4	Effect of Primary Pressure on Maximum Efficiency	8.3-6
8.3-5	Typical Effect of Tertiary Exit Velocity or Base Pressure on Maximum Efficiency	8.3-7
8.3-6	Typical Effect of Primary Total Pressure on Optimum Area Ratio	8.3-8
8.4-1	Gas Horsepower as a Function of Pressure Ratio, Inlet Temperature and Weight Flow	8.4-6
8.4-2	Required Compressor Horsepower	8.4-7
8.4-3	J69-T-35 High Bleed Pumping Engine (Mock-Up)	8.4-8
8.4-4	J69-T-35 High Bleed Pumping Engine (Schematic)	8.4-9
8.4-5	Specific Thrust as a Function of Pressure Ratio for an Ejector Operating with Bleed Air and Bleed Air with Afterburning	8.4-10
8.4-6	Total Weight (Engine and Fuel) for Various Propulsion Devices as a Function of Time	8.4-11
8.5-1	Forward Flight Performance	8.5-5
8.5-2	Projected GEM Performance	8.5-6
8.6.1-1	Two-Dimensional Annular Jet Water Test	8.6-3
8.6.1-2	Two-Dimensional Ejectijet Water Test	8.6-4
8.6.2-1	Condenser Microphone	8.6-10

LIST OF ILLUSTRATIONS (Cont'd)

<u>Figure</u>		<u>Page</u>
8.6.2-2	Audio Frequency Spectrometer	8.6-11
8.6.2-3	Microphone Positions - Model 3 Straight Ejector	8.6-12
8.6.2-4	Microphone Positions - Model 3 Recirculating Ejector	8.6-13
8.6.2-5	Typical Jet Engine and Rocket Engine Power Spectrum Levels	8.6-14
8.6.2-6	Comparison of Calculated and Typical Experimental Sound Spectrums	8.6-15
8.6.2-7	Model 3 Straight Ejector Sound Spectrum - $p_o' = 100$ psig, 4 ft radius	8.6-16
8.6.2-8	Model 3 Straight Ejector Sound Spectrum - $p_o' = 100$ psig, 8 ft radius	8.6-17
8.6.2-9	Model 3 Straight Ejector Sound Spectrum - $p_o' = 100$ psig, position 10	8.6-18
8.6.2-10	10,000 cps Sound Pressure Level Around Model 3 Straight Ejector	8.6-19
8.6.2-11	Model 3 Straight Ejector Peak Sound Levels	8.6-20
8.6.2-12	Model 3 Recirculating Ejector Sound Spectrum - $p_o' = 100$ psig	8.6-21
8.6.2-13	Model 3 Recirculating Ejector Sound Spectrum - $p_o' = 40$ psig	8.6-22
8.6.2-14	Comparison of Straight and Recirculating Ejector Sound Spectrums	8.6-23
8.6.2-15	Noise Levels at Representative Pilot's Location	8.6-24
9.1-1	Ejector Test Facility	9.1-16
9.1-2	Straight Ejector Dimensions	9.1-17
9.1-3	Fabrication Details of Straight Ejectors	9.1-18
9.1-4	Straight Ejector Inlet	9.1-19
9.1-5	Straight Ejector Diffuser Exit	9.1-20
9.1-6	Straight Ejector Primary Nozzles	9.1-21
9.1-7	Straight Ejector Primary Nozzle Dimensions	9.1-22
9.1-8	Straight Ejector Primary Nozzle-Header Assembly	9.1-23
9.1-9	Straight Ejector Primary Manifold	9.1-24
9.1-10	Primary Mass Flow Meter	9.1-25
9.1-11	Straight Ejector Exit Pitot-Static Rake	9.1-26

LIST OF ILLUSTRATIONS (Cont'd)

<u>Figure</u>		<u>Page</u>
9.1-12	Dimensions of Exit Pitot-Static Rake	9.1-27
9.1-13	Inlet Pitot-Static Rake	9.1-28
9.1-14	Mercury and Water Manometer Banks	9.1-29
9.1-15	Model 1 Straight Ejector Total Thrust	9.1-30
9.1-16	Model 2 Straight Ejector Total Thrust	9.1-32
9.1-17	Model 3 Straight Ejector Total Thrust	9.1-34
9.1-18	Model 4 Straight Ejector Total Thrust	9.1-36
9.1-19	Experimental Straight Ejector Tertiary Mass Flow	9.1-38
9.1-20	Straight Ejector Primary Mass Flow - Experimental Results	9.1-40
9.1-21	Effect of Mixing Section Length on Straight Ejector Mass Augmentation	9.1-41
9.1-22	Effect of Area Ratio on Straight Ejector Mass Augmentation	9.1-42
9.1-23	Effect of Mixing Section Length on Straight Ejector Thrust Augmentation	9.1-43
9.1-24	Straight Ejector Thrust Augmentation - Experimental Results	9.1-44
9.1-25	Effect of Mixing Section Length on Straight Ejector Efficiency	9.1-45
9.1-26	Effect of Area Ratio on Straight Ejector Efficiency	9.1-48
9.1-27	Effect of Primary Total Pressure Ratio on Tertiary and Primary Velocity	9.1-47
9.1-28	Model 3 Straight Ejector Longitudinal Static Pressure Distributions - $l/t = 8.03$	9.1-48
9.1-29	Model 3 Straight Ejector Longitudinal Static Pressure Distributions - $l/t = 6.1$	9.1-49
9.2-1	Small-Scale Recirculating Ejector	9.2-4
9.2-2	Close-Up of Small Scale Recirculating Ejector	9.2-5
9.2-3	Configuration A - Small Scale Recirculating Ejector	9.2-6
9.2-4	Configuration B - Small Scale Recirculating Ejector	9.2-7
9.2-5	Configuration C - Small Scale Recirculating Ejector	9.2-8
9.2-6	Water Test of Small-Scale Recirculating Ejector - Configuration A	9.2-9
9.2-7	Water Test of Small Scale Recirculating Ejector	9.2-10
9.2-8	Large Scale Recirculating Ejector Test Set-Up	9.2-34
9.2-9	Primary Nozzle-Header Combinations for Recirculating Ejectors	9.2-35

LIST OF ILLUSTRATIONS (Cont'd)

<u>Figure</u>		<u>Page</u>
9.2-10	Model 1 Recirculating Ejector Primary Manifold	9.2-36
9.2-11	Model 2 and 3 Recirculating Ejector Primary Manifold	9.2-37
9.2-12	Nozzle for Model 2 and 3 Recirculating Ejector	9.2-38
9.2-13	Recirculating Ejector Exit Pitot-Static Rake	9.2-38
9.2-14	Model 1 Recirculating Ejector	9.2-40
9.2-15	Model 1 Recirculating Ejector - Dimensional Drawing	9.2-41
9.2-16	Model 1 Recirculating Ejector Theoretical Mass Augmentation	9.2-42
9.2-17	Effect of Primary Total Pressure on the Ground Board Pressure Distribution of Model 1 Recirculating Ejector	9.2-43
9.2-18	Model 1 Recirculating Ejector Secondary and Tertiary Total Pressure Distributions	9.2-44
9.2-19	Effect of Height on the Ground Board Pressure Distribution of Model 1 Recirculating Ejector	9.2-45
9.2-20	Model 2 Recirculating Ejector	9.2-46
9.2-21	Model 2 Recirculating Ejector - Dimensional Drawing	9.2-47
9.2-22	Model 2 Primary Nozzle - Header Installation	9.2-48
9.2-23	Theoretical Mass Augmentation for Model 2 Recirculating Ejector	9.2-49
9.2-24	Effect of Height on the Ground Board Pressure Distribution of Model 2 Recirculating Ejector	9.2-50
9.2-25	Effect of Spoiler Location on Base Pressure - Model 2 Recirculating Ejector	9.2-51
9.2-26	Model 3 Recirculating Ejector - Dimensional Drawing	9.2-52
9.2-27	Model 3 Recirculating Ejector - $\theta_1 = \theta_2 = 30^\circ$	9.2-53
9.2-28	Effect of Tertiary Exit Angle on the Model-Base and Ground-Board Pressure Distributions of Model 3 Recirculating Ejector - $h = 17.2$ inches	9.2-54
9.2-29	Effect of Tertiary Exit Angle on the Model-Base and Ground-Board Pressure Distributions of Model 3 Recirculating Ejector - $h = 12.4$ inches	9.2-55
9.2-30	Effect of Tertiary Exit Angle on the Model-Base and Ground-Board Pressure Distributions of Model 3 Recirculating Ejector - $h = 8.4$ inches	9.2-56
9.2-31	Performance of Downstream Ejector in Tandem Straight Ejector Tests	9.2-57

LIST OF ILLUSTRATIONS (Cont'd)

<u>Figure</u>		<u>Page</u>
9.2-32	Model 4 Recirculating Ejector	9.2-58
9.2-33	Model 4 Recirculating Ejector - Dimensional Drawing	9.2-59
9.2-34	Modified Model 1 Recirculating Ejector	9.2-60
9.2-35	Recirculating Ejector Efficiency (Experimental Results) - Modified Model 1 Recirculating Ejector	9.2-61
9.2-36	Effect of Ejector Area Ratio on Base Pressure and Primary Horsepower - Modified Model 1 Recirculating Ejector	9.2-62
10.1-1	Straight Ejector Mass Augmentation - Comparison of Theory with Experiment	10-4
10.1-2	Straight Ejector Thrust Augmentation - Comparison of Theory with Experiment - Effect of Mixing Section Length	10-5
10.1-3	Straight Ejector Thrust Augmentation - Comparison of Theory with Experiment - Effect of Area Ratio	10-6
10.1-4	Straight Ejector Efficiency - Comparison of Theory with Experiment	10-7
10.2-1	Comparison of Theoretical and Experimental Values of Mass Augmentation - Models 1 and 3 Recirculating Ejectors	10-10
10.2-2	Comparison of Theoretical and Experimental Values of Efficiency - Model 1 Recirculating Ejector	10-11
10.2-3	Comparison of Theory and Experiment for Base Pressure and Cavity Pressure - Model 3 Recirculating Ejector $\theta = 30^\circ$, $\theta_2 = 60^\circ$	10-12
10.2-4	Comparison of Theory and Experiment for Base Pressure and Cavity Pressure - Model 3 Recirculating Ejector $\theta_1 = 30^\circ$, $\theta_2 = 45^\circ$	10-13
10.2-5	Comparison of Theory and Experiment for Base Pressure and Cavity Pressure - Model 3 Recirculating Ejector $\theta_1 = 30^\circ$, $\theta_2 = 30^\circ$	10-14

LIST OF TABLES

<u>Table</u>		<u>Page</u>
8.1-1	Ejector Performance Equations	8.1-2
8.1-2	Annular Jet Performance Equations	8.1-3
8.4-1	Engine Compressor Units	8.4-2
9.2-1	Summary of Recirculating Ejector Experimental Results	9.2-31
9.2-2	Summary of Modified Model 1 Recirculating Ejector Experimental Results	9.2-33

LIST OF SYMBOLS

<u>Symbol</u>	<u>Quantity</u>	<u>Dimension</u>
A'	Total exit area of ejector primary nozzles	ft ²
A''	Total area of ejector secondary stream in exit plane of primary nozzles	ft ²
A'*	Total throat area of ejector primary nozzles	ft ²
A _w	Wetted area of ejector mixing section	ft ²
a	Wetted area shape parameter for ejector mixing section	—
b	Length parameter for ejector mixing section	—
c	Perimeter	ft
c _p	Specific heat at constant pressure	BTU/lb°R
c _v	Specific heat at constant volume	BTU/lb°R
C _D	Total drag coefficient = $\frac{D}{qs}$	—
C _{D_f}	Profile drag coefficient = $\frac{D_f}{qs}$	—
C _{D_{mom}}	Momentum Drag Coefficient = D_{mom}/qS	—
C _f	Total skin friction coefficient	—
C _L	Lift coefficient = L/qs	—
D	Total drag	lb
D _f	Profile drag	lb
D _{mom}	Momentum drag	lb
F	Total friction force on walls of ejector mixing section	lb
F _A	Force applied to air in ejector ducting	lb/ft
F _H	Horizontal component of momentum action on ejector ducting	lb/ft
F _V	Vertical component of momentum acting on ejector ducting	lb/ft
F _Z	Lifting force in heave	lb
HP	Horsepower	
h	Height of vehicle base above the ground plane	ft
\bar{h}	Mean height of pitched or rolled vehicle	ft

LIST OF SYMBOLS (Cont'd)

<u>Symbol</u>	<u>Quantity</u>	<u>Dimension</u>
I_{yy}	Pitch moment of inertia	ft-lb-sec ²
\hat{i}	Unit vector in axial direction of flow in ejector mixing section	—
J	Total momentum flux of tertiary exit flow t_e	lb
j	Unit momentum flux of tertiary exit flow = $\int V_4 dt$	lb/ft
L	Lift	lb
ℓ	Length of ejector mixing section or length of vehicle	ft
\bar{L}	Distance between centroids of forward and aft recirculating flow cavities	—
M	Pitching moment	ft-lb
M_{CF}	Pitching moment due to cross flow	ft-lb
\dot{m}	Ejector tertiary mass flow	slugs/sec
\dot{m}'	Total mass flow through ejector primary nozzles	slugs/sec
\dot{m}/\dot{m}'	Mass augmentation	—
\vec{n}	Unit vector normal to area of integration	—
p	Absolute static pressure	lb/ft ²
p_o	Absolute total pressure	lb/ft ²
p_a	Absolute ambient static pressure	lb/ft ²
p_b	Gage base (air cushion) pressure	lb/ft ²
p_{br}	Gage base pressure behind right jet of pitched vehicle	lb/ft ²
p_{bl}	Gage base pressure behind left jet of pitched vehicle	lb/ft ²
p_c	Gage cavity pressure, static pressure interior to recirculating flow between ejector exit and inlet	lb/ft ²
p_c	Difference between right and left cavity pressures of pitched vehicle	lb/ft ²
q	Freestream dynamic pressure = $\frac{1}{2} \rho_\infty V_\infty^2$	lb/ft ²
q_j	Jet dynamic pressure of conventional annular jet	lb/ft ²
R	Universal gas constant	1715 ft lb/slug °
S_b	Vehicle base area	ft ²
S_c	Vehicle cavity area	ft ²

LIST OF SYMBOLS (Cont'd)

<u>Symbol</u>	<u>Quantity</u>	<u>Dimension</u>
T	Total thrust	lb
T	Temperature	°F or °R
T _o	Total temperature	°R
t	Ejector mixing section thickness	ft
t _e	Exit jet thickness measured normal to exit flow	ft
V	Velocity	ft/sec
W	Vehicle weight	lb
w	Ejector or vehicle width	ft
z	Vertical displacement in heave from steady-state condition	ft
α	Pitch angle	rad
γ	Ratio of specific heats, $\frac{c_p}{c_v}$	—
ε	Ejector efficiency	—
ε _o	Overall Ejectijet efficiency	—
η _o	Overall annular jet efficiency	—
θ ₁	Angle of ejector secondary inlet measured from the horizontal	deg
θ ₂	Angle of ejector tertiary exit measured from the horizontal	deg
μ	Viscosity of air	lb sec/ft ²
ρ	Density of air	slugs/ft ³

Subscripts

0	Stagnation conditions
I	Condition at ejector inlet in exit plane of primary nozzles
2	Condition at end of ejector mixing section
3	Condition at end of ejector diffuser section
4	Condition at ejector exit
l	Condition at left jet of pitched vehicle
r	Condition at right jet of pitched vehicle
∞	Freestream conditions

Superscripts

'	Ejector primary flow conditions
"	Ejector secondary flow conditions
$\overline{(\quad)}$	Simple average or integrated average
*	Non-dimensionalized value

One dot over a variable denotes the first derivative with respect to time; two dots denote the second derivative with respect to time.

1.0 SUMMARY

This report represents an experimental and theoretical investigation to determine the feasibility of utilizing a recirculation concept as a lift system for ground effect machines. Several recirculation methods are considered and it is concluded that the annular recirculating ejector referred to as "Ejectijet" is superior.

A theory is developed to predict the performance of an ejector, both straight and recirculating. Correlation with this theory is shown with the large scale two-dimensional models. Overall Ejectijet-GEM hovering performance estimates are presented along with a brief study of the effects of forward flight. Stability and control in hover are also considered including a cursory examination of forward flight effects. Some propulsion aspects are shown primarily as a comparison with the conventional annular jet GEM.

2.0 CONCLUSIONS

2.1 RECIRCULATION METHODS

The annular recirculating ejector concept, referred to as "Ejectijet", is superior to other recirculation methods.

2.2 HOVERING POWER

Comparison of the hovering power required for the Ejectijet as compared with conventional annular jets in terms of lifting power per installed engine horsepower involves the question of efficiency of various components in each system. At present, such a comparison cannot be made between specific configurations, since two comparable machines have not yet been designed. However, based upon a range of efficiencies outlined in the foregoing investigation, it can be concluded that it is possible to build a Ground Effect Machine using the Ejectijet recirculating principle with a higher value of lift per horsepower. The theory presented here indicates that a further reduction in hovering power is possible.

2.3 PROPULSION POWER

An appreciable reduction in momentum drag will be encountered by the Ejectijet machine. Therefore, the Ejectijet will require less propulsive power than the comparable annular jet and the margin of difference in favor of the Ejectijet will increase with increasing speed.

2.4 PAYLOAD

An advantage in structural and mechanical simplicity will be realized. In particular, the weight of the lift system favors the Ejectijet. This results in a significant advantage for the Ejectijet in such ratios as payload per horsepower and payload per gross weight.

2.5 STABILITY

An analog simulation study, as well as tests of a small scale 3-dimensional model, indicate that the recirculation GEM is inherently statically stable without resorting to compartmentation of the base area by such means as air curtains.

2.6 CONTROL

Many control devices have been under investigation. Analysis indicates that varying the angular position of the Ejectijets with respect to the base plane provides an effective control system while maintaining the characteristically low profile of the recirculation system.

2.7 DUST AND SPRAY SUPPRESSION

Recirculation of the air curtain confines the majority of the dust and spray under the base of the machine. Tests of the small scale 3-dimensional model over a water tank as well as a series of comparative tests of 2-dimensional models of an annular jet and a recirculating jet confirm that the spray pattern of the recirculating machine will be an order of magnitude less than conventional annular jets.

3.0 RECOMMENDATIONS

As a result of this study the following recommendations are made:

- a. Continued experimental and theoretical investigations should be conducted to determine the maximum efficiency obtainable from the recirculating ejector.
- b. A theoretical analysis of the external flow of recirculating ejectors should be continued. In particular, it appears that a conformal mapping solution is possible and may provide useful information.
- c. The study of the effects of forward flight should include the testing of man-carrying test vehicle.
- d. A detailed design study and operational analysis for an Ejectijet GEM to perform a specific mission is recommended.

4.0 INTRODUCTION

The Martin-Marietta Company began its effort in the field of GEM research as early as 1958. Extensive experimental and analytical work was done at the Orlando Aerospace Division on flow phenomena, performance, and static stability of conventional annular jet configurations. Martin-Marietta began studying the general concept of recirculation in 1959, and the development of the Ejectijet principle was the result of this effort.

To substantiate and extend the existing theoretical analysis, and to prove the practical feasibility of the recirculating ejector concept, the research program described in this report was undertaken:

The theoretical analysis of straight and recirculating ejectors is presented. The experimental program to substantiate the theoretical analysis, justify the necessary assumptions, and define the limits of applicability and accuracy, is also presented.

The application of recirculating ejectors to a GEM is analyzed quantitatively and qualitatively with regard to

- a. Hovering performance
- b. Forward flight
- c. Stability and control
- d. Propulsion
- e. Dust and spray generation
- f. Noise generation

Experimental results are used wherever possible to correlate with theoretical predictions and to formulate empirical relationships whenever theory becomes inadequate. The results of these studies should prove useful as a guide to future research.

5.0 GENERAL RECIRCULATION METHODS

The general principle of recirculation applied to ground effect machines (GEM) is an intriguing concept which in the ideal case requires zero lift power input. The high potential efficiency and low momentum drag in forward flight has stimulated considerable research, as witnessed by References 1 through 4, in devising systems which will produce the recirculating flow pattern. The logical evolution of the Martin-Marietta recirculation concept is demonstrated in the following critical analysis of several general recirculation methods.

5.1 DIFFUSER RECIRCULATION CONCEPT

In the diffuser-recirculation concept of Reference 1 the kinetic energy of an air jet is converted into pressure energy through diffusion. Air exhausted at an inward and downward angle from an annular slot is diffused between the ground surface and lower surface of the GEM. The resultant static pressure is applied over the base area to produce the lift force. Pressurized air from the base cavity is then recirculated by a fan. This process is presented schematically in Figure 5-1.

A study of this process presents several serious disadvantages which negate the possible improvement in efficiency and reduction in dust and spray generation.

- a Since this concept is simply a plenum chamber with a recirculation cycle, it is inherently restricted to heights that are equal to or less than the thickness of the exhaust nozzles.
- b Operation at very low heights becomes critical especially if the jet is "overfed" (Reference 5). In this condition the jet splits at the ground surface with a larger portion exhausting out from under the base. The recirculating flow is then no longer balanced, air is pumped out of the base region, and the vehicle is sucked to the ground.

- c Performance is dependent on efficient diffusion of the flow as it moves inward under the vehicle and irregularities in the surface over which the vehicle moves would adversely effect this diffusion process.
- d The use of a fan or compressor in a contaminated air stream is objectionable due to the short operating life and consequent maintenance problems.

5.2 LABYRINTH SEALS

The labyrinth or powered seals described in References 2 and 3 are pseudo-peripheral recirculation devices applied to a plenum lift system for the purpose of retarding the escape of air from the air cushion. The principle involved is that of a high loss system in which both velocity and static pressure of the flow are reduced. In the limiting case of zero velocity and ambient pressure at the periphery theoretically no air would escape, hence no air need be added and the efficiency would approach 100 percent.

Figure 5-2 shows the labyrinth chambers with fans and the intended flow directions through the system. Air tending to escape from the base cavity enters the vicinity of the first labyrinth chamber whereupon the flow splits and a portion of it is drawn into the chamber by a fan. This portion of the flow is then expelled through a slot and directed against the remainder of the escaping flow. The process is repeated at the next chamber where more energy is extracted from the flow. The author of Reference 2 claims a reduction of 25 percent in power input for a two-stage seal with fans and an expected reduction of 40 percent with a three-stage system.

The undesirable features of the labyrinth seal concept are similar to those of the diffuser-recirculation concept. Both are restricted to relatively low operating heights, and both require numerous fan installations near the periphery of the vehicle. Fan operating life may be sufficient in a labyrinth seal system since flow contamination by dust and spray is not so severe; however, the mechanical complexity and additional weight of such a fan system appear prohibitive.

5.3 ANNULAR JET RECIRCULATION SYSTEMS

In the recirculation systems illustrated in Figure 5-3 the exhaust jet is entrained by a return duct after ground impingement, and recirculated through the system. This system is referred to as an annular jet recirculation system since turning of an air curtain in the manner of a conventional annular jet is still utilized to generate the cushion pressure. Figure 5-3a depicts an inward closed annular jet recirculation system. Here the cushion pressure is generated by the flow as it turns into the return duct after ground impingement. In the outward recirculation system of Figure 5-3b the base pressure is generated before ground impingement.

Of the recirculation systems discussed, only the annular jet system shows promise of substantially improving the performance of ground effect machines without compromising operating height. However, some mechanical problems are apparent. It is noted in Figure 5-3 that no means of maintaining the recirculating flow are indicated. A series of fans could be located around the perimeter of a vehicle to create the desired flow pattern but,

the mechanical complexity of such a system precludes this possibility. Figure 5-4 shows two possible duct systems that could be utilized with a central fan (Reference 4). In this case, the increased weight and internal losses due to the additional ducting penalize performance significantly. Also, both systems must operate in a contaminated air stream leading to short fan life.

The crux of the problem of developing a successful recirculation system is in implementing the concept in a practical mechanical form. Utilizing an ejector to maintain the circulatory flow appears to be the only practical method.

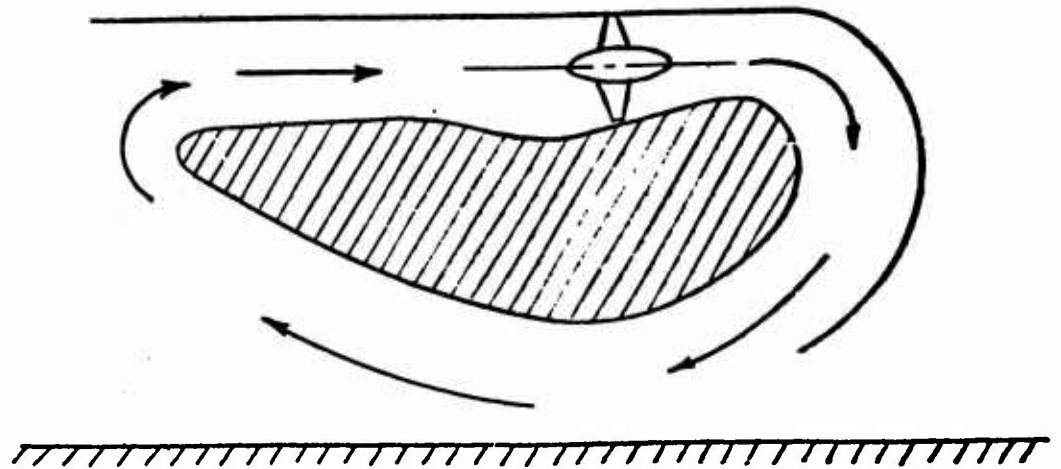


FIGURE 5-1 DIFFUSER - RECIRCULATION CONCEPT

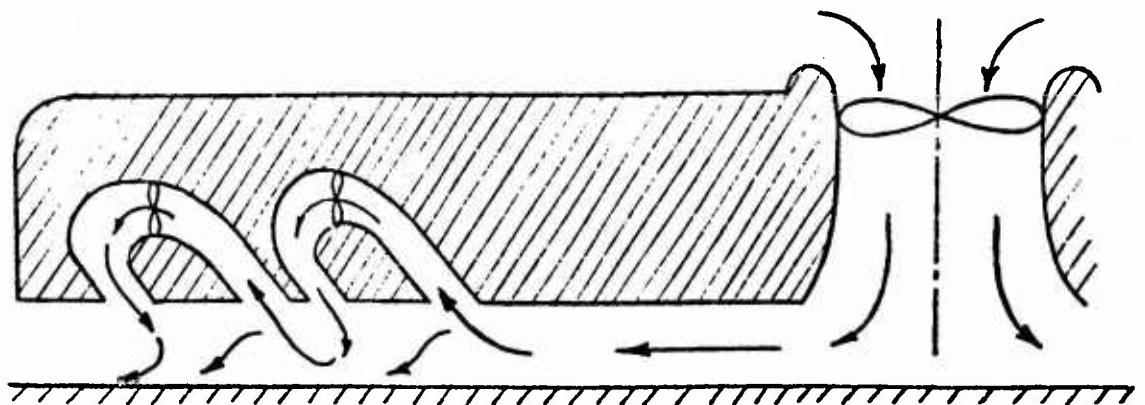


FIGURE 5-2 LABYRINTH - SEAL CONCEPT

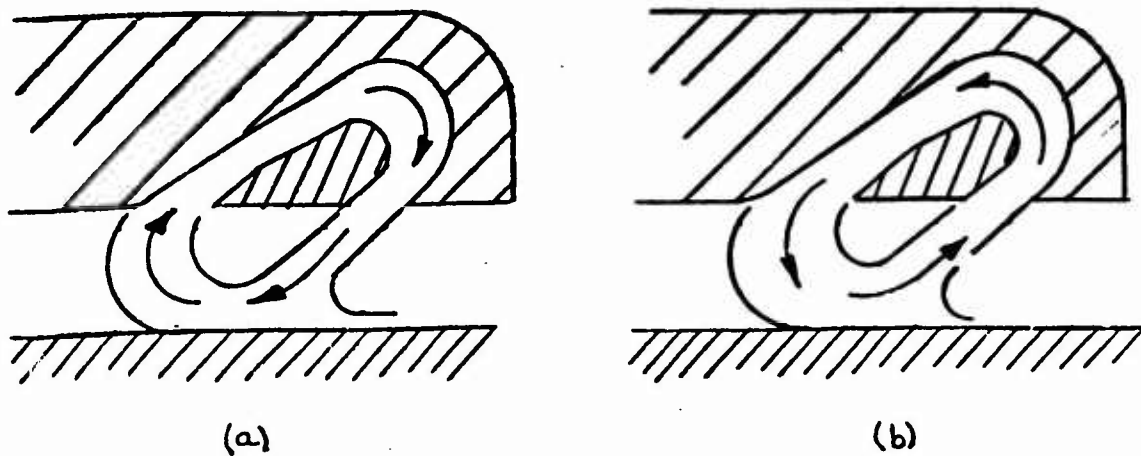
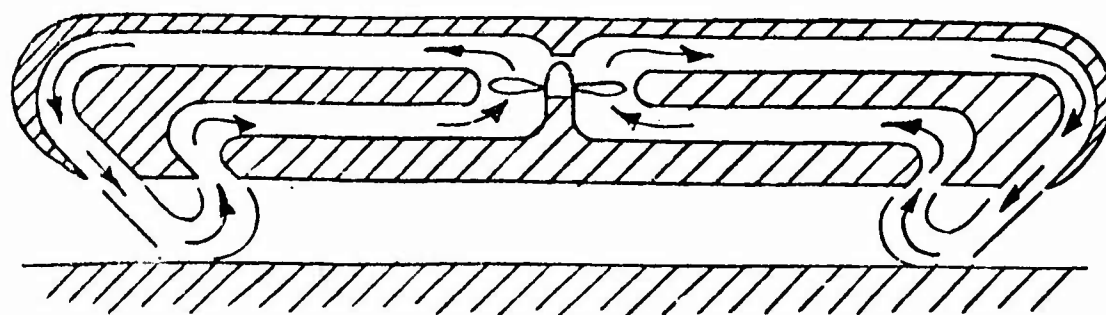
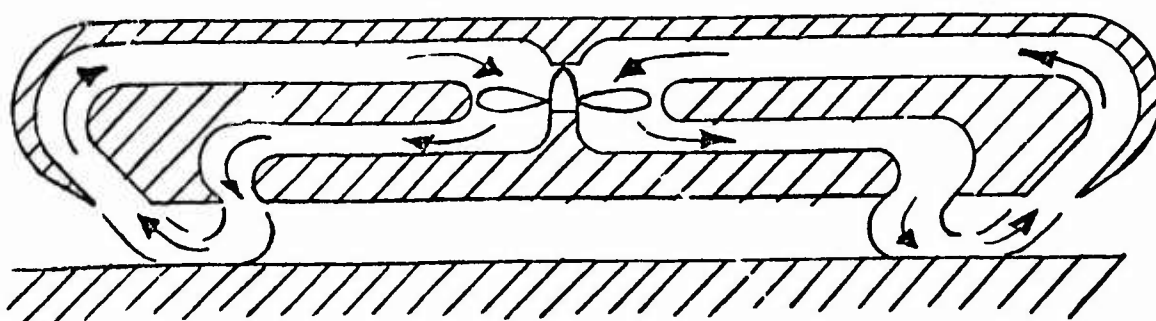


FIGURE 5-3 ANNULAR JET RECIRCULATION CONCEPT



(a) INWARD FLOW



(b) OUTWARD FLOW

FIGURE 5-4 CENTRAL FAN INSTALLATION FOR ANNULAR JET RECIRCULATION SYSTEM

6.0 MARTIN-MARIETTA RECIRCULATION CONCEPT

It is concluded that the recirculating annular jet system is the most promising of the various recirculation schemes known. The single problem area is the development of a power system that can impart the necessary momentum to a highly contaminated recirculating airstream. Various possible power systems have been examined, including axial flow fans, centrifugal compressors, rotary vanes, piston compressors, gear blowers, valveless pulsejets, and ejectors. Of these, the ejector presents a practical solution to the problem.

Figure 6-1 demonstrates schematically how the recirculating flow is achieved by means of an ejector. The process is as follows: High velocity air from the primary nozzle (station 1) entrains a secondary air stream, and turbulent mixing of the two streams occurs in the mixing section. At the end of the mixing section (station 2) complete mixing has occurred and the combined flow is then diffused to slightly above ambient pressure (station 3). The flow is next turned through the curved ducting and exhausted at station 4. At the design height and mass augmentation, with the optimum jet exhaust angle, there will be no static pressure gradient across the outboard jet. Atmospheric pressure will then exist interior to the circulating flow. The jet exhaust impinges on the ground surface in the manner of a free jet impinging on a flat plate. The laws of fluid continuity require the jet to split after impingement such that the mass flow introduced through the primary nozzle is blown out (station 6). This requirement determines the proper jet angle. The remaining mass flow, at station 5, is turned up and into the ejector inlet and forms a curved reverse flow annular jet which generates a lifting pressure or base pressure in the same manner as the conventional annular jet.

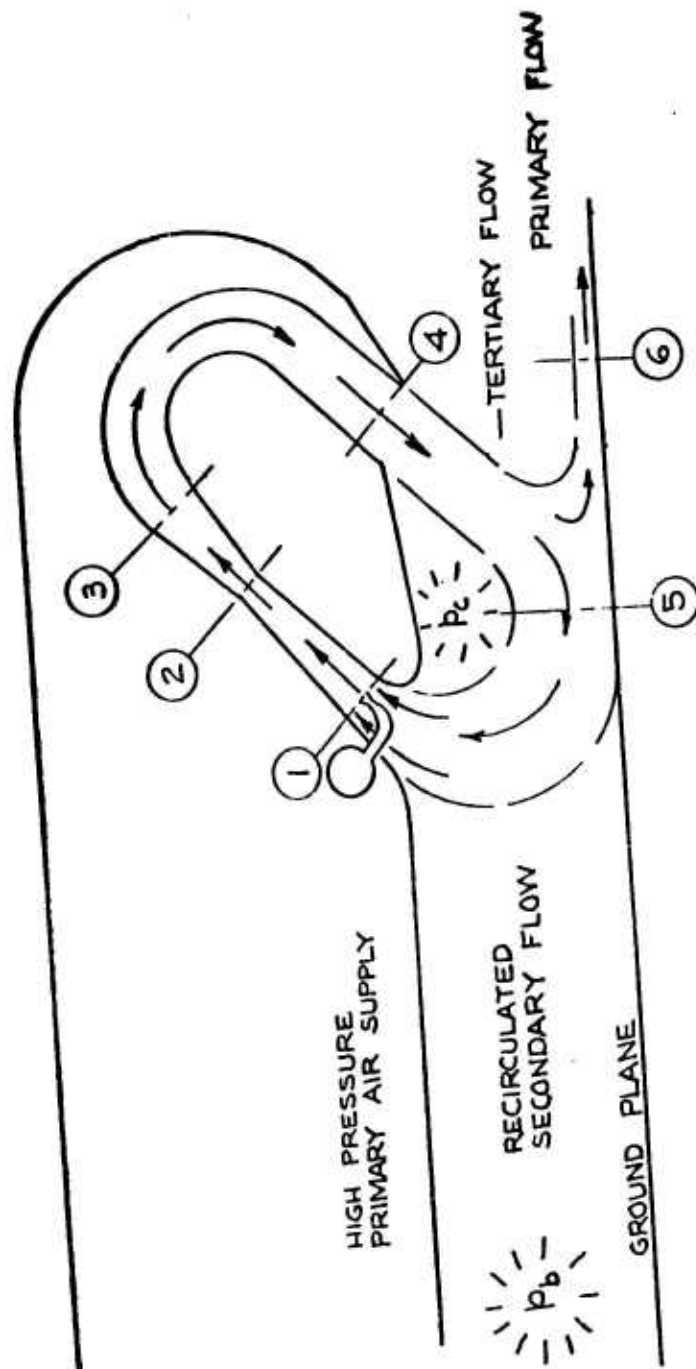


FIGURE 6-1 RECIRCULATING EJECTOR LIFT SYSTEM

7.0 ANALYTICAL STUDIES

7.1 STRAIGHT EJECTOR

The problem of the conventional straight ejector is treated here in the manner of References 6 and 7 with some modification. In Figure 7.1-1 it is seen that the reservoir conditions for the primary and secondary flows are known. The tertiary or combined flow is specified by three independent quantities; total head, P_{03} , static pressure, P_3 , and the mass flow, m . It is assumed that the flow is quasi-one-dimensional; i.e., each stream (primary, secondary, and tertiary) is uniform vertically and laterally at the entrance and exit. Isentropic flow is assumed everywhere except in the mixing section, and for the present analysis, it is assumed that there is no heat transfer across the walls. These assumptions indirectly require that the mixing process be completed in the mixing section regardless of the mixing section length. The governing equations for the mixing process are:

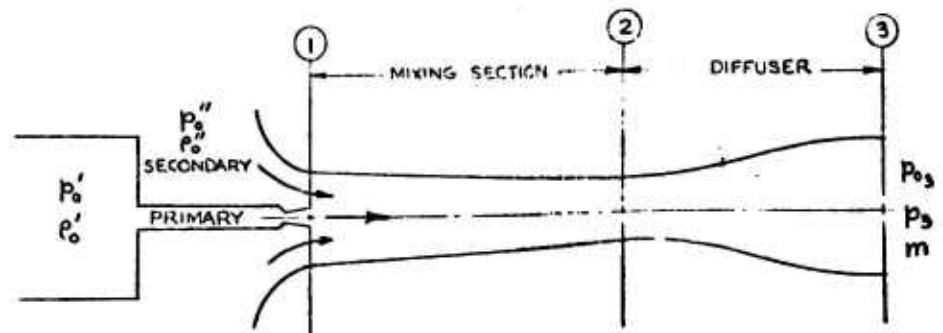


Figure 7.1-1 Conventional Straight Ejector

7.1-1

1 Continuity

$$m' + m'' = m \quad (7.1-1)$$

2 Momentum

$$m'V_1' + m''V_1'' = mV_2 + F + \iint_A (p\vec{n}) \cdot \vec{i} dA \quad (7.1-2)$$

Since it is assumed that the mixing section shape results in a constant pressure along its length ($p_1 = p_2$), the net pressure force on the control surface enclosing the mixing section is zero. Therefore, equation 7.1-2 becomes

$$m'V_1' + m''V_1'' = mV_2 + F \quad (7.1-3)$$

3 Energy

$$c_p m' T_0' + c_p m'' T_0'' = m \left[c_p T_2 + \frac{V_2^2}{2} \right] \quad (7.1-4)$$

This is the general energy relation for adiabatic (zero heat transfer) flow. It states that the energy entering the mixing section is the sum of the total enthalpies of the primary and secondary streams, and the energy leaving is the total enthalpy at the end of mixing. From the equation of state for an ideal gas

$$T = \frac{p}{\rho R}$$

$$\text{where } R = C_p - C_v$$

Substitutions of these relations into equation 7.1-4 leads to the more useful form of the energy equation.

$$\frac{\gamma}{\gamma-1} \left[\frac{m' p_0'}{\rho_0'} + \frac{m'' p_0''}{\rho_0''} \right] = m \left[\left(\frac{\gamma}{\gamma-1} \right) \left(\frac{p_2}{\rho_2} \right) + \frac{V_2^2}{2} \right] \quad (7.1-5)$$

7.1.1 Inviscid Solution

The inviscid solution obtained in this section describes the flow in the ejector in terms of the given flow variables and the mixing section static pressure. The details of the turbulent mixing process are avoided

by assuming constant mixing-section pressure and maintaining a simultaneous balance in mass, momentum, and energy across the mixing section.

Solving equations 7.1-1 and 7.1-3 for the primary and secondary mass flows with $F = 0$

$$m' = \frac{V_2 - V_1'}{V_1' - V_1''} m \quad (7.1-6)$$

$$m'' = \frac{V_1' - V_2}{V_1' - V_1''} m \quad (7.1-7)$$

It is assumed that the static pressure is uniform in the plane of the primary nozzle exit and that the flow in this plane is isentropic, therefore

$$\left(\frac{\gamma}{\gamma-1}\right)\left(\frac{p_0'}{\rho_0'}\right) = \left(\frac{\gamma}{\gamma-1}\right)\left(\frac{p_1}{\rho_1}\right) + \frac{V_1'^2}{2} \quad (7.1-8)$$

$$\left(\frac{\gamma}{\gamma-1}\right)\left(\frac{p_0''}{\rho_0''}\right) = \left(\frac{\gamma}{\gamma-1}\right)\left(\frac{p_1}{\rho_1}\right) + \frac{V_1''^2}{2} \quad (7.1-9)$$

Equations 7.1-8 and 7.1-9 in conjunction with the relations

$$\frac{p_1}{p_0'} = \left(\frac{\rho_1}{\rho_0'}\right)^\gamma \quad \frac{p_1}{p_0''} = \left(\frac{\rho_1}{\rho_0''}\right)^\gamma$$

may be used to determine expressions for the primary and secondary velocities, V_1' and V_1'' in terms of the unknown mixing section static pressure, p_1

$$V_1' = \sqrt{\frac{2\gamma}{\gamma-1} \left(\frac{p_0'}{\rho_0'}\right) \left[1 - \left(\frac{p_1}{p_0'}\right)^{\frac{\gamma-1}{\gamma}}\right]} \quad (7.1-10)$$

$$V_1'' = \sqrt{\frac{2\gamma}{\gamma-1} \left(\frac{p_0''}{\rho_0''}\right) \left[1 - \left(\frac{p_1}{p_0''}\right)^{\frac{\gamma-1}{\gamma}}\right]} \quad (7.1-11)$$

Examination of Equation 7.1-5 indicates that the velocity at the end of mixing, V_2 , can also be expressed in terms of the mixing section static pressure ($p_1 = p_2$) if ρ_2 can be expressed in terms of p_1 and V_2 . Since the flow between locations (2) and (3) (see Figure 7.1-1) is assumed to be isentropic, the energy equation for this region provides the desired expression for ρ_2

$$\left(\frac{\gamma}{\gamma-1}\right)\left(\frac{p_0}{\rho_0}\right) = \left(\frac{\gamma}{\gamma-1}\right)\left(\frac{p_2}{\rho_2}\right) + \frac{V_2^2}{2} \quad (7.1-12)$$

$$\frac{p_2}{\rho_2} = \left(\frac{\rho_2}{\rho_0}\right)^{1/\gamma} \quad (7.1-13)$$

Solving equation 7.1-12 for ρ_2 using equation 7.1-13 yields

$$\rho_2 = \left(\frac{\gamma}{\gamma-1}\right)\left(\frac{p_0}{V_2^2}\right)\left(\frac{p_2}{\rho_0}\right)^{1/\gamma} \left[1 - \left(\frac{p_2}{p_0}\right)^{\frac{\gamma-1}{\gamma}}\right] \quad (7.1-14)$$

Substitution of Equations 7.1-6, 7.1-7, and 7.1-14 into Equation 7.1-5 yields the following quadratic equation in V_2

$$V_2^2 - \left\{ \frac{2\gamma}{\gamma-1} \left(\frac{p_0'}{\rho_0'} - \frac{p_0''}{\rho_0''} \right) \left[\frac{1 - \left(\frac{p_1}{p_2} \right)^{\frac{\gamma-1}{\gamma}}}{V_1' - V_1''} \right] \right\} V_2 - \left\{ \frac{2\gamma}{\gamma-1} \left(V_1' \frac{p_0''}{\rho_0''} - V_1'' \frac{p_0'}{\rho_0'} \right) \left[\frac{1 - \left(\frac{p_1}{p_0} \right)^{\frac{\gamma-1}{\gamma}}}{V_1' - V_1''} \right] \right\} = 0 \quad (7.1-15)$$

This equation for V_2 completes the solution in that the remaining flow conditions and areas can now be determined.

Analysis of Equation 7.1-15 indicates a rather startling simplification when the stagnation temperatures of the primary and secondary flows are the same.

$$\text{When } T_0' = T_0''$$

$$\frac{p_0'}{\rho_0'} = \frac{p_0''}{\rho_0''} = \frac{p_0}{\rho_0} = RT_0$$

Then

$$V_2^2 = RT_{c_3} \left(\frac{2\gamma}{\gamma-1} \right) \left[1 - \left(\frac{p_3}{p_2} \right)^{\frac{\gamma}{\gamma-1}} \right] \quad (7.1-16)$$

Equation 7.1-16 is simply the energy equation for the flow between location (2) and (3) as expressed by Equation 7.1-12. The significance of this simplification becomes evident in the viscous solution of the ejector problem.

Equations for the remaining inviscid flow conditions and areas are now developed. For a given value of mixing section pressure, $p_1 = p_2$, a value for V_2 can be obtained from Equation 7.1-15. The remaining variables in Equation 7.1-15 are known from the outset or are also functions of p_1 . Having determined V_2 , the density ρ_2 is given by Equation 7.1-14 and the stagnation density of the tertiary flow is given by Equation 7.1-13. The tertiary velocity is then determined from

$$V_3 = \sqrt{\left(\frac{2\gamma}{\gamma-1} \right) \left(\frac{p_2}{p_3} \right) \left[1 - \left(\frac{p_3}{p_2} \right)^{\frac{\gamma}{\gamma-1}} \right]} \quad (7.1-17)$$

and

$$\rho_3 = \rho_{c_3} \left(\frac{p_3}{p_{c_3}} \right)^{1/\gamma} \quad (7.1-18)$$

$$A_2 = \frac{m}{\rho_2 V_2} \quad (7.1-19)$$

$$A_3 = \frac{m}{\rho_3 V_3} \quad (7.1-20)$$

Returning to the initial flows

$$\rho' = \rho'_c \left(\frac{p_1}{p'_c} \right)^{1/\gamma} \quad (7.1-21)$$

$$\rho'' = \rho''_c \left(\frac{p_1}{p''_c} \right)^{1/\gamma} \quad (7.1-22)$$

Since the primary and secondary mass flows are given by Equations 7.1-6 and 7.1-7, the areas may be determined from

$$A' = \frac{m'}{\rho' V'} \quad (7.1-23)$$

$$A'' = \frac{m''}{\rho'' V''} \quad (7.1-24)$$

$$A_1 = A' + A'' \quad (7.1-25)$$

Flow conditions and areas are now specified at locations (1), (2) and (3) for a given mixing section pressure. Thus it is clear that there are many possible area ratios or ejector configurations which deliver the required flow and operate out of given reservoirs.

In the outlined solution it has been necessary to consider only the exit area of the primary nozzle. For a supersonic primary nozzle, the throat area is easily determined from the Laval equations since the primary reservoir conditions and the primary mass flow are known, thus

$$A'^* = \frac{1}{m'} \sqrt{\gamma \left(\frac{2\gamma}{\gamma+1} \right)^{\frac{\gamma+1}{\gamma-1}} \rho'_e \rho'_s} \quad (7.1-26)$$

7.1-2 Viscous Solution

The inviscid solution gives unrealistic results, but is nevertheless useful in the solution of the viscous problem. In particular, the inviscid solution suggests the proper approach to the viscous problem.

To solve the viscous case a shear function, F , is defined as

$$F = \frac{\bar{\rho} \bar{V}^2}{2} A_w \left\{ \frac{0.455}{\left[\text{LOG}_{10} \left(\frac{\bar{\rho} \bar{V} l}{\mu} \right) \right]^{2.58}} \right\} \quad (7.1-27)$$

Where the bracketed term is the Prandtl-Schlichting incompressible flat plate turbulent skin-friction coefficient, and A_w and L are the wetted area and length, respectively, of the mixing section. A bar over a symbol indicates the average of the secondary stream value at location (1) and the tertiary or mixed stream at location (2), specifically,

$$\bar{\rho} = \frac{\rho'' + \rho_2}{2} \quad (7.1-28)$$

$$\bar{V} = \frac{V_1'' + V_2}{2} \quad (7.1-29)$$

$$\bar{\mu} = .333 \left(\frac{\bar{T}}{459} \right)^{.75} \times 10^{-6} \text{ (FOR AIR)} \quad (7.1-30)$$

$$\bar{T} = \frac{p_1}{R \bar{\rho}} \quad (7.1-31)$$

The viscosity law expressed by Equation 7.1-30 is suggested in Reference 8.

The wetted area is, of course, a function of the ejector cross-sectional shape (e.g., rectangular, annular, circular) and length. This area can be therefore expressed as

$$A_w = a \bar{A} \quad (7.1-32)$$

Where
$$\bar{A} = \frac{A_1 + A_2}{2} \quad (7.1-33)$$

and a is a shape parameter. Similarly, the length may be written as

$$L = b \sqrt{\bar{A}} \quad (7.1-34)$$

where b is another independent shape parameter. Together, a and b

specify the shape, but not the size, of the mixing section. In this manner some three-dimensionality is introduced.

The primary and secondary mass flows are obtained from the viscous form of Equations 7.1-1 and 7.1-3.

$$m' = \frac{m(V_2 + V_1'') + F}{V_1' - V_1''} \quad (7.1-35)$$

$$m'' = \frac{m(V_1' - V_2) + F}{V_1' - V_1''} \quad (7.1-36)$$

Substitution of Equations 7.1-14, 7.1-35, and 7.1-36 into Equation 7.1-5 results in the following quadratic equation in V_2 .

$$V_2^2 - \left\{ \left(\frac{2\gamma}{\gamma-1} \right) \left(\frac{p_0'}{\rho_0'} - \frac{p_0''}{\rho_0''} \right) \frac{\left[1 - \left(\frac{p_2}{p_{0,2}} \right)^{\frac{\gamma-1}{\gamma}} \right]}{V_1' - V_1''} \right\} V_2 - \left\{ \left(\frac{2\gamma}{\gamma-1} \right) \left[\left(V_1' - \frac{F}{m} \right) \frac{p_0''}{\rho_0''} - \left(V_1'' - \frac{F}{m} \right) \frac{p_0'}{\rho_0'} \right] \frac{\left[1 - \left(\frac{p_2}{p_{0,2}} \right)^{\frac{\gamma-1}{\gamma}} \right]}{V_1' - V_1''} \right\} = 0 \quad (7.1-37)$$

Since the frictional force F is a function of V_2 , an iterative process is required to solve Equation 7.1-37. F is evaluated to a first approximation by using the flow values obtained from the inviscid solution of Equation 7.1-15. This value of F when substituted into Equation 7.1-37 provides the first approximation to V_2 . With the values for V_2 and F , the first approximations to the primary and secondary mass flows are determined from Equations 7.1-35 and 7.1-36. The remaining variables (area and density) that influence F can be determined and substituted into Equation 7.1-27 to provide the second approximation to F . The iteration is continued in this manner until satisfactory convergence is obtained; i.e., until Equation 7.1-37 is balanced.

The solution associates the mixing section pressure uniquely with an area ratio, A''/A' . The optimum ejector is determined by obtaining solutions for several mixing section pressures and choosing the one for which the power ratio (efficiency) is a maximum. Power ratio is herein defined as the ratio between tertiary and primary kinetic energy, thus

$$\epsilon = \frac{m V_3^2}{m' V_1^2} \quad (7.1-38)$$

The questions now remain - what is the shape of the mixing section that will result in a constant pressure along its length, and what is the length of tube required to obtain complete mixing? The mixing section length is required to determine the shape parameters for the solution and can be determined from experimental data. Since the areas A_1 and A_2 of the entrance and exit of the mixing section are known, the intermediate shape should be reasonably well approximated by a straight line. This is justifiable since such a fairing is an interpolation rather than an extrapolation. The fact that the computed entrance and exit areas for an optimum ejector are not far from equal reinforces this reasoning. This implies that constant pressure mixing and constant area mixing are not vastly different.

7.1-3 Simplified Solution of Special Ejector Problem

For the special case in which the stagnation temperatures of the primary and secondary flows are the same, Equation 7.1-37 reduces to the energy equation expressed by equation 7.1-12. The iteration process is then applied only to F since the difference between the inviscid and viscous values for m' and m'' cause a corresponding change in cross sectional and wetted areas. However, an order analysis performed on Equation 7.1-36

shows that the influence of F on secondary mass flow, and consequently secondary area, is small (unless $V_1' \approx V_2$) such that the first approximation to F is satisfactory and the iteration can generally be omitted.

The simplifications created by this special case make the ejector problem amenable to graphical solution. For example, the velocities, V_1' , V_2'' , V_2 , and V_3 can be determined from the curves of Figure 7.1-2, which are simply solutions of the compressible Bernoulli equation. The value for the Prandtl-Schlichting skin friction coefficient is provided by Figure 7.1-3. The first approximation to F is then used to calculate m' and m'' and the corresponding ejector cross-sectional areas.

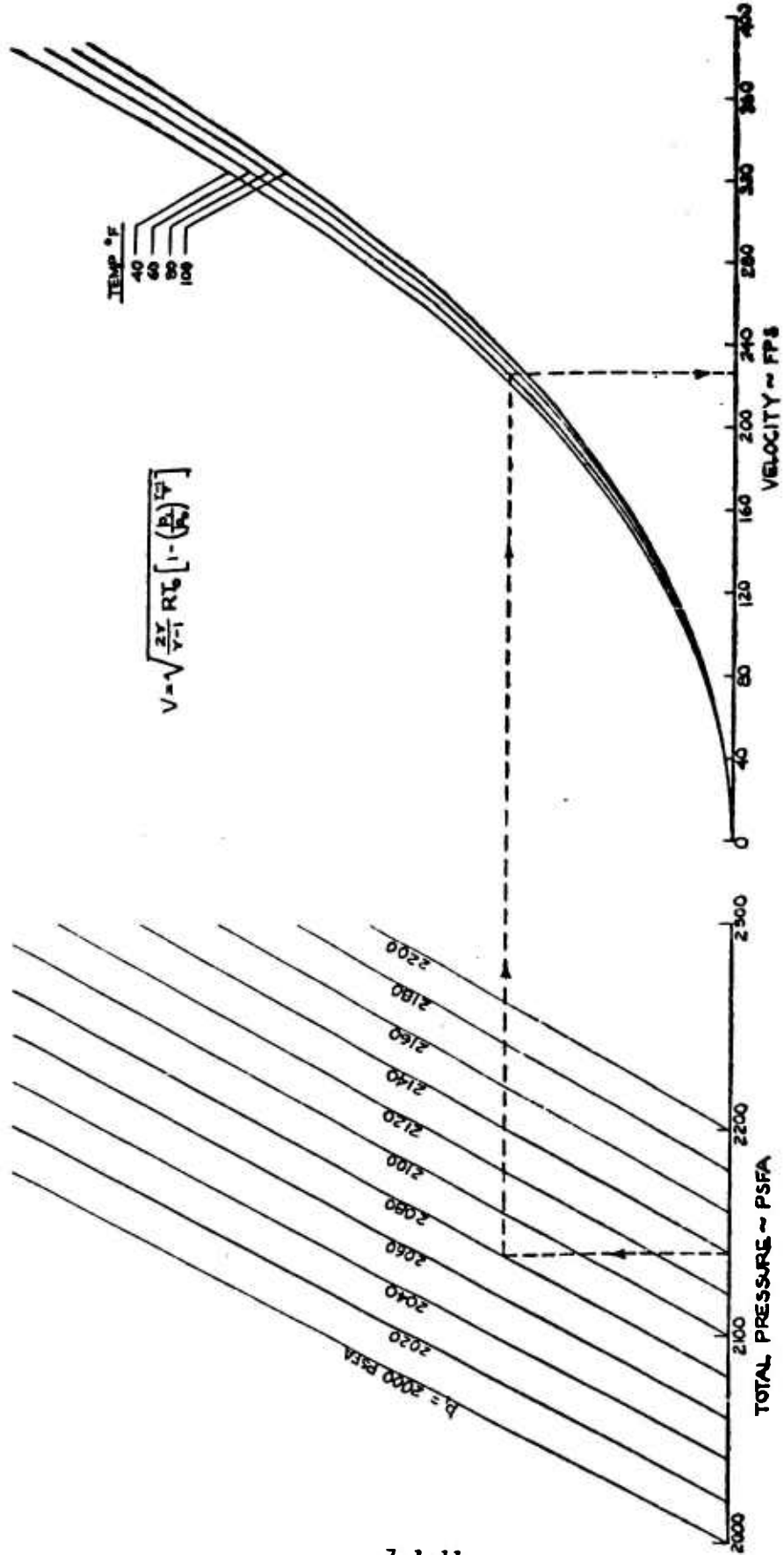
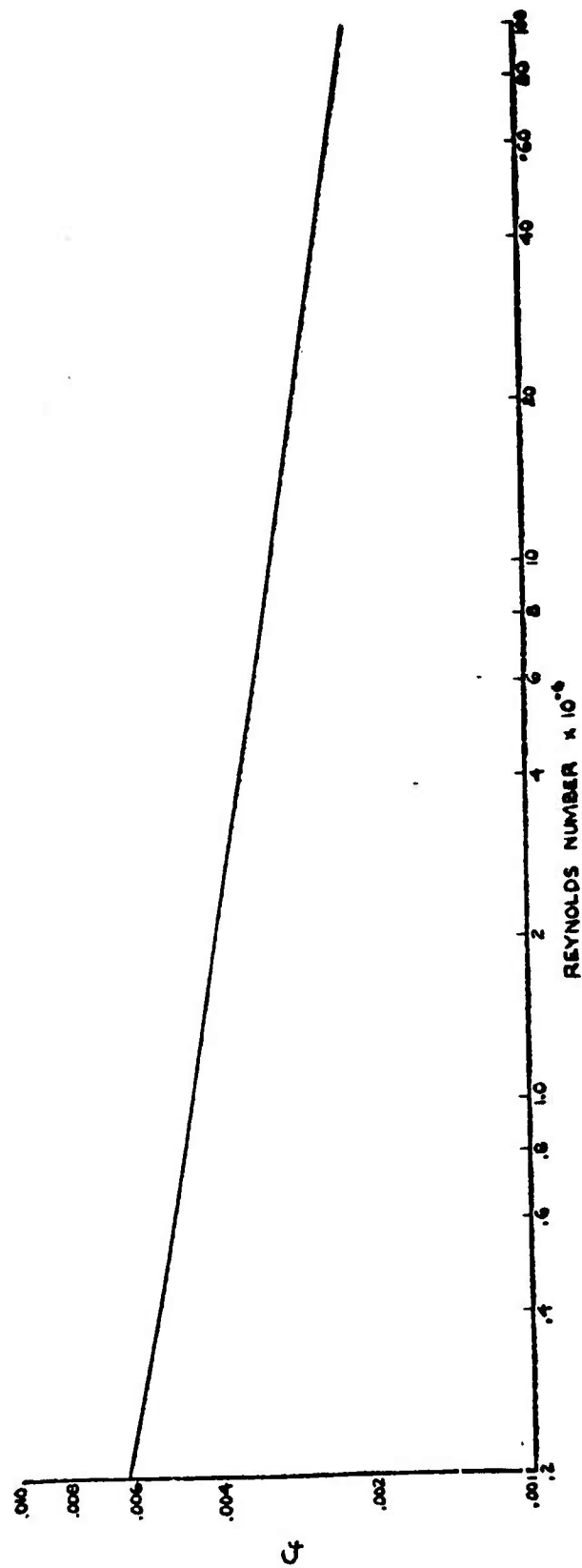


FIGURE 7.1-2 GRAPHICAL SOLUTION OF COMPRESSIBLE BERNOULLI EQUATION



7.1-12

FIGURE 7.1-3 PRANDTL - SCHLICHTING INCOMPRESSIBLE FLAT PLATE TURBULENT SKIN FRICTION COEFFICIENT

7.2 EJECTIJET CONCEPT

The basic principle of the concept is explained in detail in Section 6.0. The analysis of the recirculating ejector will be considered in three distinct parts; ejector, diffuser plus turn, and external flow.

7.2.1 Ejector

The recirculating ejector is treated as a straightforward extension of the conventional straight ejector in terms of efficiency of recirculation. This efficiency can be defined as the fraction of the tertiary total pressure recovered at the secondary inlet. To determine the effect of pressure recovery, various values, ranging from atmospheric pressure (conventional straight ejector) to the total pressure of the tertiary flow (full recovery), are assigned to the total pressure of the secondary flow. Figures 7.2-1 and 7.2-2 present the mass augmentation and power ratio for a series of hypothetical ejector configurations operating at several values of secondary pressure recovery.

A theoretical solution has been obtained for the straight and recirculating ejector problem, however, certain aspects of the solution somewhat limit its usefulness. For example, the problem of determining the flow conditions for a given primary mass flow and ejector geometry cannot be solved directly. A number of flow conditions must be evaluated until one is found that matches the given primary mass flow and ejector geometry. A digital computer has been employed to facilitate this iterative solution technique.

For the case of the recirculating ejector, the flow conditions between the tertiary exit and secondary inlet are expressed only in terms of secondary pressure recovery. Specifying the pressure recovery during the design of a GEM recirculating ejector provides no information concerning the inlet and exit angles, height above the ground, or distance

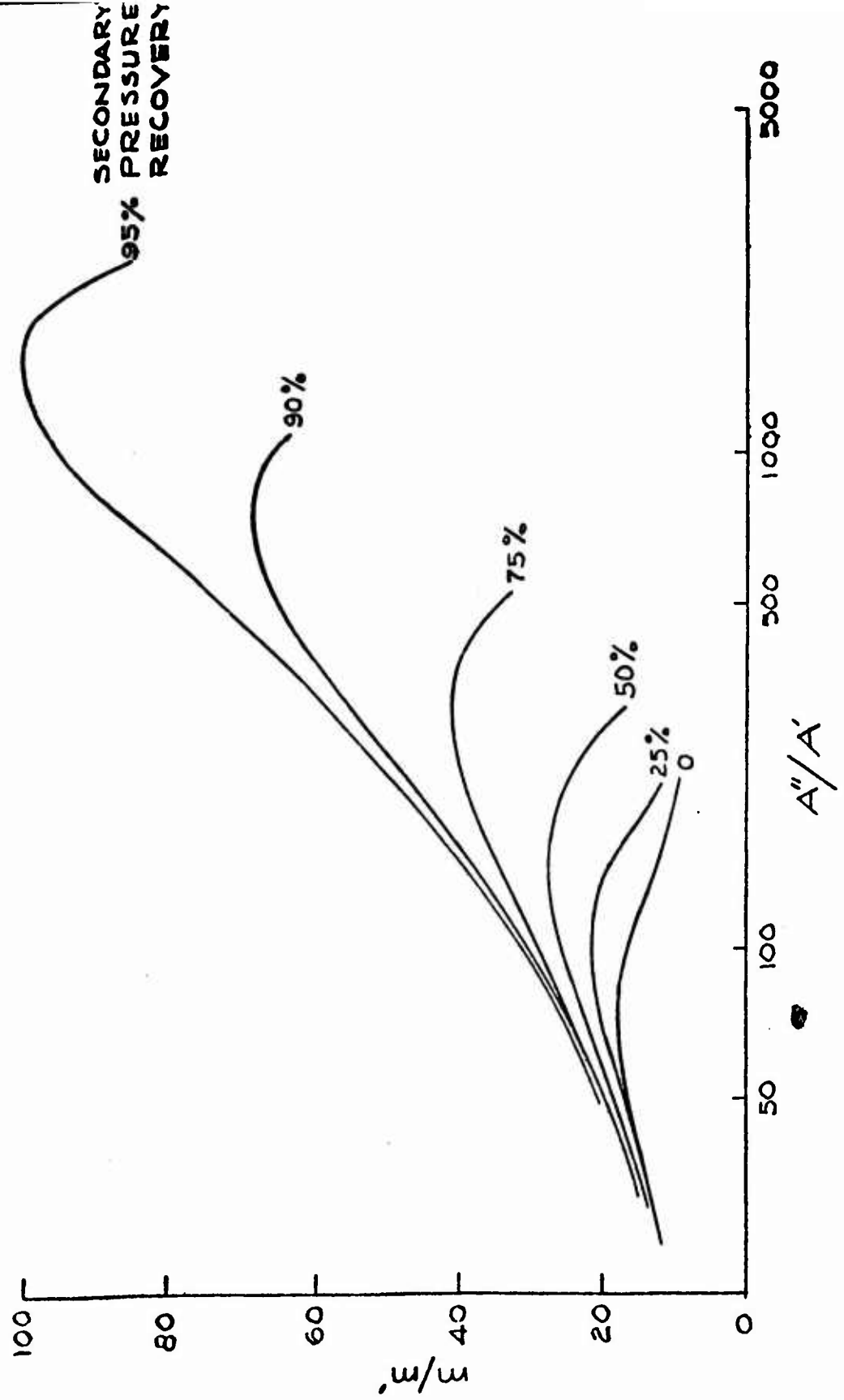


FIGURE 7.2-1 MASS AUGMENTATION OF A RECIRCULATING EJECTOR

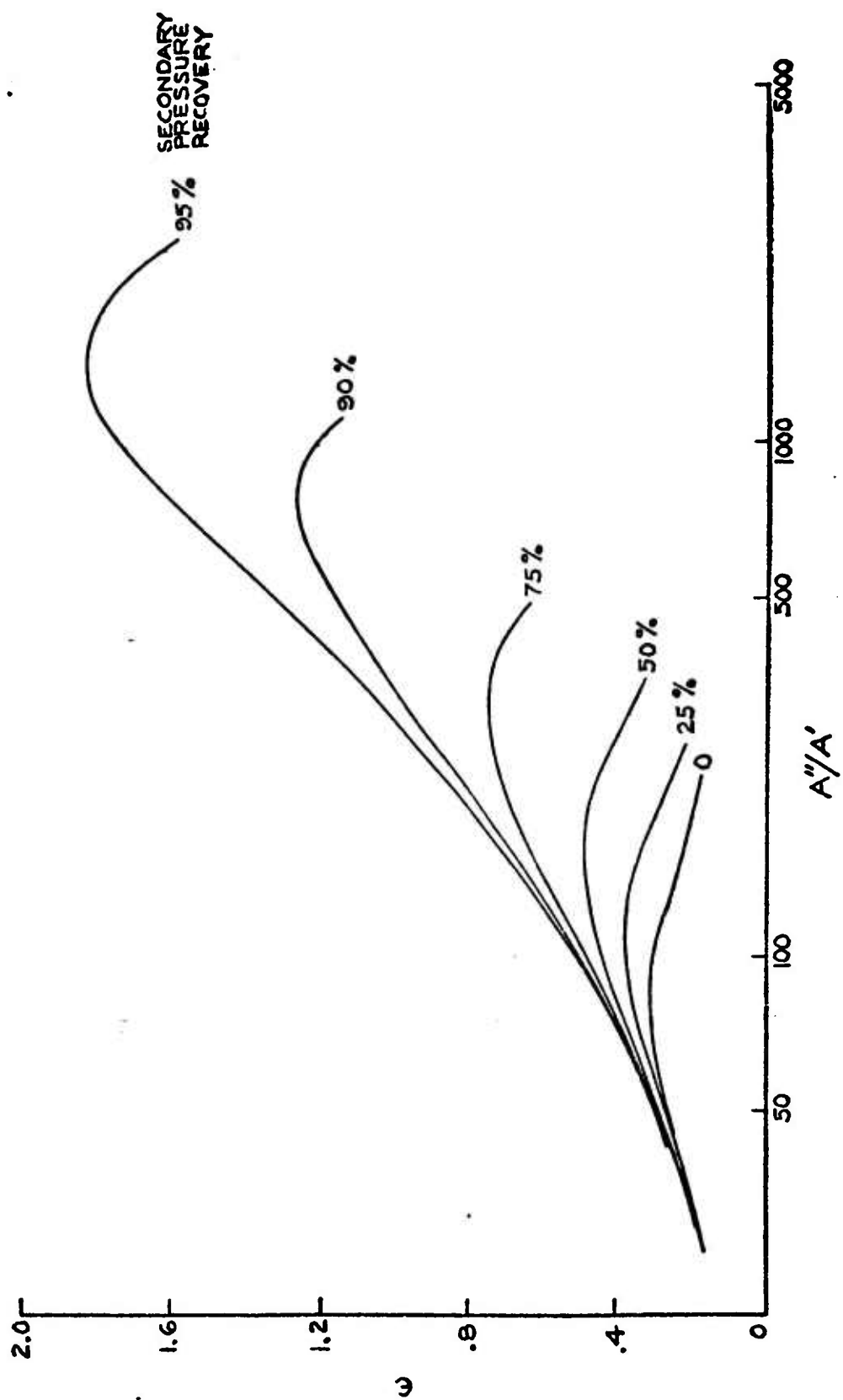


FIGURE 7.2-2 EFFICIENCY OF A RECIRCULATING EJECTOR

between inlet and exit required to obtain this desired recovery. Although the theory "closes the loop", so to speak, for the recirculating ejector, it is still primarily an ejector theory and an additional analysis is required to describe the flow conditions under the vehicle.

7.2.2 Diffuser and Turn

Thus far in the ejector analysis, only frictional losses in the mixing section have been considered. Equation (7.1-35) is therefore valid for determining primary mass flow for the constant pressure mixing process. However, when diffuser and turn losses are significant, or the static pressure along the mixing section is not constant, Equation (7.1-35) must be written in the form

$$\dot{m}' = \frac{\dot{m}(V_2^* - V_1') + F + \iint_A (\vec{p}\vec{n}) \cdot \vec{i} dA}{V_1' - V_1''} \quad (7.1-39)$$

where

$$V_2^{*2} - \left\{ \left(\frac{2\gamma}{\gamma-1} \right) \left(\frac{p_0'}{\rho_0'} - \frac{p_0''}{\rho_0''} \right) \frac{\left[1 - \left(\frac{p_2}{p_0^*} \right)^{\frac{\gamma-1}{\gamma}} \right]}{V_1' - V_1''} \right\} V_2^* -$$

$$\left\{ \left(\frac{2\gamma}{\gamma-1} \right) \left[\left(V_1' - \frac{F}{\dot{m}} \right) \frac{p_0''}{\rho_0''} - \left(V_1'' - \frac{F}{\dot{m}} \right) \frac{p_0'}{\rho_0'} \right] \frac{\left[1 - \left(\frac{p_2}{p_0^*} \right)^{\frac{\gamma-1}{\gamma}} \right]}{V_1' - V_1''} \right\} = 0$$

and

$$p_{02}^* = p_{04} + \Delta p_{\text{TURN LOSS}} + \Delta p_{\text{DIFFUSER LOSS}}$$

The latter equation states that the total pressure of the flow at the end of the mixing section must be greater than the total pressure at the exit by an amount equal to the total pressure drop in the diffuser and turn.

The diffuser and turn losses can be estimated from the empirical data such as contained in Reference 9. This reference contains sufficient data to design optimum diffusers and turns for specific conditions.

7.2.3 External Flow

The flow in the recirculating ejector has previously been described in terms of conditions at the ejector exit (Station 4) and the pressure recovery at the secondary inlet (Station 1). The flow under the recirculating ejector remains to be analyzed.

Since exit total pressure and secondary pressure recovery are interrelated with the base pressure, p_b , the formulation of a method which will satisfactorily predict the base pressure is obviously a worthwhile endeavor.

Two methods for predicting the base pressure are presented below. These methods are based on simple momentum theory (thin-jet) and on the thick-jet theory developed by Stanton-Jones. A third method utilizing conformal mapping techniques is contemplated and discussed.

7.2.3.1 Thin-Jet Theory

Figure 6-1 schematically shows that a ground effect vehicle utilizing the recirculating ejector concept is subjected to base pressure p_b and cavity pressure p_c . Analysis of the flow pattern of Figure 6-1 is simplified by separating the flow region into two regions as shown in Figure 7.2-3.

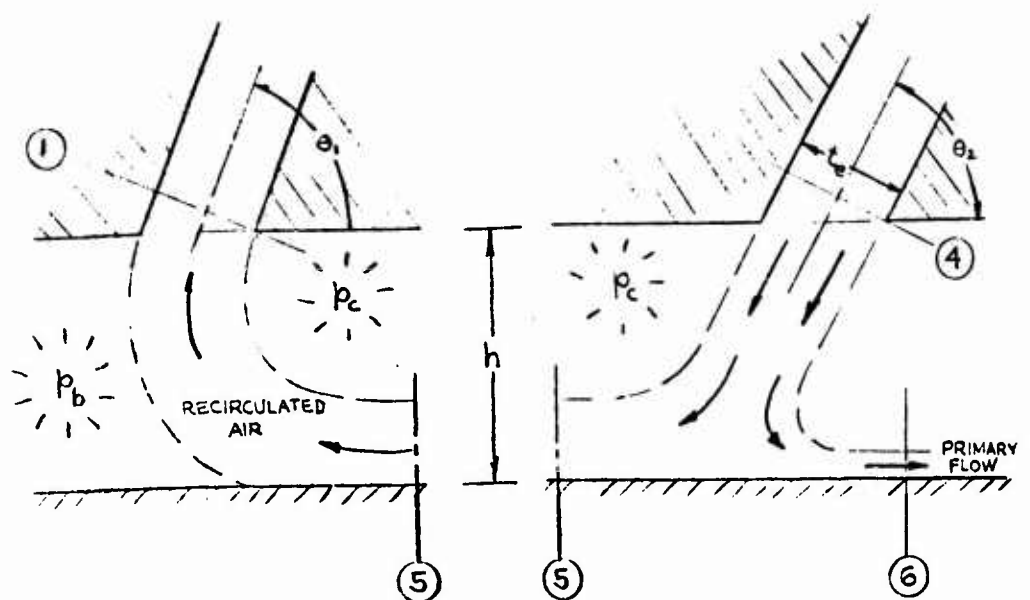


Figure 7.2-3 Two Flow Regions in Recirculation

Diagram illustrating the flow field and momentum distribution around a curved surface, showing the interaction between recirculated air and expelled primary air.

Key components and labels:

- Free Surface:** Indicated by a horizontal line at the top, with a height h marked on the left.
- Flow Direction:** Indicated by a horizontal arrow labeled tF .
- Curved Boundary:** A dashed line representing the boundary of the flow field.
- Pressure Region:** A circular region labeled p_c is shown within the flow.
- Vertical Arrow:** A vertical arrow labeled j points downwards.
- Angle:** A curved arrow labeled θ_2 indicates the angle of the flow.
- Regions:** Circular regions labeled 4, 5, and 6 are shown.
- Momentum Labels:**
 - MOMENTUM OF RECIRCULATED AIR:** Associated with region 5, labeled $(1 - \frac{1}{m/m'})j$.
 - MOMENTUM OF EXPELLED PRIMARY AIR:** Associated with region 6, labeled $(\frac{1}{m/m'})j$.

With the aid of Figure 7.2-4 the horizontal components of momenta and forces can now be equated.

$$p_c = -\frac{j}{h} \left[\left(1 - \frac{2}{m/m'} \right) - \cos \theta_2 \right] \quad (7.2-1)$$

It is noted in Equation (7.2-1) that when the term, $(1 - \frac{2}{m/m'})$, is equal to $\cos \theta_2$ the cavity pressure is zero. This means the angle of the jet at the exit (Station 4) is equal to the impingement angle, and the flow corresponds to a straight jet (no transverse pressure gradient) impinging on a flat plate. As long as the exit angle is greater than the impingement angle required by the existing mass augmentation, the cavity pressure is less than ambient. The possibility of a positive pressure occurring under the ejector is also demonstrated by Equation (7.2-1). It is interesting to observe that the cavity pressure is independent of the secondary inlet angle, θ_1 and the distance between the secondary inlet and tertiary exit. Experimental results presented later tend to confirm this theoretical conclusion.

When thin-jet theory is used to determine the pressure rise across the recirculated secondary flow depicted in the left hand sketch of Figure 7.2-4, the following equation results

$$\Delta p = \frac{(1 - \frac{1}{m/m'})j(1 + \cos \theta_2)}{h} \quad (7.2-2)$$

Since this pressure rise is referenced to the cavity pressure rise the equation for base pressure is

$$p_b = \Delta p + p_c \quad (7.2-3)$$

or

$$p_b = \frac{(1 - \frac{1}{m/m'})j(1 + \cos \theta_1)}{h} - \frac{j}{h} \left[\left(1 - \frac{2}{m/m'}\right) - \cos \theta_2 \right] \quad (7.2-4)$$

It is subsequently demonstrated in Section 10.2 that thin-jet theory adequately predicts cavity pressure. However, only fair correlation with experimental base pressures can be expected from this theoretical treatment.

This is due to the fact that thin-jet theory predicts infinite base pressure at zero height when in reality base pressure asymptotically approaches the jet total pressure as height approaches zero. Note that Equation (7.2-4) reduces to the thin-jet base pressure equation for a conventional annular jet whenever mass augmentation decreases to 1.

7.2.3.2 Thick Jet Theory

The limitations of thin-jet theory in predicting the base pressure generated by a recirculation system can be avoided by using the thick-jet or exponential theory of Reference 11 to calculate the pressure rise across the secondary jet, thus

$$\Delta p = \Delta p_{o_4} \left[1 - e^{-2 \left(\frac{t_e}{h} \right) (1 + \cos \theta_1)} \right] \quad (7.2-5)$$

where

Δp_{o_4} = gauge total pressure at station 4

t_e = jet thickness

h = height from ground to vehicle base

Since this pressure rise is referenced to p_c , the base pressure, p_b , is

$$p_b = \Delta p + p_c$$

$$p_b = \Delta p_{o_4} \left[1 - e^{-2 \left(\frac{t_e}{h} \right) (1 + \cos \theta_1)} \right] + p_c \quad (7.2-6)$$

The gage total pressure of Equation (7.2-6) can be expressed in terms of the jet momentum through the following algebraic manipulations.

$$\Delta p_q = q_{a.} = \frac{\rho V_4^2}{2} = \frac{\rho V_4^2 t_e}{2 t_e} = \frac{j}{2 t_e}$$

Substitution of the latter expression for exit total pressure, along with Equation (7.2-1) for p_c , into Equation (7.2-6) yields the following equation for base pressure

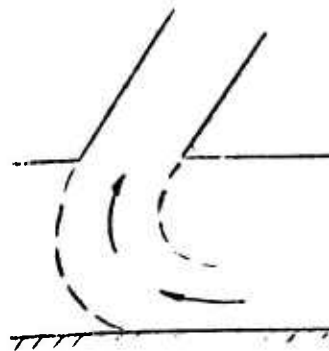
$$p_b = \frac{j}{2 t_e} \left[1 - e^{-2 \frac{t_e}{h} (1 + \cos \theta_2)} \right] - \frac{j}{h} \left[\left(1 - \frac{2}{m/m'} \right) - \cos \theta_2 \right] \quad (7.2-7)$$

A comparison of base pressures calculated from Equation (7.2-7) with experimental results is presented in Section 10.2.

7.2.3.3 Conformal Mapping Solution

Recently Ehrich, in Reference 12 extended the conformal mapping techniques pioneered by Strand and Chaplin of References 13 and 14 to the case of the bifurcated jet. This bifurcated jet solution deals with the flow properties generated by a jet splitting into two separate streams.

The flow pattern external to the recirculating ejector can be divided into a bifurcated jet and a deflected jet, as shown in the previous sections. As a result, this conformal mapping procedure potentially has a direct application to the present recirculation studies.



Deflected jet case



Bifurcated jet case

The digital computer programs for both cases have been loaned to the Martin Company by Dr. Ehrich and have been recoded on the Orlando Aerospace Division IBM 7090. Initial problems have been run to compare with coding check-out problems, and the checkout procedure is complete.

Although the present methods for predicting base and cavity pressures are considered good, it is expected that, as in the conventional annular jet, the conformal mapping predictions will give improved correlation with experiment. Also since the conformal mapping describes the nature of the whole flow field underneath the ejector, a more detailed study of the region can be made with particular application to the design of the ejector inlet.

No problems other than checkout problems have been run as yet, but it is anticipated that a full study will be made on the applicability of this conformal mapping program in the near future.

Although relatively simple methods for predicting base pressure as a function of height have been devised, which essentially close the recirculating flow loop, certain limitations of both the ejector analysis and the base pressure analysis should be pointed out. Since inviscid flow is assumed, no means are provided for predicting the pressure recovery at the secondary inlet. Also, the base pressure analysis assumes that the total pressure of the tertiary exit flow is known, when in reality this total pressure varies with vehicle height and secondary pressure recovery. This means that any attempts at optimization will naturally be performed at values of secondary pressure recovery that are consistent with experimental results.

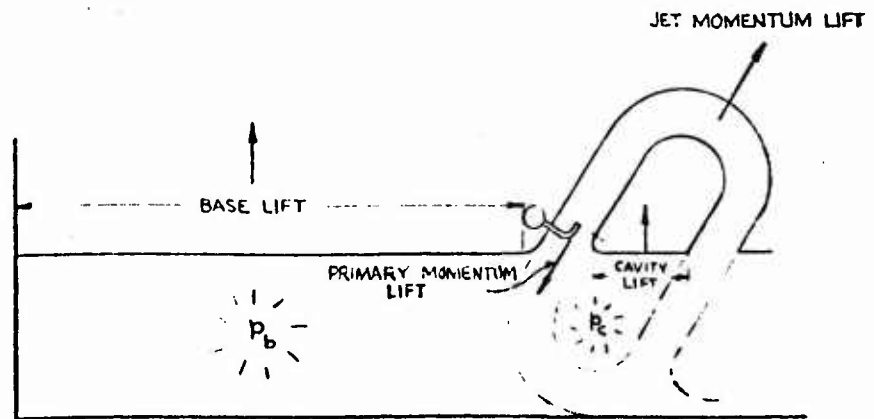
7.3 HOVERING

7.3.1 Lift

In the initial thin-jet analysis of the recirculation system, an IBM optimization program was devised to determine the inlet and exhaust angles, θ_1 , and θ_2 , that would maximize the total lift. The planform was assumed to be rectangular and the total lift was considered to be composed of the following four parts:

1. Base lift
2. Cavity lift
3. Primary momentum lift
4. Jet momentum lift

The geometry of the recirculating stream and the different lift regions is shown below.



The parameters used in the optimization equation are

1. l - length of machine - ft
2. w - width of machine - ft
3. m/m' - mass augmentation
4. K_1 - empirical correction constant for the base lift equation to make theory agree with experiment

5. K_2 - empirical correction constant for the cavity lift equation
6. K_3 - empirical correction constant for the primary momentum lift equation
7. K_4 - empirical correction constant for the jet momentum lift equation
8. j' - primary momentum per foot - lb/ft
9. j - tertiary jet momentum per foot - lb/ft

$$\text{Lift}_{\text{total}} = p_b S_b + p_c S_c + \text{PRIMARY MOMENTUM LIFT} \\ + \text{JET MOMENTUM LIFT}$$

$$= K_1 \left[-\frac{j}{h} \left\{ \left(1 - \frac{2}{m/m'} \right) - \cos \theta_2 \right\} + \frac{j}{h} \left\{ 1 - \frac{1}{m/m'} \right\} (1 + \cos \theta_1) \right] \cdot \\ \left[S_{\text{ref}} - 2h \left\{ \frac{\sin \theta_2 - \sin \theta_3}{\cos \theta_3 - \cos \theta_2} + \frac{\sin \theta_1}{1 + \cos \theta_1} \right\} \left\{ \ell + w - 2h \left(\frac{\sin \theta_2 - \sin \theta_3}{\cos \theta_3 - \cos \theta_2} + \frac{\sin \theta_1}{1 + \cos \theta_1} \right) \right\} \right] \\ - K_2 \left[\frac{j}{h} \left\{ \left(1 - \frac{2}{m/m'} \right) - \cos \theta_2 \right\} \right] \cdot \\ \left[2h \left\{ \frac{\sin \theta_2 - \sin \theta_3}{\cos \theta_3 - \cos \theta_2} + \frac{\sin \theta_1}{1 + \cos \theta_1} \right\} \left\{ \ell + w - 2h \left(\frac{\sin \theta_2 - \sin \theta_3}{\cos \theta_3 - \cos \theta_2} + \frac{\sin \theta_1}{1 + \cos \theta_1} \right) \right\} \right] \\ - K_3 \left[2j' \left\{ \ell + w - 4h \left(\frac{\sin \theta_2 - \sin \theta_3}{\cos \theta_3 - \cos \theta_2} + \frac{\sin \theta_1}{1 + \cos \theta_1} \right) \right\} \sin \theta_1 \right] \\ + K_4 \left[j \left\{ \sin \theta_1 + \sin \theta_2 \right\} \left\{ 2 \left(\ell + w - 2h \left[\frac{\sin \theta_2 - \sin \theta_3}{\cos \theta_3 - \cos \theta_2} + \frac{\sin \theta_1}{1 + \cos \theta_1} \right] \right) \right\} \right]$$

where

$$\theta_3 = \cos^{-1} \left(1 - \frac{2}{m/m'} \right) \quad (7.3-1)$$

To maximize the total lift of Equation 7.3-1 the aforementioned IBM program evaluates the function over a prescribed grid of θ_1 and θ_2 and selects the particular value of θ_1 and θ_2 that yields this maximum value. The lifts at all combinations of θ_1 and θ_2 are also printed out so that the penalty in lift, due to the use of other than the optimum θ 's, could be evaluated.

The initial recirculating ejectors, models 1 and 2, were designed from the output of this program in conjunction with control force considerations.

In using this approach it was not anticipated that the mass augmentation and resultant tertiary momentum would be such strong functions of exhaust and inlet angles. It was initially assumed that these parameters would be functions of the ejector design only. For this reason unrealistic results were obtained. It was found from subsequent experiments on model 3 that the best angles for maximum lift were relatively flat - i.e., $\theta_1 = \theta_2 = 30^\circ$.

Because the initial thin-jet theory did not compare well with experiment at the lower heights, the thin-jet theory for predicting the jump in pressure from the cavity region to the base region was replaced by Stanton-Jones equation. The final equation for predicting total lift is now

$$\begin{aligned} \text{LIFT}_{\text{TOT}} = & K_1 \left\{ \frac{j}{2t_e} \left[1 - e^{-2\frac{t_e}{h}(1+\cos\theta_1)} \right] - \frac{j}{h} \left[\left(1 - \frac{2}{m/m'} \right) - \cos\theta_2 \right] \right\} S_b \\ & + K_2 \left\{ -\frac{j}{h} \left[\left(1 - \frac{2}{m/m'} \right) - \cos\theta_2 \right] \right\} S_c \\ & - K_3 \left\{ j c_1 \sin\theta_1 \right\} + K_4 \left\{ j (\sin\theta_1 + \sin\theta_2) c_2 \right\} \end{aligned} \quad (7.3-2)$$

where

c_1 = perimeter over which the primary momentum acts ~ ft

c_2 = perimeter over which the jet momentum acts ~ ft

Comparisons are given in Figure 7.3-1 between experimentally measured total loads and the ones predicted by equation 7.3-2 using all the k's equal to 1.

7.3.2 Stability

An analysis of the hovering stability of the Ejectijet is presented in this section. This analysis is the first of its kind for the recirculation system of the Ejectijet and, as such, is preliminary in nature. However, since the lift in the Ejectijet is produced by an air curtain supporting a pressure under the vehicle, as in the annular jet, extensive use has been made of the existing theories on annular jets. The results of this analysis are substantiated in part by experimental data, for both the static and dynamic stability of the machine.

7.3.2.1 Static Stability

7.3.2.1.1 Pitch and Roll

The problems of static stability in pitch and roll for a rectangular planform GEM are the same except for the magnitude of the moments and forces which depend on the vehicle length in pitch, and on the vehicle width in roll. Therefore, the two dimensional analysis and results presented herein for the pitch case can also be used for the roll case. A limited amount of data has been obtained from the tests of a 3 ft x 5 ft three dimensional wind tunnel model tested at DTMB.

There are three factors that contribute to the pitch static stability.

1. Cross flow
2. Momentum thrust (jet reaction)
3. Cavity pressure

a. Pitching Moment due to Cross Flow

Figure 7.3-2 illustrates the mechanism of cross flow for two types of GEMs when pitched at angle α .

A thin-jet theory developed by Webster (Reference 15) for the annular jet in pitch will be used here to analyze the cross flow in the Ejectijet.

The assumptions made here are the same as in Reference 15. The jet curtain is thin and small changes in pressure under the machine produce no sensible change in the mass flow, m , or the jet velocity, V_a . This can be considered correct for small values of α . Viscous mixing of the jet with the surrounding air is neglected including the viscous dissipation of the cross flow under the machine.

Using momentum balance for the outer right hand jet (Figure 7.3-3a).

$$p_{cr} h_r = j \left(\cos \theta_r + \frac{2-\beta}{m/m'} - 1 \right) - \beta m' (V_{cr} - V_a) \quad (7.3-3)$$

where β is that portion of the primary flow that cross flows under the machine and p_{cr} is gage pressure.

Assuming that for small α the heights h_r of both jets on the right hand side is the same, the momentum balance for the inner right hand jet (Figure 7.3-3b) gives

$$h_r (p_{br} - p_r) = j \left(1 - \frac{m'}{m} \right) (1 + \cos \theta_r) - \beta m' (V_{br} - V_{cr}) \quad (7.3-4)$$

substituting (7.3-3) in (7.3-4)

$$p_{br} h_r = j \left[\cos \theta_r \left(2 - \frac{m'}{m} \right) + \frac{m'}{m} (1 - \beta) + m' (V_a - V_{br}) \right] \quad (7.3-5)$$

Similarly, the momentum balance on the left hand jet curtain (Figures 7.3-3c and d)

$$p_{cl} h_l = j \left(\cos \theta_l + \frac{m'}{m} \right) + \beta m' (V_a - V_{cl}) - j \left(1 - \frac{m'}{m} \right) \quad (7.3-6)$$

and

$$p_{bl} h_l = j \left[\left(2 - \frac{m'}{m} \right) \cos \theta_l + \frac{m'}{m} \right] + \beta m' (V_{al} - V_{bl}) \quad (7.3-7)$$

Making the following substitutions

$$h_L = h + l\alpha/2$$

$$h_r = h - l\alpha/2$$

$$\theta_r = \theta - \alpha$$

$$\theta_L = \theta + \alpha$$

$$j = mV_a$$

equations 7.3-5 and 7.3-7 can be written

$$p_{br} \left(h - \frac{l\alpha}{2} \right) = mV_a \left[\cos(\theta - \alpha) \left(2 - \frac{m'}{m} \right) + \frac{m'}{m} (1 + \beta) \right] + \beta m' (V_a - V_{br}) \quad (7.3-8)$$

$$p_{bL} \left(h + \frac{l\alpha}{2} \right) = mV_a \left[\cos(\theta + \alpha) \left(2 - \frac{m'}{m} \right) + \frac{m'}{m} \right] + \beta m' (V_{aL} - V_{bL}) \quad (7.3-9)$$

V_{aL} in general will not be equal to V_a due to viscous losses.

Defining $\phi = \frac{V_{bL}}{V_a}$ the horizontal momentum balance across the entire

machine gives

$$\left[2mV_a \sin \theta_L + \eta_a (p_{br} + p_{bL}) l \right] \alpha = m' V_a (1 + \phi) \beta \quad (7.3-10)$$

Now, assuming that the energy equation for the cross flow air under the left hand jet is approximately valid in the immediate vicinity of the jet

$$(V_{aL} - V_{bL}) = \frac{2 p_{bL}}{\rho (V_{aL} + V_{bL})} \quad (7.3-11)$$

Substituting equation 7.3-11 with 7.3-9, non-dimensionalizing by dividing by $\rho V_a^2 h$ and substituting

$$\sin \alpha = \alpha$$

$$\cos \alpha = 1 - \frac{\alpha^2}{2}$$

a set of linear equations is obtained. An asterisk is used to signify quantities non-dimensionalized by $\rho V_a^2 h$.

$$p_{br}^* \left(1 - \alpha \frac{l^*}{2} \right) = m^* \left\{ \left(2 - \frac{m'}{m} \right) \left(1 - \frac{\alpha^2}{2} \right) \cos \theta - \alpha \left(2 - \frac{m'}{m} \right) \sin \theta + \frac{m'}{m} (1 + \beta) \right\} + \beta m' \phi \quad (7.3-12)$$

$$p_{bL}^* \left[1 + \alpha \frac{l^*}{2} - \frac{2 \beta m'^*}{\phi (1 + V_{bL}/V_{aL})} \right] = m^* \left[\left(2 - \frac{m'}{m} \right) \left(1 - \frac{\alpha^2}{2} \right) \cos \theta - \left(2 - \frac{m'}{m} \right) \alpha \sin \theta + \frac{m'}{m} \right] \quad (7.3-13)$$

$$\left[2 m^* \sin \theta + l^* \eta_a (p_{br}^* + p_{bL}^*) \right] \alpha = m'^* \beta (1 + \phi) \quad (7.3-14)$$

In order to obtain a solution to the above equations, which have been linearized by assuming small values of $\alpha = \sin \alpha$, p_{b_1} , p_{b_2} , θ are expanded in a perturbation series around $\alpha = 0$. This series is assumed to be convergent for small α .

$$\begin{aligned} p_{b_r}^* &= p_{b_{r_0}}^* + \alpha p_{b_{r_1}}^* + \alpha^2 p_{b_{r_2}}^* + \dots \\ p_{b_{\ell}}^* &= p_{b_{\ell_0}}^* + \alpha p_{b_{\ell_1}}^* + \alpha^2 p_{b_{\ell_2}}^* + \dots \\ \beta &= \beta_0 + \alpha \beta_1 + \alpha^2 \beta_2 + \dots \end{aligned} \quad (7.3-15)$$

Substituting equations 7.3-15 into 7.3-13 and 7.3-14

$$\begin{aligned} 0 &= \left[p_{b_{r_0}}^* - m^* \left(2 - \frac{m'}{m} \right) \cos \theta - m'^* \right] + \alpha \left[p_{b_{r_1}}^* - \frac{\ell^*}{2} p_{b_{\ell_0}}^* + m^* \left(2 - \frac{m'}{m} \right) \sin \theta \right. \\ &\quad \left. + m'^* (1 - \phi) \beta_1 \right] + \alpha^2 \left[p_{b_{r_2}}^* - \frac{\ell^*}{2} p_{b_{r_1}}^* + \frac{m^*}{2} \left(2 - \frac{m'}{m} \right) \cos \theta + m'^* (1 - \phi) \beta_2 \right] + \dots \\ 0 &= \left[p_{b_{\ell_0}}^* - m^* \left(2 - \frac{m'}{m} \right) \cos \theta + m'^* \right] + \alpha \left[p_{b_{\ell_1}}^* + \frac{\ell^*}{2} p_{b_{\ell_0}}^* - \frac{2m'^*}{\phi(1 + V_{b_2}/V_{a_2})} \beta_1 p_{b_{\ell_0}}^* \right. \\ &\quad \left. + m^* \left(2 - \frac{m'}{m} \right) \sin \theta \right] + \alpha^2 \left[p_{b_{\ell_2}}^* + \frac{\ell^*}{2} p_{b_{\ell_1}}^* - \frac{2m'^*}{\phi(1 + V_{b_2}/V_{a_2})} (\beta_2 p_{b_{\ell_0}}^* + \beta_1 p_{b_{\ell_1}}^*) \right. \\ &\quad \left. + \frac{m^*}{2} \left(2 - \frac{m'}{m} \right) \cos \theta \right] + \dots \\ 0 &= \left[2m^* \sin \theta + \ell^* \eta_A (p_{b_{\ell_0}}^* + p_{b_{r_0}}^*) - m'^* (1 + \phi) \beta_1 \right] \alpha \\ &\quad + \left[\ell^* \eta_A (p_{b_{\ell_1}}^* + p_{b_{r_1}}^*) - m'^* (1 + \phi) \beta_2 \right] \alpha^2 + \dots \end{aligned}$$

By equating each of the coefficients of the powers of α to zero, the solution to the previous set of simultaneous equations is found

$$\begin{aligned} p_{b_{r_0}}^*/m^* &= \left[\left(2 - \frac{m'}{m} \right) \cos \theta - \frac{m'}{m} \right] \\ p_{b_{r_1}}^*/m^* &= \frac{\ell^*}{2} (p_{b_{r_0}}^*/m^*) + \left(2 - \frac{m'}{m} \right) \sin \theta + m'^* (1 - \phi) \beta_1 \\ p_{b_{r_2}}^*/m^* &= \frac{\ell^*}{2} (p_{b_{r_1}}^*/m^*) + \left(2 - \frac{m'}{m} \right) \frac{\cos \theta}{2} + m'^* (1 - \phi) \beta_2 \\ p_{b_{\ell_0}}^*/m^* &= \left[\left(2 - \frac{m'}{m} \right) \cos \theta - \frac{m'}{m} \right] \end{aligned}$$

$$\begin{aligned}
p_{b_{x_1}}^*/m^* &= - \left[\frac{\ell^*}{2} \left(p_{b_{x_1}}^*/m^* \right) + \frac{2m'^*}{\phi(1+V_{b_L}/V_{a_L})} \theta_1 \frac{p_{b_{x_1}}^*}{m^*} + \left(2 - \frac{m'}{m} \right) \sin \theta \right] \\
p_{b_{x_2}}^*/m^* &= - \left[\frac{\ell^*}{2} \left(\frac{p_{b_{x_1}}^*}{m^*} \right) - \frac{2m'^*}{\phi(1+V_{b_L}/V_{a_L})} \left(\theta_2 \frac{p_{b_{x_1}}^*}{m^*} + \theta_1 \frac{p_{b_{x_2}}^*}{m^*} \right) + \left(2 - \frac{m'}{m} \right) \frac{\cos \theta}{2} \right] \\
\theta_1 &= \left[2 \sin \theta + \ell^* \eta_A (p_{b_{x_1}}^* + p_{b_{x_2}}^*)/m^* \right] \div m'(1+\phi) \\
\theta_2 &= \left[\ell^* \eta_A (p_{b_{x_1}}^* + p_{b_{x_2}}^*)/m^* \right] \div m'(1+\phi)
\end{aligned}$$

A solution is thus obtained for p_{b_v} and p_{b_L} in terms of m , m' , θ , w , η_A , ϕ , and V_{b_L}/V_{a_L} . All of these quantities are known with the exception of η_A , ϕ , and V_{b_L}/V_{a_L} . However, η_A is the ratio of the actual mean pressure to the theoretically predicted mean pressure under the vehicle and is very close to 1. The value of ϕ , as indicated in Reference 15, can be bounded by 1 as the upper limit when $V_{a_L} = V_a$, and by $\sqrt{2p_{b_L}/V_a^2 \rho}$ as the lower limit, when the cross flow is expanded from p_{b_L} to atmospheric pressure. The value of V_{b_L}/V_{a_L} can be bounded from continuity between 0 and $\theta_1 m'/\phi$. Finally the pitching moment due to cross flow per unit length can be written

$$M_{CF} = 2 \xi \ell^2 (p_{b_v} - p_{b_L})$$

where ξ is a function of the pressure distribution under the vehicle. A linear distribution of the pressure gives a value of $\xi = .167$ while for a sinusoidal distribution $\xi = .203$.

While numerical values of M_{CF} have not been calculated, the form of the solution is the same as that for an annular jet. This indicates that the cross flow moments will be destabilizing.

b. Pitching Moment Due to Jet Reaction

In the recirculating ejector internal loads are produced by the recirculating air inside this duct system. The resultant load is referred to as momentum thrust or jet reaction, which has

been discussed in Section 7.3.1. The magnitude of the reaction depends on the strength of the jet, j . Since this reaction is applied to the machine some distance from the center of gravity, each jet will produce a moment about the c.g. During the normal operation of the vehicle, in a horizontal position, the jet strength at both ends of the machine will be the same and the moments about the c.g. will cancel.

In the recirculation process, the strength of the jet is a function of height. Experimental results have shown that as the ejector moves closer to the ground j increases and conversely j decreases when the ejector moves away from the ground. For the Ejectijet in pitch or roll, this effect creates a stabilizing moment not present in the conventional annular jet. Since at present there is no theory to predict the magnitude of this moment, only experimental results can be used. Figure 7.3-4 shows the variation of j with height for the model 3 recirculating ejector.

c. Pitching Moment due to Cavity Pressure Changes

The contribution of cavity pressure (p_c) to pitching moment was found experimentally to be a function of design, height, and pitch angle. A theoretical expression for p_c obtained from momentum theory gives

$$p_c = \frac{j}{h \pm \lambda \alpha / 2} \left[1 - 2 \frac{m'}{w} - \cos(\theta_1 \pm \alpha) \right]$$

which correlates well with experiment. The variation of p_c with height and angle shown in Figure 7.3-5 was obtained from the above expression using experimental data from the wind tunnel model. These results indicate that the contribution of p_c to pitching moment is stabilizing, since $\partial p_c / \partial \alpha < 0$

Summarizing, the cavity pressure and jet thrust contribute positive pitch static stability while the cross flow is the destabilizing element. Preliminary results of the wind tunnel tests show that the Ejectijet is statically stable in pitch at height-to-width ratios considerably greater than those of the annular jet.

These results are of extreme importance since it is well known that all conventional annular jet GEMs are statically unstable in pitch, except perhaps at very low heights. To overcome this problem on conventional annular jet GEMs, a jet partitioning of the base for pitch stability is required resulting in penalties in installed horsepower, cost, and weight.

7.3.2.1.2 Yaw

In this mode of motion the Ejectijet, like other ground effect machines, has essentially neutral stability in hovering flight. Therefore, the machine will have to depend on controls for yaw stabilization in hover.

7.3.2.1.3 Heave

The static stability in heave is given by the slope of the lift versus height curve. The lift of the Ejectijet, as given by equation 7.3-2 in Section 7.3.1, is presented in Figure 7.3-1. It may be seen that, except at very low heights, the Ejectijet is stable in heave.

7.3.2.2 Dynamic Stability

7.3.2.2.1 Pitch and Roll

As in the case of static stability, the following study of pitch dynamic stability can be used for roll by properly substituting the width for the length of the machine.

Since all the factors affecting the pitch dynamic stability of the Ejectijet are not linear, a simulation of the vehicle motions is required and can be accomplished by means of an IBM or analog computer.

Therefore, in order to obtain a preliminary indication of the Ejectijet dynamic stability in pitch the motions of the 3-dimensional wind tunnel model were simulated on an analog computer. The model was used instead of a full scale machine so that experimental data obtained from tests of the model could be used directly. The vehicle characteristics used in this study are shown in Figures 7.3-5 through 7.3-9. The computer schematic is shown in Figure 7.3-10.

The pitch damping term used in this simulation is composed of two parts, a jet damping as defined by Chaplin, $m(\lambda/l)^2 \dot{\alpha}$, and an aerodynamic damping given by

$$\rho \frac{l^4 w}{64} \dot{\alpha} |\dot{\alpha}|$$

This is fairly crude and can be refined in the future by experimental correlation. The oscillations of a 3-dimensional model can be recorded and the damping coefficients computed from these data. The equation of motion in pitch is

$$I_{yy} \ddot{\alpha} = -m \left(\frac{l}{2} \right)^2 \ddot{\alpha} - \rho \frac{l^2 w}{64} \dot{\alpha} |\dot{\alpha}| + M_{\alpha}$$

where

$$M_{\alpha} = 2w\ell \sin \theta (j_1 - j_2) + S_c \bar{\ell} \frac{\partial \Delta p_c}{\partial \alpha} \alpha + M_{CF}$$

$\bar{\ell}$ = mean distance between fore and aft recirculating flow cavities

At the time this study was conducted, the analyses above, presented for the cross flow moment, was not completed, and a simplified expression for the mass flow moment was used. This expression was obtained assuming a complete diffusion of the cross flow under the vehicle as a function of pitch angle as follows

$$M_{CF} = \frac{w\ell^2}{12} (p_o - p_b) \alpha$$

where

$$p_o = j/2t_e$$

and w and ℓ are the width and length of the vehicle respectively while p_o is the tertiary jet total pressure. A linear distribution of the pressure under the vehicle was assumed ($\xi = .167$).

While the destabilizing cross flow term in this form is questionable, the analog simulation indicated that a cross flow 10 times that estimated would be required to make the model unstable. On the other hand, it is obvious from continuity that the cross flow in the Ejectijet is limited by mass augmentation. Therefore its magnitude is much smaller than in the annular jet. Also, in actual flight the model did not exhibit any tendency toward divergence. Hence, it can be concluded that the estimated cross flow is of the proper magnitude.

The estimated damping in pitch was evidently much too low since the model was very well damped in flight, and the simulation exhibited only negligible damping. An analog trace of the pitch motion is shown in Figure 7.3-11.

The effect of the non-linearity of the vehicle characteristics is clearly depicted. This indicates that care should be exercised when using analytical techniques requiring linearized data.

7.3.2.2.2 Heave

As the dynamic stability in pitch, the heave motions of the wind tunnel model were also simulated in the analog computer. The vehicle characteristics were obtained from experimental data also, and are presented in Figures 7.3-5 and 7.3-9.

The equation of motion in heave is

$$\frac{W}{g} \ddot{z} = F_z - W - \frac{\partial F_z}{\partial \dot{z}} \dot{z}$$

where

$$F_z = p_b S_b + 20 K_j j \sin \theta + 4 K_p S_c p_c$$

and

$$\frac{\partial F_z}{\partial \dot{z}} = \frac{S_b z}{t_e^2 + h^2} \sqrt{\frac{\rho W}{2\pi}}$$

is the damping in heave, from Reference 16. K_j and K_p are analog gain constants. A typical analog trace of the heave motion of the model is shown in Figure 7.3-12.

Figures 7.3-6 and 7.3-7 show that the slope of p_b versus Z and j versus Z are negative, indicating a stable motion. The slope of p_c versus Z is positive or unstable; however, it is of small magnitude compared to the

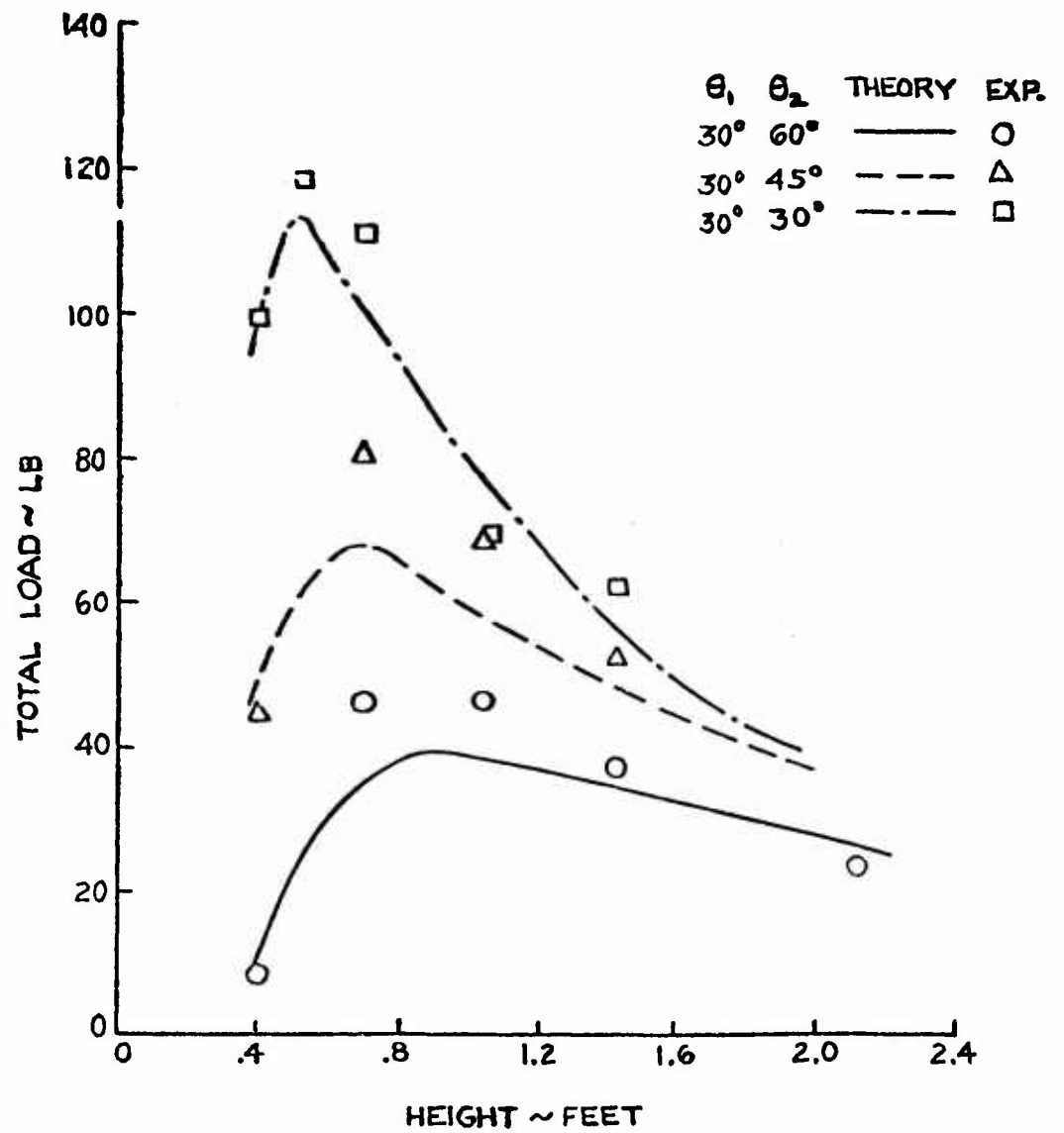


FIGURE 7.3-1 COMPARISON OF PREDICTED TOTAL LOAD WITH EXPERIMENT

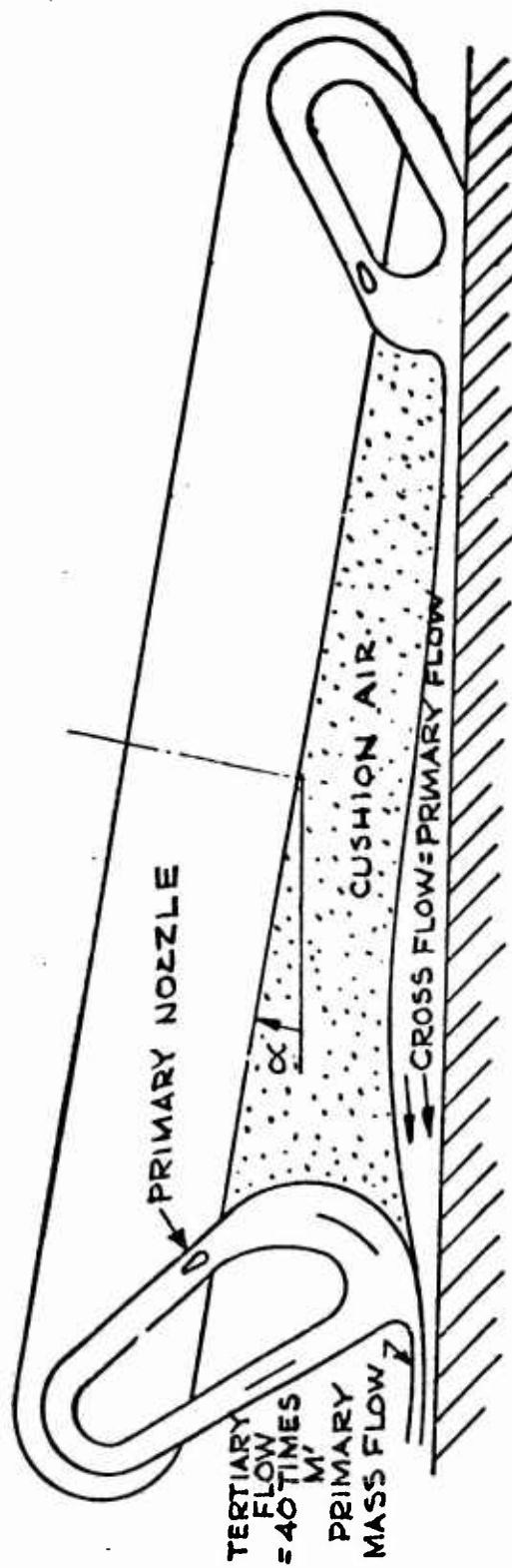


FIGURE 7.3-2 TWO-DIMENSIONAL EJECTORJET CROSSFLOW IN PITCH (ROLL)

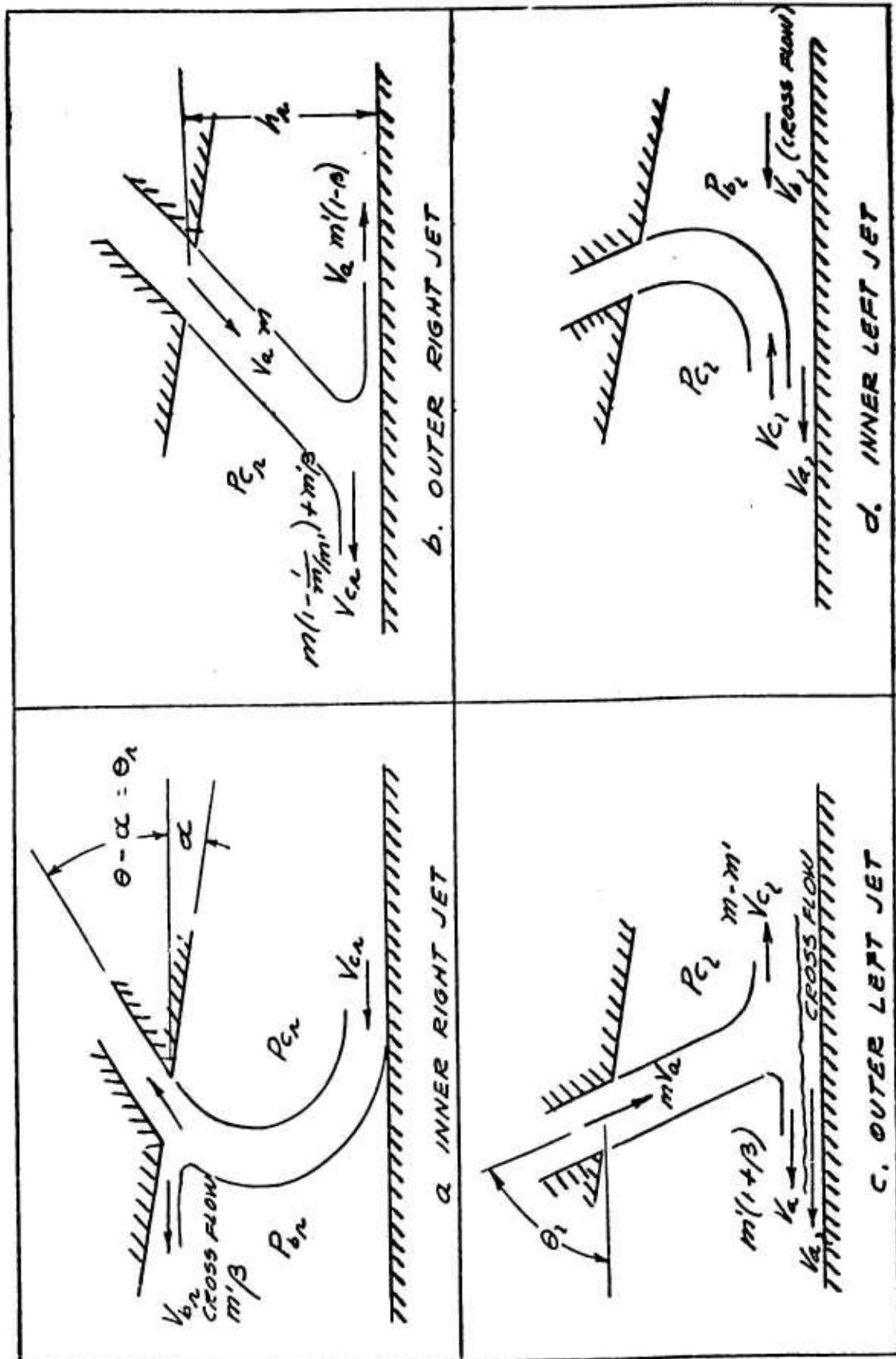


FIGURE 7.3-3 FLOW PATTERN UNDER PITCHED EJECTNET

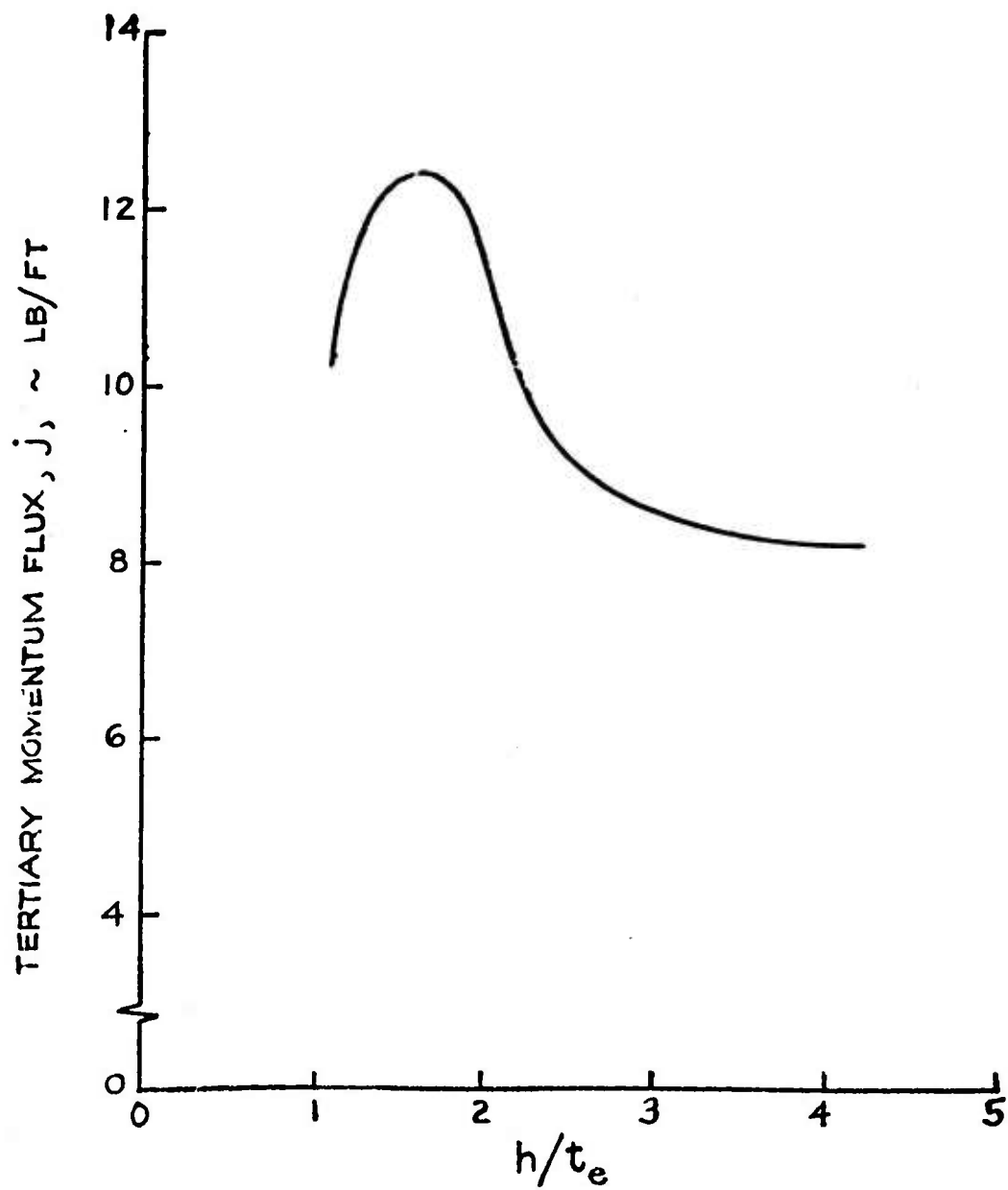


FIGURE 7.3-4 EFFECT OF HEIGHT ON MOMENTUM THRUST

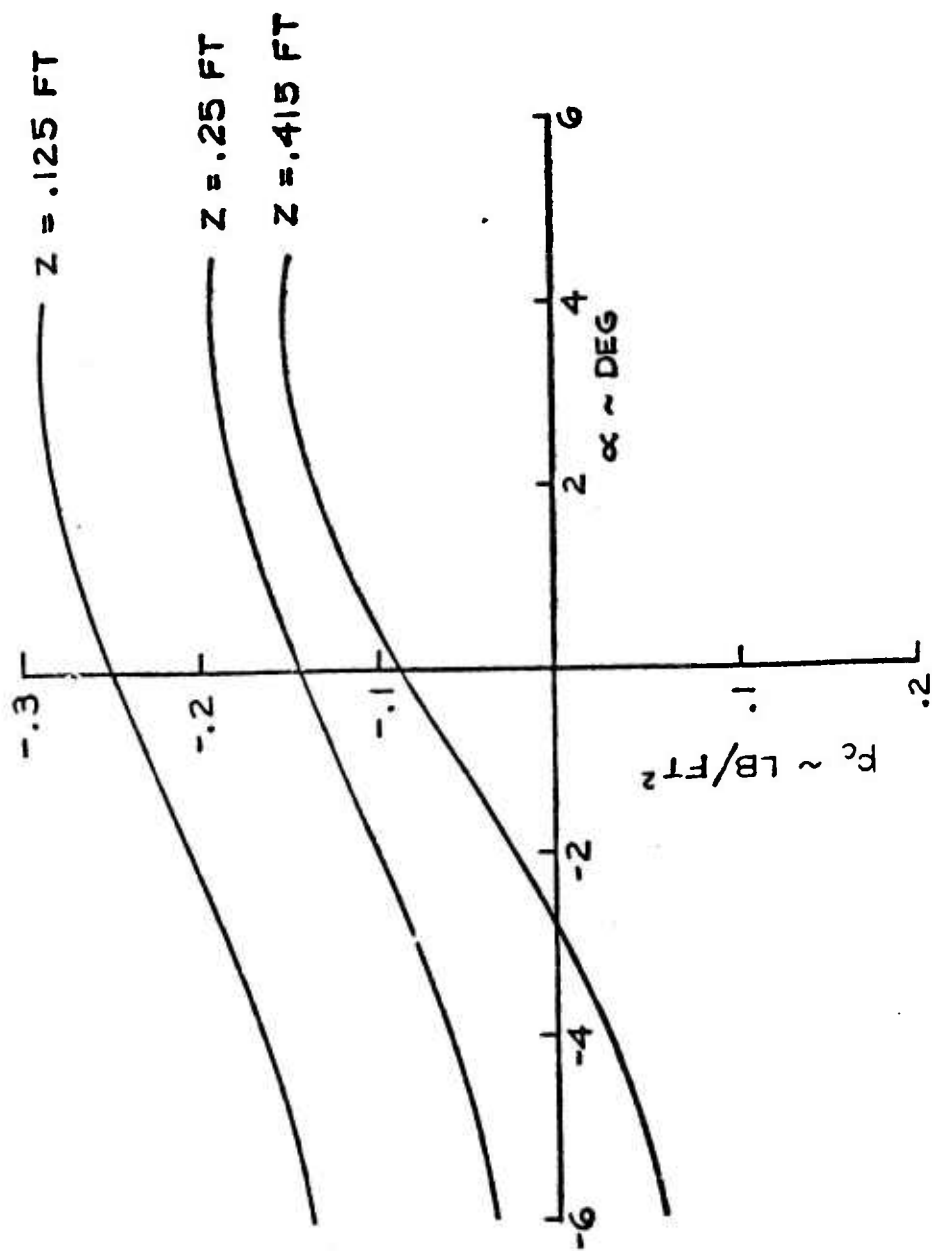


FIGURE 7.3-5 EFFECT OF PITCH ANGLE ON CAVITY PRESSURE (WIND TUNNEL MODEL)

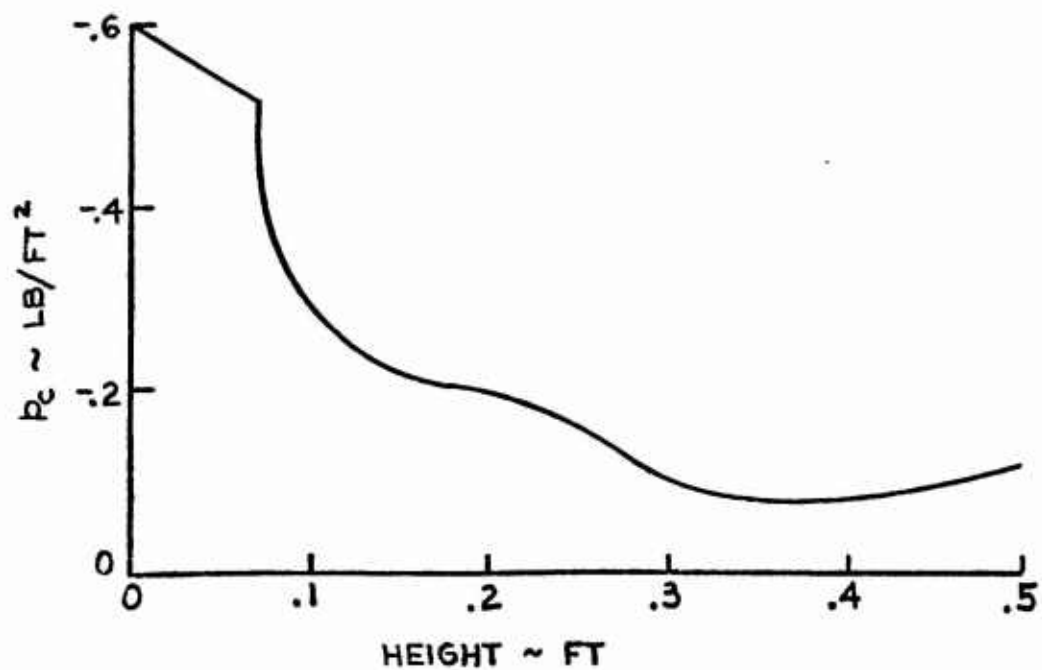
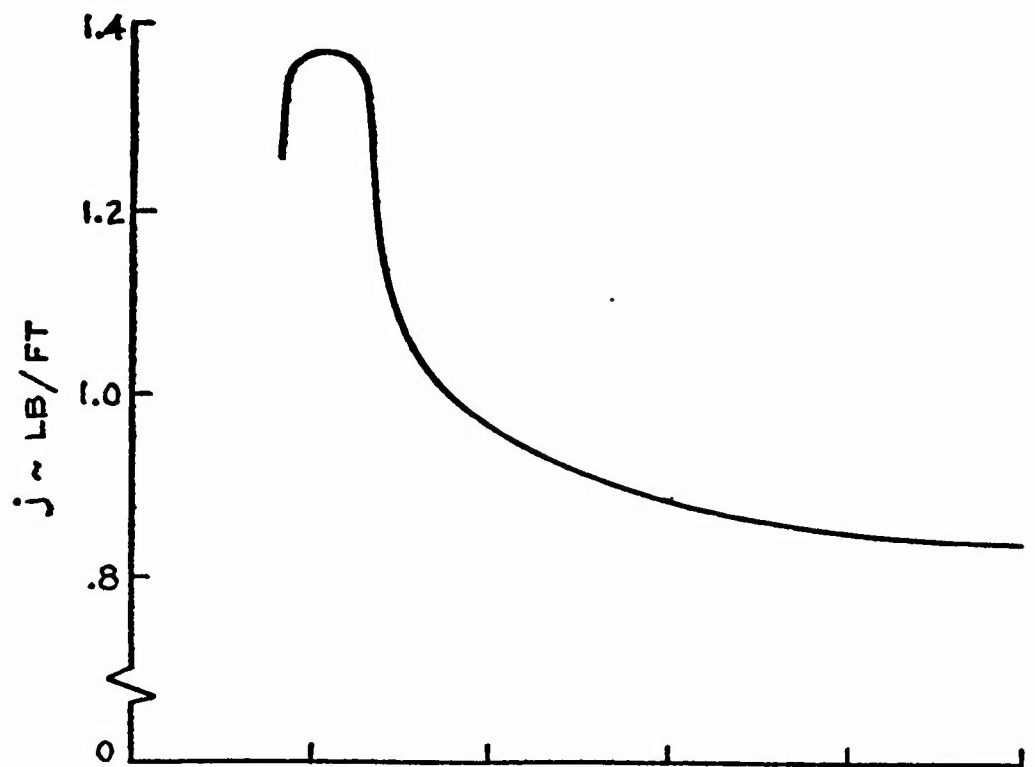


FIGURE 7.3-6 EFFECT OF HEIGHT ON CAVITY PRESSURE AND JET MOMENTUM (WIND TUNNEL MODEL)

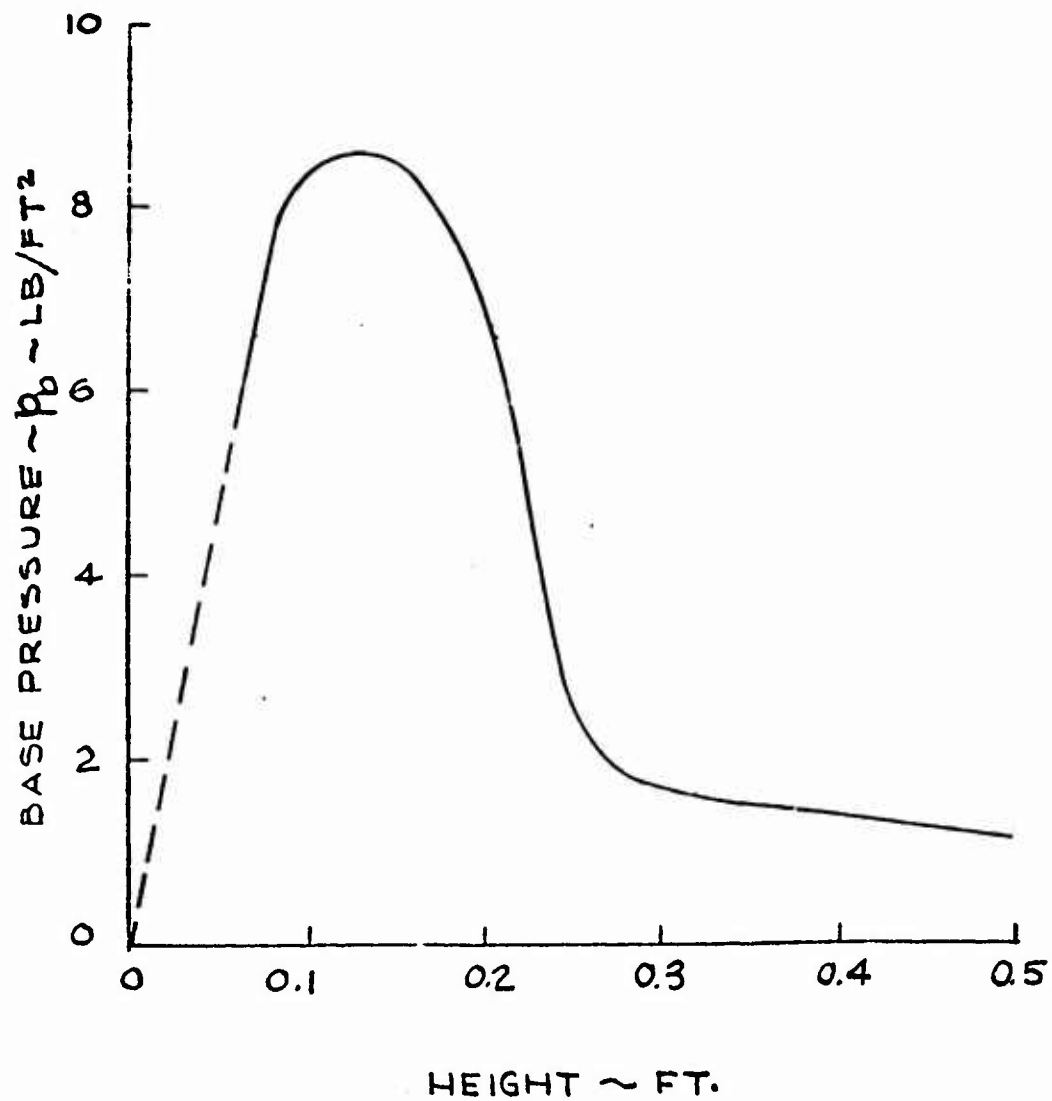


FIGURE 7.3-7 BASE PRESSURE VS HEIGHT
(WIND TUNNEL MODEL)

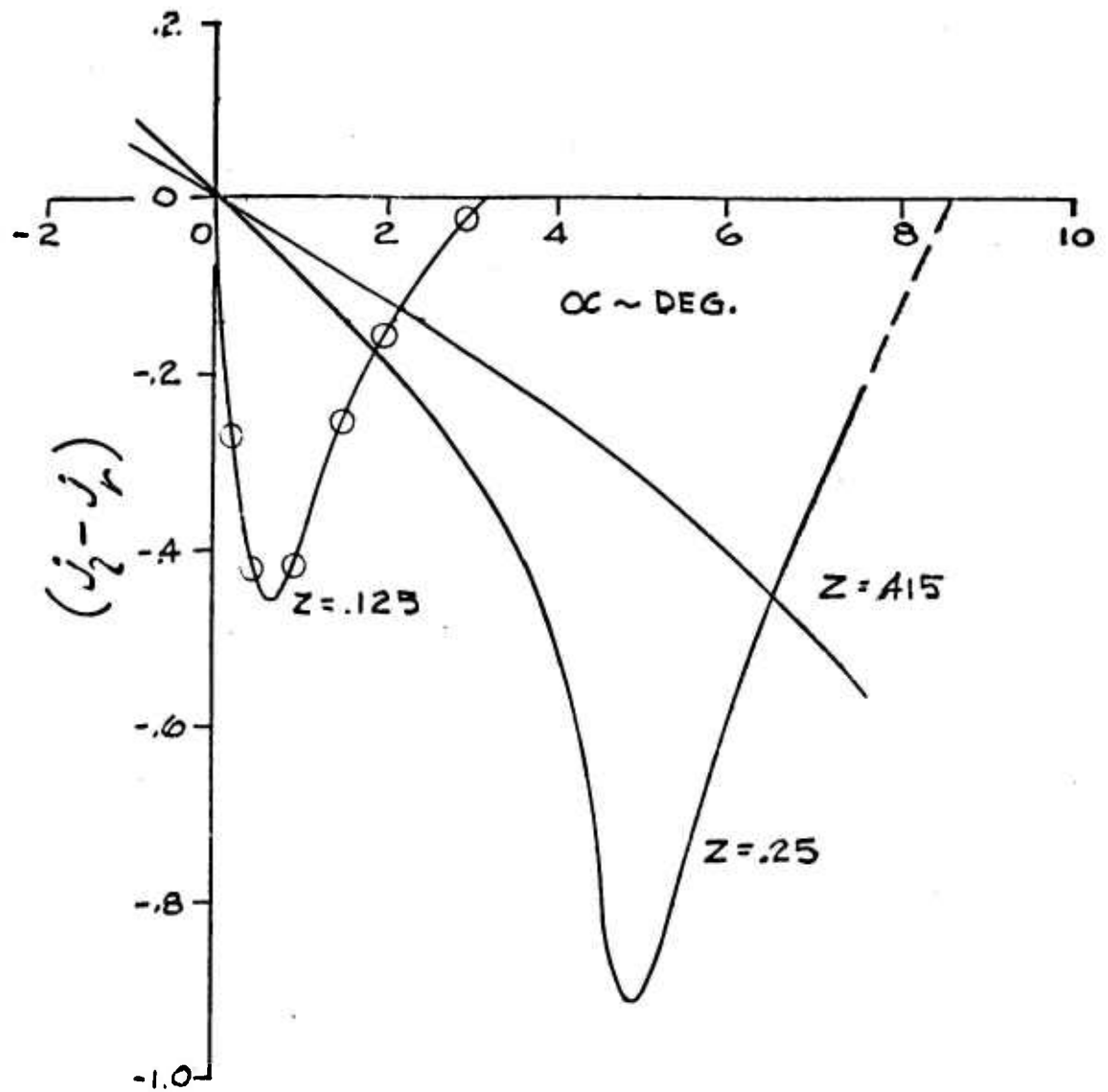


FIGURE 7.3-8 JET THRUST VS PITCH ANGLE
(WIND TUNNEL MODEL)

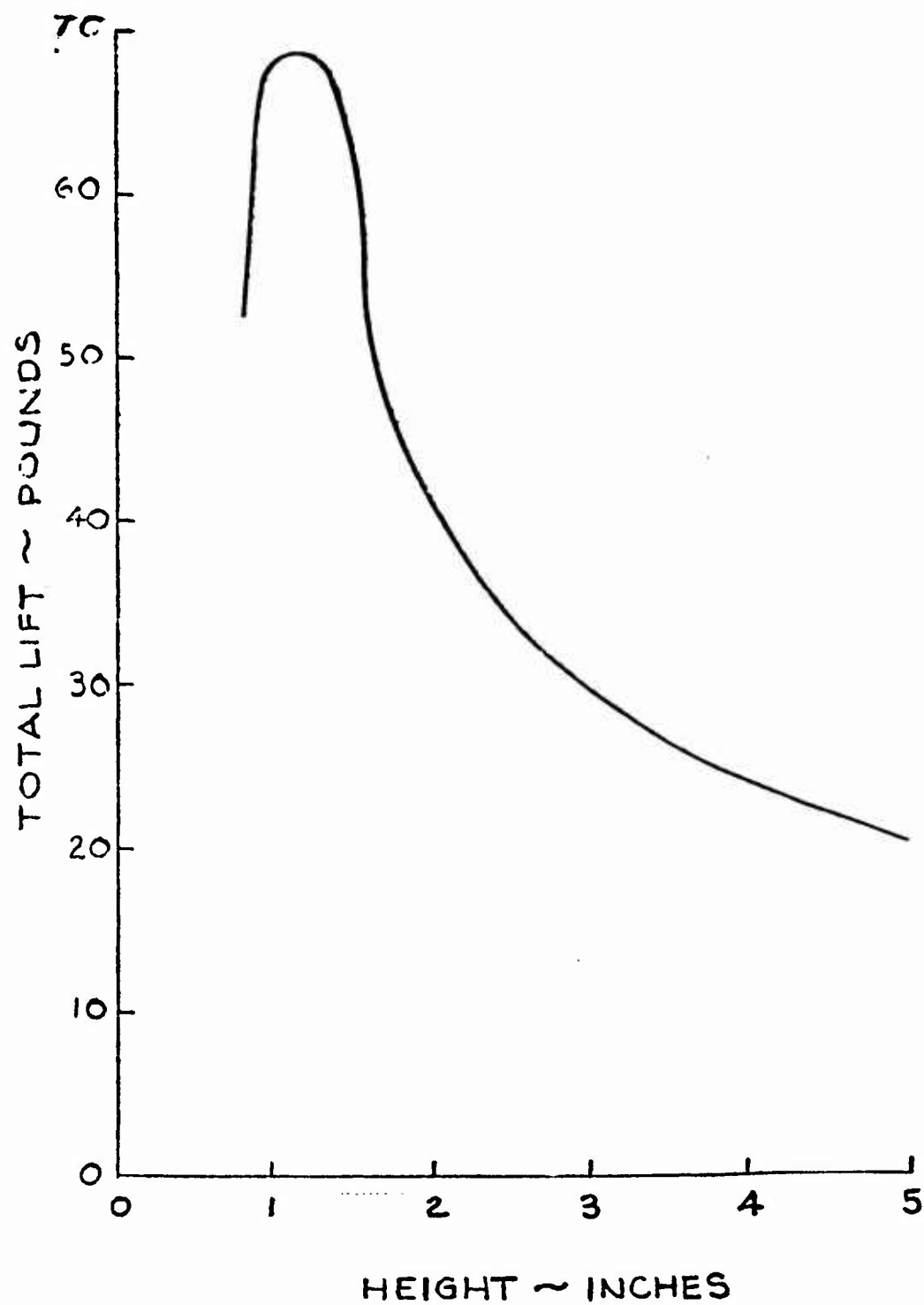


FIGURE 7.3-9 LIFT VS HEIGHT (WIND TUNNEL MODEL)

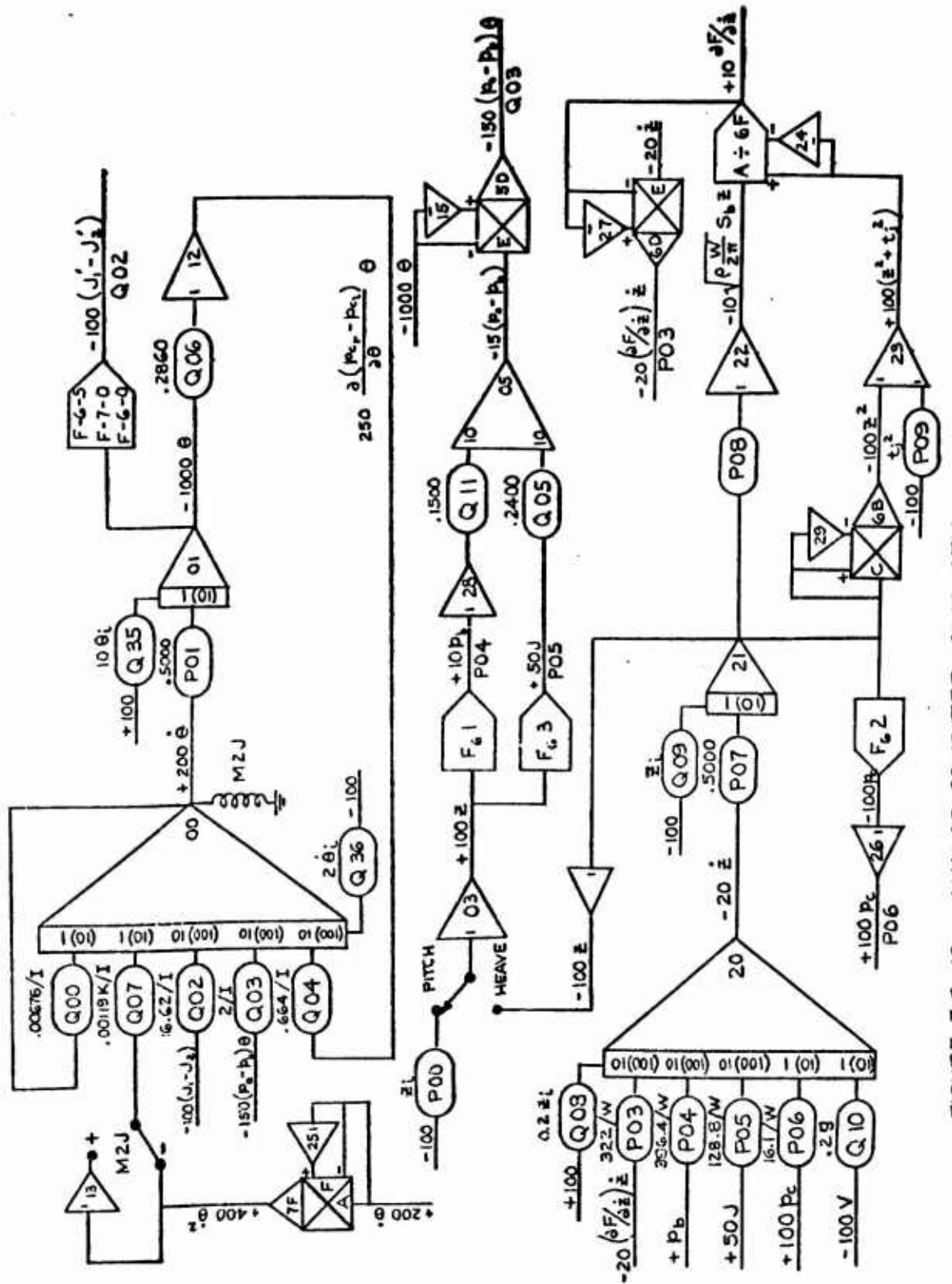


FIGURE 7.3-10 ANALOG COMPUTER SCHEMATIC

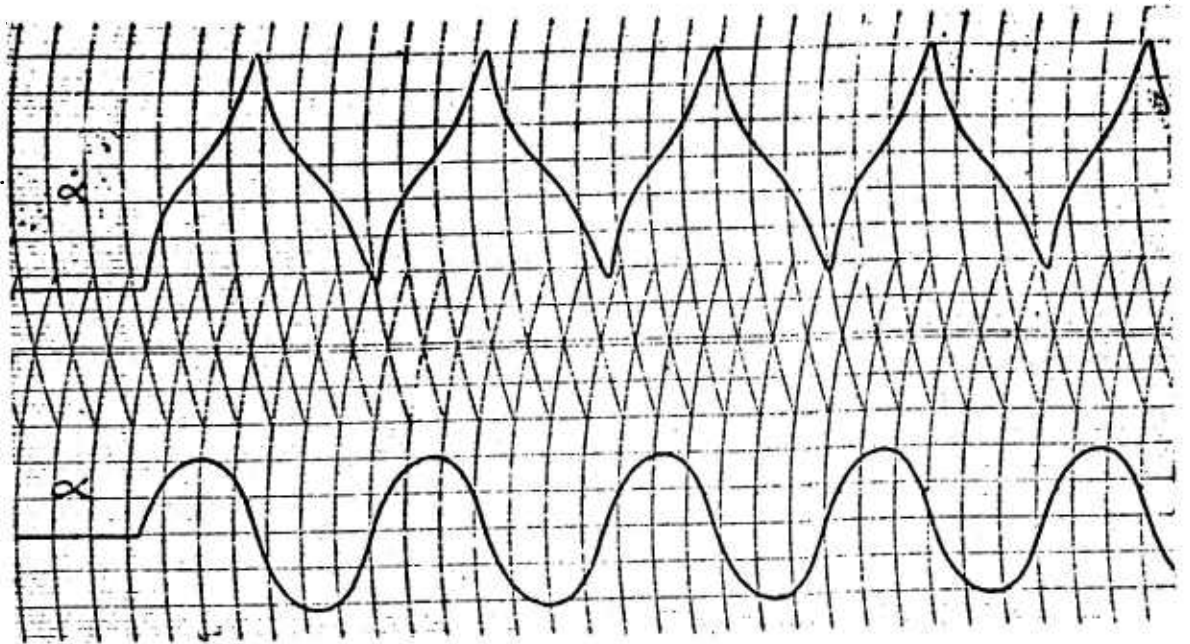


Figure 7.3-11 Pitch Motion for the Wind Tunnel Model

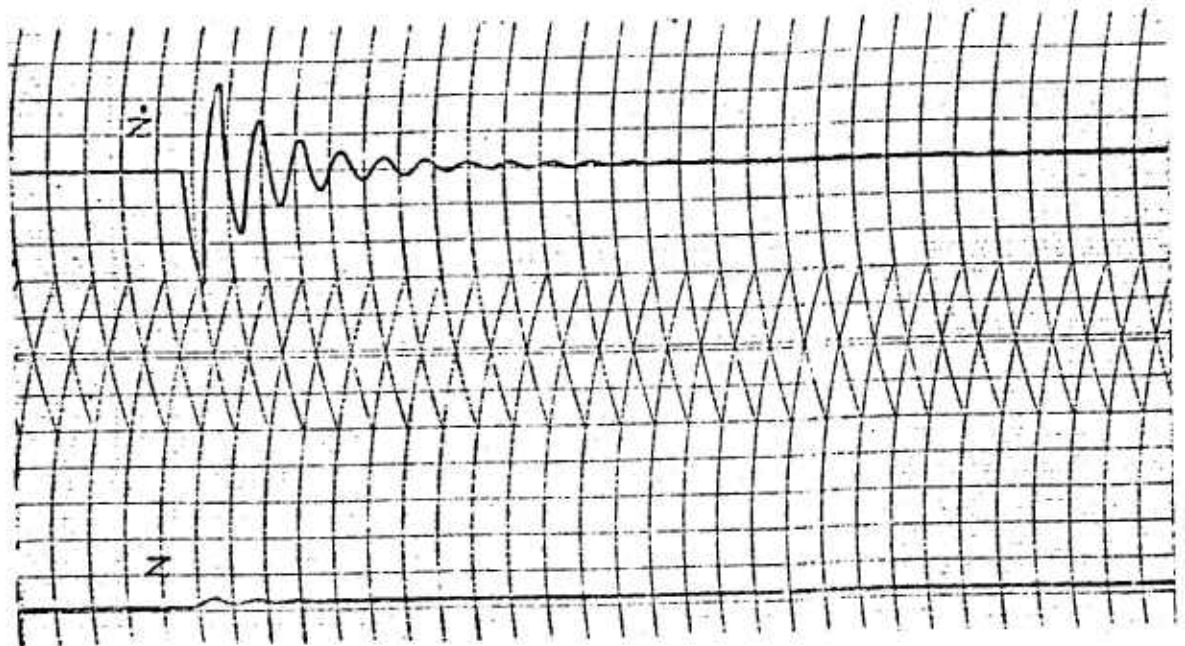


Figure 7.3-12 Heave Motion for the Wind Tunnel Model

slope of p_b and j . Thus we can see that the recirculation machine is inherently statically stable. The undamped natural frequency in heave is given by

$$\omega_n = \frac{1}{2\pi} \sqrt{\frac{\partial F_z}{\partial z} \frac{g}{W}} \quad \text{cycles per second}$$

The damping in heave was defined as shown in the equations of motion. Due to the uncertainty of this quality, values 50 percent above and below that defined by the equation were investigated on the computer. Even with the low value of damping, the oscillations in heave were rapidly damped.

7.3.3 Control

Many control methods, similar to those being used on the conventional annular jet, will be available for use on the Ejectijet GEM. Among these are:

- a. External power plants and propellers
- b. Vectored engine exhausts
- c. Bleed air from the base region
- d. Flaps in the jet region

Inasmuch as these and other methods are already available, an investigation was made to determine a method that would be uniquely applicable to a GEM using recirculation. Since the Ejectijet system affords a low external profile due to the small amount of air required for the primary nozzles, this new method should ideally maintain this low profile.

The analysis of the lift acting on a vehicle using recirculation shows that an internal duct load, approximately double the tertiary momentum, is

exerted on the vehicle. Control forces and moments can be obtained in two ways using this internal force. The first would be a prescribed rotation of this induced force vector about the periphery of the machine. This is a mechanical procedure - a physical rotation of the ejector assemblies.

The second is aerodynamic. The mass flow distribution to the primary nozzles, located about the periphery of the machine, is regulated as desired. This in turn regulates the total mass flow through the ejectors resulting in a change in the magnitude of the force vector.

7.3.3.1 Method Utilizing the Rotation of the Force Vector

In the process of recirculating the large mass of air through the ejectors, an internal force is produced whose direction is defined by the internal geometry of the ducts and whose magnitude is dependent on the amount of flow recirculated. The geometry is shown in Figure 7.3-13.

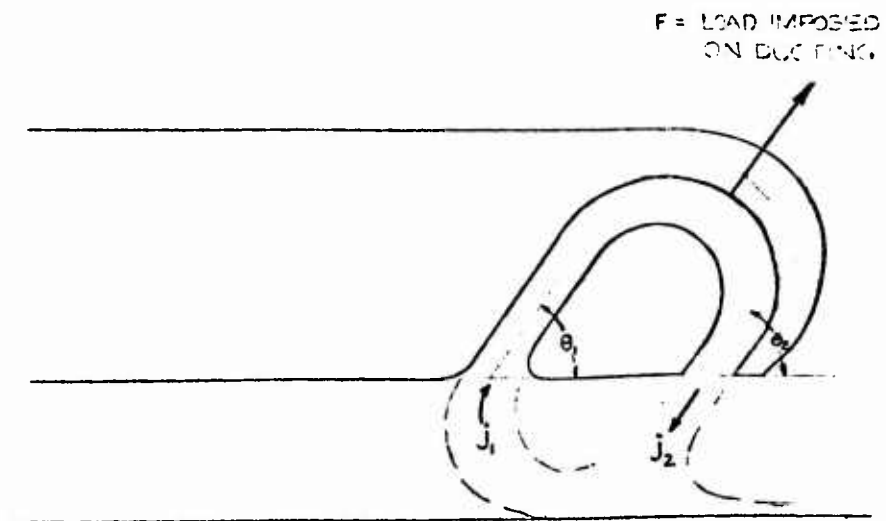


Figure 7.3-13 Internal Geometry

In complex notation the initial force vector at A is $j_1 e^{i\theta_1}$.
 The force vector at B is $j_2 e^{i(\theta_2 + \pi)}$. A load must be applied to
 the air stream to turn it through the ducting. A force diagram is
 used to solve for this force in magnitude and direction.

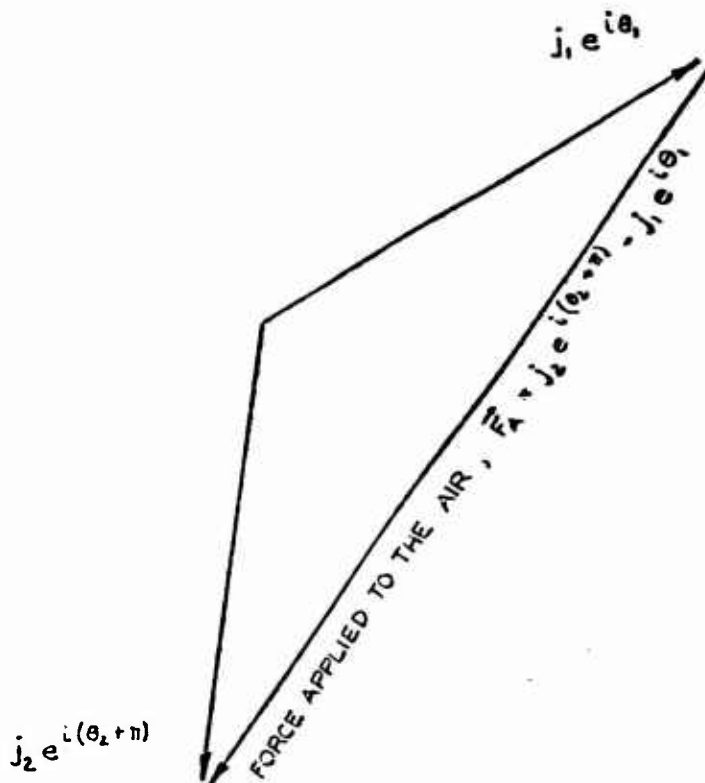


Figure 7.3-14 Force Vector Diagram

The force vector, \vec{F} , applied to the ducting is the negative of \vec{F}_A . This is

$$\begin{aligned}\vec{F} &= -\vec{F}_A = j_1 e^{i\theta_1} - j_2 e^{i(\theta_2 + \pi)} \\ &= j_1 (\sin \theta_1 + i \cos \theta_1) - j_2 [\sin(\theta_2 + \pi) + i \cos(\theta_2 + \pi)]\end{aligned}\quad (7.3-16)$$

Since

$$\begin{aligned}\sin(\theta_2 + \pi) &= -\sin \theta_2 \quad \text{AND} \quad \cos(\theta_2 + \pi) = -\cos \theta_2 \\ \vec{F} &= (j_1 \sin \theta_1 + j_2 \sin \theta_2) + i(j_1 \cos \theta_1 + j_2 \cos \theta_2)\end{aligned}\quad (7.3-17)$$

The horizontal and vertical components of this force are

$$\begin{aligned}\vec{F}_H &= (j_1 \cos \theta_1 + j_2 \cos \theta_2) \\ \vec{F}_V &= (j_1 \sin \theta_1 + j_2 \sin \theta_2)\end{aligned}\quad (7.3-18)$$

Assuming $j_1 = j_2$, Equation 7.3-18 reduces

$$\begin{aligned}\vec{F}_H &= j (\cos \theta_1 + \cos \theta_2) \\ \vec{F}_V &= j (\sin \theta_1 + \sin \theta_2)\end{aligned}\quad (7.3-19)$$

A comparison is given in Figure 7.3-15 between the theoretical vertical forces \vec{F}_V and the experimental data for two configurations. In the first configuration $\theta_1 = \theta_2 = 50$ degrees and in the other one $\theta_1 = 30$ degrees and $\theta_2 = 45$ degrees so that $\vec{F}_V/j = 1.53$ and 1.22 respectively. Although Figure 7.3-15 shows the experimental data to be non-linear, the incremental difference between the two curves compares well with the predicted difference. This indicates that the flow does not enter the ducting at the angle θ_1 , but at some other angle which is the same function of height for both models.

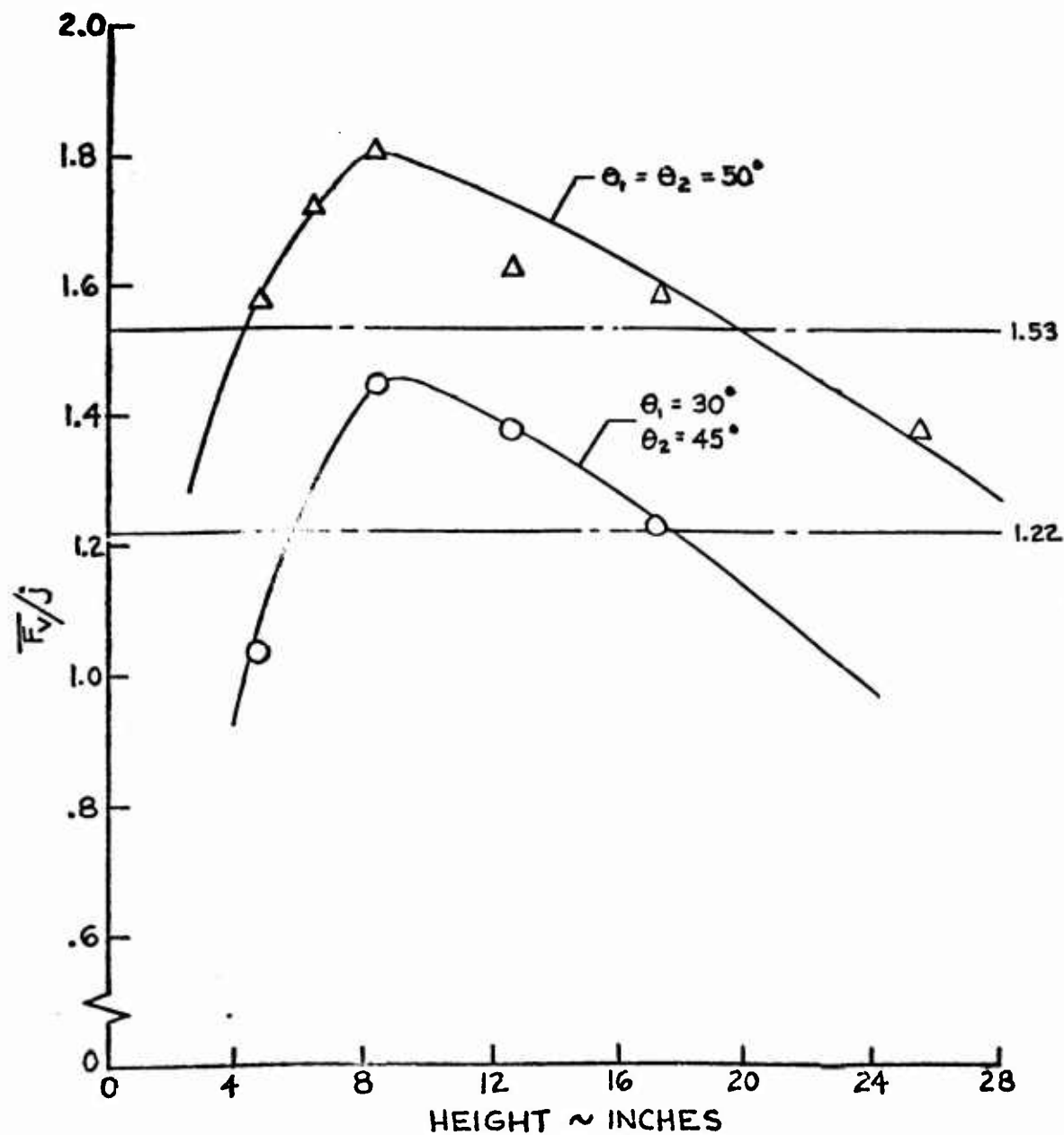


FIGURE 7.3-15 COMPARISON OF THEORETICAL VERTICAL EJECTOR FORCE WITH EXPERIMENT

This incremental change in vertical or horizontal forces can be utilized to create pitching, rolling, and yawing moments or lateral and longitudinal forces by the proper manipulation of ejector banks. To achieve these control moments the ejector assembly can be divided into banks as shown in the plan view of Figure 7.3-16. A pitching motion is obtained by forces from banks C and F, a rolling motion from banks AB and ED, a yawing motion from banks BE and AD.

The example of creating a pitching moment can be demonstrated by taking a two-dimensional cut through the machine of Figure 7.3-16 to show ejectors F and C in the side view.

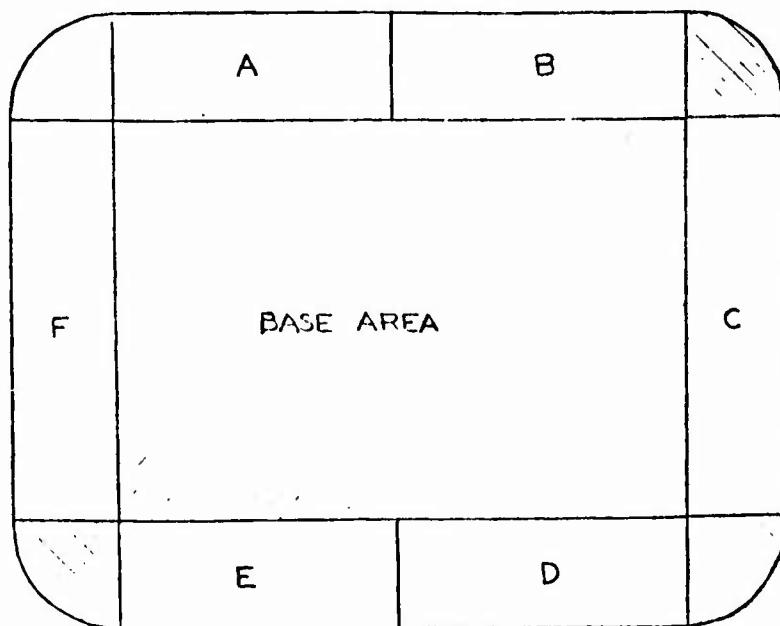
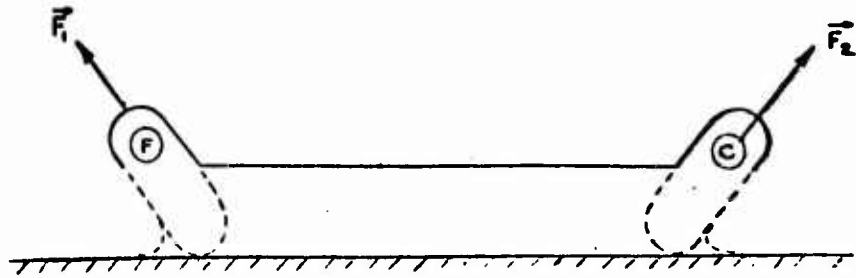
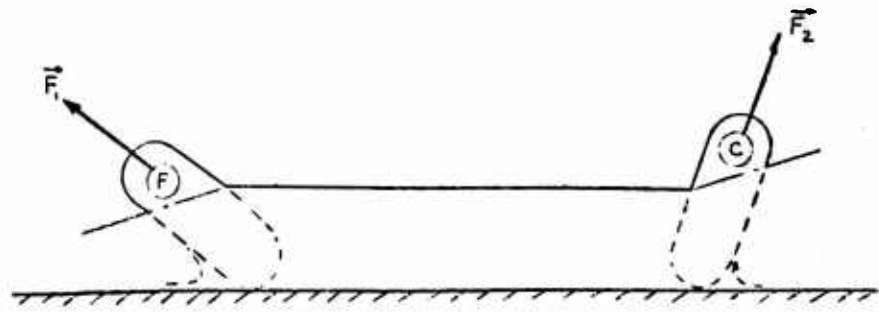


Figure 7.3-16 Plan View of Ejector Assemblies for Control



(1) Untilted Position $(\vec{F}_1)_v = (\vec{F}_2)_v$



(2) Tilted Position $\vec{F}_v = (\vec{F}_2)_v - (\vec{F}_1)_v$

Figure 7.3-17 Ejector Tilting Procedure

An unbalance in vertical forces is created by the tilted pattern, (2), of Figure 7.3-17 so that $(\vec{F}_2)_v > (\vec{F}_1)_v$. The desired pitching moment is then created by this unbalance of forces. A rolling moment can be created in the same manner by the use of ejectors, A, B, D, and E. These same four assemblies can be used to create a yawing moment by changing the horizontal components of \vec{F} in each ejector. The yawing moment is produced by rotating ejectors B and E down while ejectors D and A are rotated up or vice versa.

Figure 7.3-17 shows that the rotation of the ducts, while producing a change in vertical forces, produces a thrust force due to the change in horizontal components of forces. This horizontal force is zeroed out by either increasing the flow in ejector C with the introduction of more primary air to the nozzles, or by allowing the machine to ride with a slight tilt angle using the horizontal component of the inclined total lift vector. This latter method is shown in Figure 7.3-18.

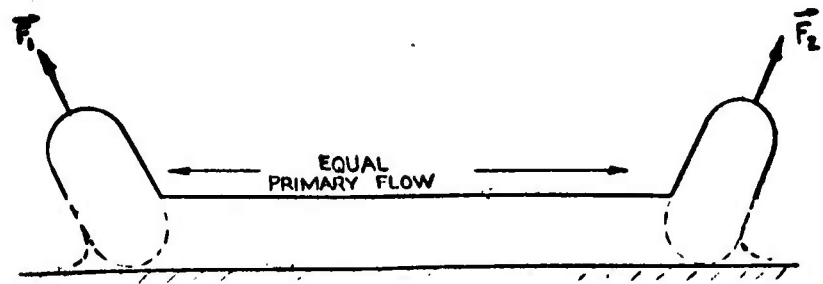
There are many other apparent advantages in being able to tilt the ejector banks. They are:

- 1 Control is obtained in all three planes.
- 2 The available control moments increase at higher heights since the required j increases. Thus, the maximum control moments occur at the heights where they are needed most.

- 3 Static tests on the 3-D wind tunnel model shows that the curve of p_B versus height can be translated by a uniform rotation of the ejector banks. Thus, the ejectors can be used as a trim device to obtain the maximum L/HP over a restricted height range, as shown in Figure 7.3-19.
- 4 The starting problem over water, in light of recent 2-D tests, can be resolved by tilting the ejectors down and pumping the water out from under the base with the primary air. Recirculation can then be started.
- 5 Low profile is maintained.
- 6 The interaction produced is cancelled readily.

7.3.3.2 Method Utilizing the Change in Magnitude of the Force Vector

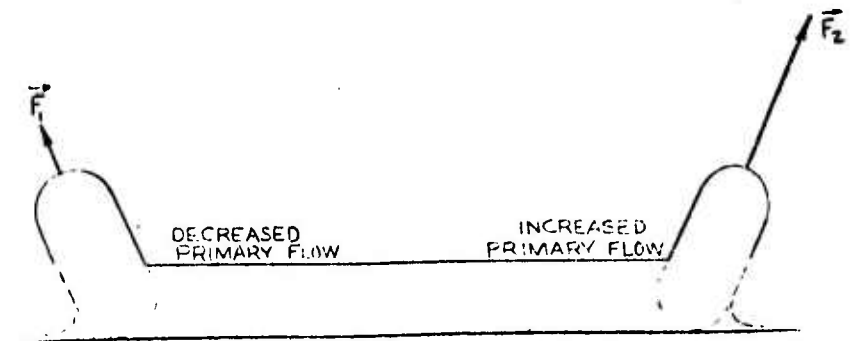
Control forces and moments can be obtained by regulating the flow to the primary nozzles of segments of the ejectors in a pattern that will produce the desired effect. If a rolling moment is desired, the amount of primary air to one side of the machine can be increased while decreasing the flow to the opposite side. The result is shown in the following figure.



EQUAL FLOW CONDITION

$$(\vec{F}_H)_1 = -(\vec{F}_H)_2$$

$$(\vec{F}_V)_1 = -(\vec{F}_V)_2$$



UNEQUAL FLOW CONDITION

$$(\vec{F}_H)_1 < (\vec{F}_H)_2$$

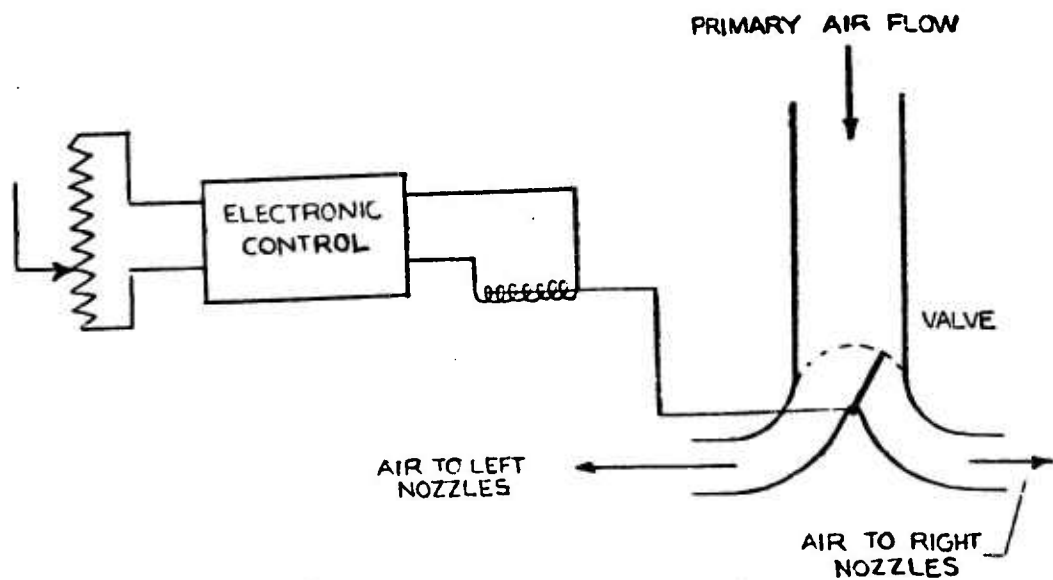
$$(\vec{F}_V)_1 < (\vec{F}_V)_2$$

Yawing moment and thrust forces can be obtained by this method in a manner similar to that described in the section on the rotation of the force vector.

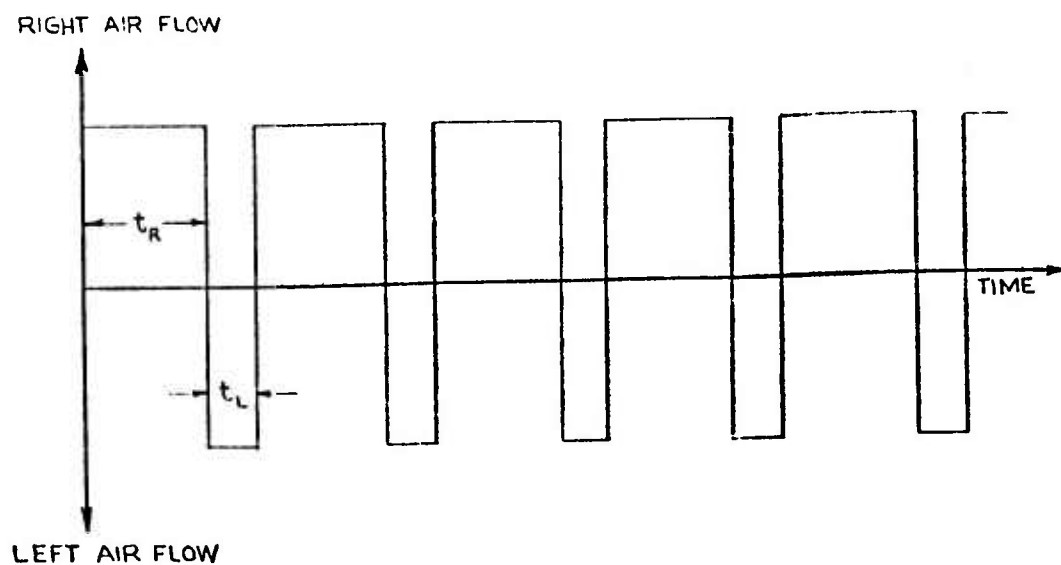
The amount of primary air flow can be controlled two ways. They are:

- a. Time-dwell-modulation - (TDM)
- b. Throttling

In the T-D-M control, air flow to the primary nozzles is modulated by a simple air-controlled right-left valve.



In this procedure the air flow to the left and right nozzles is regulated in a bang-bang fashion as shown below.



Air flow is controlled either right or left by the valve. The primary air would flow to the right nozzles for a time period of T_R and to the left nozzles for a time period of T_L . Since T_R is greater than T_L , in this case, more force would be exerted by the right ejector than the left one. By varying the time dwell (varying the ratio of T_R to T_L) a proportional control can be achieved. The repetition time, T_S , which is T_R plus T_L is small, on the order of 0.2 seconds, so the air pulsing would appear to be continuous.

A similar method would be differential throttling of the primary air flow. This could be accomplished by varying the primary total pressure to the ejectors so that the force vector would again be regulated.

Although the results of this study indicate that rotation of the ejectors provides the most promising control system, a test facility is now being constructed to test these methods and evaluate their relative merits as compared to the more conventional control systems. A one-half scale version of the facility shown in Figure 7.3-20 will be used.

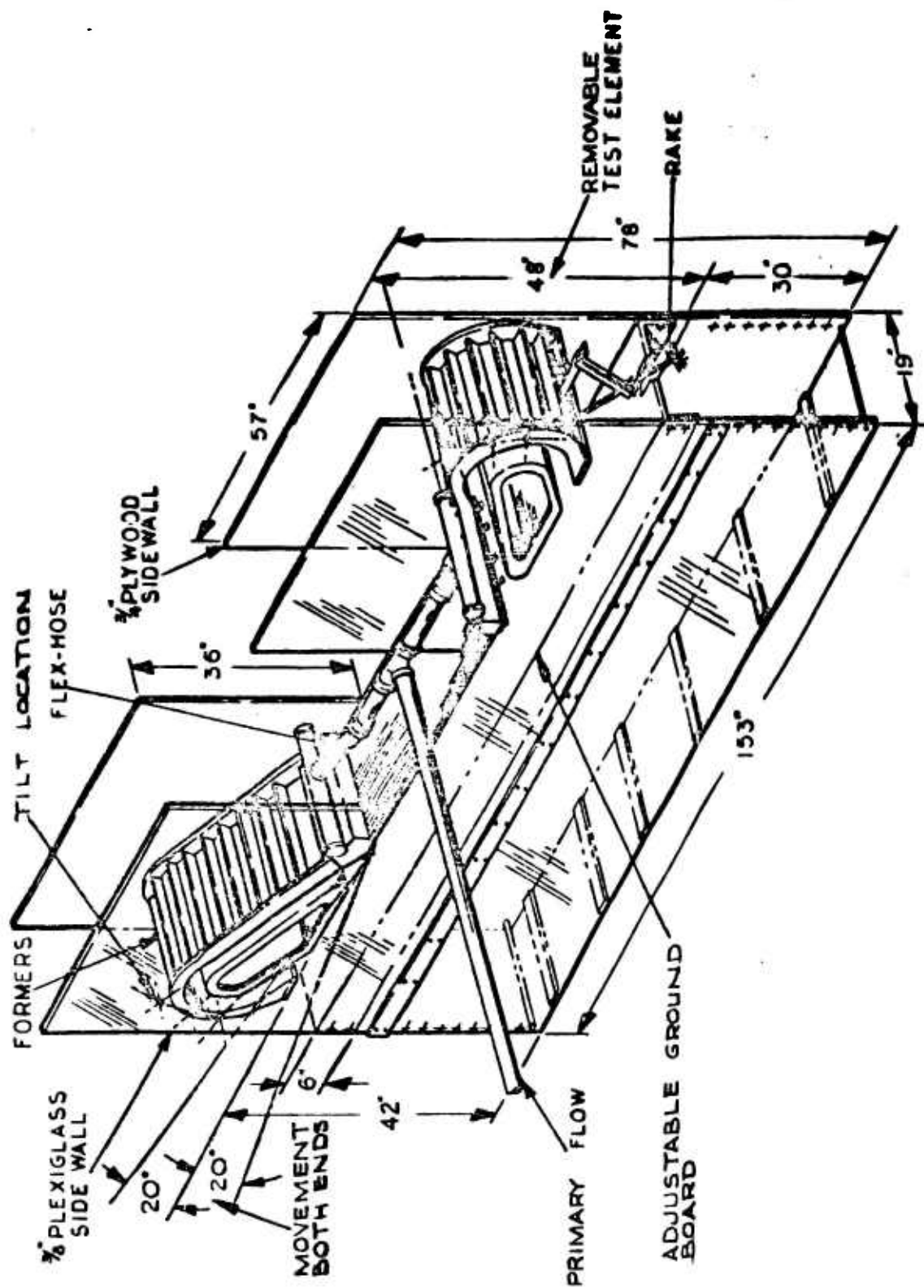


FIGURE 7.3-20 DOUBLE EJECTOR CONTROL MODEL

7.4 FORWARD FLIGHT

The forward flight aspects of GEM performance do not lend themselves readily to theoretical analyses. The complexity of the flow patterns created by forward velocity and cushion flow is such that meaningful theoretical models are difficult if not impossible to create. Thus, forward flight analysis must rely heavily upon experimental data for verification of the basic performance equations.

The only data available is from a model recirculation GEM which was tested in the wind tunnel at the David Taylor Model Basin, Washington, D. C. (Reference 17). The model was rectangular in planform with a 4.5 ft length and a 3.5 ft beam. The model height was 7 inches and the top was a smooth flat surface blending into the sidewalls with a generous radius. The recirculation air curtain was also rectangular in planform with "open" corners. The resultant square curtain corners were imperfect in that some air leakage from the pressurized base region was observed. No attempt was made to streamline the model for the purpose of maximizing lift and minimizing drag due to the external flow field. The primary purpose of the tests was to investigate the performance of the recirculation cushion under the effects of forward flight.

Although the final analysis of the wind tunnel data is not complete at this time, sample preliminary data are presented where they assist in substantiating the basic performance equations.

7.4.1 Lift in Forward Flight

The lift in forward flight is composed of all the elements present in hovering, plus aerodynamic lift due to the external flow field. The lift equation in forward flight must then account for aerodynamic lift as well as for the effects of forward flight on the other lift

components. In forward flight the lift equation becomes:

$$L = p_b S_b + J(\sin \theta_1 + \sin \theta_2) - J' \sin \theta_1 + p_c S_c + C_L q S \quad (7.4-1)$$

Base Pressure Lift
Vertical Component of Tertiary Momentum
Vertical Component of Primary Momentum
Cavity Pressure Lift
Aerodynamic Lift

Chaplin (References 18 and 19) has found that $C_L = 0.4$ for an annular GEM. Preliminary results from Reference 20 indicate that this finding is valid for a recirculation GEM. Apparently the value of lift coefficient is relatively independent of the shape or contour of the lifting surface. Figure 7.4-1 presents representative lift data at extreme operating heights of 1 and 5 inches for the wind tunnel model. These data substantiate the lift equation (7.4-1) within a reasonable degree of accuracy.

At the 1 inch height, base pressure, cavity pressure, and momentum lifts were unaffected by forward flight when a constant cushion power input was maintained. The increase in total lift with forward speed is due to the aerodynamic lift on the top surface. The variation of aerodynamic lift with flight speed is in substantial agreement with that for an annular GEM.

At the 5 inch height the total lift curve shows a sharp rise between 45 and 60 feet per second which was not observed at the 1 inch height. Tests were conducted with constant cushion power at all heights and the resultant base pressure at 5 inch height was approximately equal to q at a flight velocity of 45 feet per second. As q increased above the base pressure level between 45 and 60 feet per second, base pressure tends to follow q , hence the rapid increase in total lift. It is apparent that the forward flight q was being fed into the base region. At high speeds then, where q values of 30 to 60 psf are available, it is apparent that reduced curtain power is required

to support a given base pressure. It is possible that only rear and side curtains will be required with forward flight q providing base pressurization.

7.4.2 Drag in Forward Flight

The drag of a ground effect machine in forward flight is expected to consist of profile drag plus a momentum drag due to the capture of free stream air to supply the jet curtain. The drag equation may be written

$$D = C_{D_f} q_\infty S_b + C_{D_{mom}} m' V_\infty \quad (7.4-2)$$

It might be anticipated that the profile drag coefficient (C_{D_f}) is a strong function of vehicle shape or streamlining and may assume a wide range of values. The momentum drag coefficient ($C_{D_{mom}}$) may be expected to depend strongly on intake location and shape.

One of the advantages of the recirculation GEM principle is the reduction in total drag compared to an annular GEM due to the lower magnitude of air (m') which must be brought on board to supply the jet curtain. A typical ejector recirculation GEM might have mass augmentation ratios of 30:1 to 40:1 thus implying that the momentum drag component of total drag should be 1/40 to 1/30 of a comparable annular jet design.

In order to gain an appreciation for the relative order of magnitude of the two drag components, consider a hypothetical 50 foot diameter recirculation GEM of 60,000 pounds gross weight operating at 3 foot height. For a base pressure of 45 psf and a jet width (t_j) to height (h) ratio of .25 the required curtain mass flow is 1500 pounds/second. Assuming a mass augmentation ratio of 30:1, the required primary airflow is 50 pounds per second. Further, assuming a profile drag coefficient (C_{D_f}) of .074 compatible with Chaplin's findings

(Reference 18), and a momentum drag coefficient of 1.0, the drag for this hypothetical machine may be calculated as a function of speed. A comparison of the annular and recirculation GEM is given in the following table.

TABLE 7.4-1 DRAG OF A HYPOTHETICAL GEM

mph	Profile Drag	Intake Drag		Total Drag	
	Pounds	Pounds		Pounds	
	Recirculation or Annular	Recircu- lation	Annular	Recircu- lation	Annular
20	140	46	1380	186	1520
40	560	91	2730	651	3290
60	1260	137	4100	1397	5360
80	2230	182	5450	2412	7680

While the total drag of the conventional GEM is composed primarily of intake momentum drag, the recirculation GEM total drag is dominated by profile drag which, as mentioned previously, is controlled by vehicle shape.

Preliminary wind tunnel data (Figure 7.4-2) indicate that in addition to profile drag there is a "cushion drag" which may be as great as the profile drag at certain combinations of speed and height. An adequate understanding of the "cushion drag" is not available currently, although a cushion drag of appreciable magnitude has been observed for some annular GEM models by Norman K. Walker (Reference 20).

While the cushion drag may be as great as the profile drag, it is apparent that a recirculation GEM with this extra cushion drag would still have a total drag of approximately 1/2 that of a comparable

annular GEM. Since an annular GEM will probably have a comparable "cushion drag", it is expected that the total recirculation drag will be on the order of $1/3$ that of the annular machine as shown in Table 7.4-1.

Because the additional "cushion drag" will require greater propulsive power than anticipated from profile and momentum drag consideration alone, additional experimental studies are advisable to find means of eliminating or minimizing this extra drag. The effects of "open" corners and streamlining the cushion in plan form should probably be determined first.

7.4.3 Stability in Forward Flight

Recirculation GEM stability in hovering has been described in detail in Section 7.3.2. The effects of forward flight are expected to be similar to those observed for annular GEM's. That is, as forward flight speed increases, stability margin decreases until at some point the basic machine becomes unstable and artificial stabilization is required. This is due to a combination of crossflow in pitch and external aerodynamic forces. The recirculation machine enjoys a big advantage over the annular machine in that hovering stability is maintained over a wide range of operating conditions. Hovering performance of the 3-D model has verified that this stability is present. The primary purpose of forward flight stability investigation is to determine, experimentally, the rate at which stability margin deteriorates with forward speed, and the point at which instability is encountered.

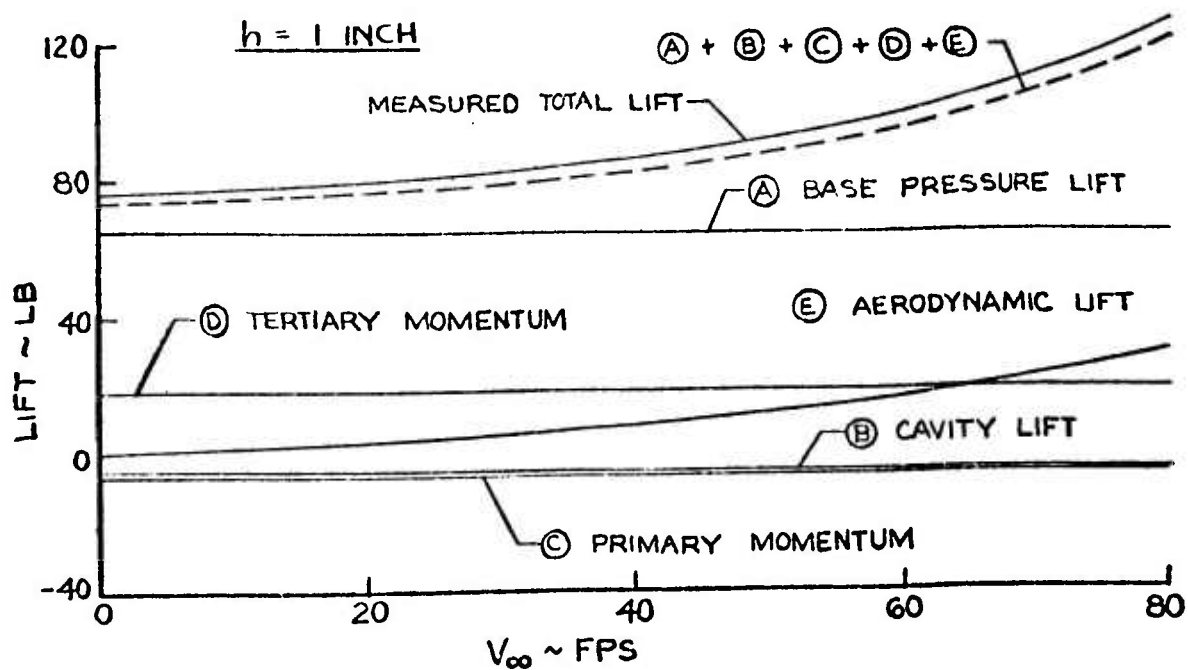
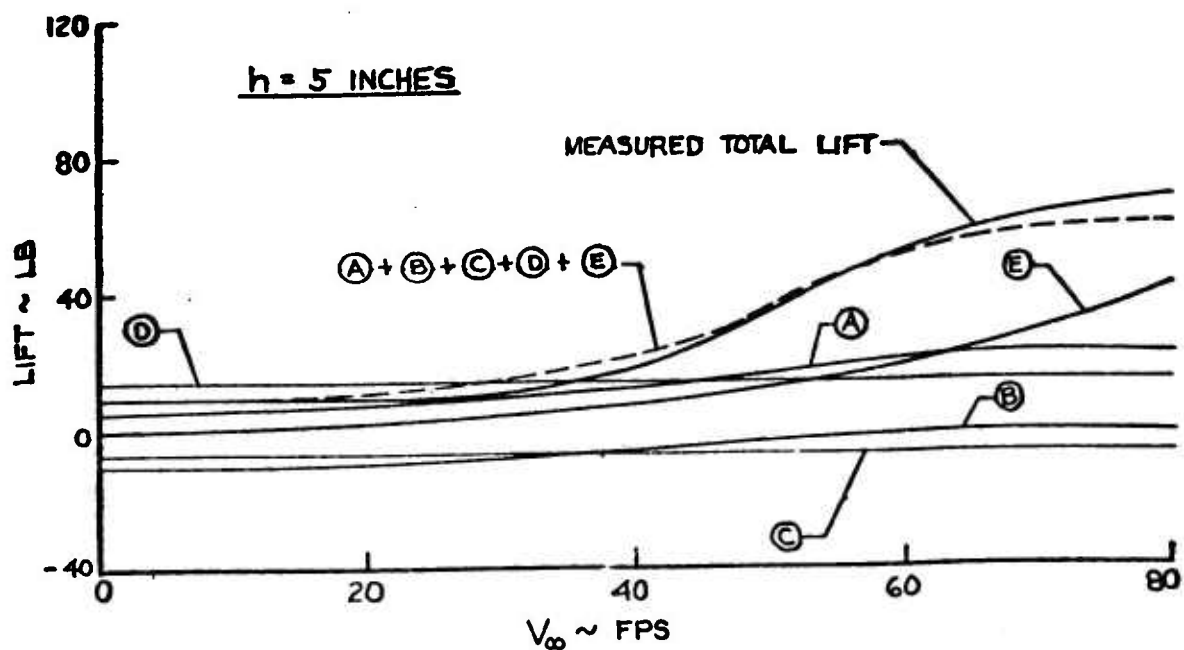


FIGURE 7.4-1 FORWARD FLIGHT OF 1/4 SCALE RECIRCULATION GEM MODEL (PRELIMINARY WIND TUNNEL RESULTS)

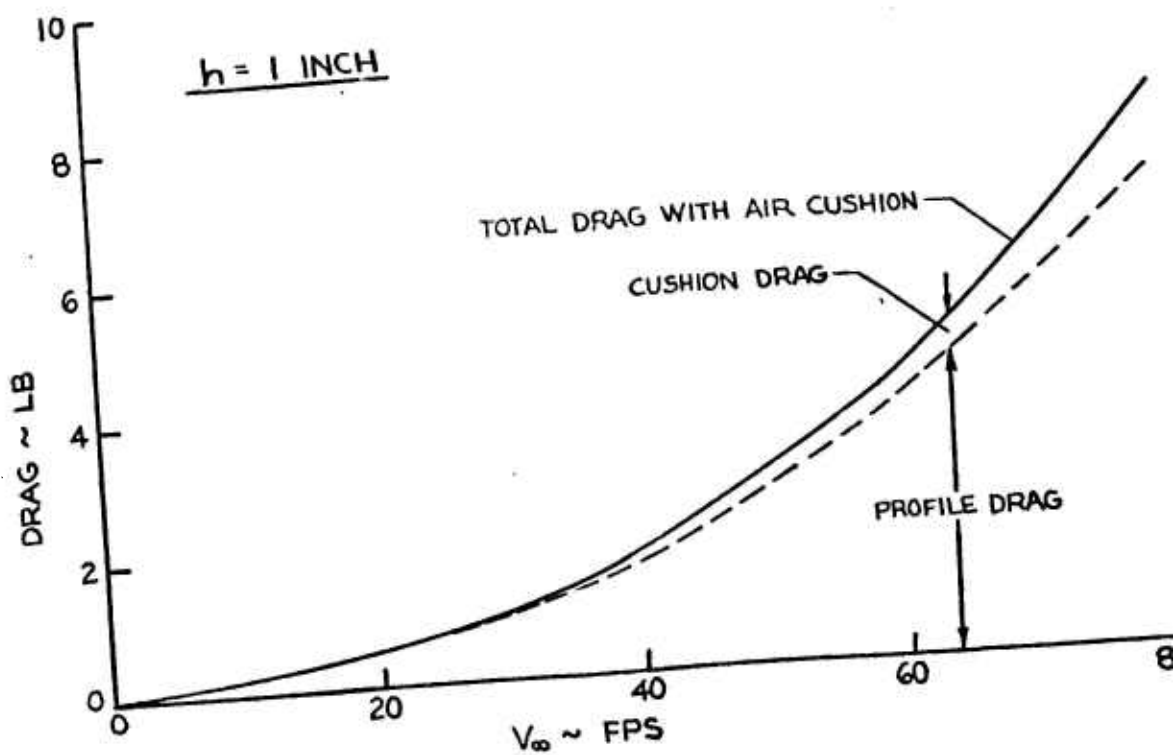
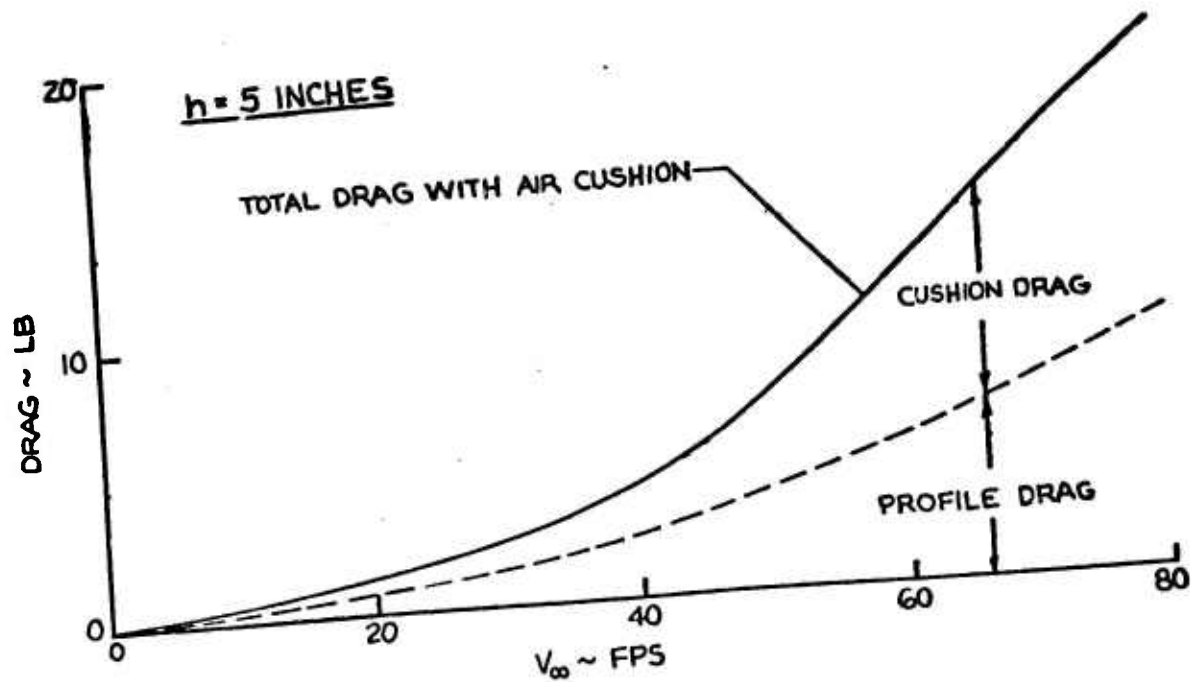


FIGURE 7.4-2 FORWARD FLIGHT DRAG OF 1/4 SCALE RECIRCULATING GEM MODEL (PRELIMINARY WIND TUNNEL RESULTS)

8.0 EJECTIJET GEM PERFORMANCE

The ultimate goal of the recirculation ejector studies is to demonstrate performance capability in a full scale vehicle. While actual hardware for a full scale vehicle has not been built at this date it is possible to predict the performance of an Ejectijet GEM by developing the basic performance equations and inserting the appropriate ejector performance parameters as derived from two-dimensional testing. This section is devoted to the development of the Ejectijet GEM performance equations, comparison with annular GEM performance equations, and finally, utilization of the equations to predict power requirements of a typical vehicle.

8.1 TABULATION OF BASIC PERFORMANCE EQUATIONS

The basic equations for estimating the performance of the Ejectijet and annular jet GEMs are summarized in Tables 8.1-1 and 8.1-2. The equations for the Ejectijet have been substantiated elsewhere in this report. For the annular jet, the equations were obtained from References 18 and 19. In preparing these tables it was necessary to make certain assumptions and simplifications. For example, power required for control and acceleration is not accounted for, however, similar assumptions were made in both cases. These equations obviously lack sufficient rigor to enable an accurate determination of the performance of either system, but a relative comparison can be obtained.

TABLE 8.1-1

Ejectijet Performance Equations

Total Power:

$$HP_T = HP_J + HP_P$$

where

 HP_J = Jet cushion power HP_P = Propulsion powerJet Cushion Power:

$$HP_J = \frac{m V^2}{1100 E_o} = \frac{(\rho t_e c)^{-1/2}}{1100 E_o} J^{3/2}$$

where

 E_o = Overall hovering efficiency $E_r \approx 0$ (Negligible inlet pressure recovery)

J is determined from the relations

$$P_b = \frac{J}{2 t_e c} \left[1 - e^{-2 \frac{t_e}{h} (1 + \cos \theta_1)} \right] - \frac{J}{c h} \left[1 - \frac{2}{m/m'} - \cos \theta_2 \right]$$

$$W = L = p_b S_b + J (\sin \theta_1 + \sin \theta_2) + 0.4 q_\infty S_b + [-J' \sin \theta_1 + p_c S_c]$$

Propulsion Power:

$$HP_P = \frac{1}{E_P} D_{TCT} V_\infty$$

where

$$D_T = D_f + D_{mom}$$

$$D_f = C_{Df} q_\infty S_b$$

$$D_{mom} = C_{Dmom} m' V_\infty$$

$$E_P = 0.8 \text{ (Propulsion efficiency)}$$

$$D_f = \text{Profile drag; } D_{mom} = \text{Momentum drag}$$

$$C_{Df} = 0.074 \text{ (Same as for annular jet)}$$

$$C_{Dmom} = \text{Momentum drag coefficient}$$

TABLE 8.1-2
Annular Jet Performance Equations

Total Power: $HP_T = HP_J + HP_P$

where $HP_J = \text{Jet cushion power}$
 $HP_P = \text{Propulsion power}$

Jet Cushion Power: $HP_J = \frac{1}{\eta_c} \sqrt{\frac{2}{\rho}} q_j \left(q_j + \frac{p_b}{2} - \eta_r q_\infty \right) t_e C \cos \theta$

where $\eta_r = \text{Inlet recovery factor}$
 $\eta_c = \text{Overall efficiency}$

(η_c includes a loss factor to account for 10 percent horsepower consumed for stabilization.)

q_j is determined from:

$$p_b = \frac{5}{2} q_j \frac{t_e}{h} \quad (\text{Assumes } \eta_A = 0.73)$$

$$W = L = (p_b + 0.4 q_\infty) S_b + J \sin \theta$$

Propulsion Power:

$$HP_P = \frac{1}{\eta_p} D_T V_\infty$$

where $D_T = D_f + D_{mom}$

$$D_f = C_{Df} q_\infty S_b$$

$$D_{mom} = C_{Dmom} m_j V_\infty$$

$$\eta_p = 0.8 \text{ (Propulsion efficiency)}$$

$$D_f = \text{Profile drag; } D_{mom} = \text{Momentum drag}$$

$$C_{Df} = 0.074 \text{ (DTMB tests)}$$

$$C_{Dmom} = \text{Momentum drag coefficient}$$

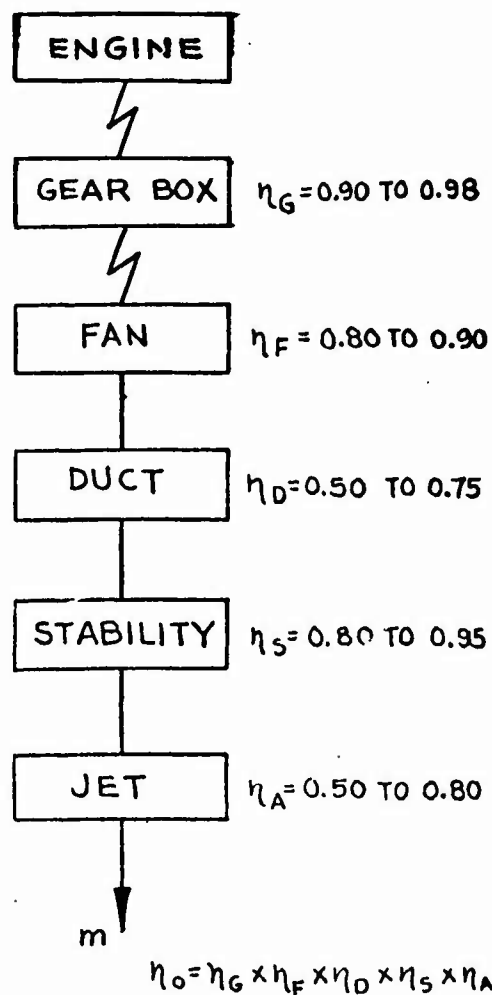
8.2 COMPONENT EFFICIENCY

The cushion power expressions for the Ejectijet and annular jet consist primarily of flow parameters and vehicle geometry. In addition, an overall hovering efficiency term must be determined. This factor accounts for difference in energy available at the output shaft of the power plant and the energy contained in the air cushion curtain.

Referring to Figure 8.2-1, it is apparent that both overall efficiencies are a function of several component efficiencies. For the annular jet, the range shown for each efficiency represents values which are obtainable, but depend largely on the design effort involved. The higher values for each component efficiency were obtained from a survey of the GEM reference literature and represent estimates which may be realized in the future. From published performance data of existing annular jet vehicles it appears that the best current values for overall hovering efficiency are 30 to 35 percent (Reference 21).

For the Ejectijet, the component efficiencies between the engine and recirculating ejector are easily determined from standard handbooks. No difficult design problems are anticipated in this section. An efficiency factor is not included for stability, as it has been shown elsewhere in this report that cross slots are not required. Of prime importance is the recirculating ejector efficiency which includes all other losses. Current best effort of ejector efficiency (obtained experimentally) is 68%. Assuming the combined compressor and line efficiency to be 80%, the predicted Ejectijet overall hovering efficiency is 54%. A direct comparison can now be made of the overall hovering efficiencies for the annular jet or Ejectijet for comparable base pressures.

ANNULAR JET



EJECTJET

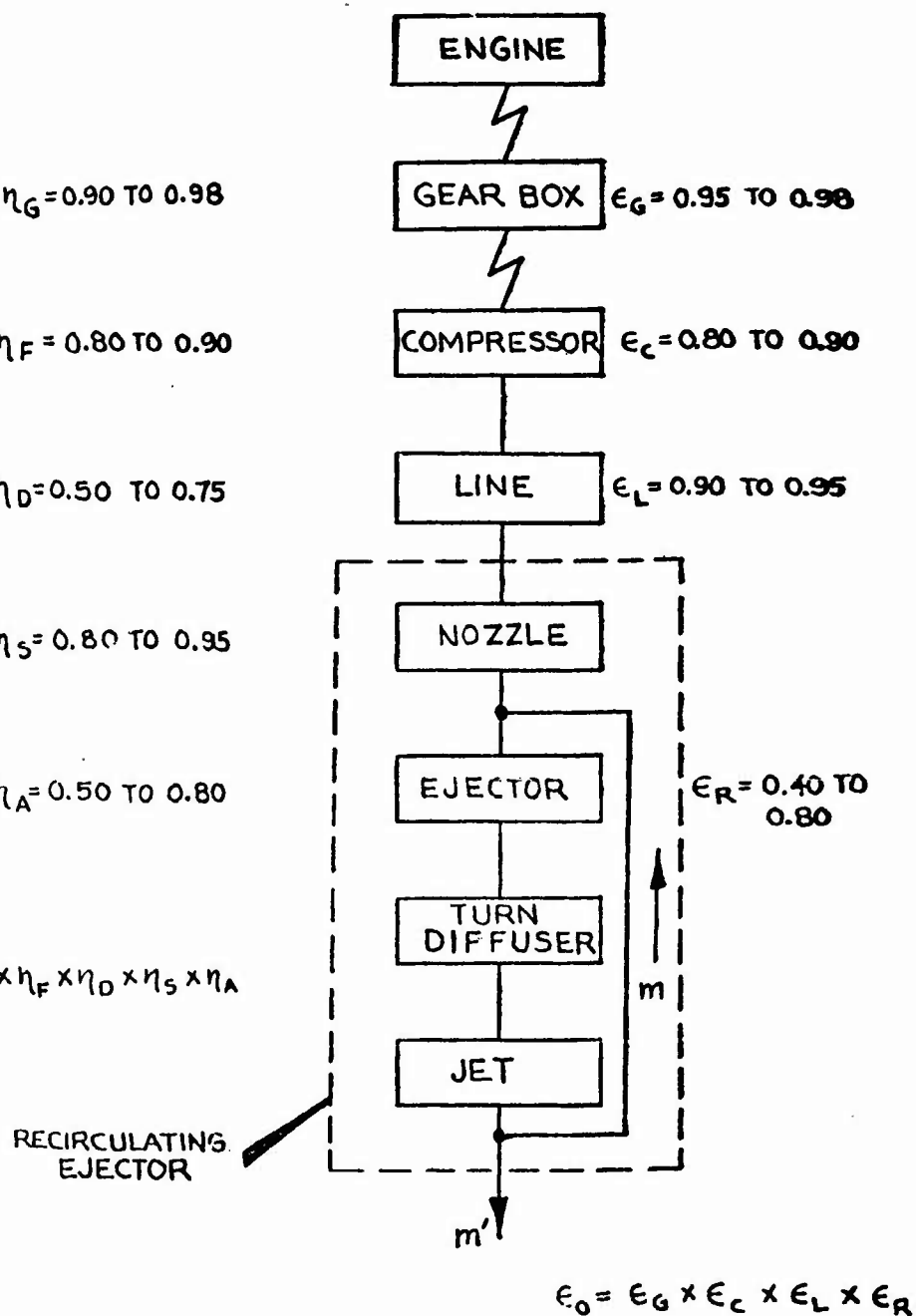


FIGURE 8.2-1 HOVER EFFICIENCY

8.3 RECIRCULATING EJECTOR PARAMETRIC STUDY

In order to determine the ejector efficiency or power ratio that might be expected, a theoretical parametric study was undertaken using the following operating conditions,

weight = 60,000 pounds

$h = 3$ feet

$P_b = 30, 50, 80$ psf

From these initial conditions the following parameters and their values were investigated.

$V_4 = 200, 256, 328$ feet per second

pressure recovery = 30, 40, 50, 60, 70, 80 and 90
percent of tertiary exit total
pressure

$P_o' = 20, 35, 70, 135, 200$ psig

$t_e/h = 0.25$

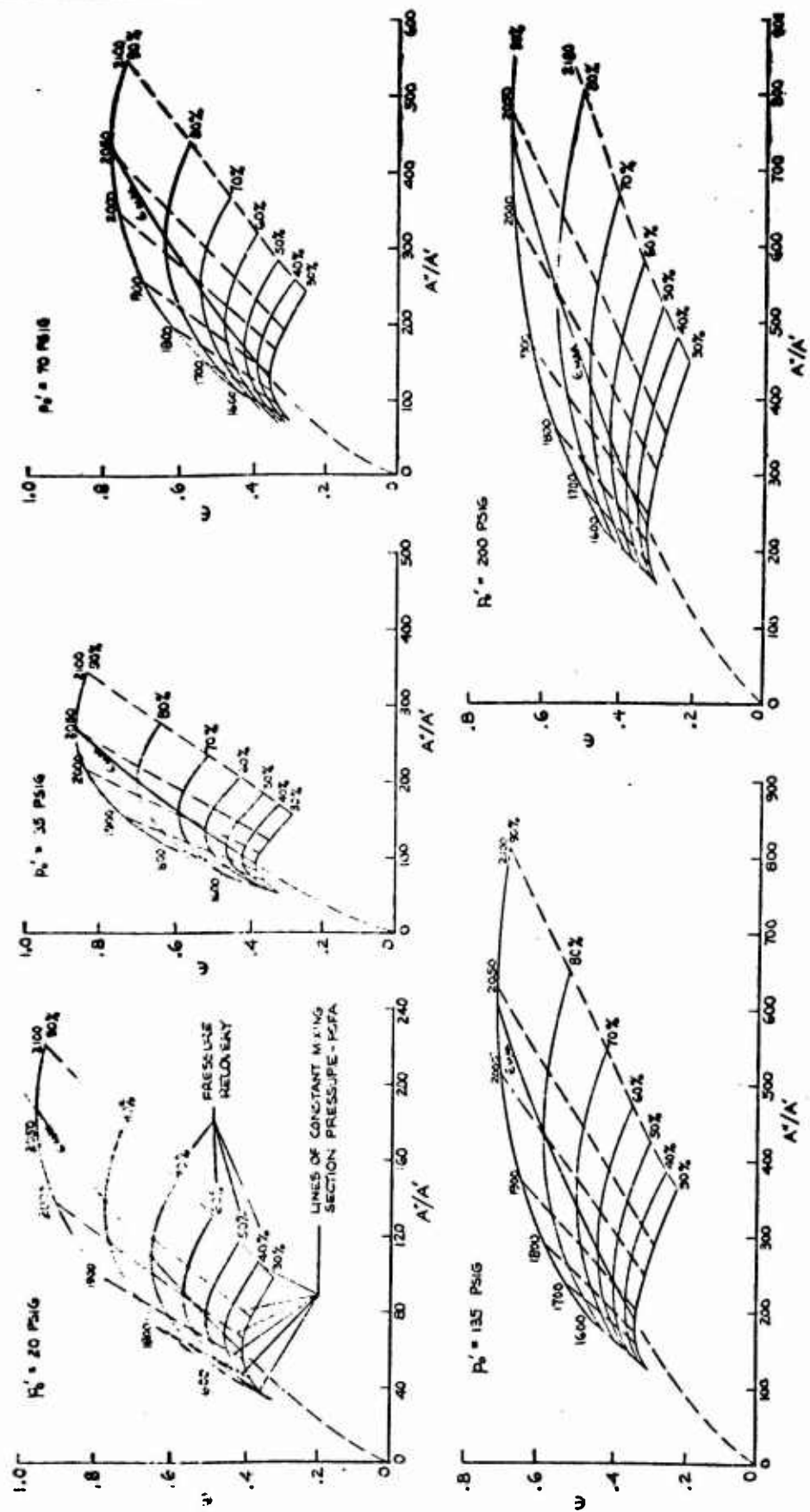
The solutions for ejector geometry and performance were obtained using the theory of Sections 7.1 and 7.2 programmed on the digital computer. Diffuser and turn losses were included in the input to insure realistic performance estimates. The input values for tertiary exit velocity were determined from the given base pressure values by means of the external flow theory of Section 7.2.3.

Plots of efficiency as a function of area ratio, pressure recovery, mixing section pressure, and primary total pressure are presented in Figures 8.3-1 through 8.3-3. It is noted that these curves have maximum values which determine an optimum area ratio for a given

secondary total pressure recovery. Also, it is shown that the possibility of attaining ejector efficiencies greater than unity exist even when realistic internal losses are included, provided the secondary total pressure recovery is sufficiently high. The effects of individual variables can be better determined from Figures 8.3-4 through 8.3-6.

Figures 8.3-4 shows how maximum ejector efficiency increases with decreasing primary total pressure and increasing tertiary exit velocity (increasing base pressure). This trend can be explained by the fact that for each curve, tertiary velocity is held constant whereas, the primary velocity decreases with decreasing primary total pressure. Since primary velocity appears in the denominator of the expression for efficiency given in equation 7.1-38, the efficiency is naturally improved as primary pressure is decreased. Figure 8.3-5 also reflects the improvement in maximum efficiency that is obtained with increased tertiary velocity. In addition, the effect of total pressure recovery at the secondary inlet is indicated.

Figure 8.3-6 is a plot of optimum area ratio (maximum power ratio) as a function of primary total pressure and pressure recovery. These curves are obtained from a cross plot of the maximum efficiency curves of Figure 8.3-1. It is seen that the optimum area ratio decreases with decreasing primary total pressure and pressure recovery.



8.3-3

FIGURE 8.3-1 THEORETICAL RECIRCULATING EJECTOR EFFICIENCY - $V_0 = 200$ FPS

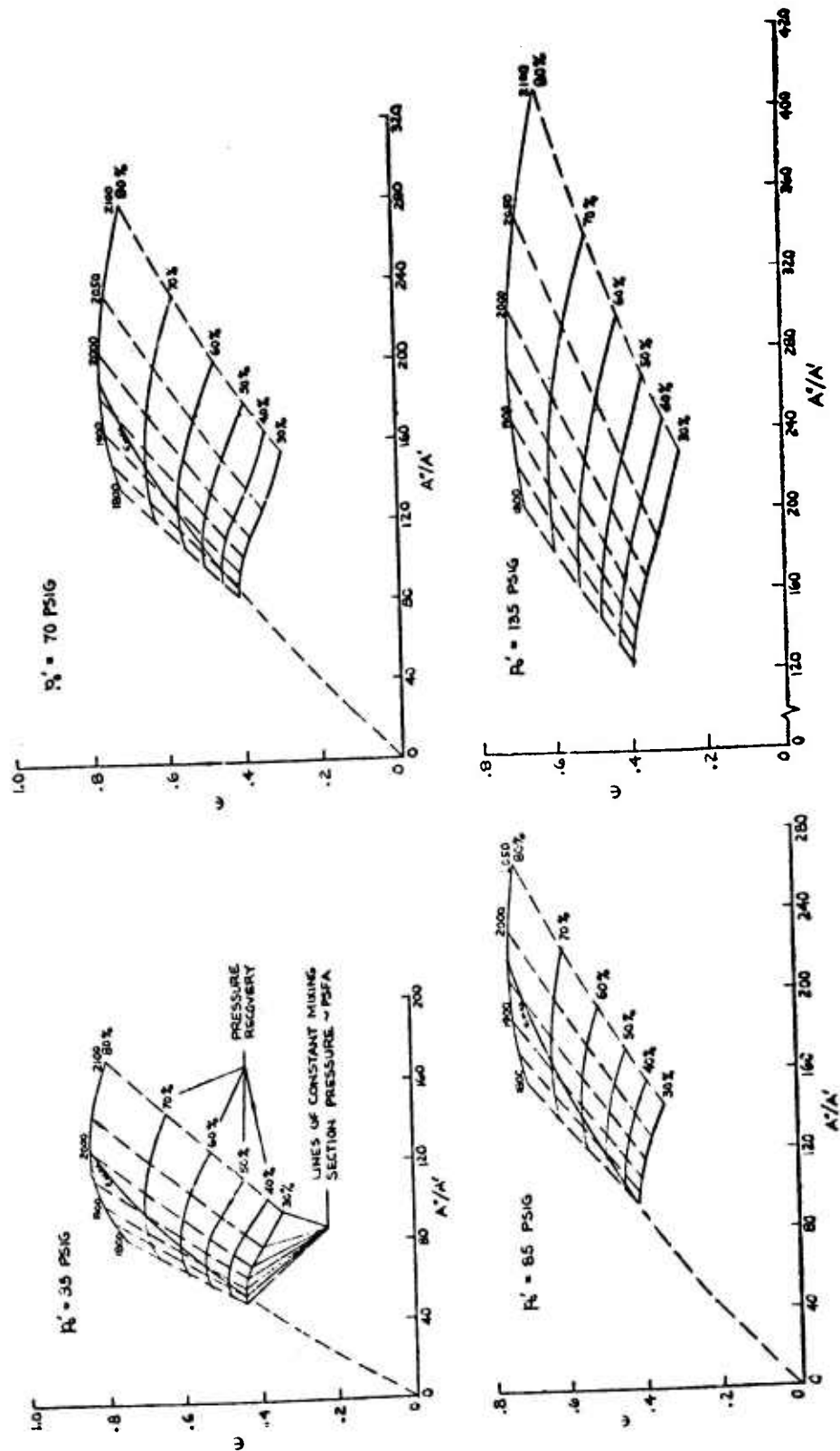
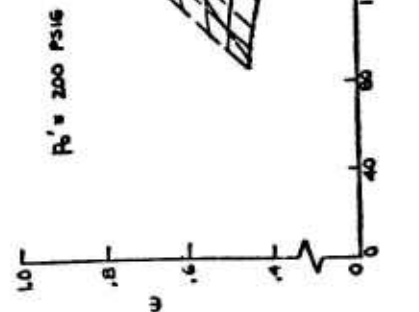
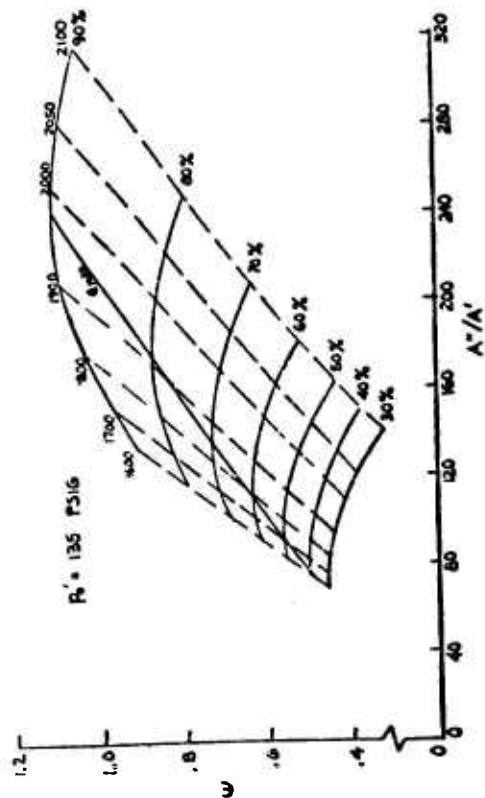
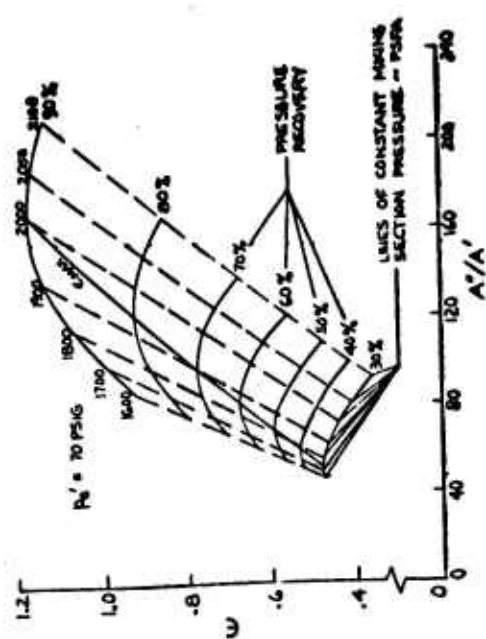
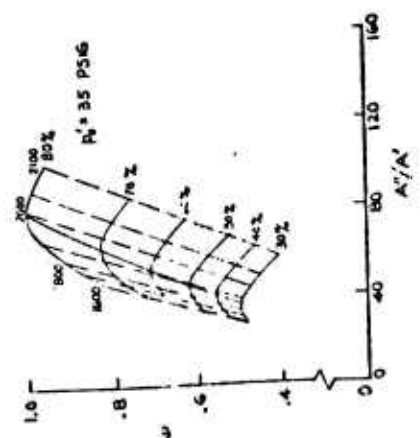
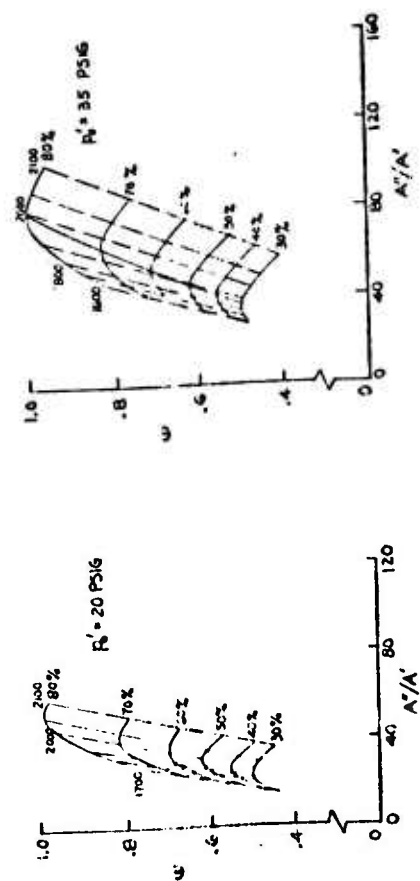


FIGURE 8.3-2 THEORETICAL RECIRCULATING EJECTOR EFFICIENCY - $V_1 = 256$ FPS



8.3-5

FIGURE 8.3-3 THEORETICAL RECIRCULATING EJECTOR EFFICIENCY - $V_1 = 328$ FPS

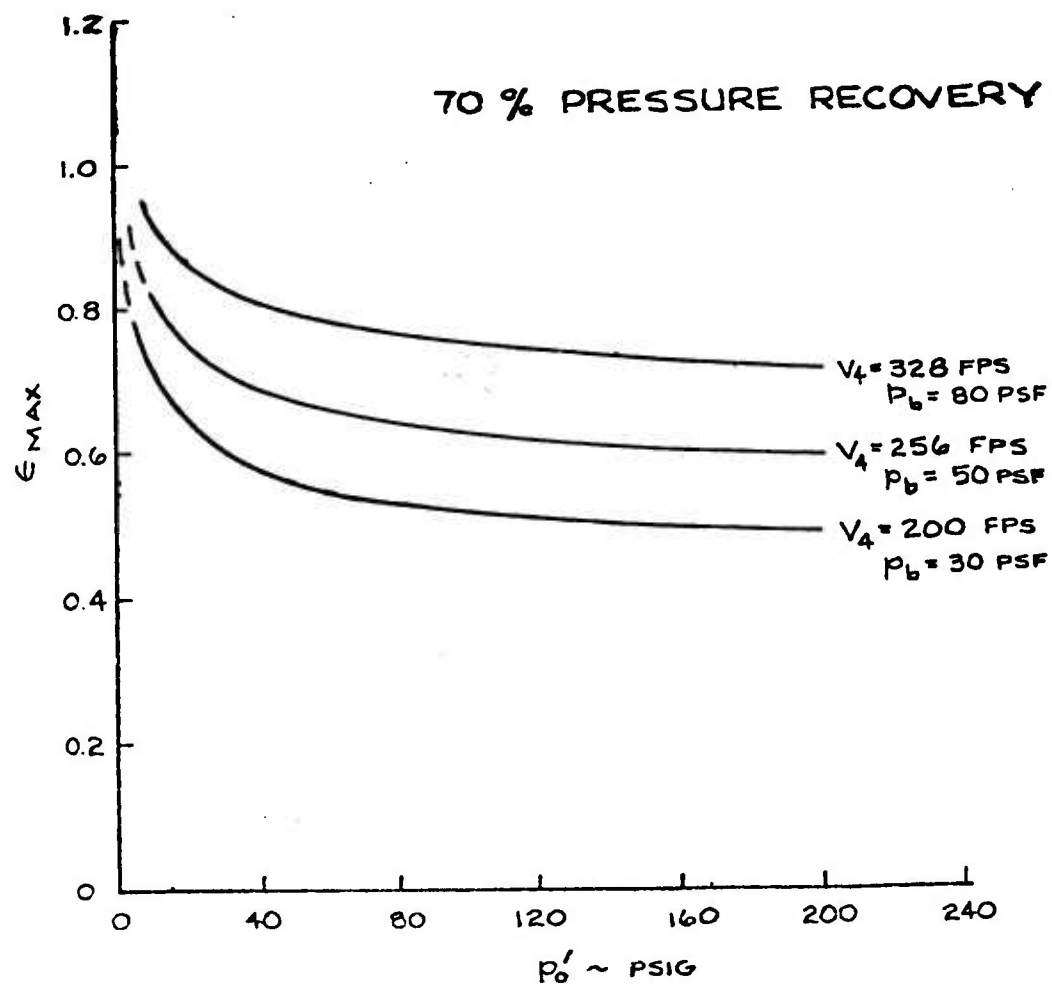


FIG. 8.3-4 EFFECT OF PRIMARY PRESSURE ON MAXIMUM EFFICIENCY

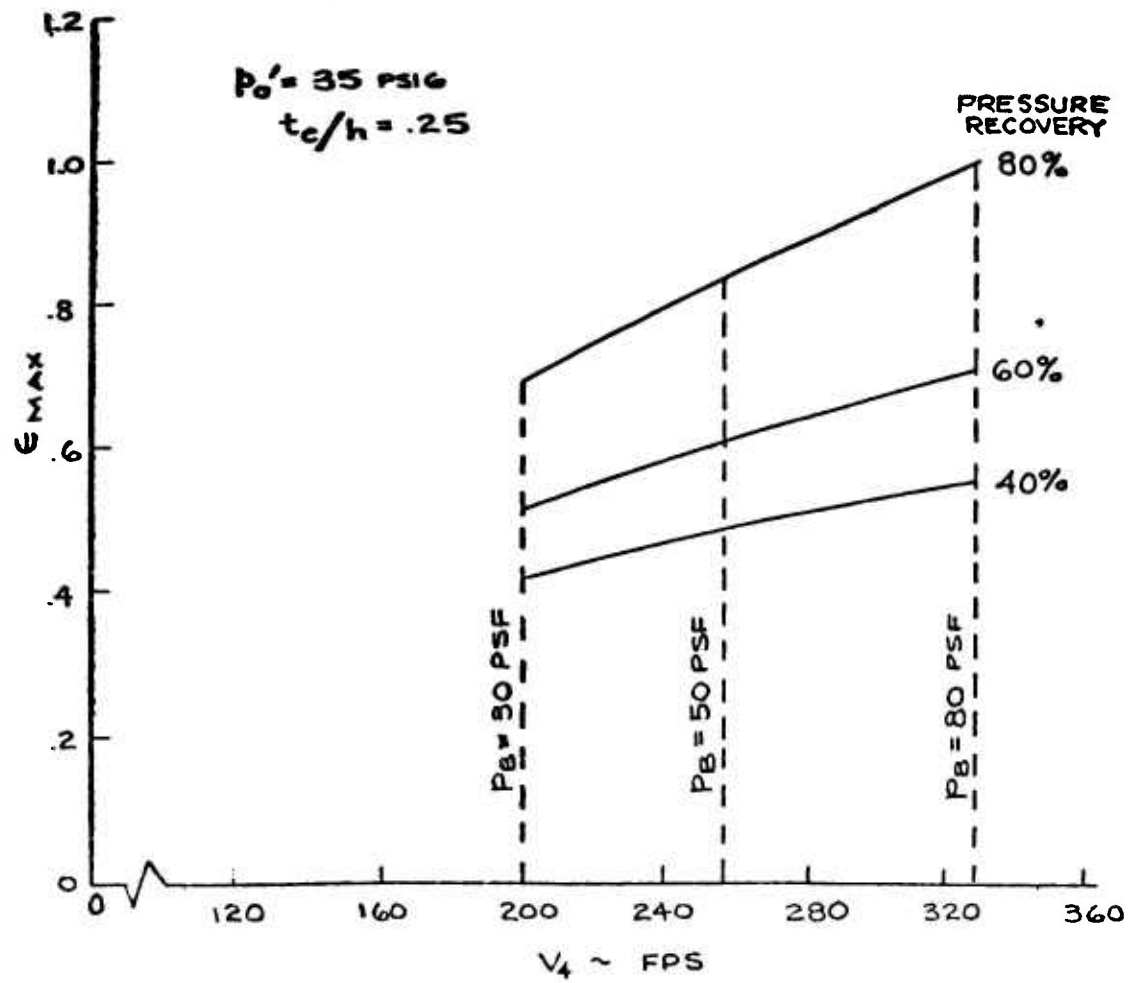


FIG. 8.3-5 TYPICAL EFFECT OF TERTIARY EXIT VELOCITY OR BASE PRESSURE ON MAXIMUM EFFICIENCY

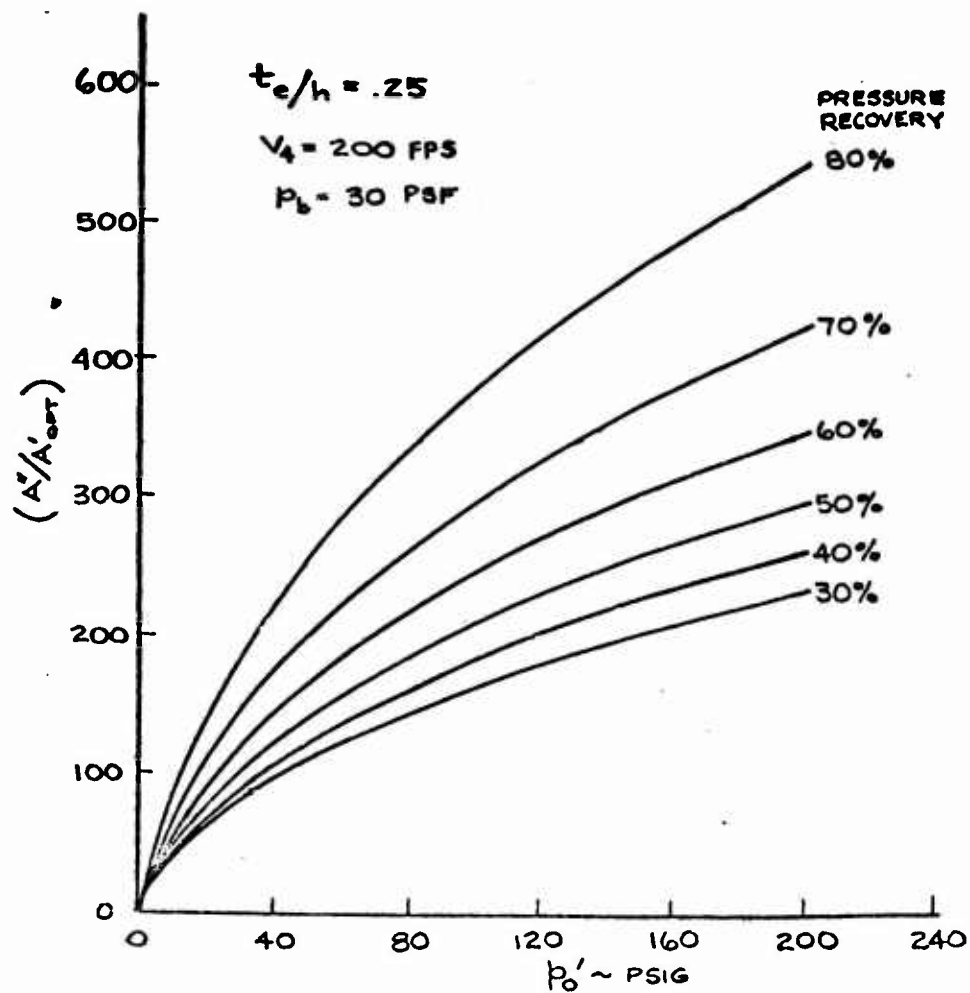


FIG. 8.3-6 TYPICAL EFFECT OF PRIMARY TOTAL PRESSURE ON OPTIMUM AREA RATIO

8.4 PROPULSION

8.4.1 Hover or Lift

The basic principles of operation of the "Ejectijet" system, as presented in previous sections, indicate that the propulsion requirements for an "Ejectijet" vehicle are substantially different than those for a conventional annular jet vehicle. Hovering with a conventional annular jet vehicle requires the propulsion system to supply large quantities of low pressure air to the annular nozzles. This is usually accomplished with a bulky system of low-pressure-ratio fans and ducting. Hovering is accomplished in the "Ejectijet" vehicle by supplying relatively small quantities of high pressure air to the ejector nozzles. A low-capacity, high pressure-ratio compressor driven by a prime mover comprises the propulsion system required by the "Ejectijet" vehicle for hover. The advantages of the latter system are readily apparent and can be summarized as follows:

1. Mechanical simplicity
2. Increased reliability and safety
3. Reduced propulsion system weight
4. Reduced propulsion system size

Only gas turbines have been considered as a power source, primarily because of their weight advantage over other conventional power plants. To obtain optimum performance for an Ejectijet GEM it will be advisable to choose a high performance gas turbine and couple it directly to a compressor with the proper flow requirements. The modular construction techniques used by most gas turbine manufacturers makes it feasible to separate or interchange the compressor unit. If it is deemed necessary to match a new combination of engines and compressor it is estimated that this development cost will be similar

or less than that for the annular jet engine-gear box-fan development. Figures 8.4-1 and 8.4-2 were used in determining the flow rate and power requirements of compressors for a broad range of Ejectijet vehicles. References 22 and 23 present a reasonably complete tabulation of the available gas turbines and compressors. Comparison of the flow requirements of a range of Ejectijet GEM's up to 60,000 pounds with the available engine and compressor units indicates no major difficulty.

Table 8.4-1 lists several engine-compressor units that are basically similar to the type proposed.

TABLE 8.4-1

Engine-Compressor Units

<u>User</u>	<u>Application</u>	<u>Engine Model</u>
Columbia Gulf Transmission Co. Clements ville, Kentucky	Compressor Station Natural Gas	J-57 Pratt & Whitney
Bethlehem Steel Corporation	Blast Furnace Compressors	J-47 Westinghouse
Texas Oil Company Dallas, Texas	Oil Refineries Cracking Process Pneumatic Source	J-47 Westinghouse
Subterranean Construction Corp. Brooklyn, New York	Pressurization of Underwater Tunnels During Construction	J-69 Continental
Boeing Aircraft Company	Boundry Layer Control - Experimental Aircraft	Model 520

A complete power plant unit for an "Ejectijet" vehicle will be comprised of an engine and a driven compressor; therefore, the weight of the driven compressor must be added to the engine weight. Contact with various engine manufacturers indicate this weight will be approximately 15% of the above referenced weights. As a result, it can be conservatively

stated that the total weight of the engine-compressor combination that will be utilized in the Ejectijet GEM should be no greater than $1/3$ lb per horsepower.

A typical example of an Ejectijet engine-compressor combination is presented in Figures 8.4-3 and 8.4-4. This specific combination delivers 1760 nozzle air HP for a unit weight of 500 lb. This corresponds to .284 lb per horsepower.

8.4-2 Forward Flight

GEM vehicles, regardless of their lift generating system, can use any of a number of possible propulsion concepts to provide forward flight capability. The Ejectijet vehicle has the unique ability, however, to utilize high pressure air from the compressor to power simple straight ejectors to generate thrust. This air can be obtained either from the excess air available from the compressor as the amount of air required to generate lift is reduced at forward speeds, or from compressors designed to provide enough air for both functions. The Ejectijet vehicle can also use the following conventional means of generating propulsive thrust

1. Air screw thrust
 - a. Turbo-prop
 - b. Piston-prop
 - c. Diesel prop
2. Jet thrust
 - a. Turbo jet
 - b. Turbo fan
 - c. Hot ejectors (using combustion products)

The selection of the power plant which meets the forward flight requirements for a specific mission normally is a function of installed weight, initial cost, and operating cost. Other considerations may influence the selection; reliability, availability, noise and vibration, plus configuration flexibility and application.

Selection of a power plant on the basis of installed weight (hardware plus fuel) can be made by analyzing the following expression:

$$\frac{W_T}{T} = \left[W_E + W_A + (S.F.C.) t \right] (P)$$

W_T = total installed weight ~ lb.

T = total thrust ~ lb.

W_E = weight of engine ~ lb/HP

W_A = weight of accessories and installation ~ lb HP

S.F.C. = specific fuel consumption ~ lb/HP min

t = operating time ~ min

P = power to thrust ratio ~ HP/lb

Specific weights and thrust are readily available for all the propulsive methods plotted except for the ejector. Figure 8.4-5 represents the specific thrust for an ejector under two conditions: (1) primary air is used directly from the compressor (curve labeled cold), (2) fuel is added in a combustion chamber to raise the temperature of the primary air prior to exhausting from the primary nozzles (curve labeled hot).

Figures 8.4-6a and 8.4-6b show graphically the expression solved for each propulsion system. The operating characteristics of each system were estimated using the best available information.

Analysis of Figure 8.4-6a indicates that for operating times in excess of one hour a turbo-prop will probably be favored from a weight standpoint. It is also obvious that as operating time increases, the piston-prop configuration becomes increasingly more attractive and due to the difference in initial cost may be favored for vehicles requiring extended operating time.

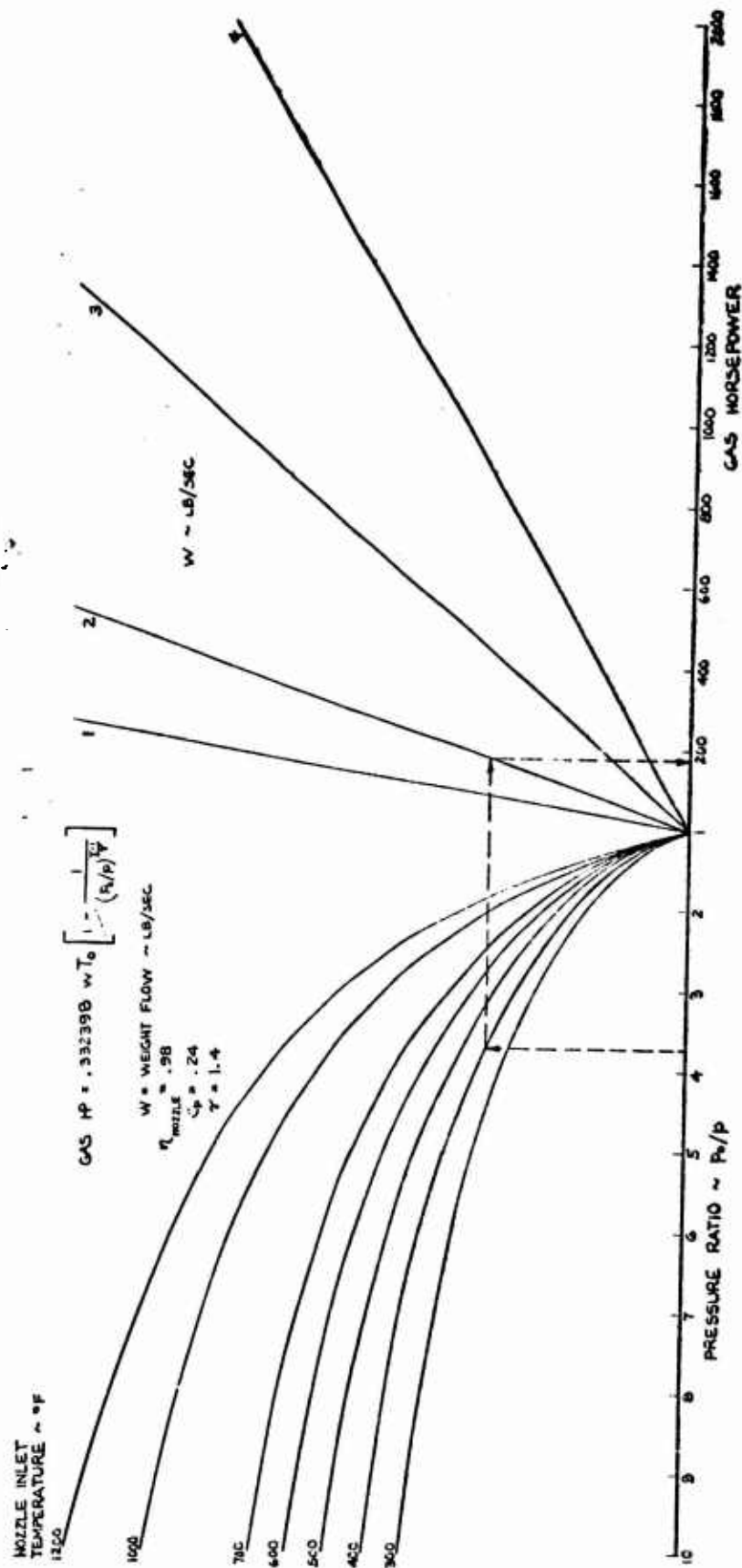
The Ejectijet GEM offers a distinct advantage over conventional annular jet vehicles in the reduction of power required to produce forward flight, especially at cruising speeds. The reduction of momentum and profile drag as discussed in Section 7.4-2 results in a significant reduction of power required to operate at cruise conditions.

8.4.3 Dash or Emergency Power Potential

It is advisable that the propulsion system of an operational GEM be able to provide power for the following functions in excess of the power needed for normal forward flight operation:

1. High speed dash capability
2. Maximum height operation (jump)
3. Grade negotiation
4. Braking

Whether this capability is integral with the forward flight propulsion system or is an auxiliary unit depends on the operational analysis of the mission. Selection of the propulsion system for emergency power requirements can again be made by use of installed weight considerations. Figure 8.4-6a indicates how the various propulsion systems compare for maximum performance, short operating time requirement. For extremely short durations both the cold and hot ejectors show distinct possibilities.



8.4-6

FIGURE 8.4-1 GAS HORSEPOWER AS A FUNCTION OF PRESSURE RATIO, INLET TEMPERATURE, AND WEIGHT FLOW

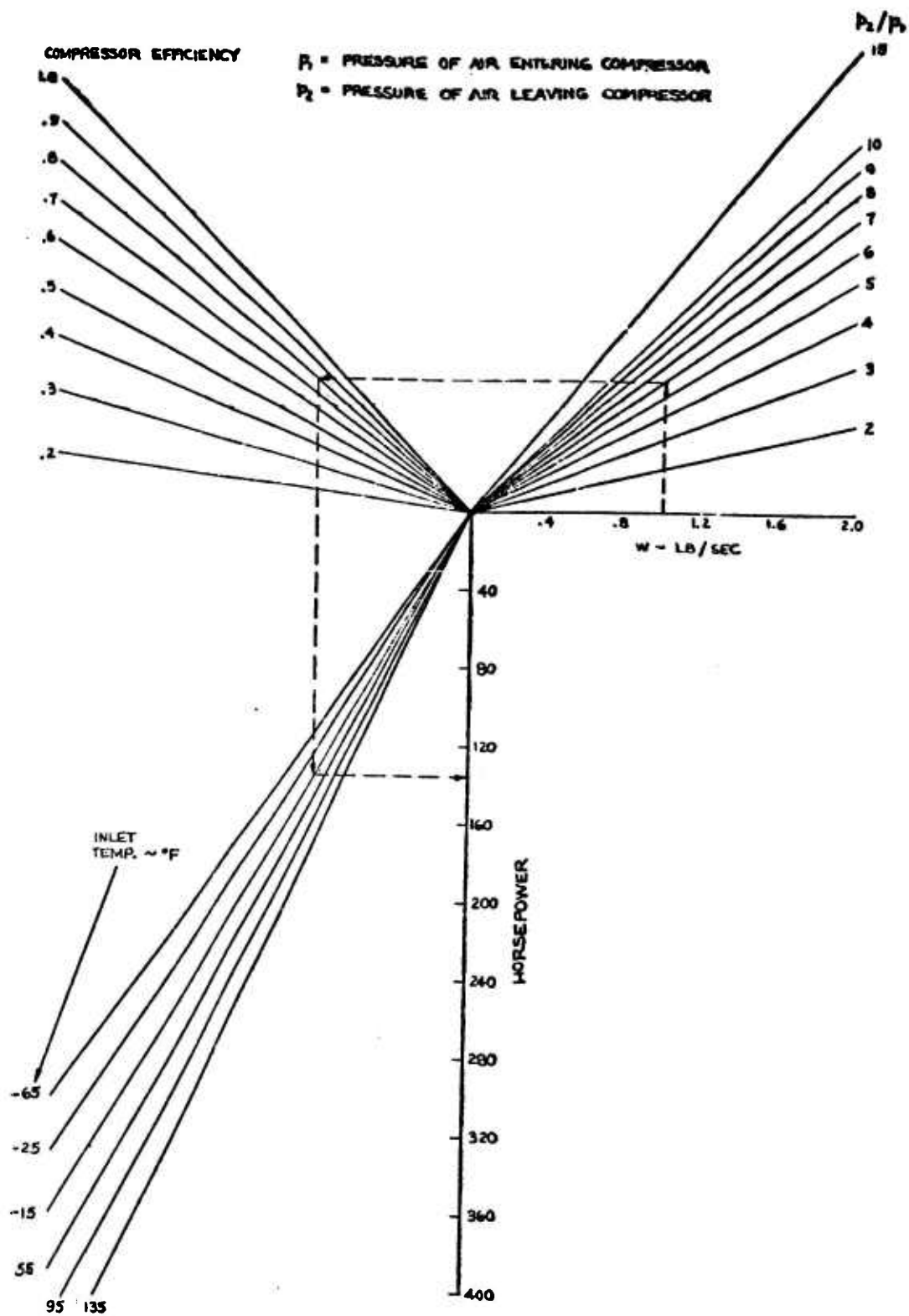


FIGURE 8.4-2 REQUIRED COMPRESSOR HORSEPOWER

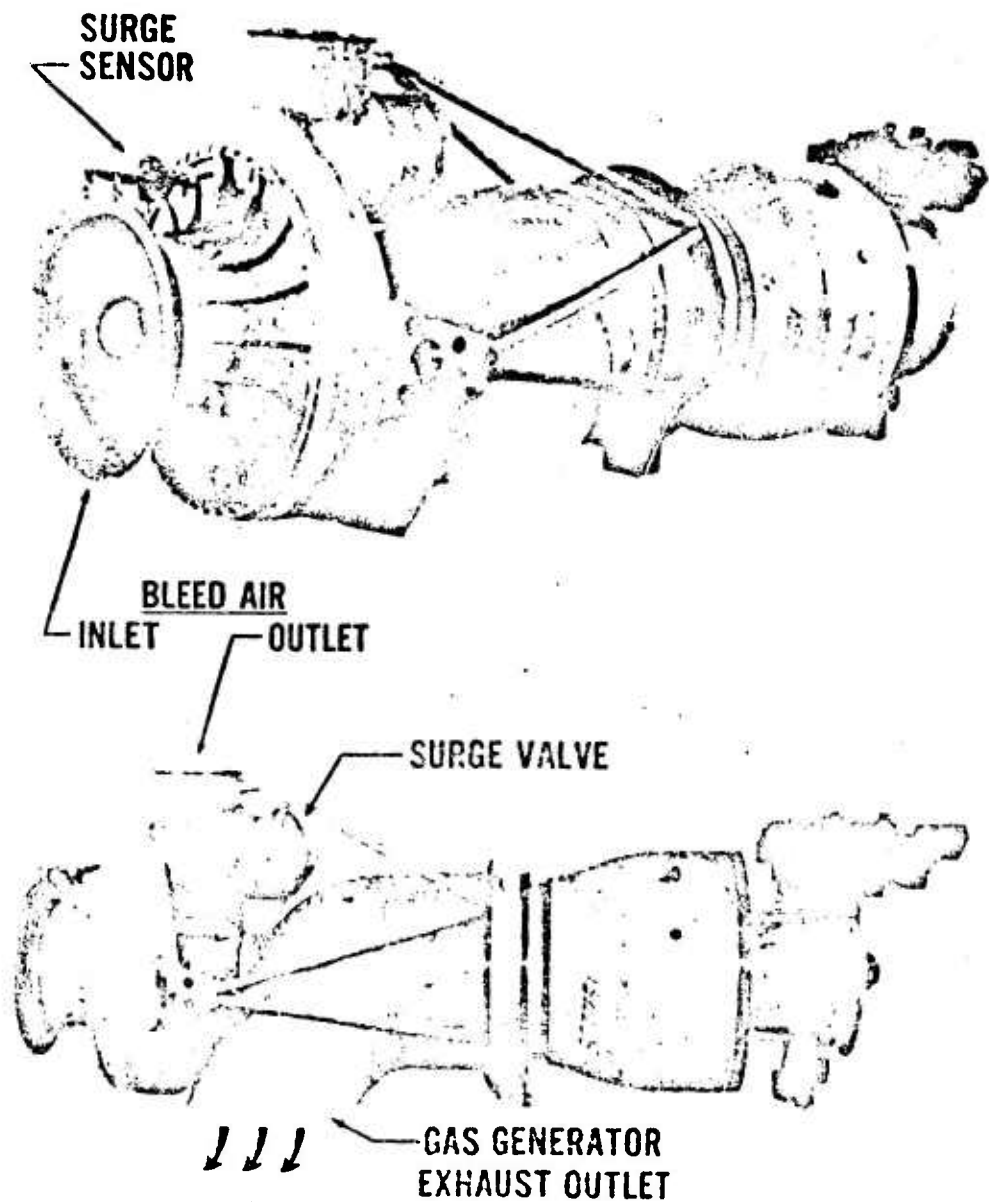


Figure 8.4-3 J69-T-35 High Bleed Pumping Engine Mockup

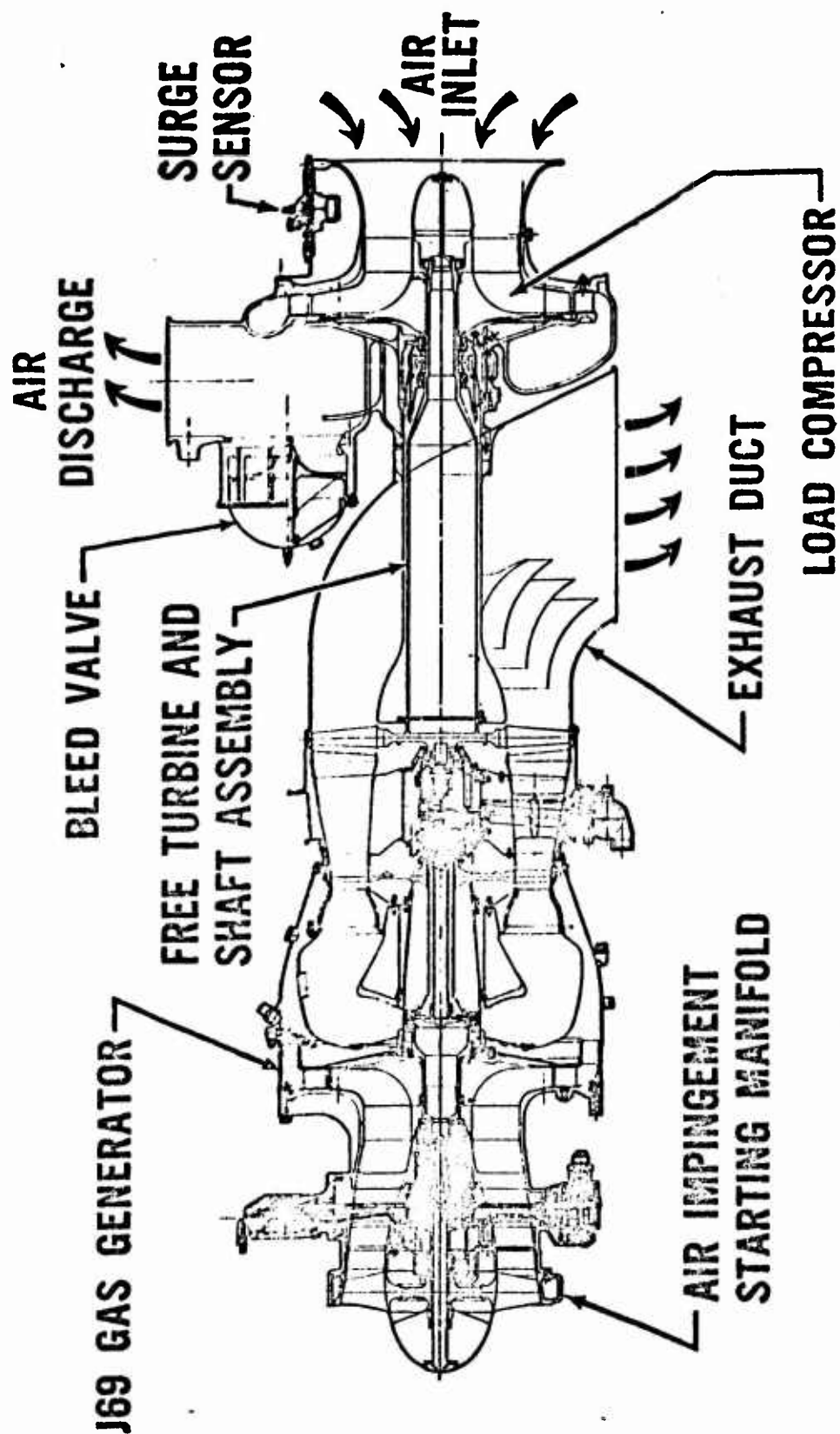


Figure 8.4-4 J69-T-35 High Bleed Pumping Engine (Cross-section)

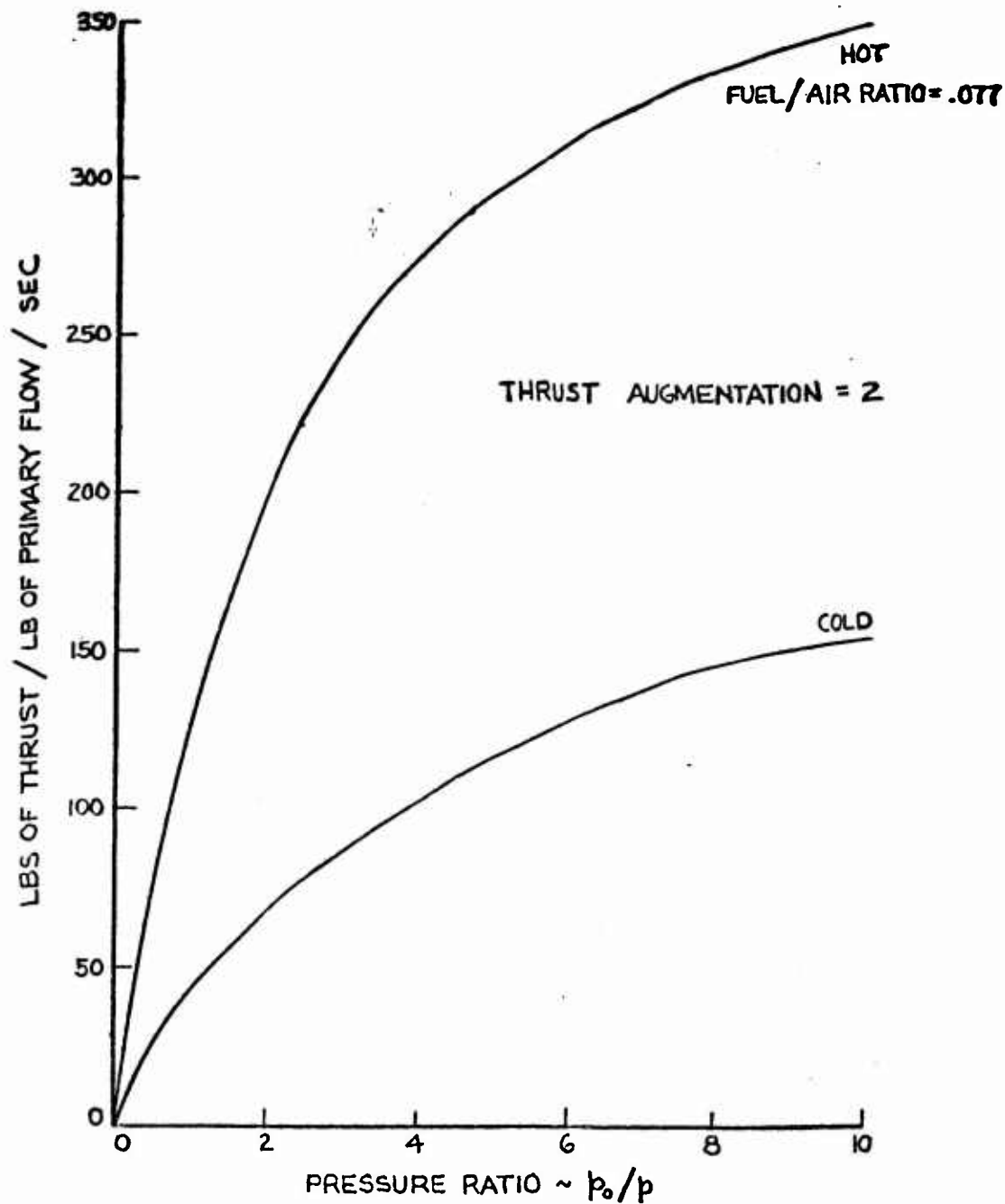


FIGURE 8.4-5 SPECIFIC THRUST AS A FUNCTION OF PRESSURE RATIO, FOR AN EJECTOR OPERATING WITH BLEED AIR AND BLEED AIR WITH AFTER-BURNING

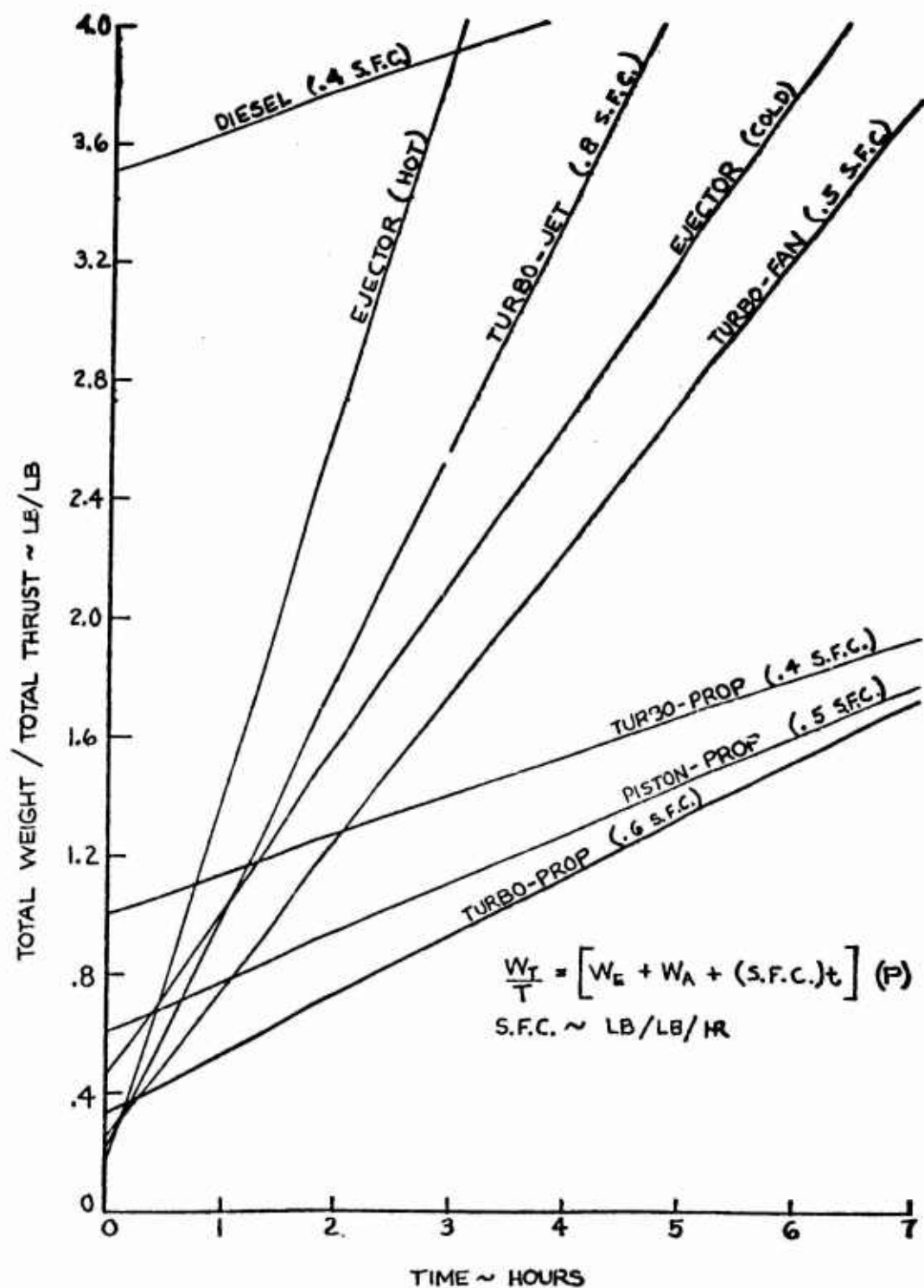


FIGURE 8.4-6a TOTAL WEIGHT (ENGINE AND FUEL) FOR VARIOUS PROPULSION DEVICES AS A FUNCTION OF OPERATING TIME

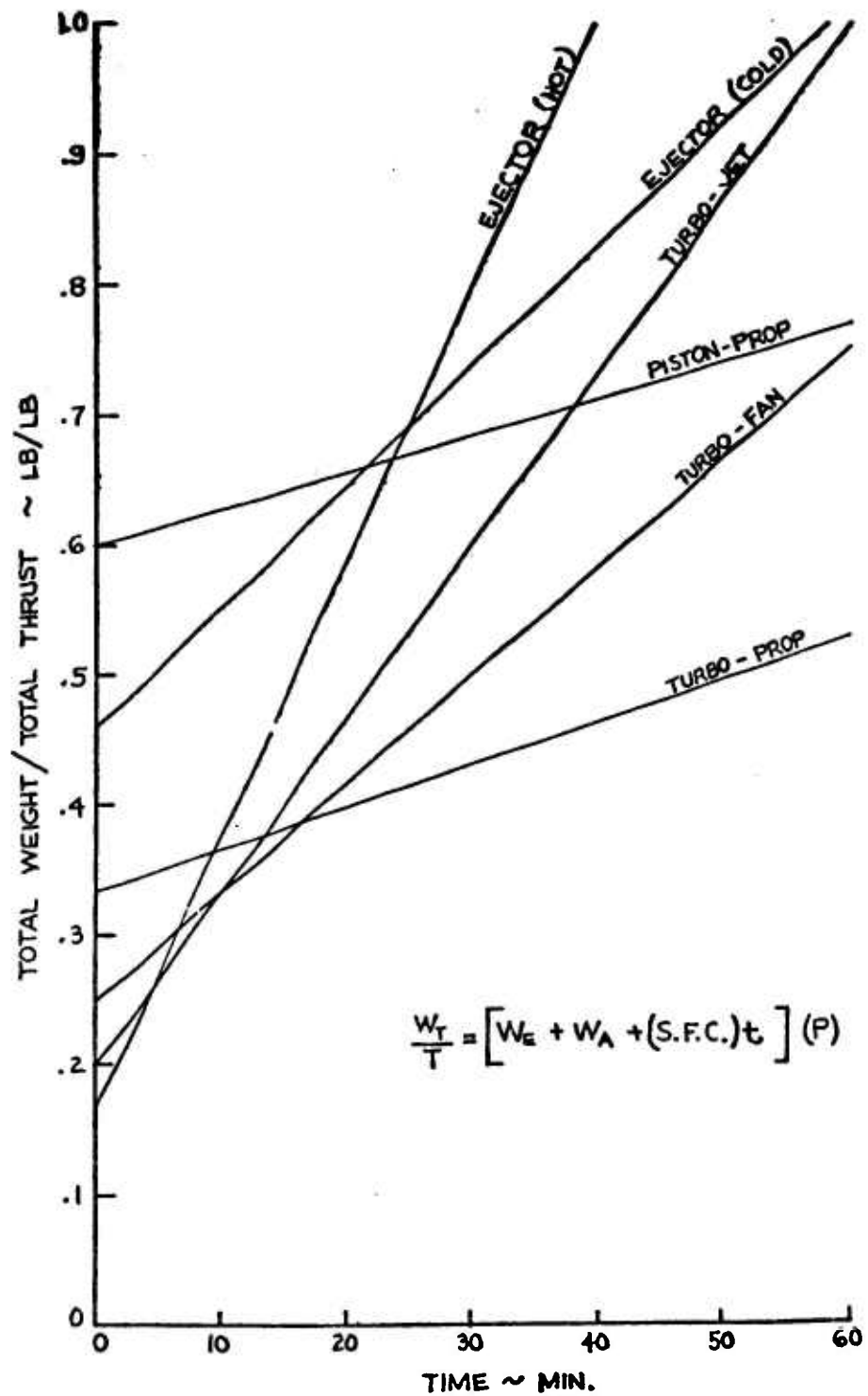


FIGURE 8.4-6b TOTAL WEIGHT (ENGINE AND FUEL) FOR VARIOUS PROPULSION DEVICES AS A FUNCTION OF OPERATING TIME

8.5 PERFORMANCE ESTIMATES

It was established previously in Section 8.1 Tabulation of Basic Equations that a performance comparison between the Ejectijet and the annular jet could not be made until their respective overall efficiency factors were determined. In Section 8.2 Component Efficiency, it was shown that overall efficiency consists of several component efficiencies. A range of each component efficiency for both concepts is given and the current best effort for overall hovering efficiency of each is listed. It was established that the total installed horsepower required to hover is presently approximately the same for both systems.

It is assumed that the overall efficiency for both concepts can be improved over the current values. Section 8.3 Recirculation Ejector indicates that it is theoretically possible to obtain significant improvements in performance for the Ejectijet. Since the efficiency values are currently comparable, it is assumed, for the following comparison, that they will also be comparable in the immediate future.

In Figure 8.5-1 the total required horsepower for the two concepts is plotted as a function of forward speed and loading parameter (L/S). The total horsepower equals the sum of the power required to support the weight of the vehicle (cushion power) plus the power required to propel it in forward flight (propulsion power). The required cushion power is reduced with increasing speed as the lift from the top surface of the vehicle increases. In addition, for the annular jet, input power requirement to the lift fans is reduced by ram recovery in forward flight. A negligible recovery will be realized for the Ejectijet due to much lower mass flow required. For both concepts

the propulsive power increases with forward speed although, as discussed previously in Section 7.4 Forward Flight, the total drag of the annular jet vehicle will be considerably larger than for the equivalent Ejectijet vehicle.

The hovering power advantage enjoyed by the Ejectijet vehicle is due in part to the lack of power required for stability (base compartmentation not required) but is mainly due to the higher momentum lift which is obtained by turning the main curtain jet through approximately 180° . This gives a momentum lift component approximately equal to $J(\sin \theta_1 + \sin \theta_2)$ for the Ejectijet vehicle while the comparable annular jet momentum lift term is $J \sin \theta_2$. The Ejectijet momentum lift is thus seen to be twice that of the annular machine for the same jet angle ($\theta_1 = \theta_2$). The resultant Ejectijet hovering power advantage varies from 15 percent for a loading of 20 psf to 25 percent for a loading of 80 psf. Thus increased loading parameter values (loading parameter is approximately equal to base pressure) increases the relative advantage of the recirculation concept (total gross weight fixed at 60,000 lbs) as well as reduces the overall size of the vehicle.

For a loading of 20 psf both vehicles will be very large. The shapes of the curves are influenced by decreased cushion power and increased propulsive power as forward speed increases. This results in a minimum power requirement at 50 to 60 mph.

At a loading parameter of 80 the hovering horsepower for both machines is higher because of the increased cushion power required to sustain the higher base pressure. For the annular jet, power initially decreases slightly with forward speed and then levels off at approximately 95% of the hovering power. The Ejectijet power-required curve decreases with forward speed until at 100 mph the total power

required is 86% of the hovering power and has not yet reached a minimum. At some speed greater than 100 mph the profile drag power would become predominate and the required power would rise, eventually becoming greater than the hovering power. The initial decrease in the power required is due to aerodynamic lift on the top surface.

The relative effects of the factors influencing the required installed horsepower are summarized in the following table:

	<u>Low Base Pressure</u>		<u>High Base Pressure</u>	
	<u>Annular</u>	<u>Ejectijet</u>	<u>Annular</u>	<u>Ejectijet</u>
Cushion power				
Aerodynamic lift	Effective	Effective	Less effective	Less effective
Ram recovery	Effective	Negligible	Less effective	Negligible
Propulsion power				
Profile drag	High	High	Low	Low
Momentum drag	High	Low	High	Low

The power loading as affected by loading parameter (base pressure) is shown in Figure 8.5-2. Again similar assumptions have been made for both concepts. The vertical and horizontal cross-hatched lines represent limiting conditions which arise from practical considerations. To be economically feasible a GEM should have a power loading in excess of 10 lbs per horsepower. Several factors indicate that higher base pressures must be designed for that is the current trend. One of the most important of these is the size of the vehicle. It is considered that the base pressure should be greater than 30 psf. Within these confines it is apparent that a 60,000 lb gross weight annular GEM would just meet minimum requirements while the Ejectijet exceeds the minimum acceptable power loading for loading parameters of 30 to 50 psf.

The superior performance of large machines is illustrated by the curves for a 300,000 lb vehicle which indicate that power loadings as high as 20:1 are attainable utilizing the Ejectijet recirculation concept. A definite advantage for the Ejectijet concept in terms of power loadings is apparent throughout a wide range of loading parameters both in hover and forward flight.

From Section 8.4 Propulsion, it was determined that the Ejectijet power source would weight approximately 1/3 pound per horsepower. By comparison, the equivalent engine-gear box-fan weight for the annular jet has been estimated at from 2 1/2 lb/HP (Reference 24) to 1 1/2 lb/HP. Part of this discrepancy involves defining the amount of weight chargeable to the fan supports and housing since they may also be structural members. To illustrate the importance of this weight differential, the following table shows a weight breakdown for comparable vehicles.

	<u>Annular GEM</u>	<u>Ejectijet GEM</u>
L/S (Assumed)	30 psf	30 psf
L/P _T (Fig. 8.5-2, V _∞ = 60 mph)	10.2	14.5
P _T (L = W _T = 60,000 lb)	5,880 HP	4,140 HP
Engine weight	11,760 lb (2 lb/HP)	1,380 lb (1/3 lb/HP)
S (L = W _T = 60,000 lb)	2,000 ft ²	2,000 ft ²
Structural weight (7 psf)	14,000 lb	14,000 lb
Fuel weight (200 mile range, V _∞ = 60 mph, S.F.C = 0.6)	11,760 lb	8,280 lb
Miscellaneous weight (.1 W _T)	6,000 lb	6,000 lb
Payload	16,480 lb	30,340 lb
L = W _T	60,000 lb	60,000 lb
<u>Payload</u> Horsepower	2.8 lb/HP	7.33 lb/HP
<u>Payload</u> Gross weight	27.5 %	50.6%

$L = 60,000 \text{ LB}$ $\theta = 30^\circ$ $S_b/S_{TOT} = .70$ $C_{Df} = .074$
 $C_{D_{mom}} = 1.0$, $t_e/h = .25$, $h = 3 \text{ FT}$, ELLIPTICAL PLANFORM ($a/b = 1.5$)

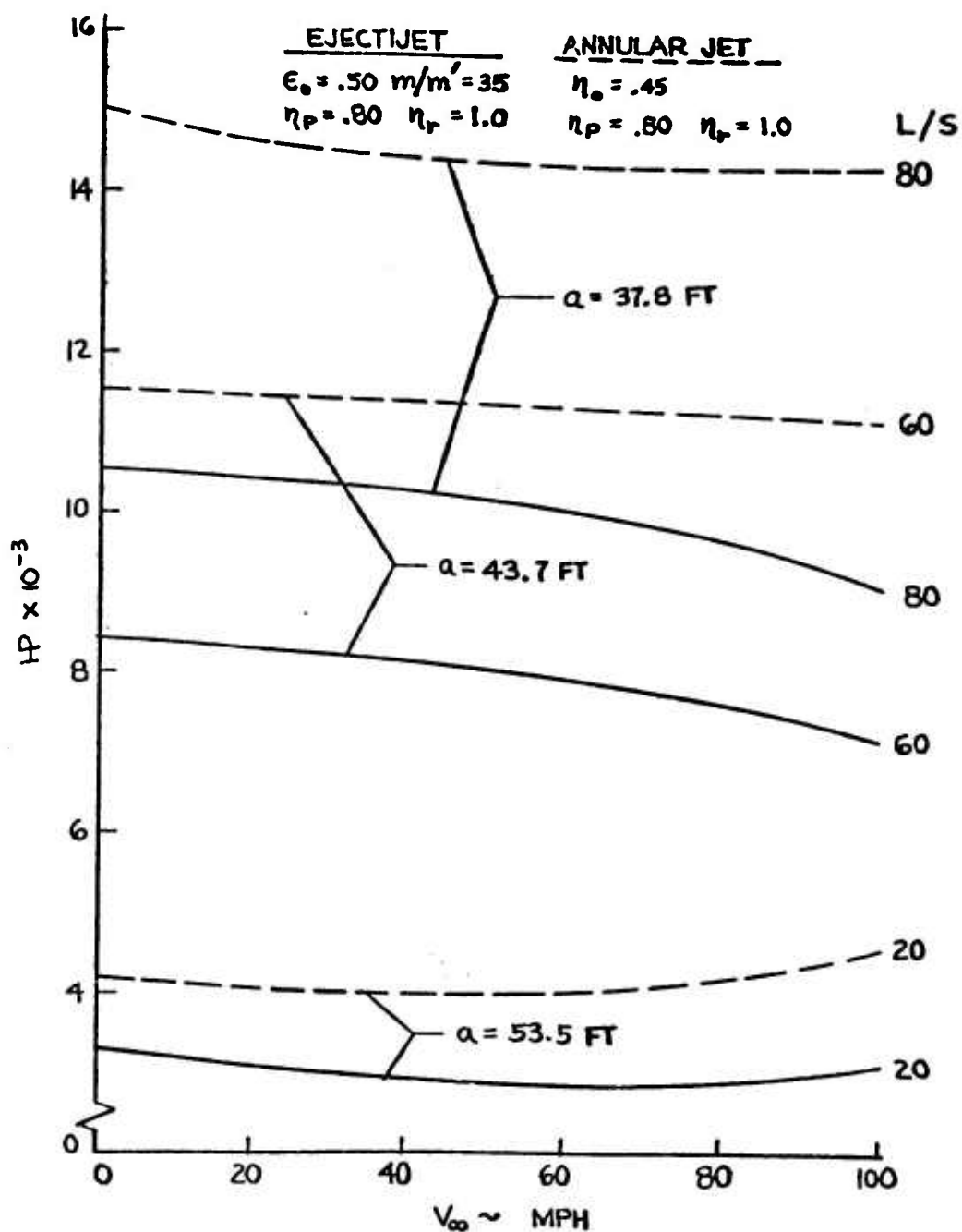


FIGURE 8.5-1 FORWARD FLIGHT PERFORMANCE

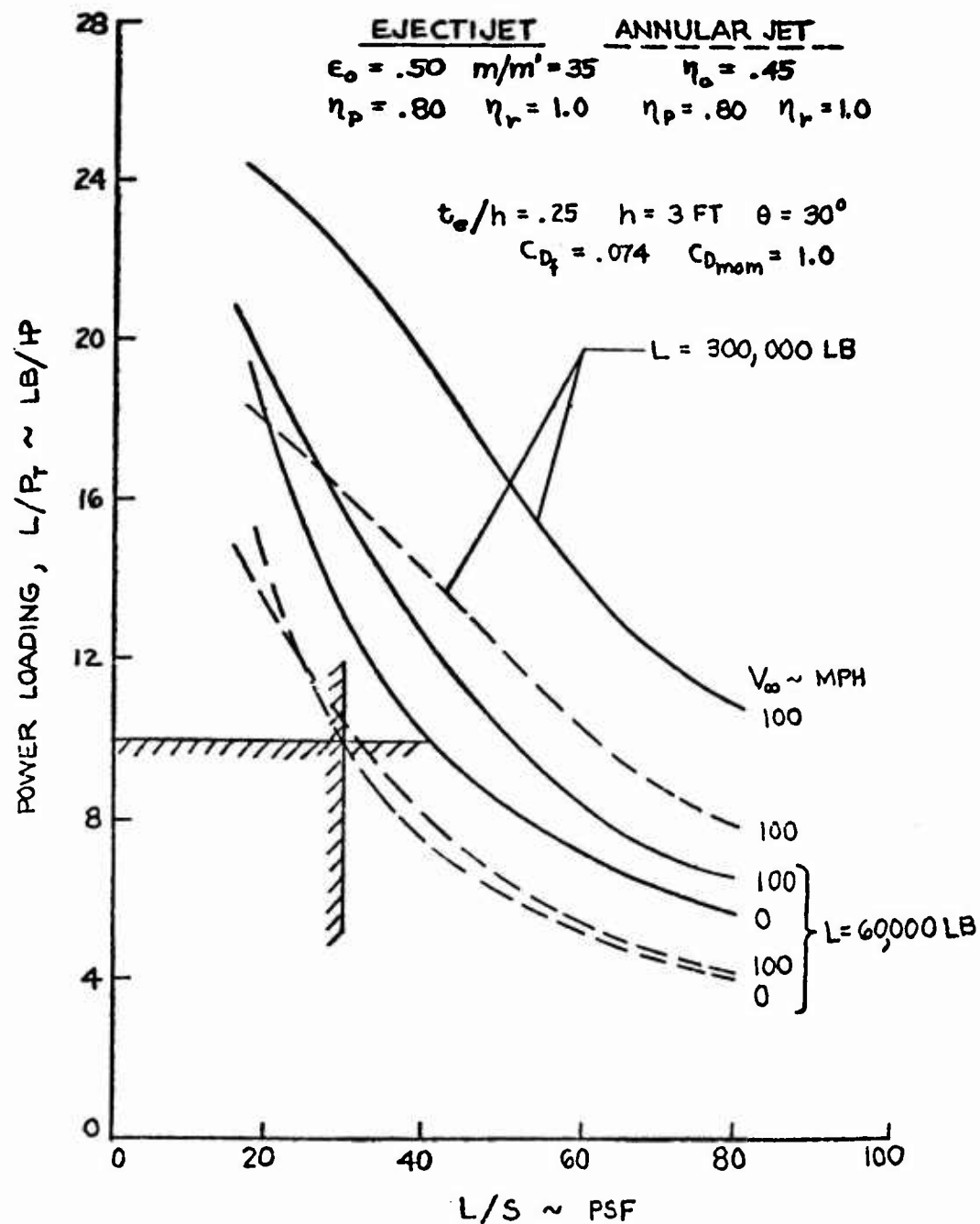


FIGURE 8.5-2 PROJECTED GEM PERFORMANCE

8.6 OPERATIONAL AND ENVIRONMENTAL CONSIDERATIONS

8.6.1 Dust and Spray Suppression

One of the fundamental operational problems affecting the practical applications of the ground effect machine is the generation of dust and spray by the lift-producing curtain. The problem is of such severity in vehicles using the conventional annular jet principle that the logistical performance of the vehicle is impaired. A GEM utilizing the recirculating-ejector principle for generating lift has distinct advantages over conventional GEM's in the suppression of dust and spray which can be summarized as follows.

The GEM using the recirculating-ejector develops the same base pressure as an annular jet GEM with similar curtain energy, but maintains approximately 95 percent of the jet flow recirculating within the system. Only approximately 5 percent of the jet curtain leaves in the manner of the annular jet. Dust and spray generation is therefore reduced by an order of magnitude.

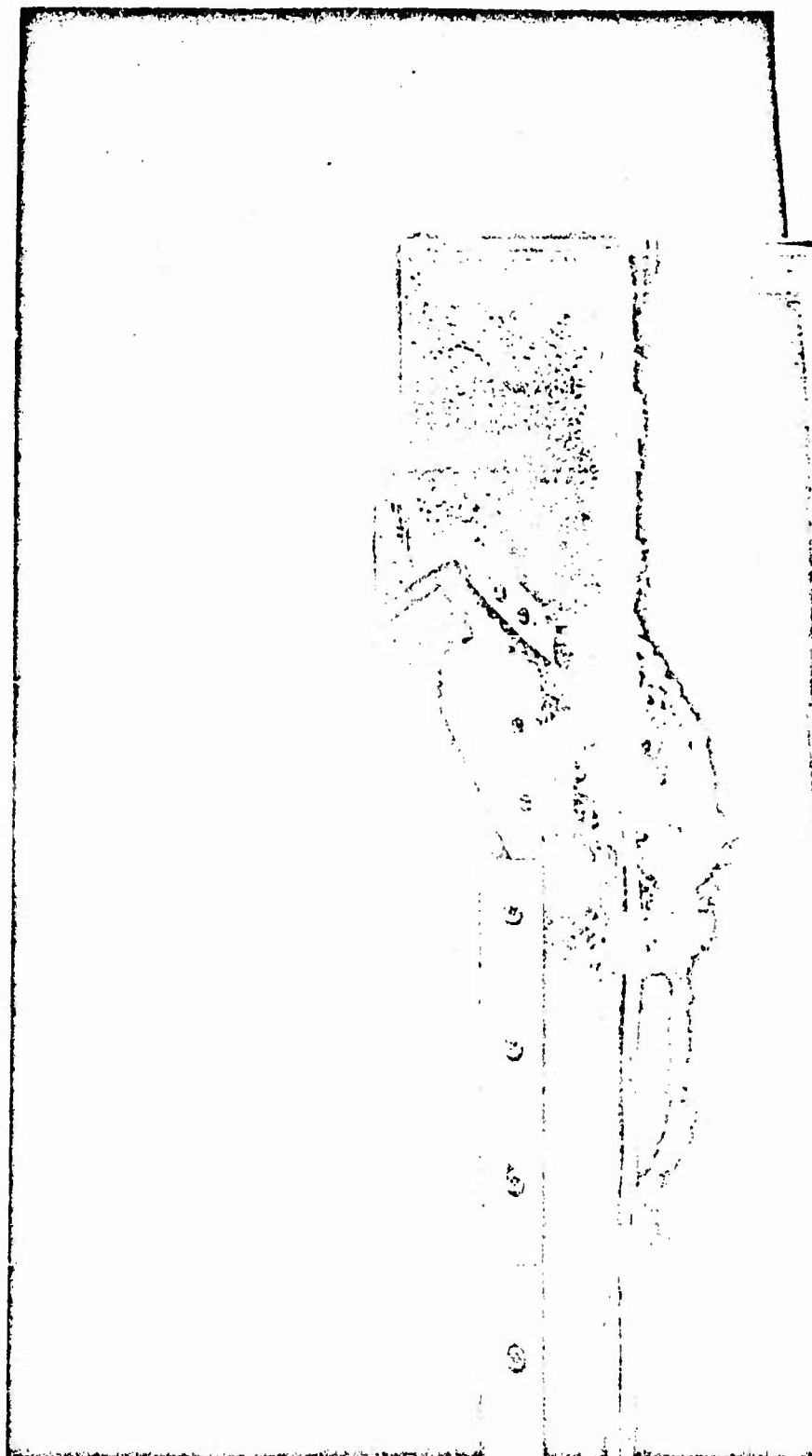
The recirculating-ejector GEM's air intake is approximately 5 percent of that required by the comparable annular jet. Since the recirculating-ejector GEM generates only a fraction of the dust or spray of the annular jet vehicle, the damage potential to the propulsion system by the ingestion of generated dust or spray is virtually non-existent.

The only area in which ingestion of debris might be a problem is in the ejector itself. However, the absence of fans, vanes, and other

obstructions reduces the problem to that of corrosion and/or erosion of the ejector surfaces.

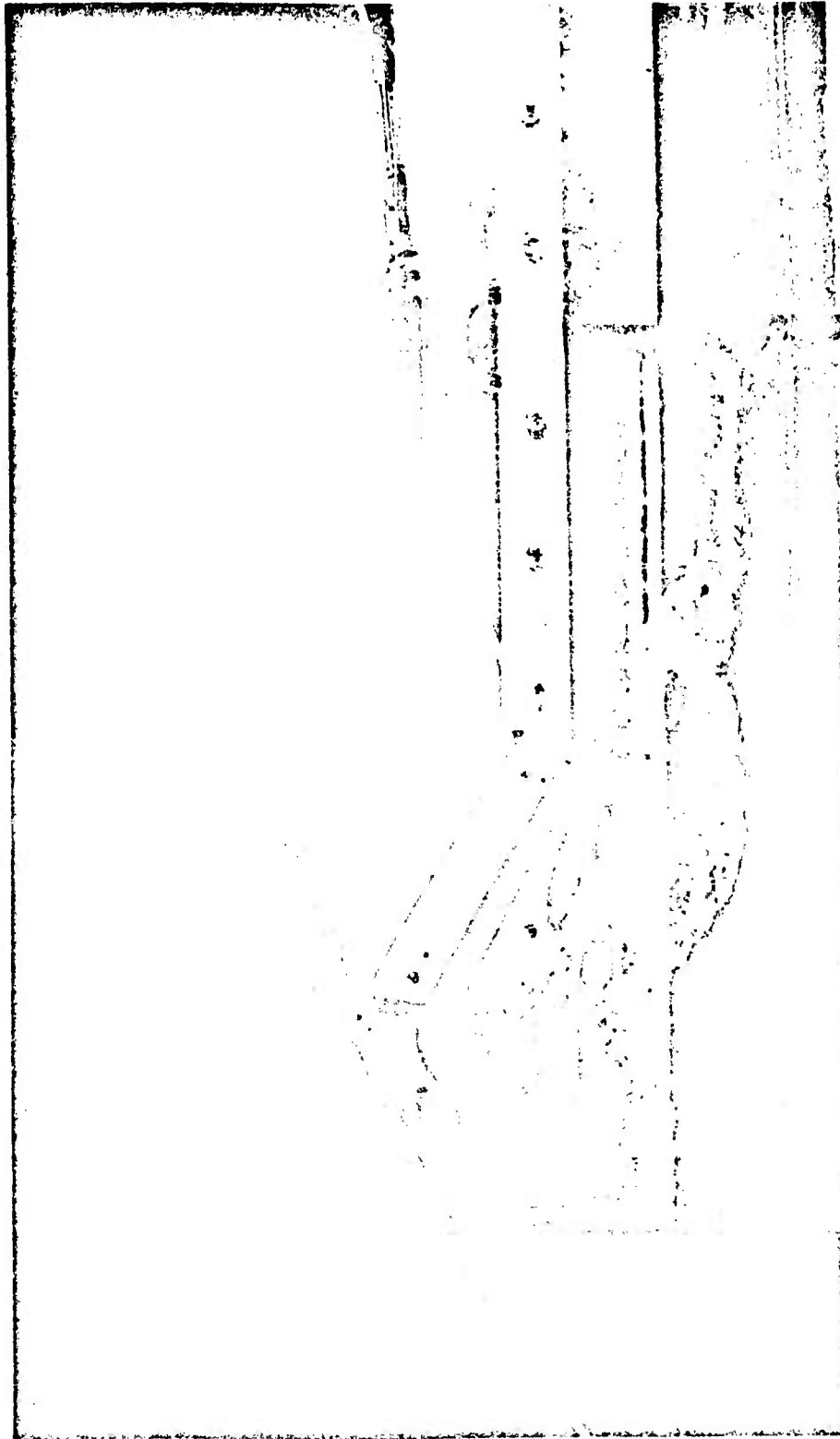
A small two-dimensional model to compare the spray generation of the conventional annular jet system and the recirculating-ejector system was built and tested. The annular jet portion was simulated by a simple straight ejector with the tertiary flow directed at an angle of 60 degrees from the horizontal. The recirculating ejector had an exit angle of 30 degrees. The ejectors for each were designed to give approximately the same tertiary mass flow and velocity and generate approximately the same base pressure. This test demonstrated the advantage of the recirculating-ejector system over the annular jet system with respect to spray generation. As shown in Figure 8.6.1-1, the flow pattern created by the annular jet was very turbulent. The creation of large amounts of spray is indicated by the abundance of droplets deposited by the stream on the tank walls and the surrounding area. The recirculating ejector configuration, as shown in Figure 8.6.1-2, exhibited a much smoother flow pattern beneath the system. It also revealed a significant reduction in spray as shown by the absence of droplets on the tank walls.

The severity of the problem of spray and dust generation by annular jet vehicles has been discussed in GEM literature and graphically illustrated by the operational testing of existing vehicles. The minimization of this problem can be accomplished with a recirculating ejector system thus enhancing the potential of GEM's for military and commercial applications.



3.6-3

Figure 3.6.1-1 Two-Dimensional Annular Jet Water Test



8.6-4

8.6.2 Noise

8.6.2.1 Measurement Procedure

In order to measure the noise generated by the recirculating ejector system, an acoustic survey was performed on both straight ejectors and recirculating ejectors. The measurements were made with a Bruel and Kjaer condenser microphone type 4134 (Figure 8.6.2-1). They were recorded and analyzed on a Brüel and Kjaer audio frequency spectrometer type 2311 (Figure 8.6.2-2) with a 50 db potentiometer.

For the straight ejector system measurements were made at 12 locations (Figure 8.6.2-3 shows the microphone locations). With the exception of stations 5 and 10, the primary pressure used was 100 psig. At stations 5 and 10 pressures of 40, 70, 85.3 and 100 psig were used.

Figure 8.6.2-4 shows the microphone locations used in the recirculating ejector acoustic tests. Measurements were made at five locations for primary pressures of 40 and 100 psig. Location 1 is representative of a pilot's position with respect to the side ejectors of a small GEM.

It should be mentioned that the test facility was located in a region of high background noise level with many reflecting surfaces nearby. This condition is manifested to an undeterminable degree in the data presented even though the background noise level was measured.

8.6.2.2 Analytical Studies

The primary nozzles used in the straight and recirculating ejectors are supersonic and comparable to rocket nozzles. As is the case for

or turbo-jet engines, the noise of the ejector is generated by the turbulent mixing of the high velocity primary air with the low velocity surrounding medium. This mixing occurs downstream of the primary nozzle and creates quadrupoles of noise in the turbulent mixing area of the shear zone. Theoretical investigation of this type of noise generation was carried out in Reference 25. It was determined that the sound power varied as a function of density squared, turbulent eddy size squared, and the eighth power of the nozzle stream velocity. The square of the turbulent eddy size was found to be directly proportional to the nozzle area. This can be expressed in equation form by

$$PWL = 10 \log_{10} \left[\frac{\rho_j^2 A v^8}{\rho_a c_a^5} \right] + 85 \quad (8.6-1)$$

where PWL = Sound power referenced to 10^{-3} watts

ρ_j = Density of the nozzle stream

ρ_a = Density of the surrounding medium

A = Exit area of the nozzle

v = Relative velocity of the nozzle stream

c_a = Speed of sound at ambient conditions

This relationship correlates well with subsonic cold air nozzle data. However, agreement is lost when correlated with supersonic nozzles and hot flows. Further investigation reported in Reference 26 indicated that sound power can be expressed as a function of the kinetic energy of the nozzle stream. This results in the following expression for sound power level

$$PWL = 78 + 13.5 \log_{10} \left[\frac{1}{2} \rho v^2 \right] \quad (8.6-2)$$

When equation (8.6-2) was applied to the primary nozzles of model 3 straight ejector, the predicted power level was 128.9 db which agrees quite well with the measured value of 129.4 db.

The frequency of the noise must also be determined to give an indication of how it will affect human beings and materials, as well as how it will attenuate through its path of travel. In Reference 26 it was found that the spectrum of the noise had a relationship between the frequency, speed of sound at the nozzle, and the nozzle exit area. This relationship is demonstrated in Figure 8.6.2-5. Figure 8.6.2-6 shows the predicted sound spectrum and several typical spectrums from the straight ejector nozzles. The measured power levels below a frequency of 1000 cps is mostly background noise and the nozzle noise level is below this value; however, without an elaborate test set-up, it was impossible to record the actual low frequency noise. The agreement between the actual spectrum and the predicted spectrum is considered satisfactory.

8.6.2.3 Discussion of Data

8.6.2.3.1 Straight Ejector

The basic straight ejector acoustic data is presented in Figures 8.6.2-7 through 8.6.2-10. In reviewing the acoustic data for the straight ejector it was found that a predominant 10,000 cps pure tone existed for primary pressures of 70, 85.3 and 100 psig. At 40 psig the pure tone component did not exist (Figure 8.6.2-11) and the sound power level was approximately 20 db lower. Subsequent investigation of this phenomenon indicated that at the higher primary pressures this nozzle design was creating an edge tone of noise which could be eliminated by proper design of the nozzle. (For example, increasing the internal surface area of the nozzle is effective.) It was further noted that the straight ejector with or without the vertical baffles had the same acoustical characteristics and approximately the same noise level (Figure 8.6.2-8) but the removal of the shroud increased the acoustical power level and the noise approached the calculated frequency spectrum (Figure 8.6.2-6).

8.6.2.3.2 Recirculating Ejector

The basic results of the sound power measurements performed on Model 3 recirculating ejector are presented in Figures 8.6.2-12 and 8.6.2-13. Conclusions drawn from Figure 8.6.2-14, which compares the acoustic level of the Model 3 recirculating ejector with the primary nozzles used in Model 3 straight ejector, must be tempered by the following considerations.

- a. The mass flow of the straight ejector nozzles was approximately twice that of the recirculating ejector nozzles.
- b. The microphone location used for the straight ejector measurements was approximately twice as far from the nozzles as the microphone location used for the recirculating ejector.

With these facts in mind Figure 8.6.2-12 shows that the noise level of the recirculating ejector was approximately 6 to 10 db lower at a primary pressure of 40 psig. Figure 8.6.2-12 also shows that the 10,000 cps peak still existed at $p_o' = 100$ psig but its intensity was 10 db lower than the straight ejector. This reduction in sound level is not unexpected since the 180° turn of the recirculating ejector should reduce straight line radiation of noise.

At a representative pilot's location the noise level at $p_o' = 40$ psig is within the damage risk criteria as shown in Figure 8.6.2-15. These criteria were set forth by the U. S. Army Ordnance Human Engineering Laboratories, Aberdeen Proving Ground, for a male person under 30 years of age who works 8 hours per day and is expected to spend six years in military service.

8.6.2.4 Conclusions

The recirculating ejector is a satisfactory device from an acoustical standpoint if the operating primary pressure is less than or equal to 40 psig. This condition allows the operation of the vehicle by the

same man for 8 hours a day without heavy damage risk. For a vehicle with enclosed cockpit the noise levels at the operator's position will still be lower. If more stringent noise requirements are imposed it is possible to use perforated ducting in the recirculating ejector thus providing some noise reduction by absorption and resonant chamber reaction.

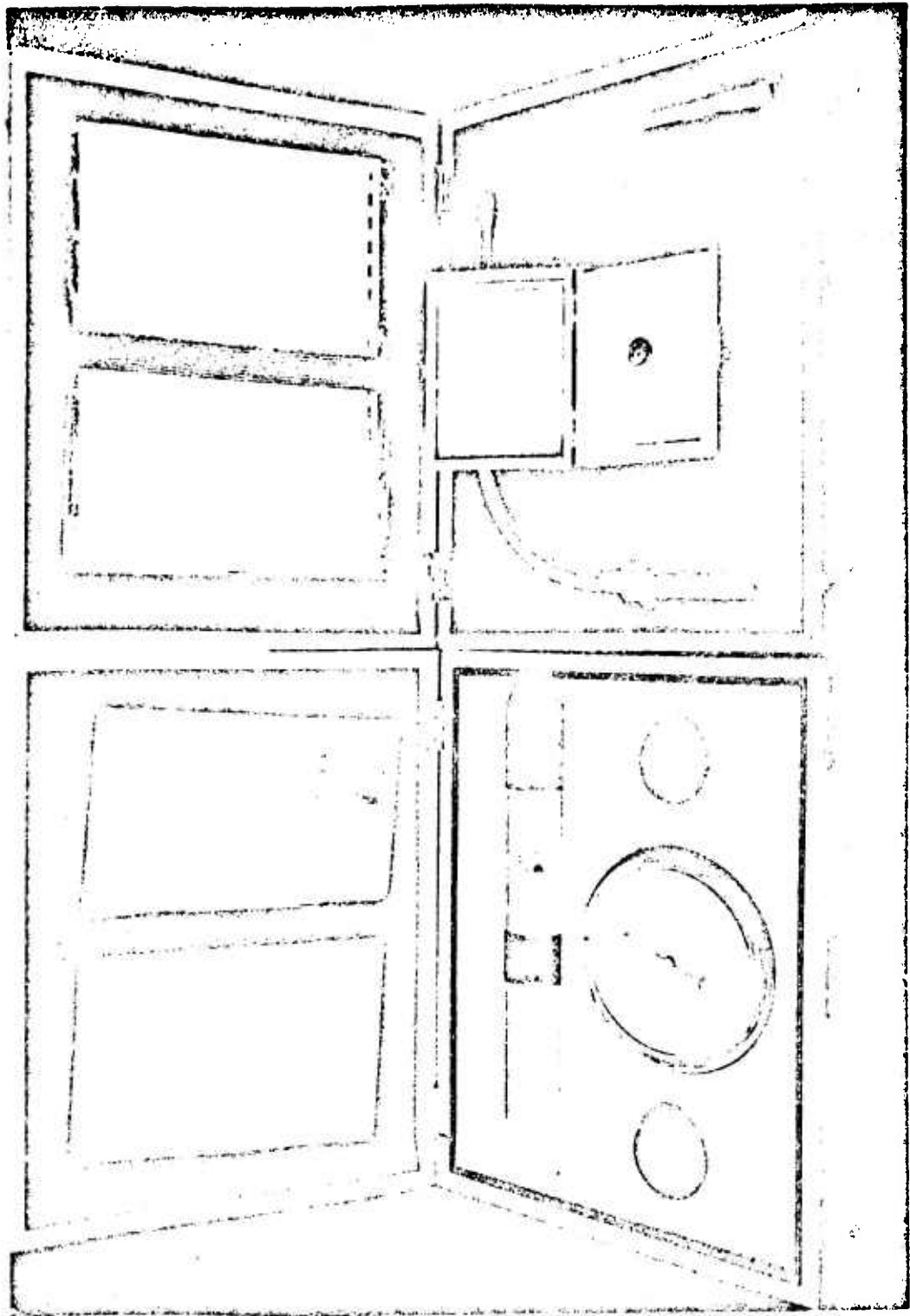


Figure 8.6.2-1 Condenser Microphone

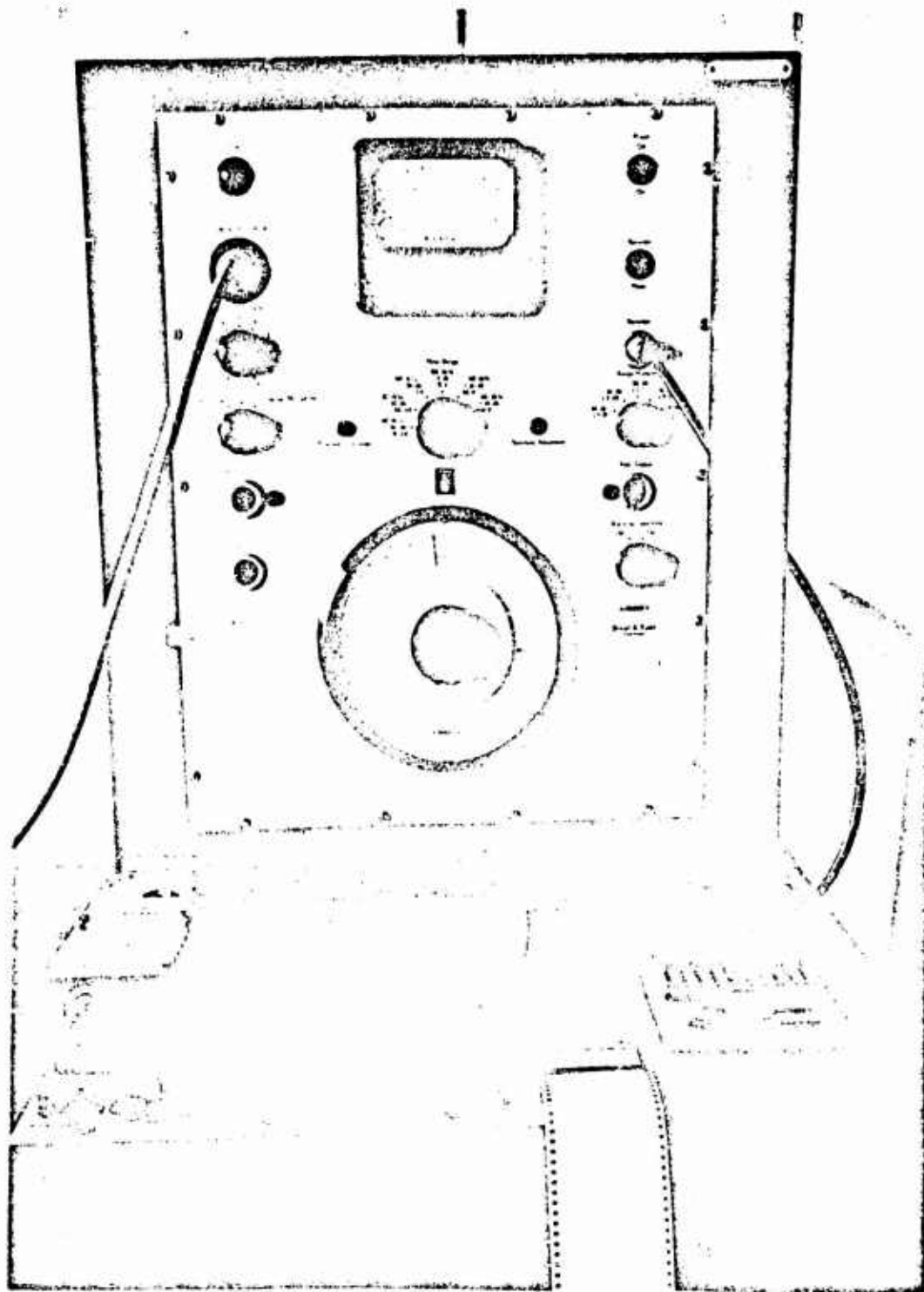
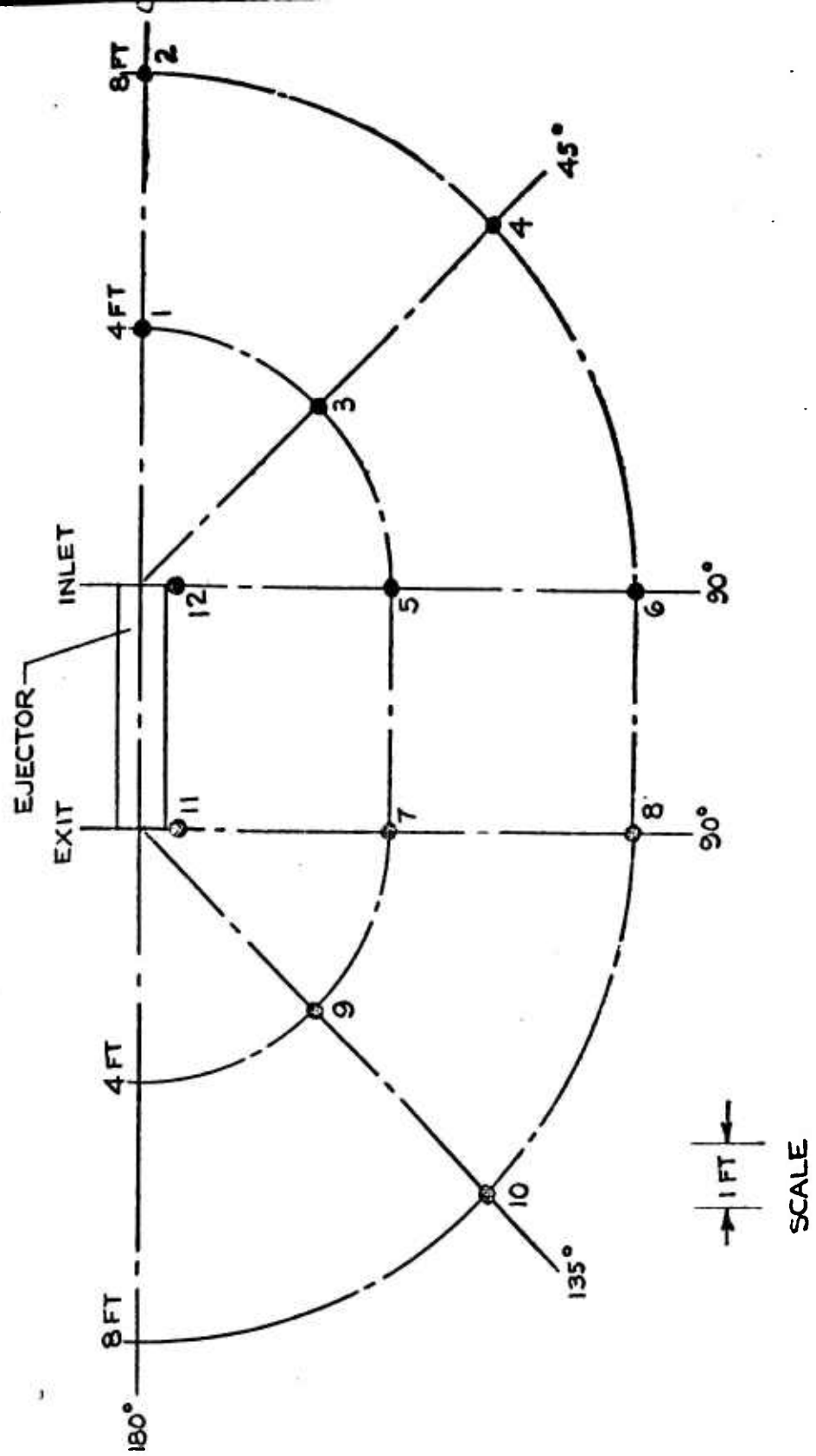
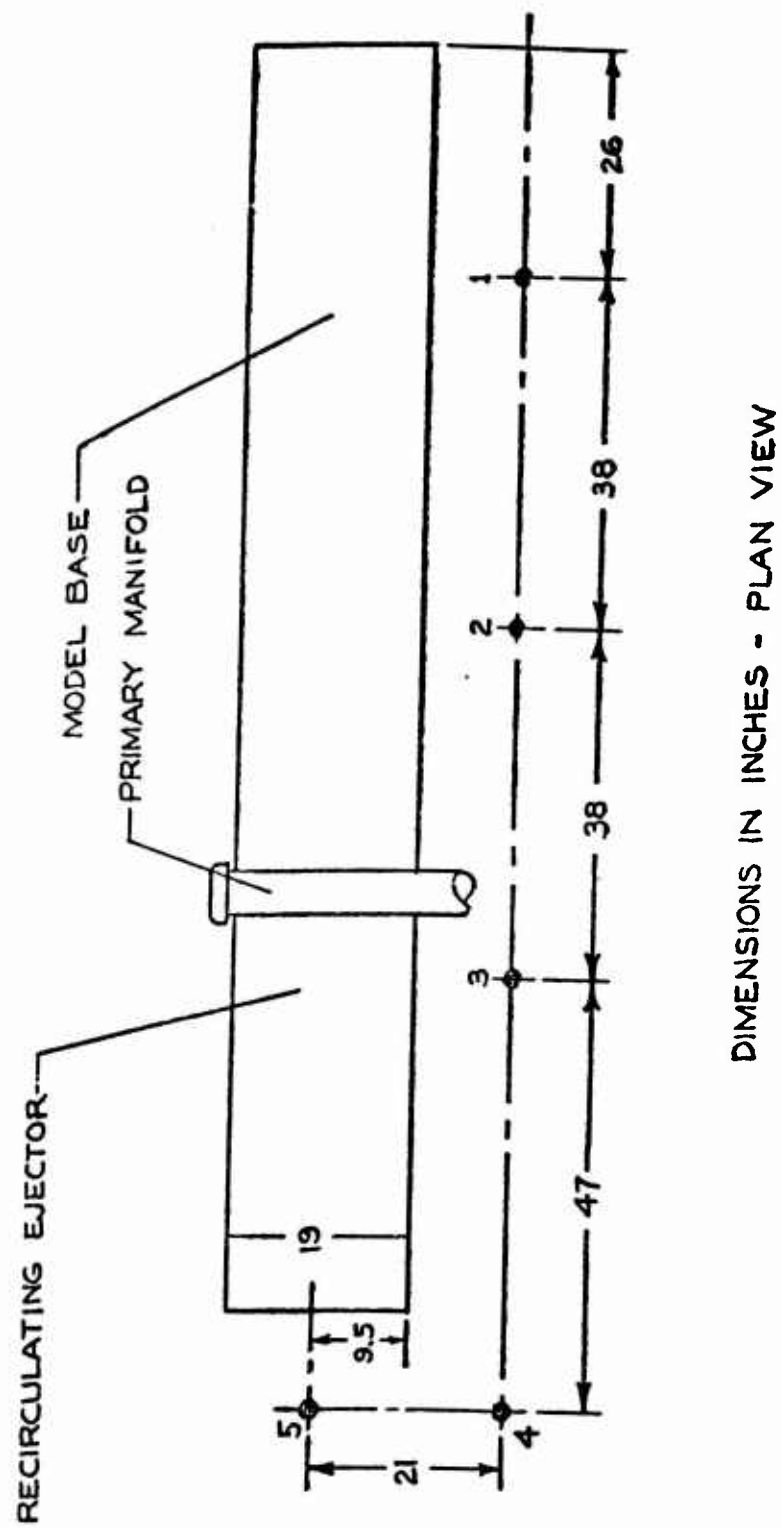


Figure 3.6.2-2 Audio Frequency Spectrometer



8.6-12

FIGURE 8.6.2-3 MICROPHONE POSITIONS - MODEL 3 STRAIGHT EJECTOR



8.6.-13

FIGURE 8.6.2-4 MICROPHONE POSITIONS - MODEL 3 RECIRCULATING EJECTOR

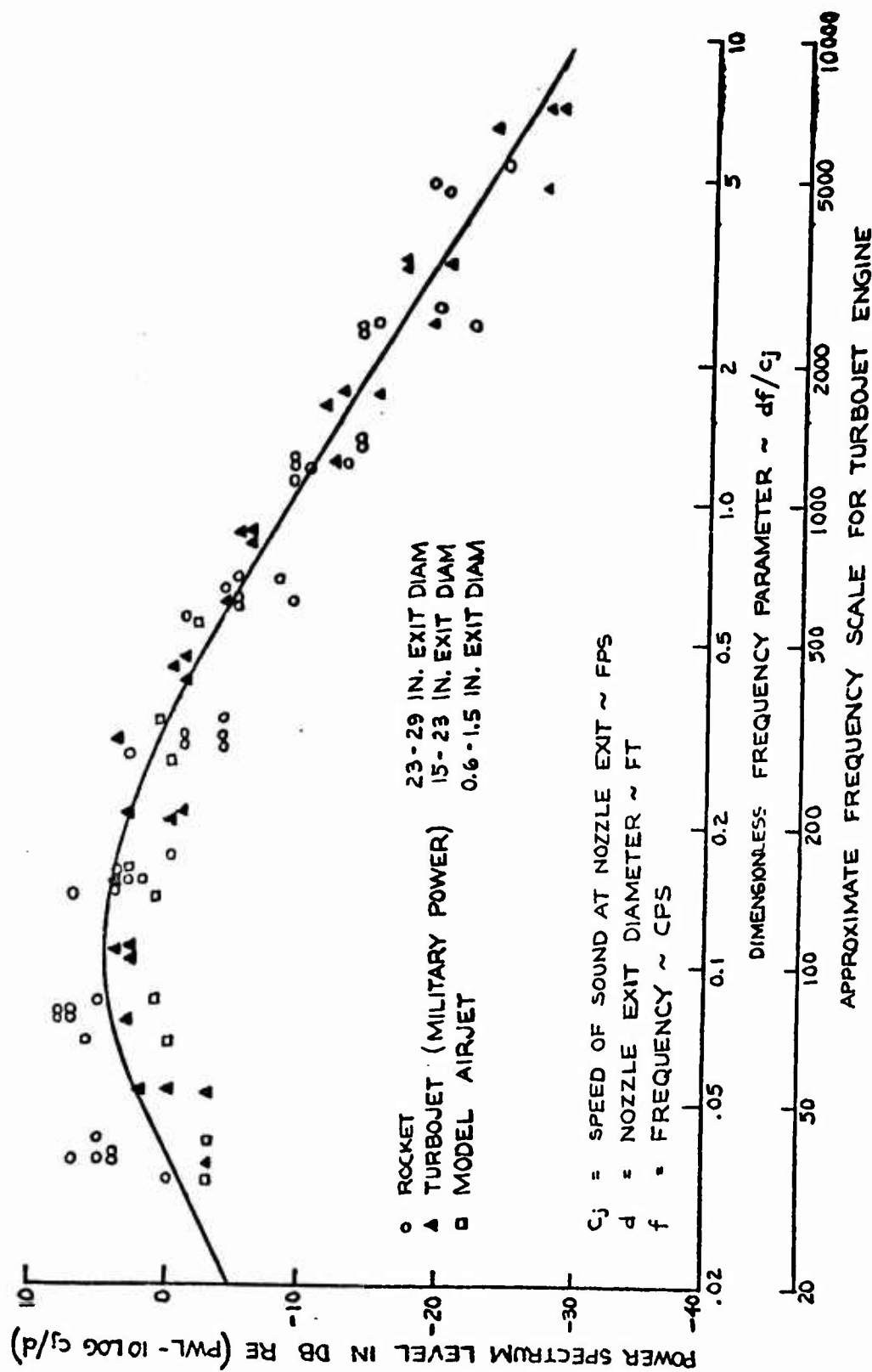


FIGURE 8.6.2-5 TYPICAL JET ENGINE AND ROCKET ENGINE POWER SPECTRUM LEVELS

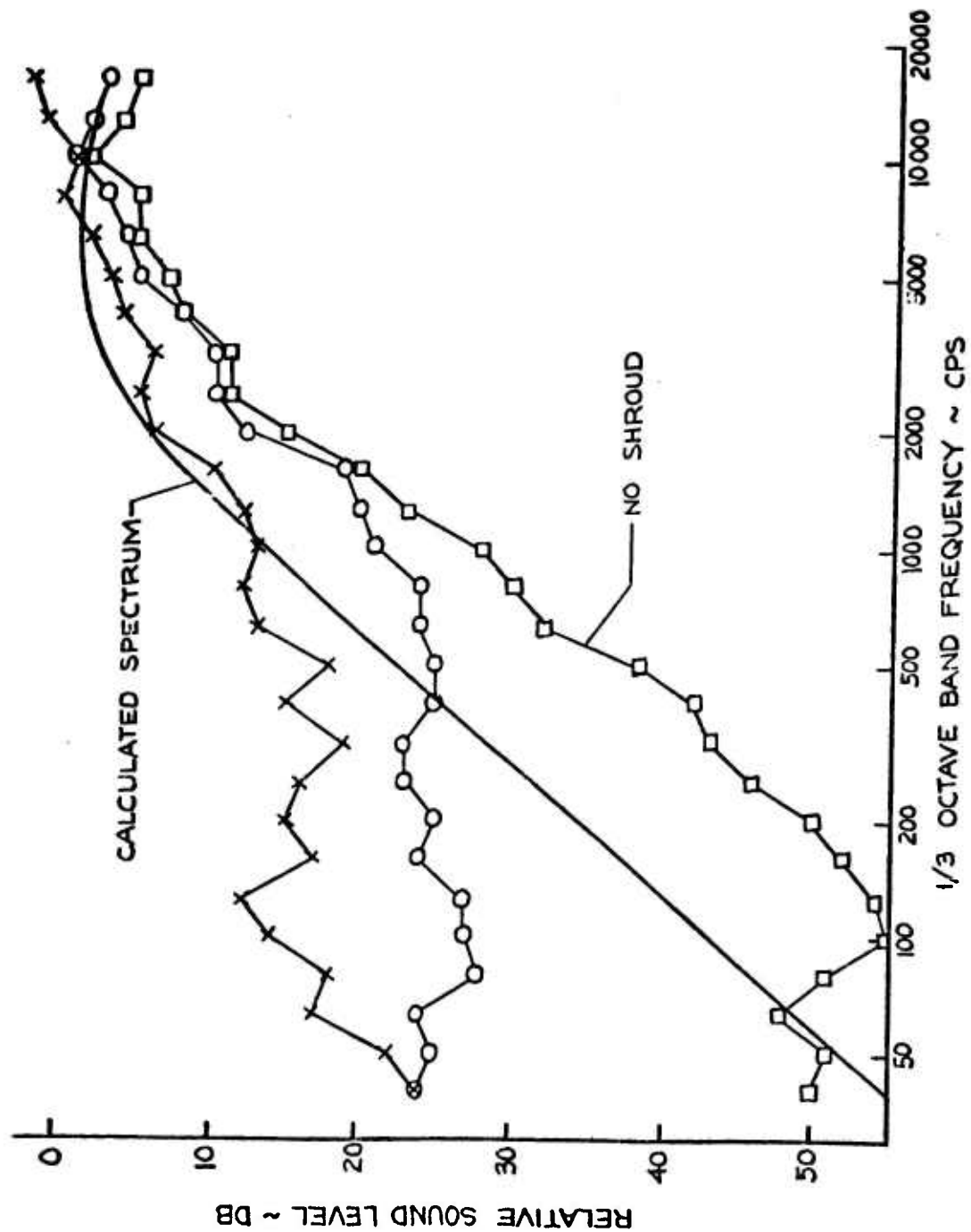


FIGURE 8.6.2-6 COMPARISON OF CALCULATED AND TYPICAL EXPERIMENTAL SOUND SPECTRUMS

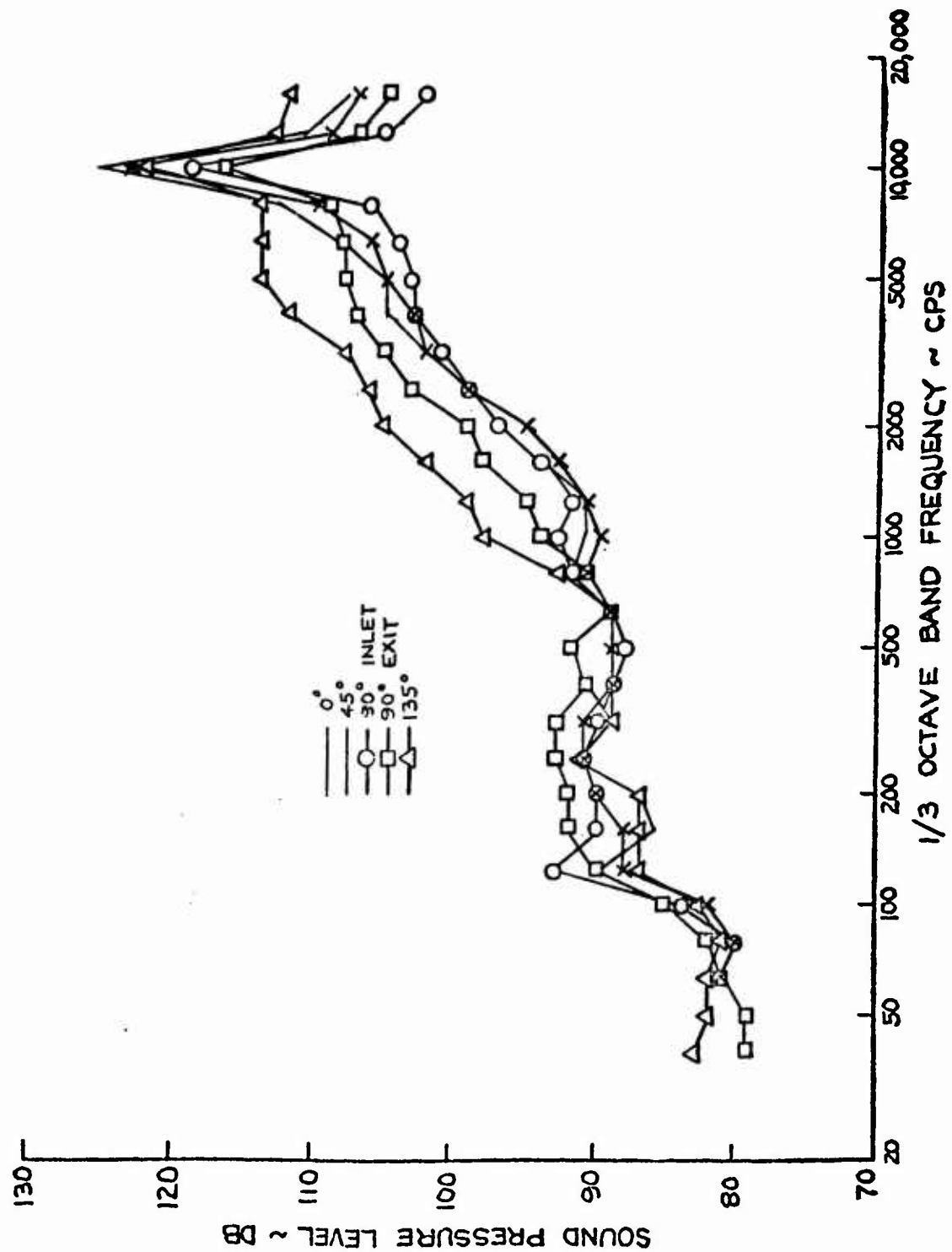


FIGURE 8.6.2-7 MODEL 3 STRAIGHT EJECTOR SOUND SPECTRUM - $P_0 = 100$ PSIG, 4 FT RADIUS

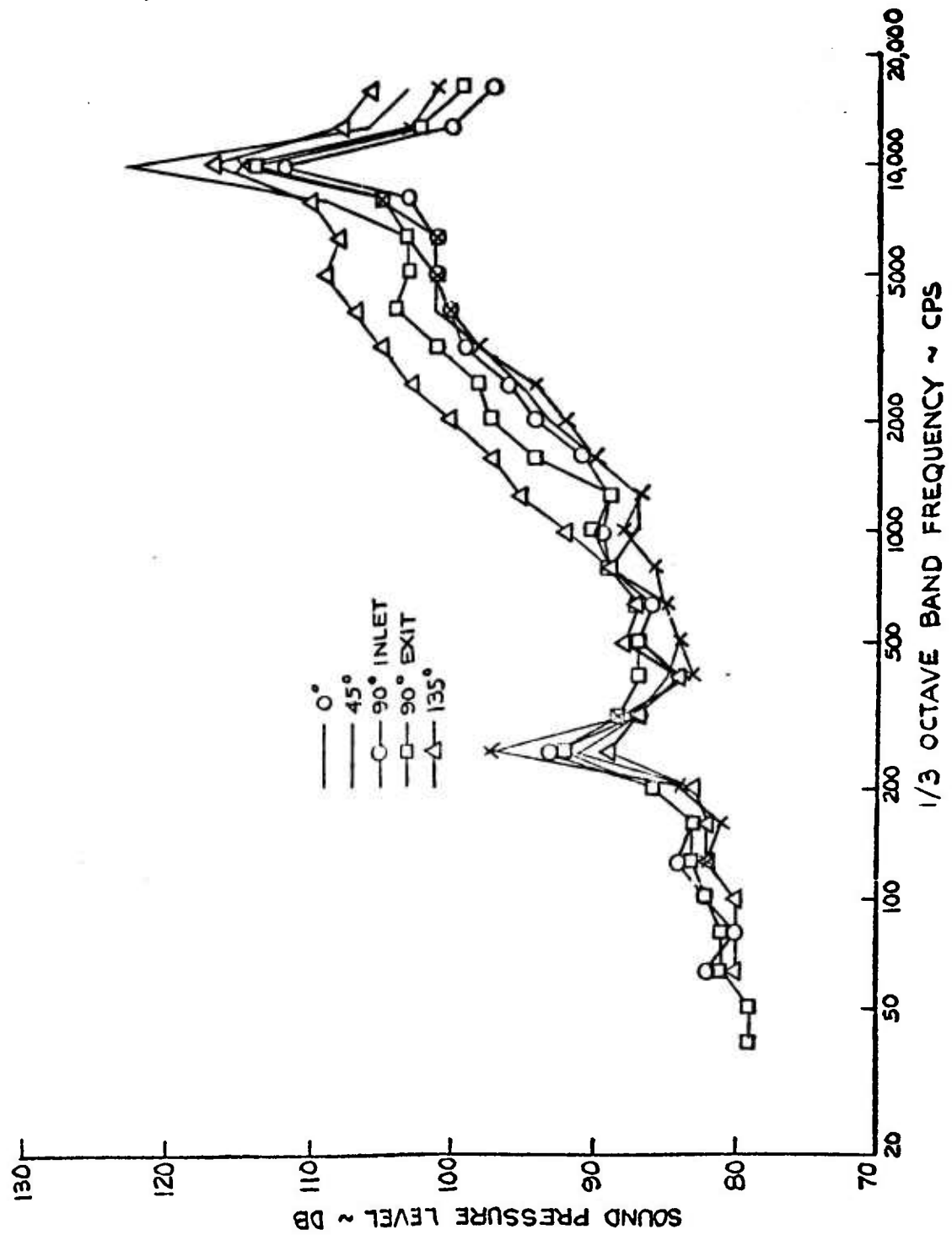


FIGURE 8.6.2-8 MODEL 3 STRAIGHT EJECTOR SOUND SPECTRUM - $p_0' = 100$ PSIG
8 FT RADIUS

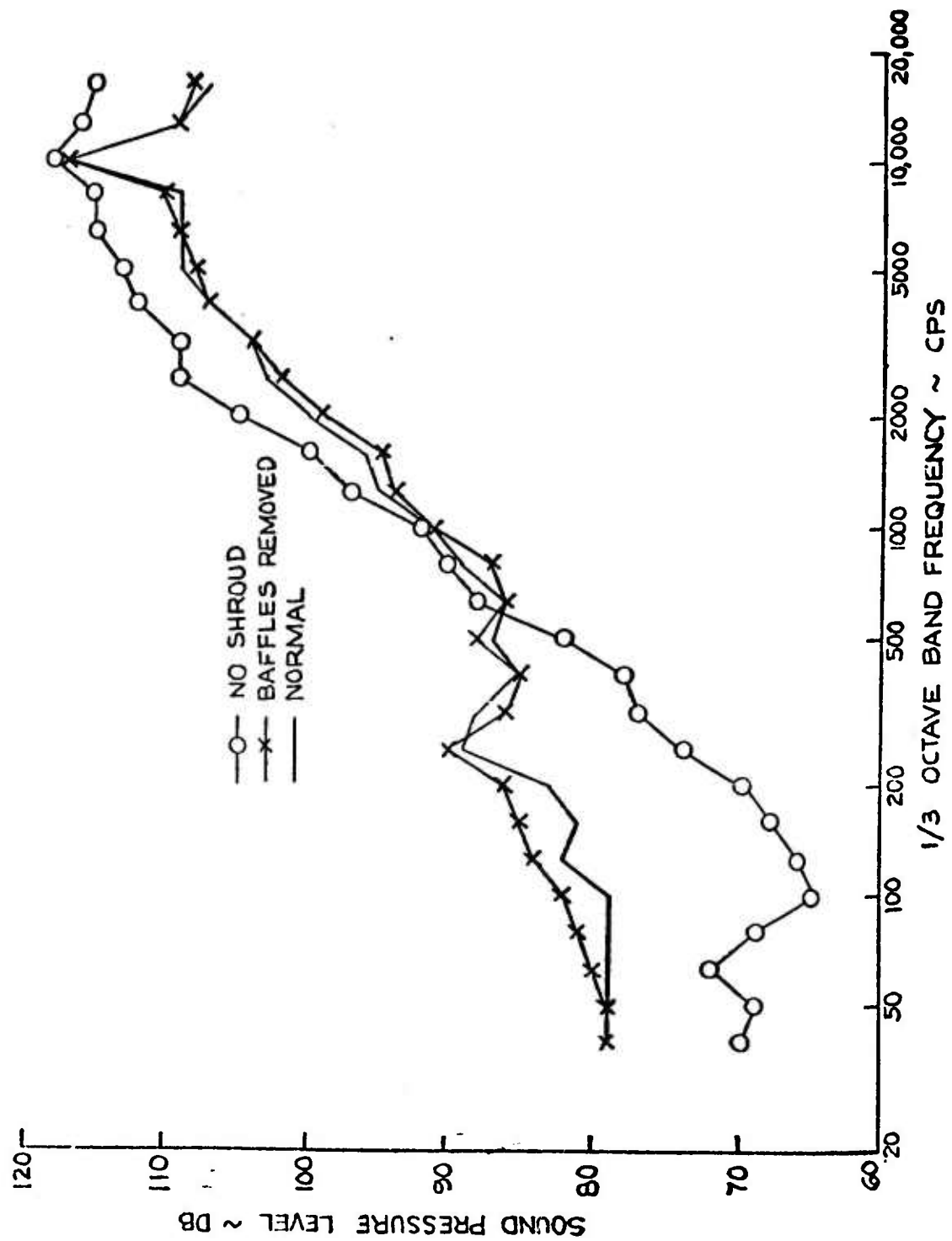
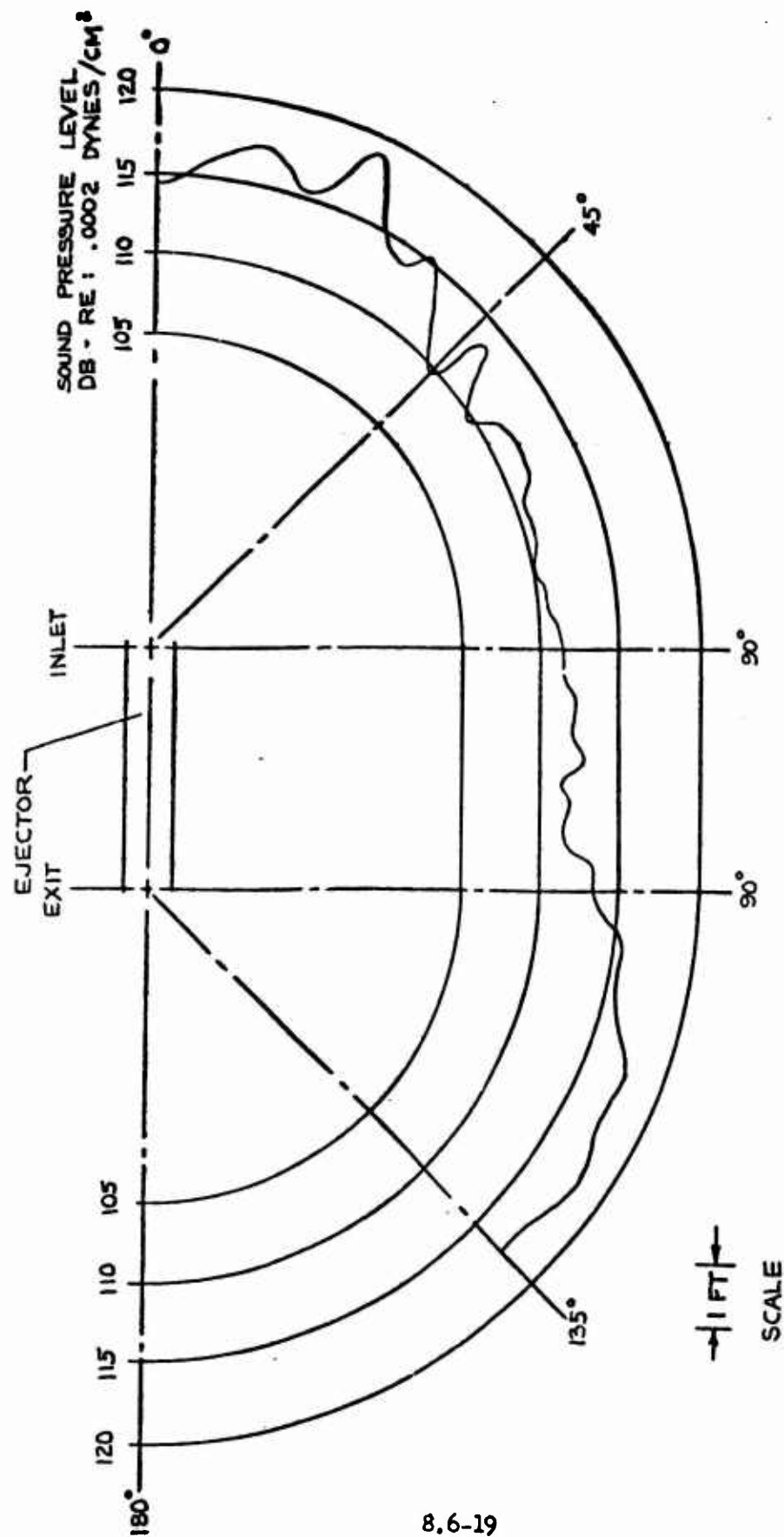


FIGURE 8.6.2-9 MODEL 3 STRAIGHT EJECTOR SOUND SPECTRUM - $p_0 = 100$ PSIG, POSITION 10



8.6-19

FIGURE 8.6.2-10 10,000 CPS SOUND PRESSURE LEVEL AROUND MODEL 3 STRAIGHT
EJECTOR - $p'_0 = 100$ PSIG, NO SHROUD, 8 FT ROVE

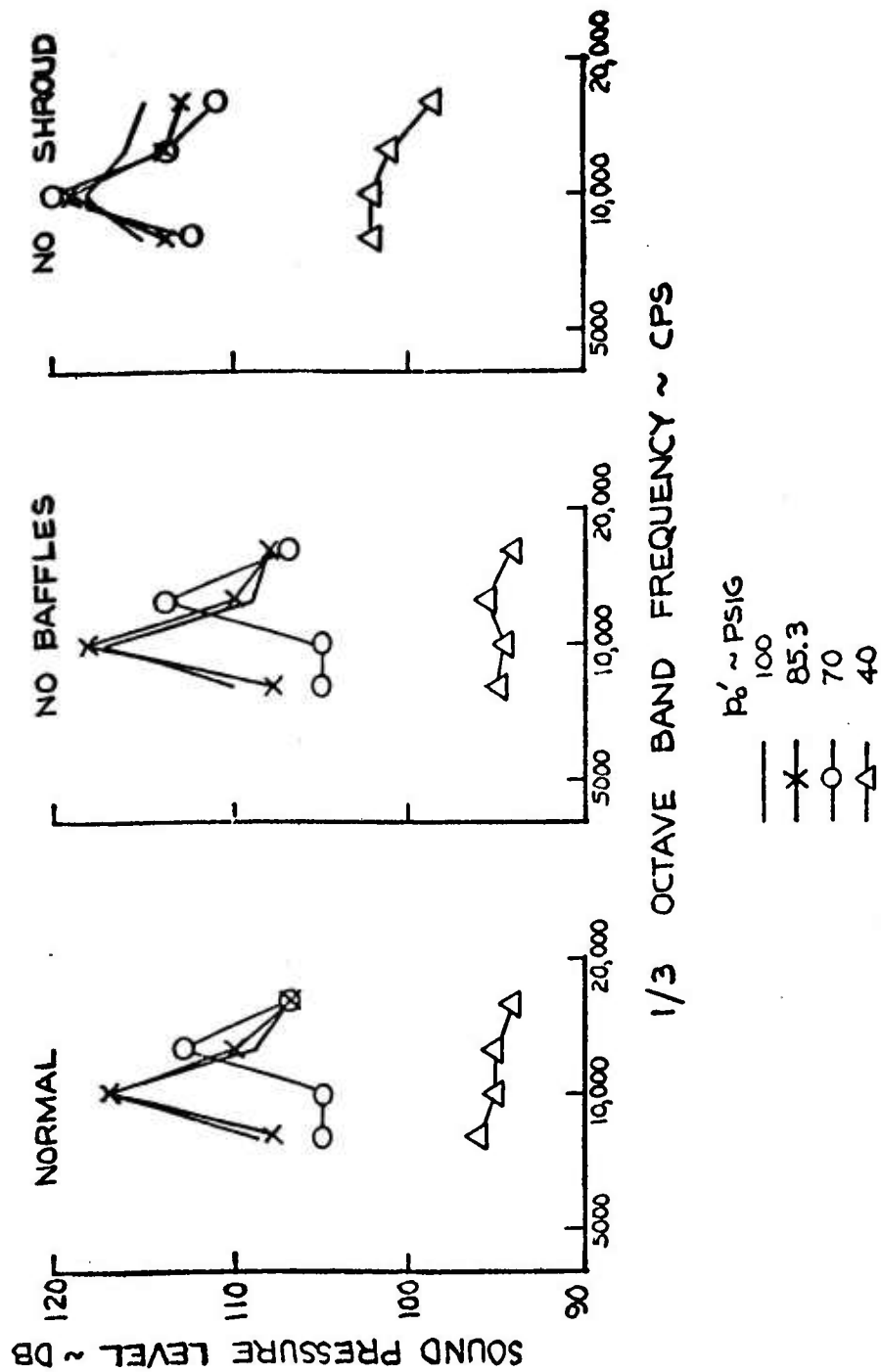


FIGURE 8.6.2-II MODEL 3 STRAIGHT EJECTOR PEAK SOUND LEVELS - POSITION 10

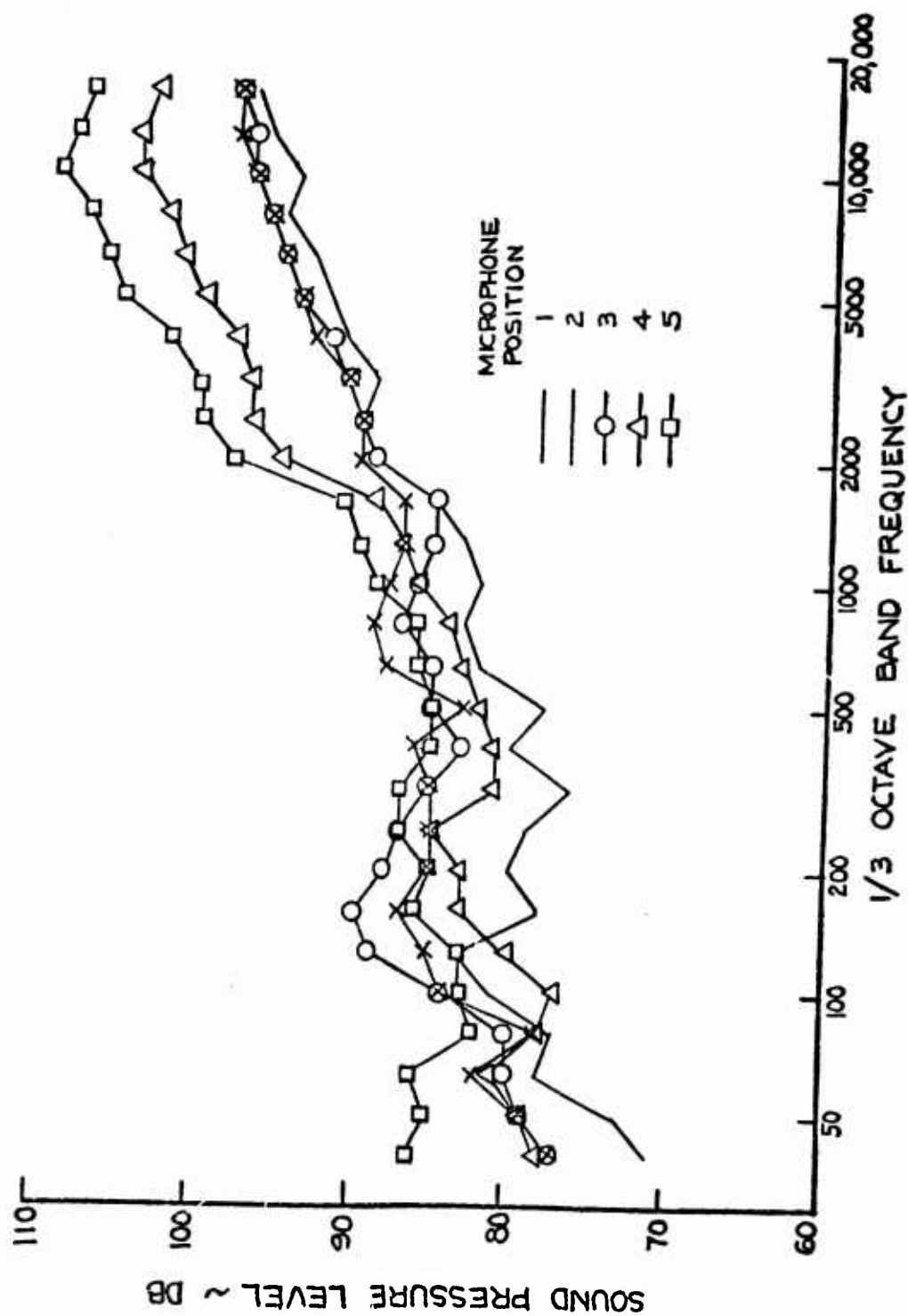


FIGURE 8.6.2-12 MODEL 3 RECIRCULATING EJECTOR SOUND SPECTRUM - $p'_0 = 100$ PSIG

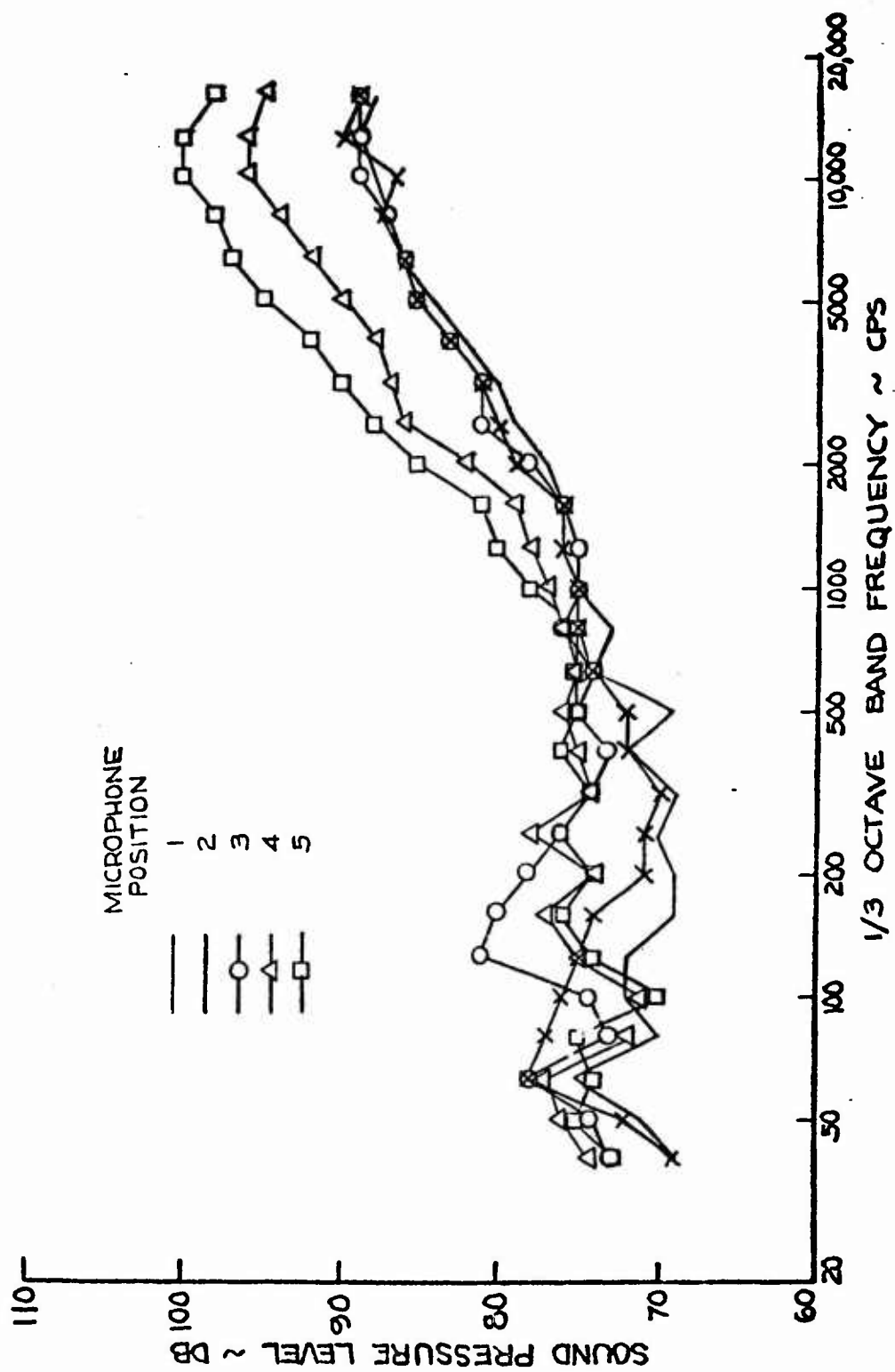


FIGURE 8.6.2-13 MODEL 3 RECIRCULATING EJECTOR SOUND SPECTRUM - $P_0' = 40$ PSIG

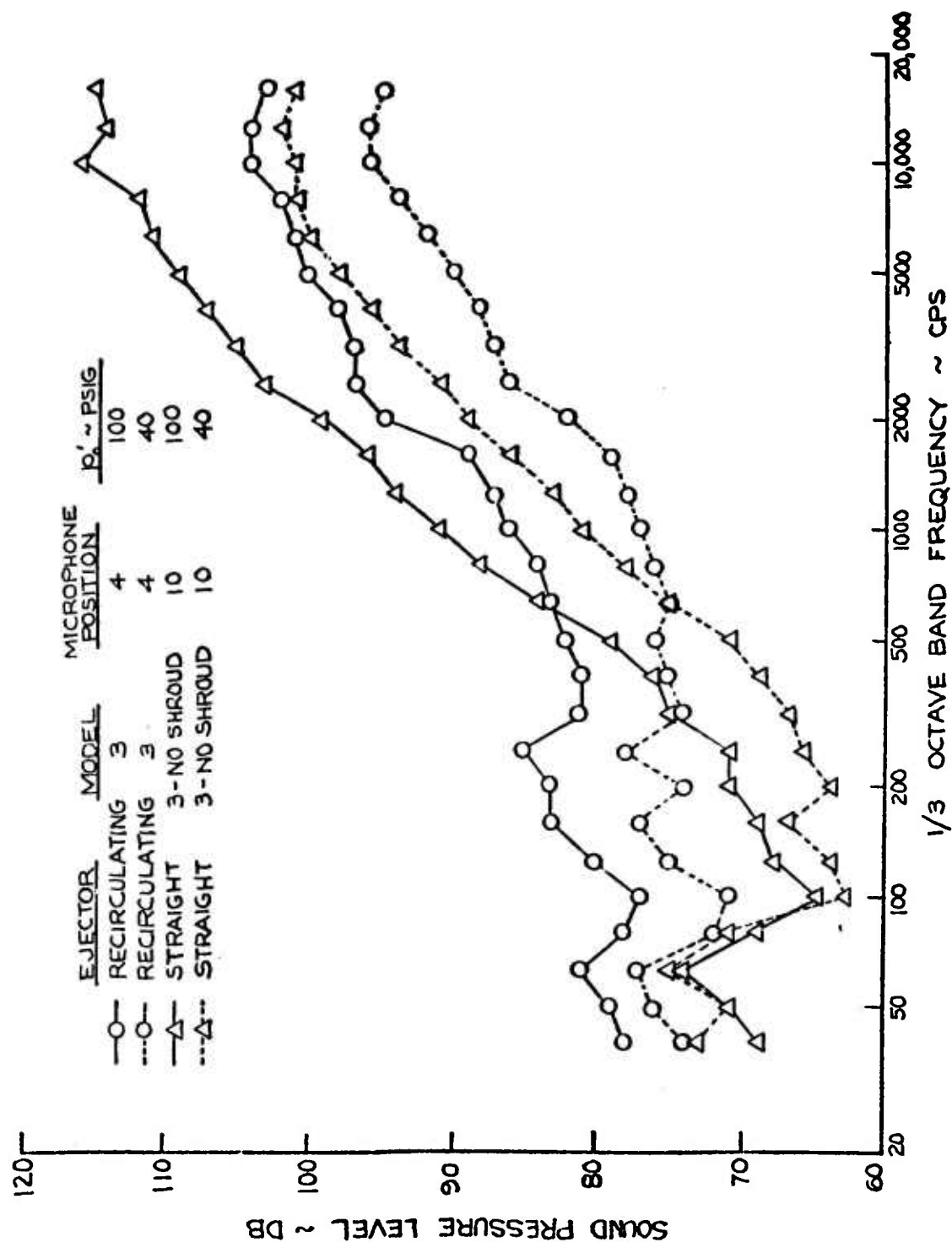


FIGURE 8.6.2-14 COMPARISON OF STRAIGHT AND RECIRCULATING EJECTOR SOUND SPECTRUMS

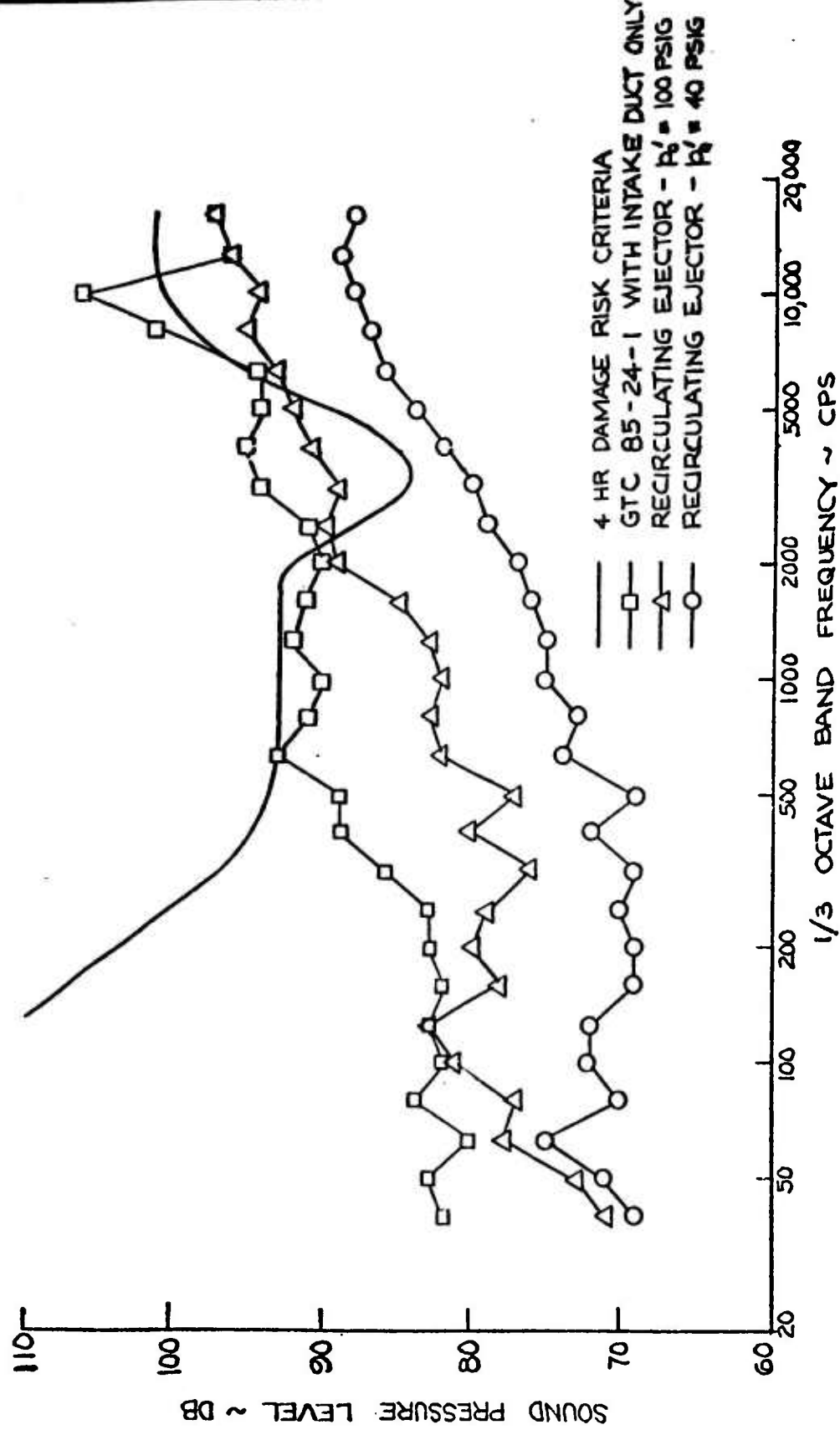


FIGURE 8.6.2-15 NOISE LEVEL AT REPRESENTATIVE PILOT'S LOCATION

9.0 EXPERIMENTAL PROGRAM

9.1 STRAIGHT EJECTOR TESTS

An experimental investigation of large scale straight ejectors was conducted prior to the recirculation test phase. This was done in order to obtain experimental correlation of the ejector theory for the case of zero inlet pressure recovery. For example, the ejector theory assumes that complete mixing is obtained regardless of ejector length. Hence, the optimum and minimum mixing section lengths must be determined experimentally for the type of ejectors utilized in the recirculation concept.

This test program also systematically isolated the effects of other variables such as primary pressure ratio, p_o'/p_a , and area ratio, A''/A' . In addition, noise measurements made during this phase can be compared with measurements obtained during the recirculating ejector test phase.

9.1.1 Description of Test Facility

The experimental investigation of straight ejectors was accomplished by modification of a test facility used in earlier company-sponsored annular jet studies (Reference 27). Figure 9.1-1 is an overall view of this test facility.

9.1.1.1 Primary Air Supply

High pressure air (110 psig) at ambient temperature was supplied directly to the test area by the plant air system. One 200 horsepower compressor operating at 3/4 capacity was capable of delivering 900 cubic feet of air per minute at an average relative humidity of 50 percent. Although the air was not filtered no contamination problems were encountered at any time during the test program.

9.1.1.2 Straight Ejector Design and Fabrication

Four basic straight ejector models were used in this test program. These were designed according to the viscous ejector theory for a primary pressure ratio, p_o'/p_a , of 6.8 and an exit velocity of 200 fps. Area ratios of 35.5, 55.5, 74.4 and 135.5 were chosen in order to bracket the theoretical optimum area ratio. The requirements of a constant mixing section pressure resulted in a nearly constant area mixing section for the four configurations.

The ejector side walls were fabricated of 1/2 inch plywood having a Harborite coating on one side. The contoured horizontal walls of the ejector shroud were formed of 1/4 inch Masonite which were held in place by means of grooves routed in the side walls. External bulkheads provided additional support between the side walls.

Dimensions of the straight ejector configurations are presented in Figure 9.1-2. Initially, the ejectors had a non-dimensional mixing section length, L/t , of 8 which was progressively reduced during the tests. Figure 9.1-3 is an isometric sketch showing fabrication details.

Baffles - Early straight ejector tests reported in Reference 6 experienced a surging of the tertiary flow. Since the area ratio of this ejector was quite large, ($A''/A' = 170$) and the diffusion angle was well below the critical value for flow separation, it was rationalized that this surge or pulsation was due to lateral flow instability. This stimulated the use of removable vertical baffles (Figure 9.1-4) in the current tests. These baffles extended the full length of the ejectors and were held in position by grooves in the horizontal walls.

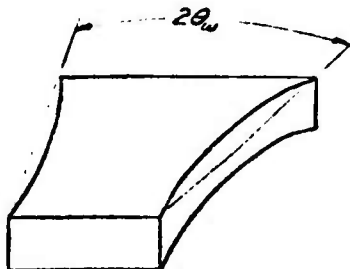
Inlet Lips - The inlet geometry was chosen to minimize losses in the inlet flow region. Although Reference 28 shows that a near optimum inlet contour is defined by a lemniscate, it is also shown in Reference 29 that the substitution of a circular inlet does not significantly decrease ejector performance (approximately one percent). Circular inlet lips having radii equal to 1/2 the height of the mixing section were incorporated into these ejector models. Reference 30 shows this value of inlet lip radius causes only a 1.5 percent loss in thrust augmentation.

The inlet section of the ejector models was detachable so that the mixing section could be sawed off and the inlet reattached to the shortened mixing section.

Diffuser - The philosophy of this design is that the rate of the area increase for short diffusers should first be small to obtain the maximum static pressure rise before boundary-layer separation occurs. As a result, a lemniscate was used for the diffuser contours. The following equation in polar form was used.

$$r^2 = a^2 \cos 2\phi$$

The diffuser is tangent to the mixing section at $\phi = 45^\circ$. The expansion angle, $2\theta_w$, of the diffuser is defined as the angle between the expanding walls. It is shown in the following sketch.



From Figure 5b of Reference 31 a value of 0.2 was chosen for the total pressure loss factor defined as

$$K = \frac{P_o/q}{1 - (1/AR)}$$

AR = ratio of diffuser exit area to diffuser inlet area

This value does not necessarily yield a minimum pressure loss, however, it does result in practical overall ejector lengths. Figure 9.1-5 is a view of the diffuser exit.

Primary Nozzles and Manifold - The primary nozzles are supersonic nozzles with exit-to-throat area ratios, A'/A'^* , determined from the Laval relations as a function of the ratio of theoretical mixing section pressure to primary total pressure, p_1/p_o' . The nozzles were threaded stainless steel male fittings which could be removed from the primary manifold as shown in Figure 9.1-6. Figure 9.1-7 is a drawing of a typical primary nozzle and includes a table of dimensions.

The primary nozzles were designed to screw into a two inch diameter stainless steel header or manifold. It was mounted upstream of the ejector inlet to minimize blockage of the entrained secondary flow. It is noted in Figure 9.1-8 that the manifold is made up of threaded sections so that the lateral position of the primary nozzles can be adjusted to fit all four straight ejector models. Figure 9.1-9 is a dimensional drawing showing the details of this header.

9.1.2 Instrumentation

The straight ejector test program utilized sufficient instrumentation to determine the primary mass flow, primary total pressure and temperature, tertiary exit total and static pressure distributions, plus the static pressure distribution around the inlet lip and along the mixing section and diffuser.

9.1.2.1 Primary Flow Instrumentation

The primary mass flow was measured by means of a sharp-edge orifice flow meter used in conjunction with a U-tube manometer. The meter was designed from the ASME procedures given in Reference 32. It is estimated that error in measuring the primary mass flow was less than one percent. Figure 9.1-10 is a photograph of the flow meter installation.

A Bourdon-type pressure gauge connected to a flush-wall tap downstream of the orifice plate was used to measure the total pressure in the flow-meter pipe. Although this pressure gauge actually measured static pressure, the error introduced was less than 0.1 percent. This was due to the fact that the cross-sectional area at the location of the pressure gauge was two orders of magnitude higher than the total primary nozzle area.

The total temperature of the primary flow was measured by an immersion thermometer of the bi-metallic type mounted in the flow meter pipe. The temperature was recorded on a dial gauge calibrated over a range from 0°F to 200°F. The maximum combined error introduced by the thermometer, and the error due to measuring stagnation temperature in a stream with a finite velocity, was estimated to be on the order of three percent.

9.1.2.2 Secondary and Tertiary Flow Instrumentation

A pitot-static rake was used to measure the tertiary flow at the diffuser exit. Figures 9.1-11 and 9.1-12 show that total and static pressures were measured by separate probes rather than integrated probes.

In the vicinity of the diffuser walls the tertiary flow is undoubtedly inclined to the rake probes. Reference 33 discusses the effect of flow inclination on the pressures sensed by total and static probes. It shows that the error in total pressure when measured with a sharp edge tube is approximately -5% at an inclination of 30°. This inclination angle is approximately the maximum divergence angle incurred at the diffuser exit. Inclinations greater than this value may exist whenever flow separation occurs. Reference 33 shows that the error in static pressure is much higher, percentage-wise, at this inclination angle. It amounts to +10% for a static pressure probe having a hemispherical nose. Since these maximum errors occur in regions of low velocity, the overall error that can occur utilizing this pitot-static rake is estimated to be on the order of one percent.

The rake-tube bundles were contained in a single large diameter tube as shown in Figure 9.1-11. The rake was mounted to the ejector side wall by means of collars which slipped over the large diameter tube. The collars contained set screws which held the rake at any desired lateral position.

A smaller pitot-static rake of similar design (Figure 9.1-13) was used in some tests to monitor the entrained secondary flow. The probes of this rake were adjustable in the spanwise direction.

The longitudinal static pressure distribution was determined by taps located around the upper inlet lip, the mixing section, and the diffuser wall. A number of pressure taps along the upper mixing-section wall were duplicated along the lower wall to aid in the vertical alignment of the primary nozzles.

Four, fifty-tube water manometer banks and a twenty-tube mercury bank were available to record the static and total pressures in the secondary and tertiary flow. The water manometers are accurate to ± 0.1 psf when tilted 11.3° from the horizontal. The mercury manometer was not tiltable and its minimum resolution is approximately ± 7 psf. A picture of these manometers is given by Figure 9.1-14.

9.1.3 Test Procedure

Before actual testing was initiated, a straight ejector configuration underwent the following preparations.

- a. By adjusting the manifold, the primary nozzles were properly spaced laterally and aligned in a single plane.
- b. The ejector shroud was placed in the desired longitudinal position relative to the primary nozzles, and then adjusted laterally and vertically until the primary nozzles were centered in the secondary cross-sectional area. The ejector shroud was held in place by the lock nuts on the primary manifold.
- c. The primary air supply was turned on and all joints were checked for leaks.

A typical straight ejector test included the recording of the following data at four primary total pressures.

- a. Primary total pressure.
- b. Primary total temperature.
- c. Pressure drop across the primary flow-meter orifice.
- d. Static pressures along the ejector shroud.
- e. Pitot-static pressure profiles at the diffuser exit.

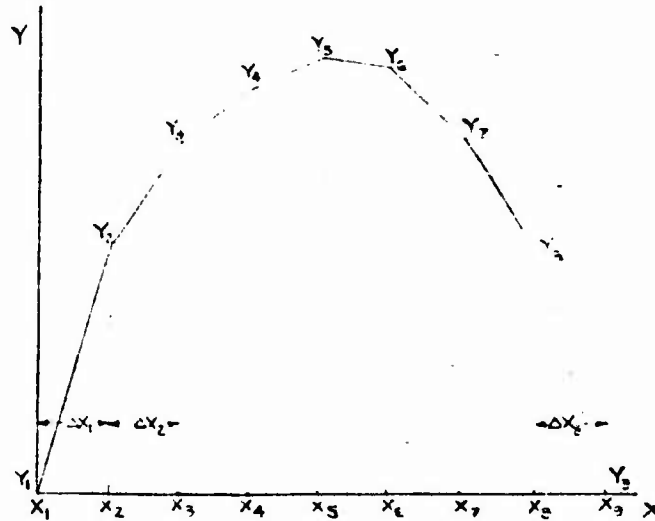
Initially, attempts were made to perform lateral velocity surveys as well as vertical surveys at the diffuser exit in order to determine precisely the effects of the vertical baffles. However, the available pitot-static rake (Figure 9.1-11) was not suitable for this type of flow measurement. These surveys were subsequently discontinued and in their place three velocity surveys in the center portion of the flow between the baffles were made. This was done to nullify the effects of flow unsteadiness which existed at the diffuser exit.

9.1.4 Data Reduction

9.1.4.1 Linear Integration Technique for Rake Data

During the period allotted for reduction of the straight ejector test data, the digital computer was not available. As a substitute, a hand-reduction method was devised. The end result was a linear integration method modified into a continuous operation for a desk calculator.

The spacing of the rake pressure probes and the rate of change of velocity between probes were sufficiently small to allow the assumption of a linear variation. This method is outlined by the following sketch and equations.



$$\int Y dX = \frac{(Y_2 + Y_1)}{2} (X_2 - X_1) + \frac{(Y_3 + Y_2)}{2} (X_3 - X_2) + \dots + \frac{(Y_9 + Y_8)}{2} (X_9 - X_8) \quad (9.1-1)$$

$$\int Y dX = (Y_2 + Y_1) \frac{\Delta X_1}{2} + (Y_3 + Y_2) \frac{\Delta X_2}{2} + \dots + (Y_9 + Y_8) \frac{\Delta X_8}{2} \quad (9.1-2)$$

Equation (9.1-2) is simply the sum of the areas of each trapezoidal strip. Rearrangement of Equation (9.1-2) results in

$$\int Y dx = Y_1 \frac{\Delta X_1}{2} + Y_2 \left(\frac{\Delta X_1 + \Delta X_2}{2} \right) + \dots + Y_n \left(\frac{\Delta X_{n-1} + \Delta X_n}{2} \right) + Y_n \frac{\Delta X_n}{2} \quad (9.1-3)$$

The latter equation is a cumulative multiplication operation on a desk calculator once the bracketed Δx terms have been determined.

9.1.4.2 Thrust Determination

Two independent methods were utilized to determine the tertiary thrust. In the first method (Reference 34) the squares of the tertiary velocities were integrated across the diffuser thickness and multiplied by the air density. The gauge static pressures were then integrated across the diffuser thickness and added algebraically to the integrated average of the squares of the velocity. The result was total thrust per foot, thus

$$T_{\text{ter 2-D}} = \rho_3 \frac{1}{t_3} \int_0^{t_3} V_3^2 dt + \frac{1}{t_3} \int_0^{t_3} \Delta p_3 dt \quad (9.1-4)$$

The total pressure across the diffuser exit, as sensed by the pitot-static rake, fluctuated to a degree that made reading the manometers difficult. Therefore, an alternate procedure of computing the exit flow was used. This method utilized the steady and well-defined longitudinal static pressures along the ejector shroud.

In this method the gauge static pressures around the inlet lip and along the diffuser were integrated in the thrust direction. The net result was thrust per foot of width of ejector shroud. Total thrust was then determined by adding the thrust of the shroud to the calculated thrust of the primary nozzles.

$$T_{TOT\ 2-D} = \left[\int |\Delta p| dy \right]_{\text{INLET}} + \left[\int |\Delta p| dy \right]_{\text{DIFFUSER}} + \left[\frac{m' V_i'}{w} \right]_{\text{PRIMARY NOZZLES}} \quad (9.1-5)$$

where

$$V_i' = \sqrt{\left(\frac{2\gamma}{\gamma-1} \right) \left(\frac{p_o'}{p_i} \right) \left[1 - \left(\frac{p_i}{p_o'} \right)^{\frac{\gamma-1}{\gamma}} \right]}$$

9.1.4.3 Primary and Tertiary Mass Flows

The pressure drop across the sharp-edge orifice was converted into primary mass flow through the use of the calibration curves associated with this orifice.

The tertiary mass flows were also determined by two independent methods similar to the methods used in the thrust computation. The average of the squares of the exit velocities can be calculated from the total ejector thrust. However, since the exit velocity profile is not rectangular (linear) in the vertical plane, the average velocity is not equal to $\sqrt{\overline{V_3^2}}$. To account for the non-linearity of the exit velocity profile, a correlation of $\overline{V_3}$ and $\sqrt{\overline{V_3^2}}$, from the rake surveys, was made as a function of mixing section length and the primary total pressure.

(Area ratio did not have an appreciable effect in this range). The average velocity determined from the total thrust by this procedure was used to calculate tertiary mass flow values which then served to "smooth" the rake survey results.

9.1.4.4 Efficiency Determination

The power ratio for ejectors given in Reference 6 is defined as

$$\epsilon = \frac{\frac{m(p_{03} - p_a)}{c_{03}}}{\frac{m'(p'_0 - p_a)}{c'_0}} \quad (9.1-6)$$

This relationship is derived from a thermodynamic description of the process using a piston analogy to represent the system. Although the relation is correct in context, it does not adequately describe the real energy ratio of the system.

A more meaningful expression for ejector efficiency, commonly used in ejector literature, is given by

$$\epsilon = \frac{\frac{1}{2} m V_3^2}{\frac{1}{2} m' V_i'^2} \quad (9.1-7)$$

This relationship is the ratio of the kinetic energies of the tertiary and primary flows which becomes

$$\epsilon = \frac{m \left(\frac{p_{03}}{c_{03}} \right) \left[1 - \left(\frac{p_3}{p_{03}} \right)^{\frac{\gamma-1}{\gamma}} \right]}{m' \left(\frac{p'_0}{c'_0} \right) \left[1 - \left(\frac{p_1}{p'_0} \right)^{\frac{\gamma-1}{\gamma}} \right]} \quad (9.1-8)$$

upon substitution of the isentropic relations for velocity. This is the form used in determining theoretical efficiency values.

In the experimental determination of the efficiency or power ratio, Equation (9.1-7) is used in the form

$$\epsilon = \frac{\rho_3 \overline{V_3^3} A_3}{m' \left(\frac{2\gamma}{\gamma-1} \right) \left(\frac{p_0'}{\rho_0'} \right) \left[1 - \left(\frac{p_1}{p_0} \right)^{\frac{\gamma-1}{\gamma}} \right]} \quad (9.1-9)$$

where $\overline{V_3^3}$ = the integrated average of the tertiary velocity-cubed profile
 m' = measured value of primary mass flow
 p_1 = average of measured mixing section static pressure
 p_0' = measured primary total pressure
 ρ_0' = primary total density calculated from perfect gas relationship

The fairing of the curves through the experimental efficiency values was accomplished by calculating additional values of tertiary power using the thrust integration of the shroud static pressures. In this case, the average of the velocity squared from the thrust integration is multiplied by the reciprocal of the correlation values used in determining average velocity for the tertiary mass flow.

9.1.5 Analysis of Basic Results

The results of the two methods for determining straight ejector total thrust are presented in Figures 9.1-15 through 9.1-18. Straight lines were faired through values derived from the static pressure thrust integration since these values were considered to be the more reliable. The agreement between the two methods is poor on Model 1 (Figure 9.1-15) except for the two-baffle configuration at $\ell/t = 8.15$ where a detailed lateral survey was performed. The scatter in the thrust values determined from the rake surveys on all ejectors is attributed generally to surging of the tertiary flow.

The thrust values of Figures 9.1-15 through 9.1-18 were used to "smooth" the mass flow and efficiency values determined from the rake data. The details of this "data smoothing" process have been previously discussed in Section 9.1.4. Some results of this process are presented in Figure 9.1-19 which shows tertiary mass flows for Model 2 plotted as function of primary pressure ratio.

It is noted in Figures 9.1-15 through 9.1-19 that the effect of the vertical baffles on the straight ejector tertiary thrust and mass flow are of the same order as the scatter in the data. As a result, no definite quantitative conclusions can be made concerning the effect of the baffles, although qualitatively their presence did reduce the severity of the fluctuations on Models 1 and 2 which had the largest diffusion angles. The qualitative observations tend to support the theory that a portion of the pulsing is due to lateral flow instability.

The experimental values of primary mass flow presented in Figure 9.1-20 are used in conjunction with the tertiary mass flows to calculate mass augmentation. The effect of mixing section length on ejector mass augmentation for constant area ratio and pressure ratio is presented in Figure 9.1-21. The usual reduction in ejector performance with decreasing mixing section length is readily apparent in Figure 9.1-21; however, the optimum mixing section length with respect to mass augmentation was not obtained in the range of values tested. Figure 9.1-21 is cross-plotted in Figure 9.1-22 to show the variation of mass augmentation with area ratio. These curves indicate an optimum area ratio of approximately 90 for all pressure ratios and mixing section lengths tested.

Similar plots of thrust augmentation are presented in Figures 9.1-23 and 9.1-24. No optimum mixing section length was obtained; however, the area ratio for maximum thrust augmentation is again approximately 90 to 100. It is interesting to note the independence of

thrust augmentation of primary total pressure. Evidently, tertiary thrust varies with primary pressure in the same proportion as the primary thrust.

The effect of mixing section length, primary pressure ratio, and area ratio on straight ejector power ratio is illustrated by Figures 9.1-25 and 9.1-26. Figure 9.1-25 shows only a small effect of mixing section length except for the case of $A''/A' = 135.5$. Reduced primary pressure has a detrimental effect on ejector efficiency, whereas the reverse occurred in the case of mass augmentation. This can be explained by an examination of the efficiency equation

$$\epsilon = \frac{m V_3^2}{m' V_1'^2} \quad (9.1-7)$$

and the variation of primary and tertiary velocity with pressure ratio as shown in Figure 9.1-27. It is seen in Figure 9.1-27 that the tertiary velocity of a typical straight ejector decreases more rapidly with primary pressure than does the primary velocity. When this observation is applied to the efficiency equation, the reason for the decrease in efficiency becomes obvious.

Typical longitudinal static pressure distributions along the straight ejector shroud are presented in Figures 9.1-28 and 9.1-29. It is seen that the mixing section pressures are fairly constant as originally intended except in the vicinity of the inlet lip. It is evident from the erratic distributions in this region that local accelerations occur in the

immediate vicinity of the walls. In Figure 9.1-28 the flow accelerates rapidly around the sharp curvature of the lip and then stabilizes apparently without separating, as it enters the mixing section. In Figure 9.1-29 it appears that boundary layer separation and reattachment occur locally on the inlet lip in a manner not unlike the laminar separation (laminar bubble) observed on thin airfoils at an angle of attack (Reference 35).

The shroud static pressures are non-dimensionalized by the primary total pressure. This shows that there is nearly linear variation of longitudinal static pressure with primary pressure. The plots of thrust versus primary pressure ratio in Figures 9.1-15 through 9.1-18 indicate the same trend.

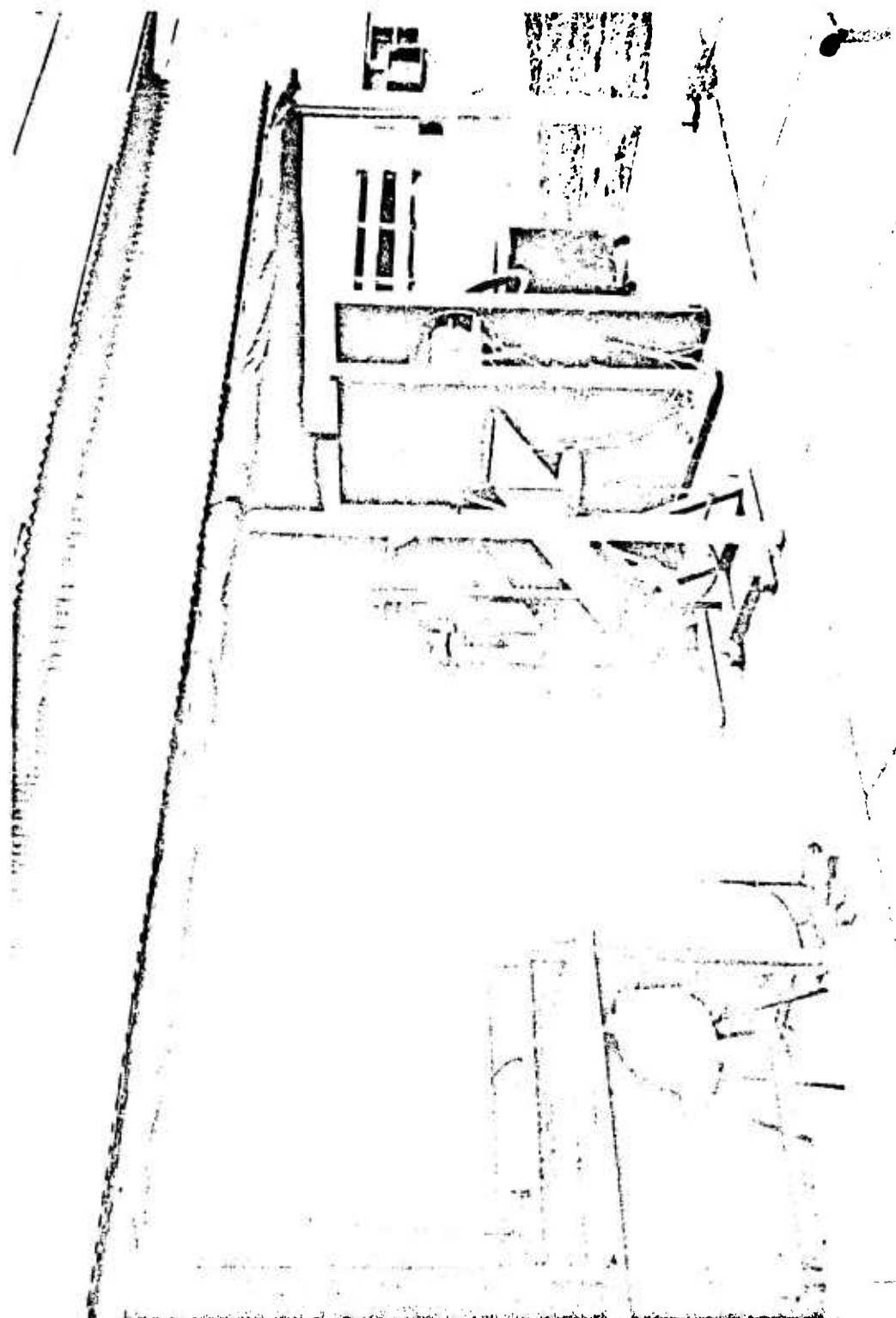
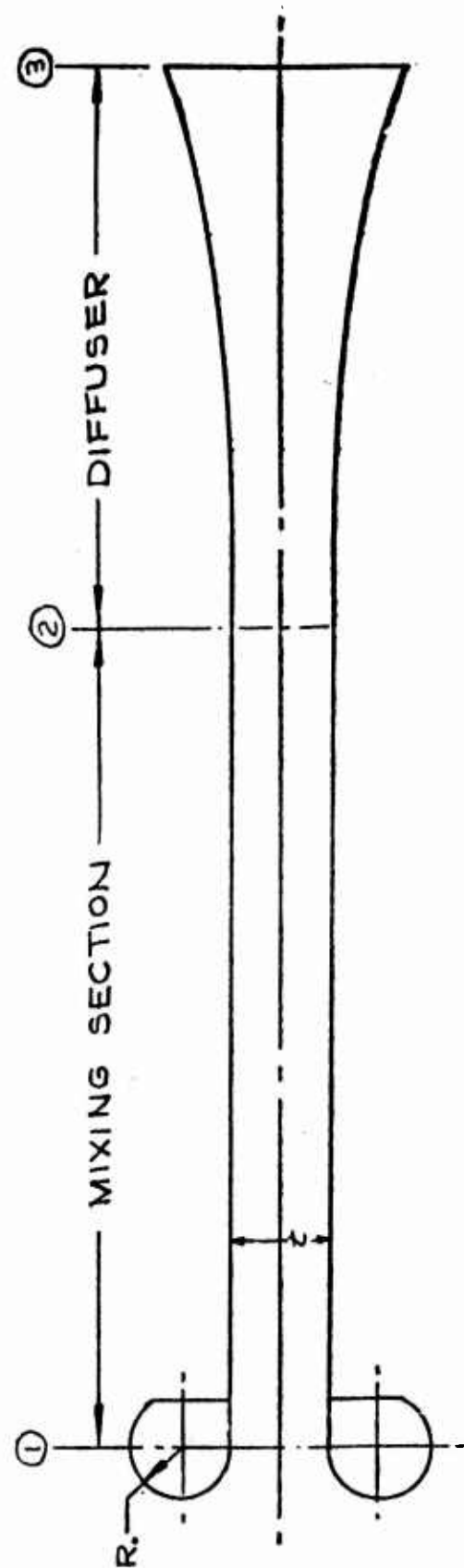


Figure 9.1-1 Ejector Test Facility



MODEL	l_{MIX}	l_{DIFF}	t	t_3	A_3/A_2	A'/A'	R
1	22.6	21.0	2.78	8.70	3.11	35.5	1.39
2	23.9	19.8	2.97	8.20	2.73	55.5	1.48
3	25.7	18.0	3.20	7.62	2.36	74.4	1.60
4	32.6	9.5	4.20	5.86	1.36	135.5	2.10

ALL DIMENSIONS IN INCHES

FIGURE 9.1-2 STRAIGHT EJECTOR DIMENSIONS

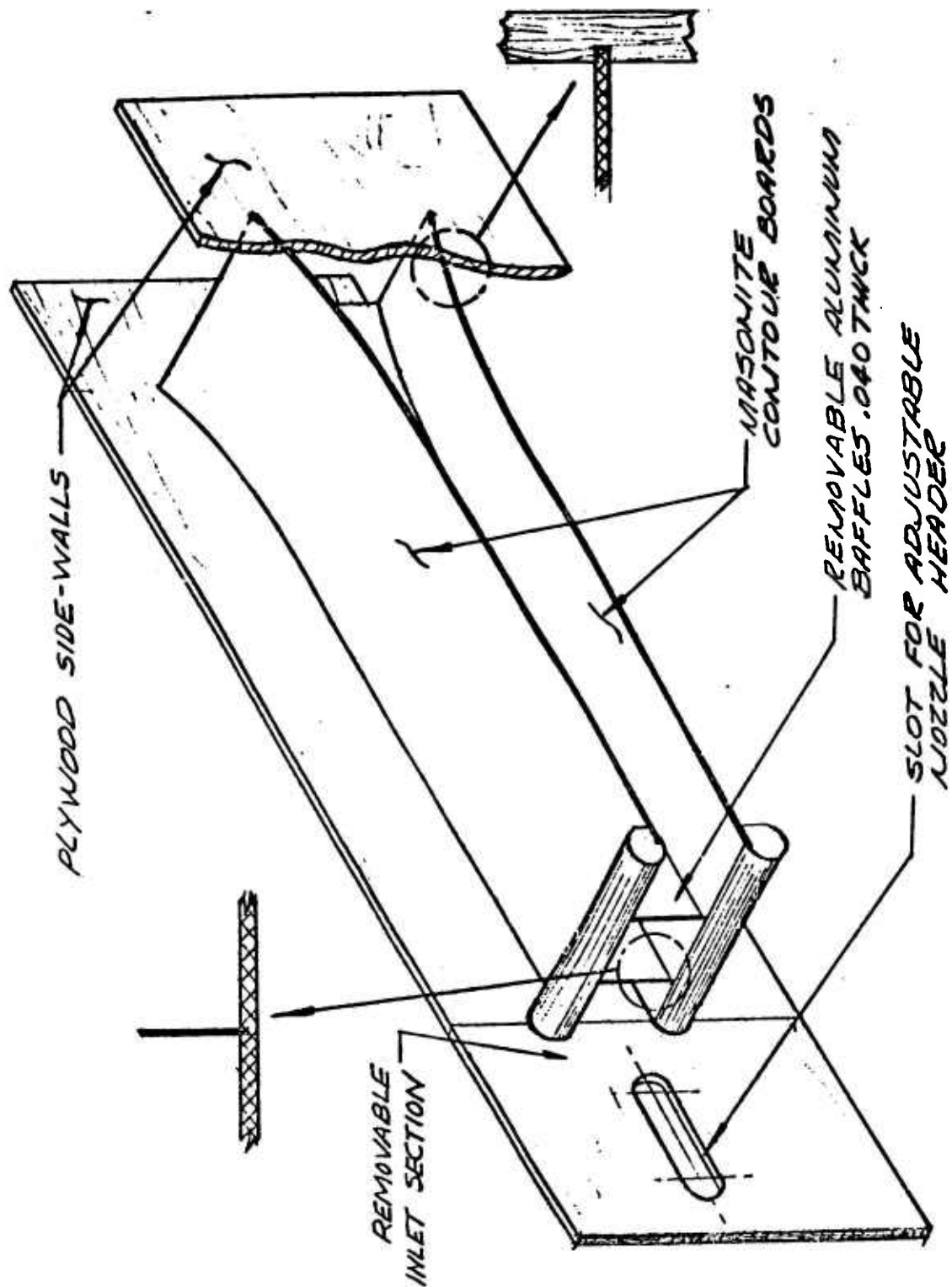


FIGURE 9.1-3 FABRICATION DETAILS OF STRAIGHT EJECTORS

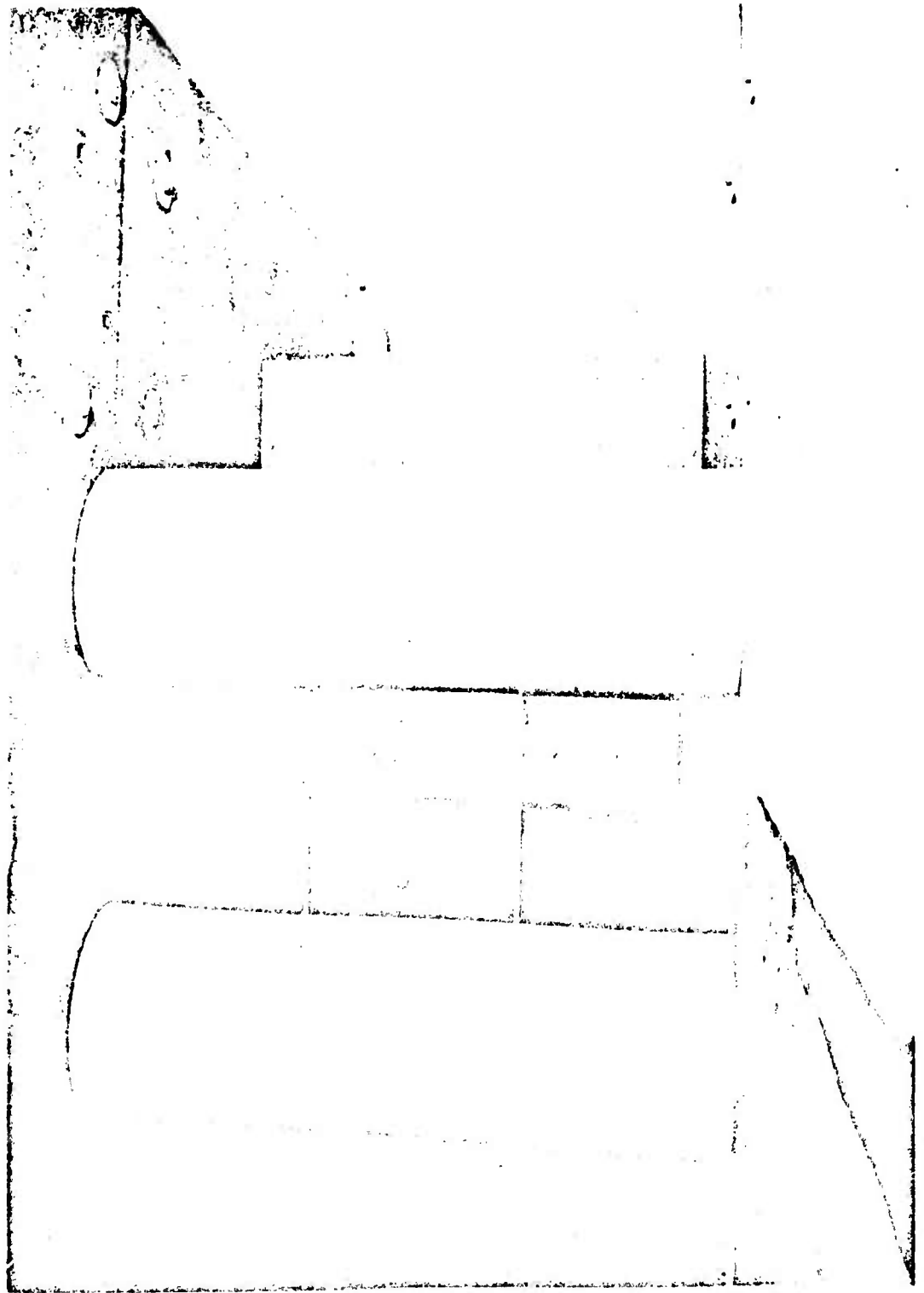


Figure 9.1-4 Straight Ejector Inlet

9.1-19

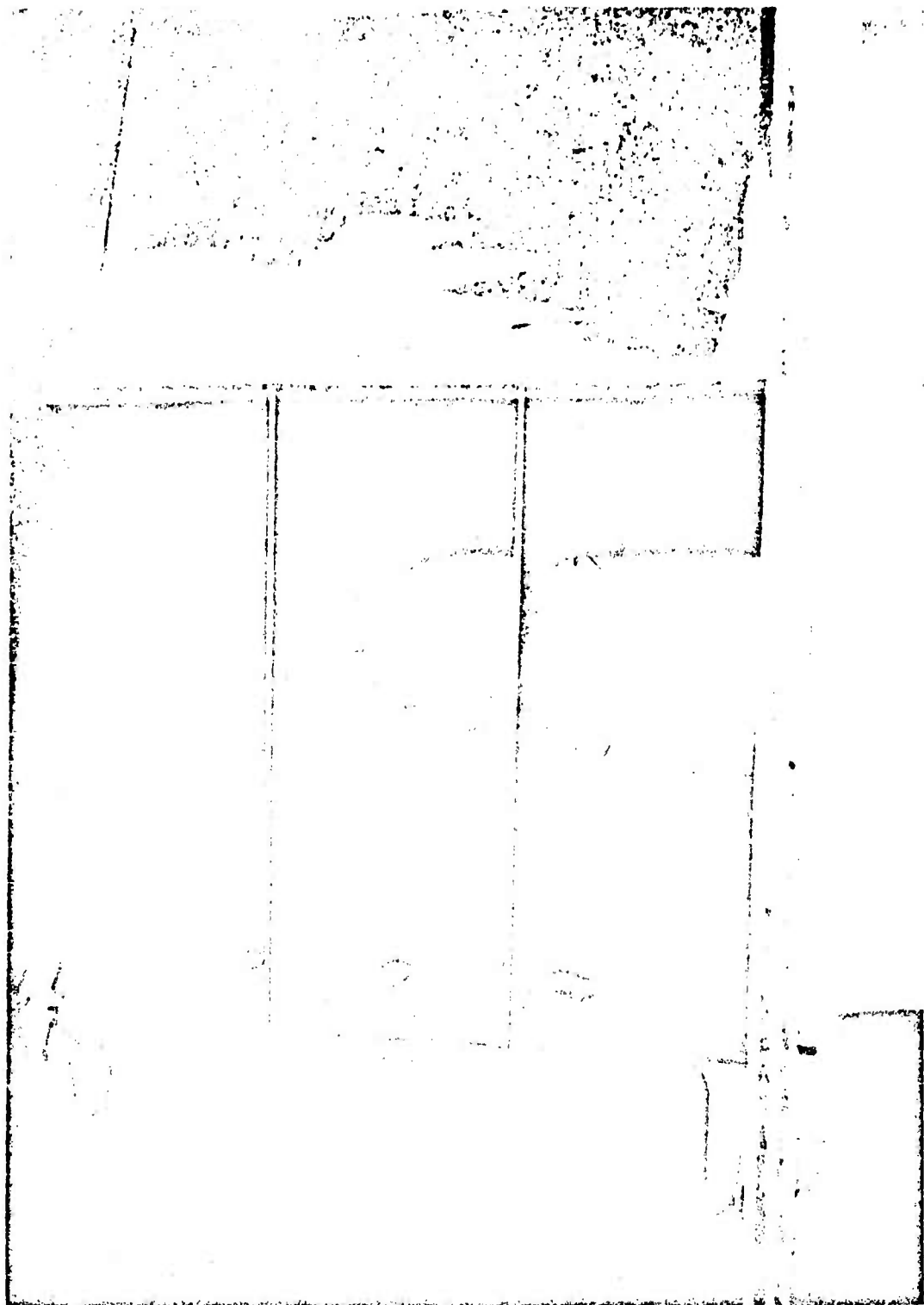


Figure 9.1-5 Straight Ejector Diffuser Exit

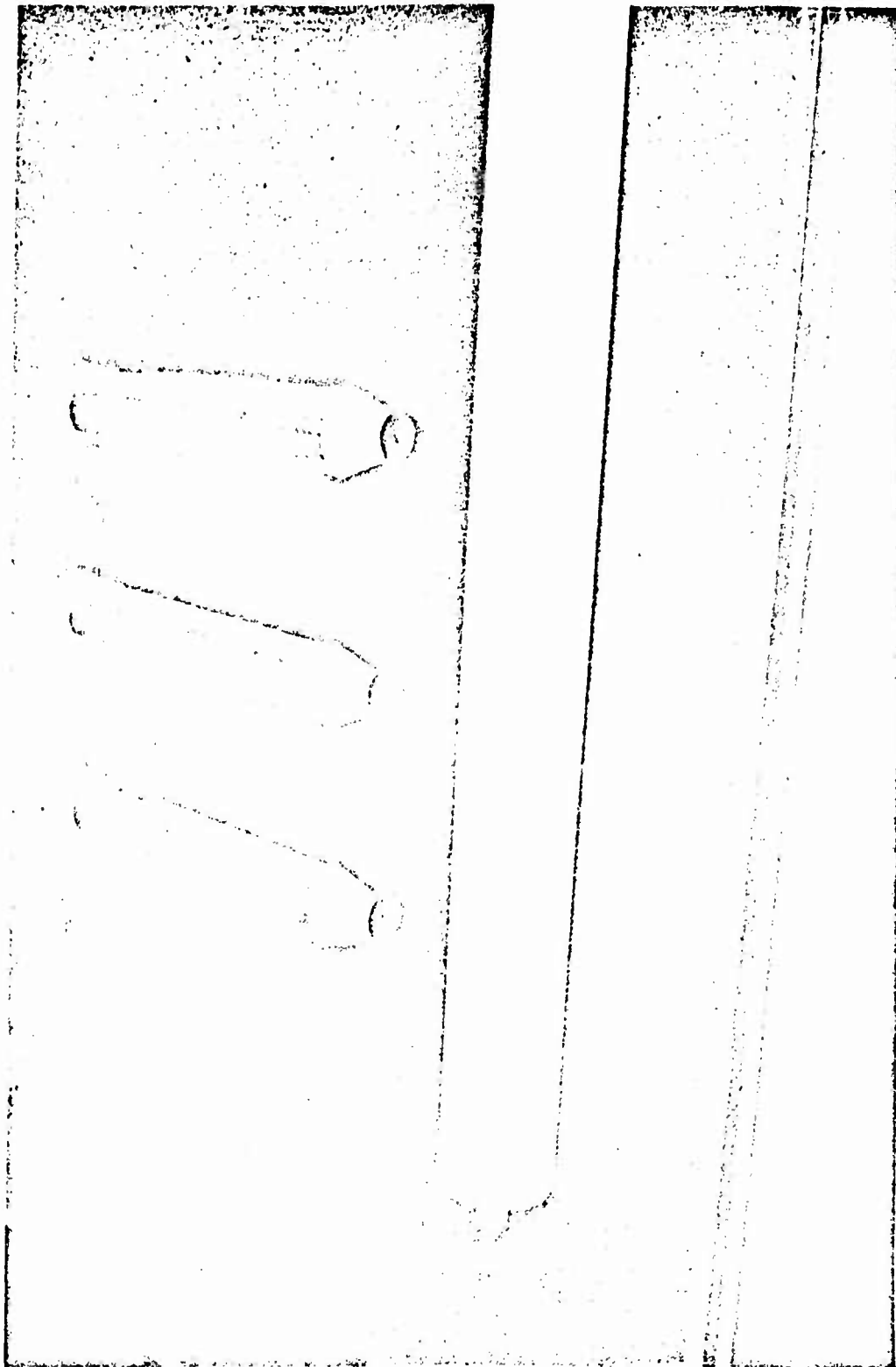
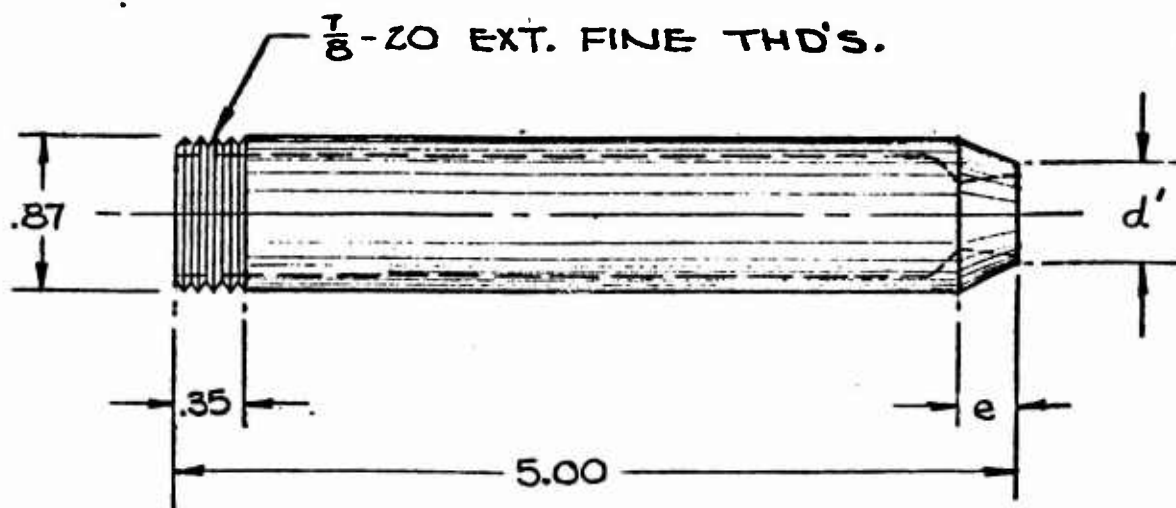
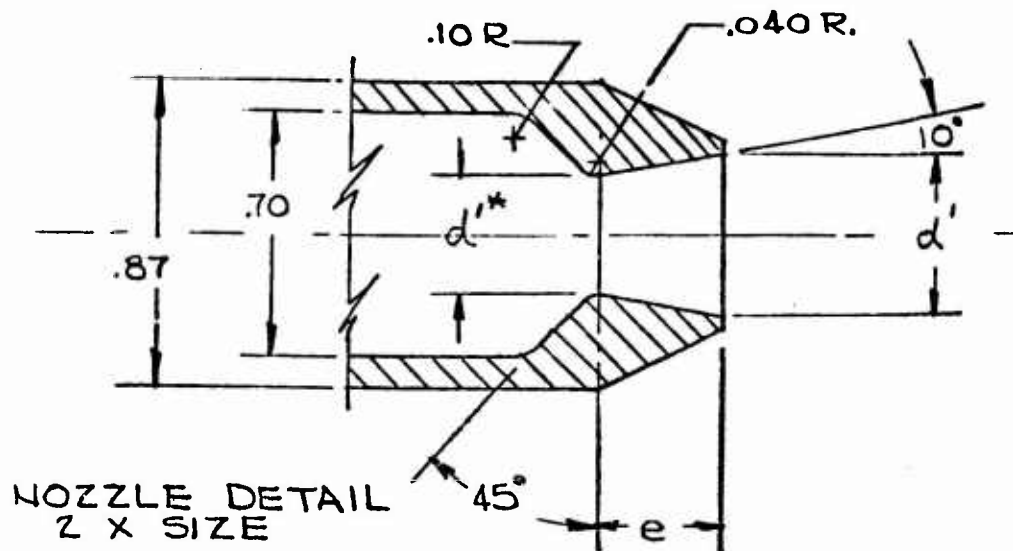


Figure 9.1-6 Straight Ejector Primary Nozzles



MATL: STAINLESS STEEL



MODEL	d'	d'^*	A'	e
1	.520	.356	.212	.52
2	.446	.330	.155	.36
3	.418	.319	.137	.27
4	.406	.319	.129	.22

ALL DIMENSIONS
IN INCHES

FIGURE 9.1-7 STRAIGHT EJECTOR PRIMARY NOZZLE

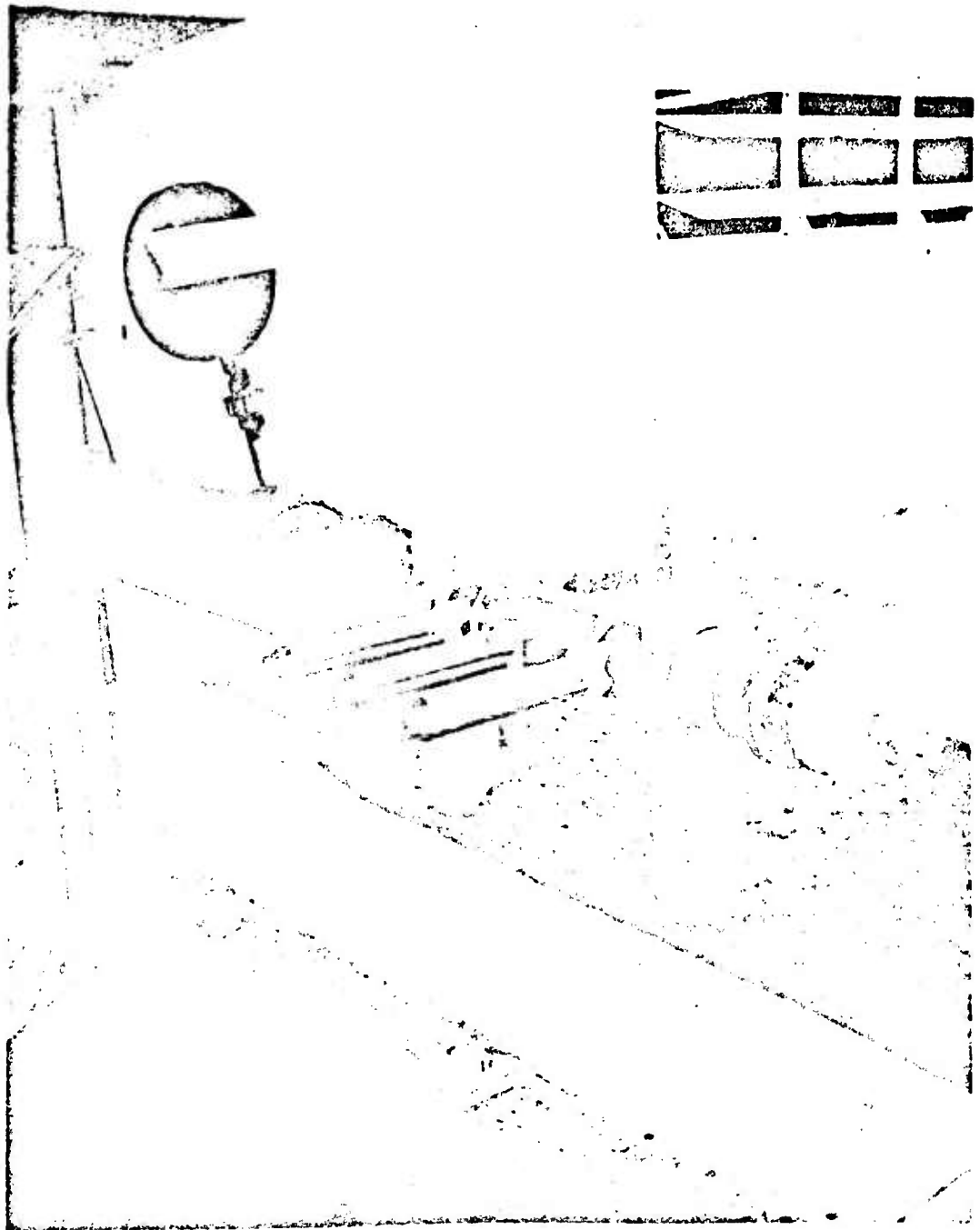


Figure 9.1-8 Straight Ejector Primary Nozzle-Header Assembly

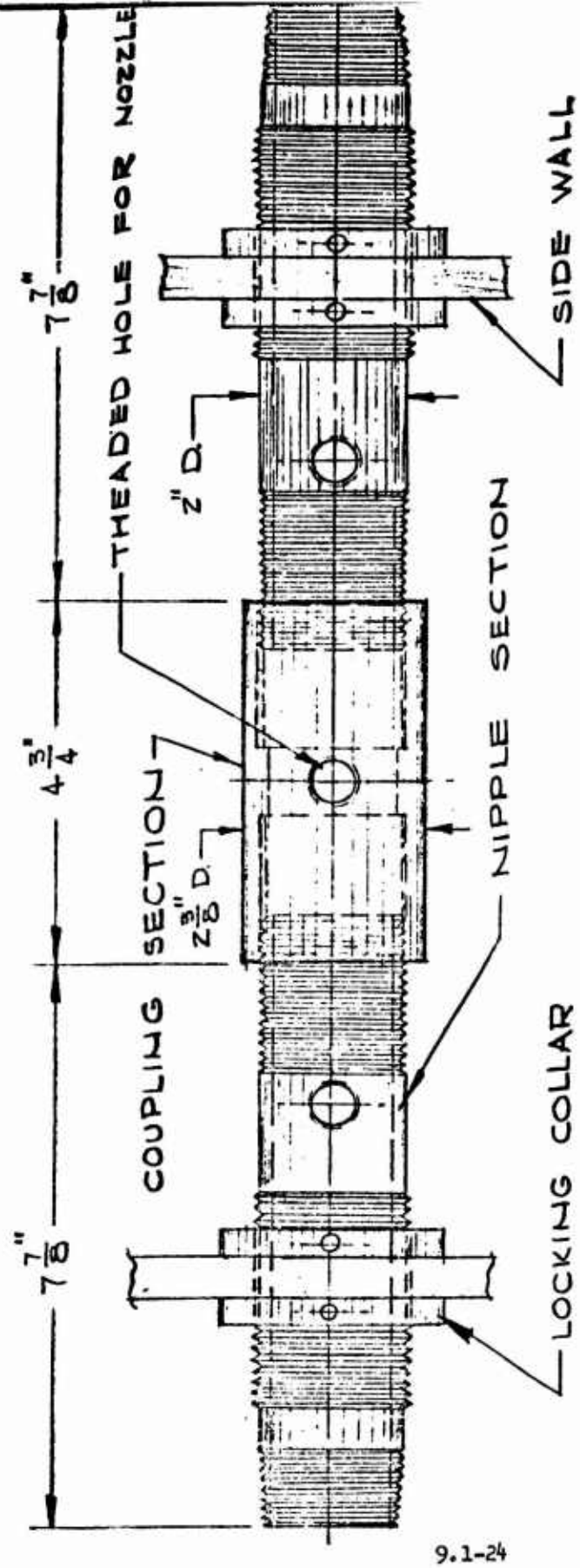


FIGURE 9.1-9 STRAIGHT EJECTOR PRIMARY MANIFOLD

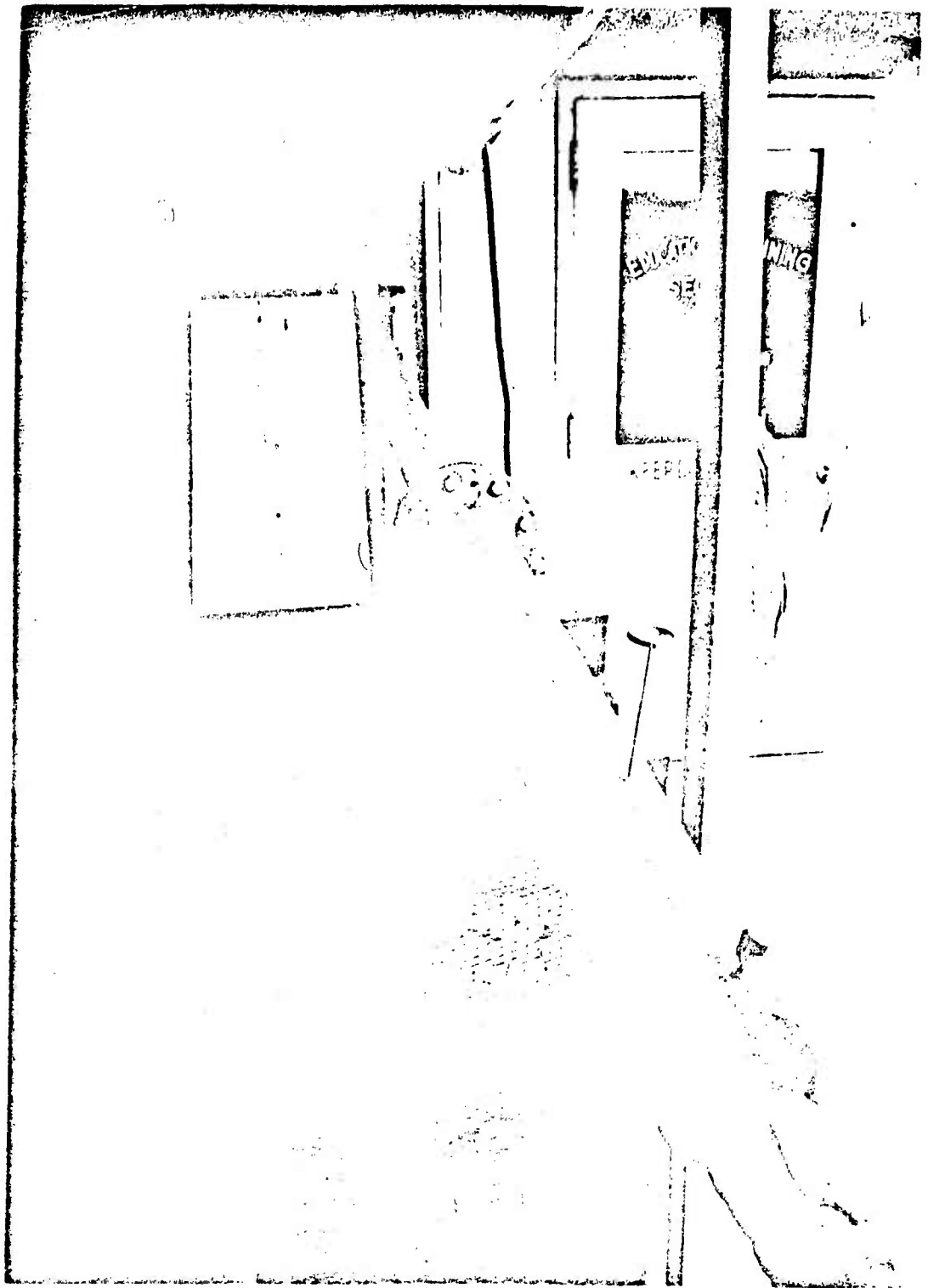


Figure 9.1-10 Primary Mass Flow Meter

9.1-25

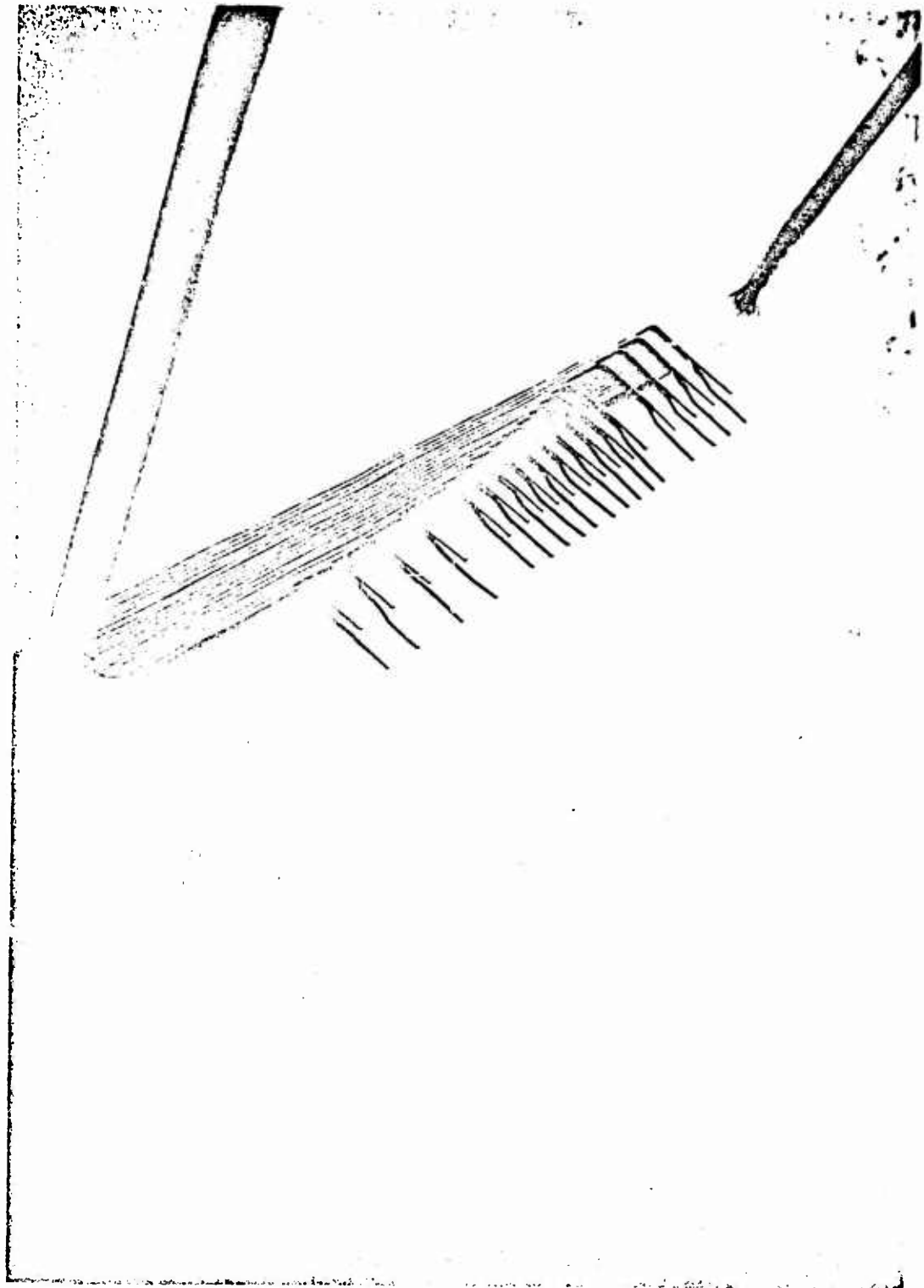


Figure 9.1-11 Straight Ejector Exit Pitot-Static Rake

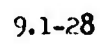


FIGURE 3.1-13 INLET PITOT - STATIC RAKE

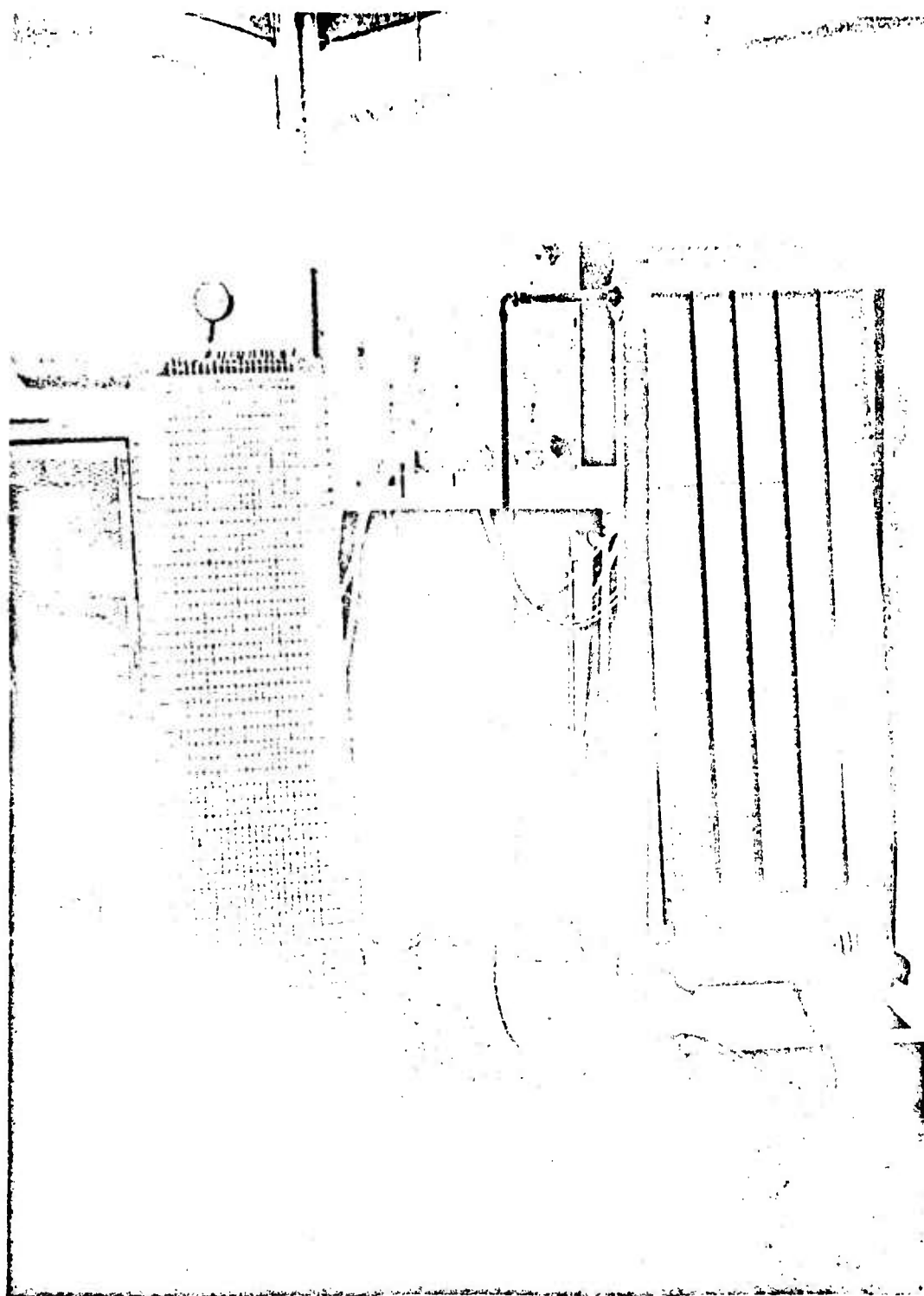
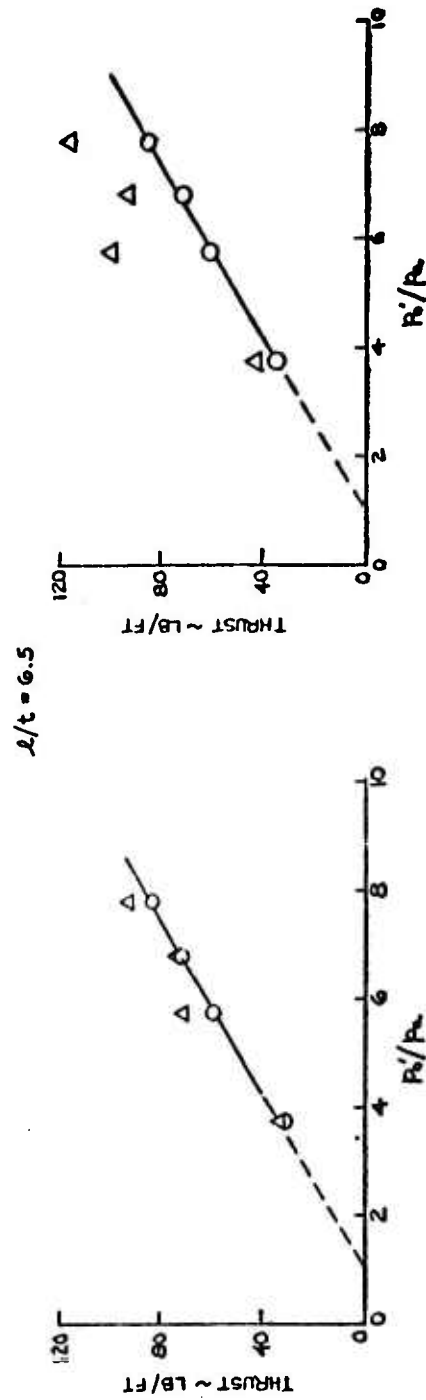
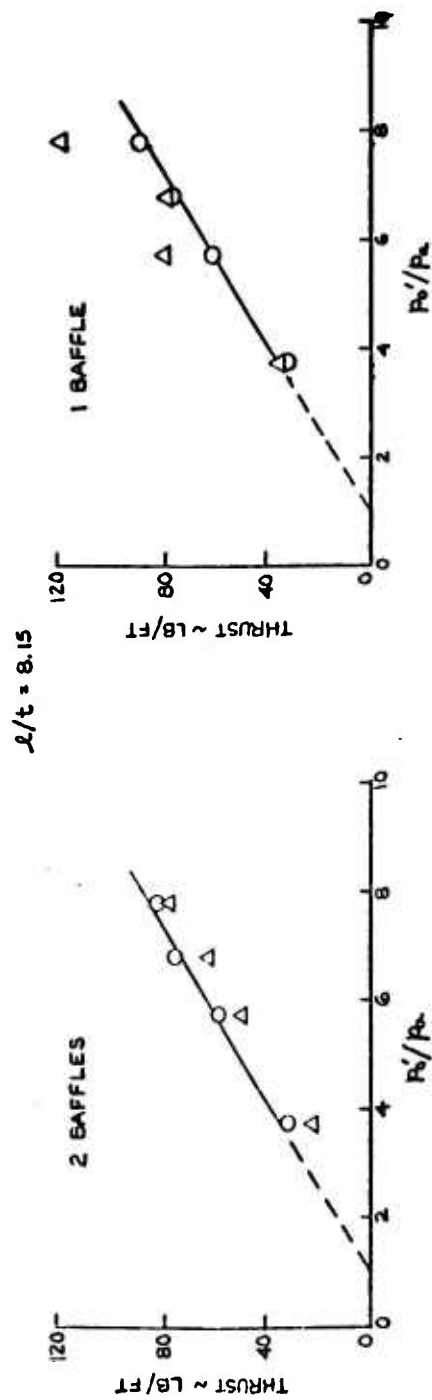


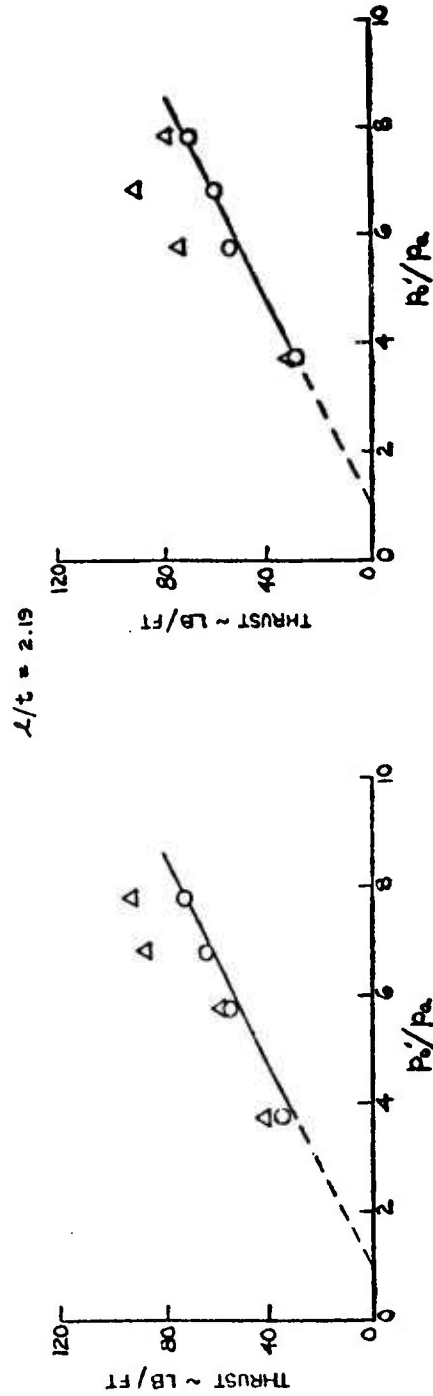
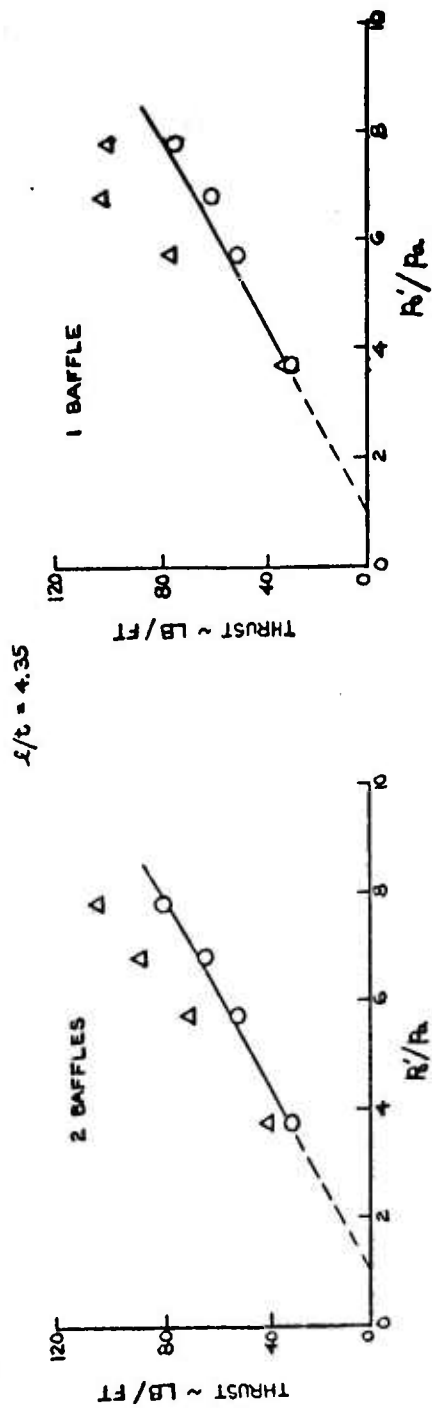
Figure 9.1-14 Mercury and Water Manometer Banks



○ INTEGRATION OF STATIC PRESSURES IN THRUST
DIRECTION PLUS PRIMARY NOZZLE THRUST

△ $T_{tot} = c_3 \frac{1}{c_2} \int V_2^2 dt + \frac{1}{c_2} \int (p_2 - p_1) dt$

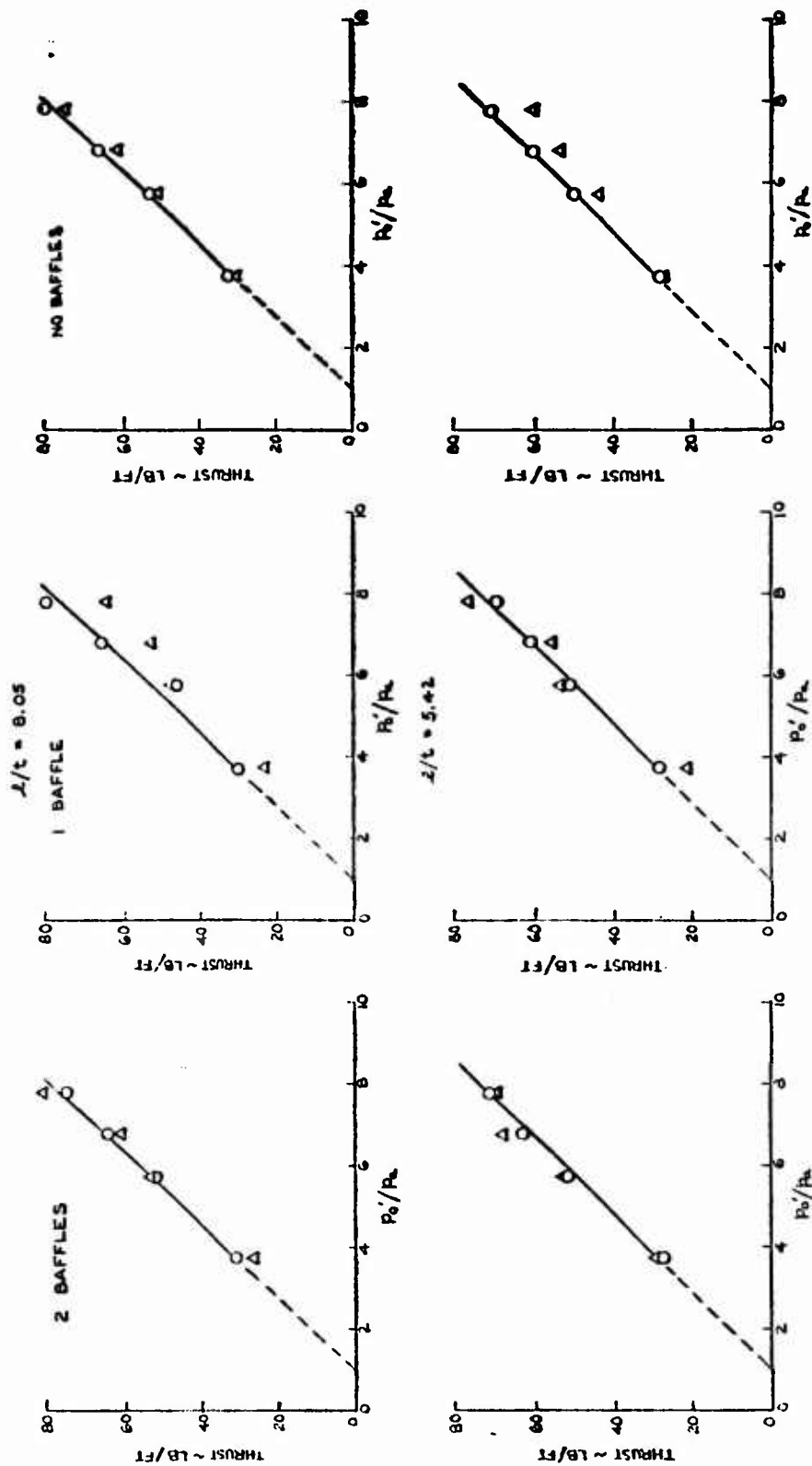
FIGURE 9.1-15 MODEL 1 STRAIGHT EJECTOR TOTAL THRUST



○ INTEGRATION OF STATIC PRESSURES IN THRUST
DIRECTION OF PRIMARY NOZZLE THRUST

△ $T_{TOT} = \rho_s \frac{1}{t_0} \int v_s^2 dt + \frac{1}{t_0} \int (p_s - p_a) dt$

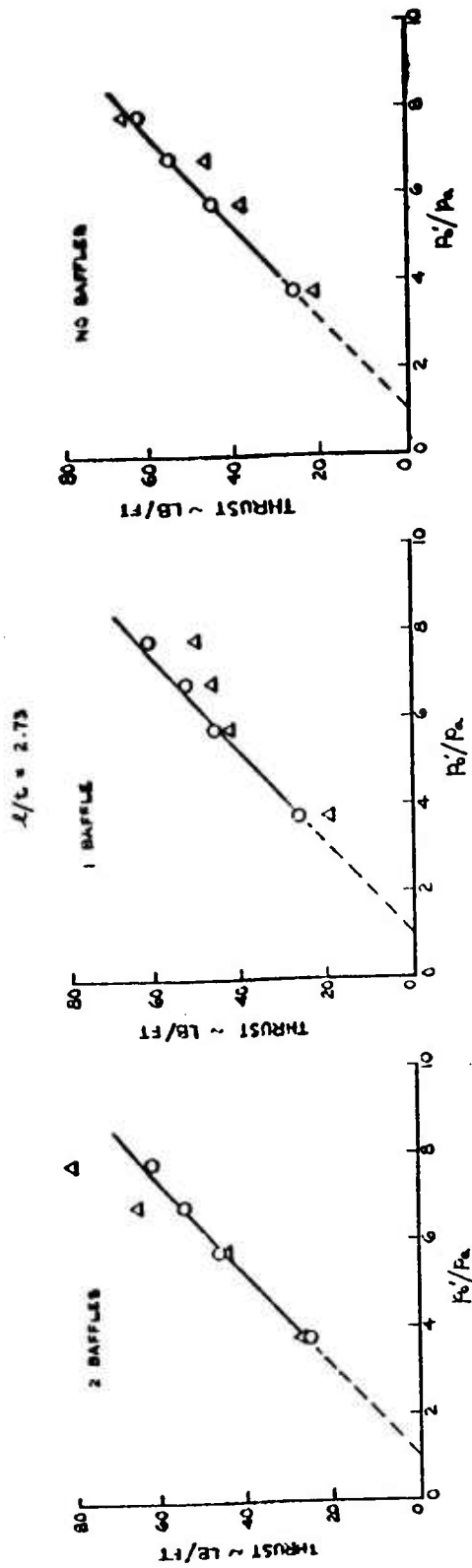
FIGURE 9.1-15 (CONT'D) MODEL 1 STRAIGHT EJECTOR TOTAL THRUST



O INTEGRATION OF STATIC PRESSURES IN THRUST
DIRECTION PLUS PRIMARY NOZZLE THRUST

$$\Delta T_{\text{Tot}} = \rho_3 \int_0^L V_3^2 dt + \frac{1}{L_0} \int_0^L (p_3 - p_\infty) dt$$

FIGURE 8.1-16 MODEL 2 STRAIGHT EJECTOR TOTAL THRUST



○ INTEGRATION OF STATIC PRESSURES IN THRUST
DIRECTION PLUS PRIMARY NOZZLE THRUST

$$\Delta T_{TOT} = C_p \frac{1}{2} \int_{t_1}^{t_2} v_1^2 dt + \frac{1}{2} \int_{t_1}^{t_2} (p_1 - p_\infty) dt$$

FIGURE 9.1-16 (CONT'D) MODEL 2 STRAIGHT EJECTOR TOTAL THRUST

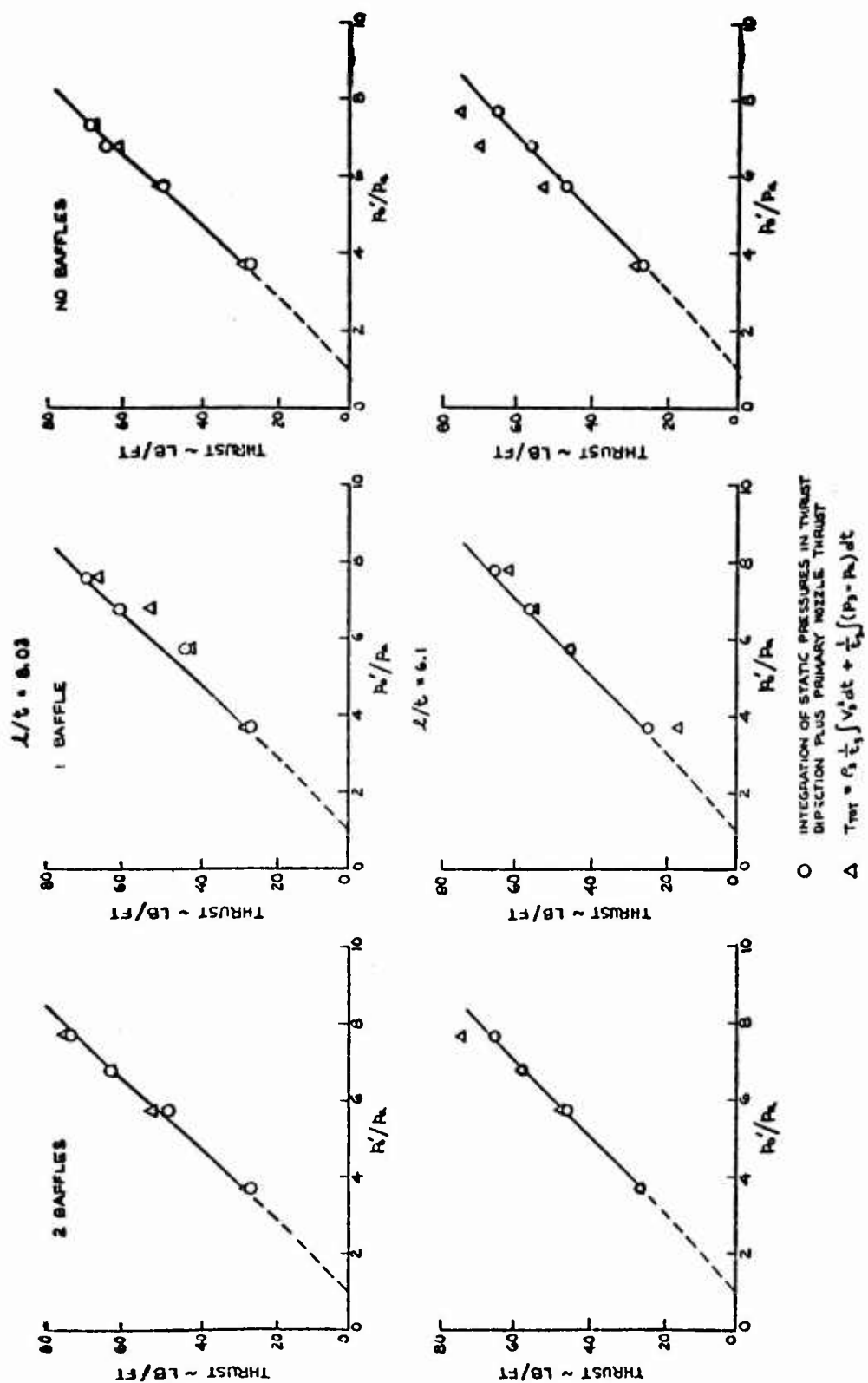
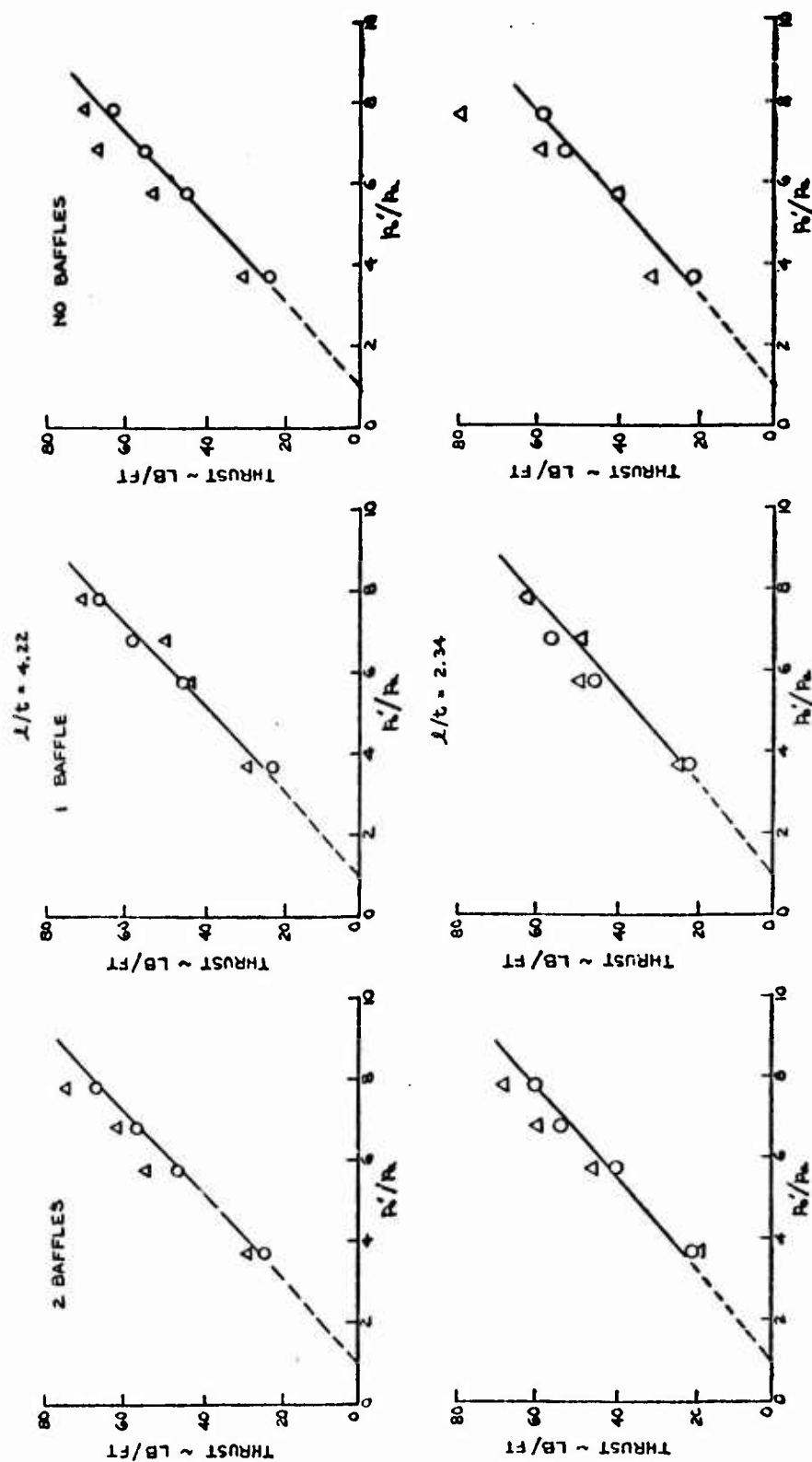
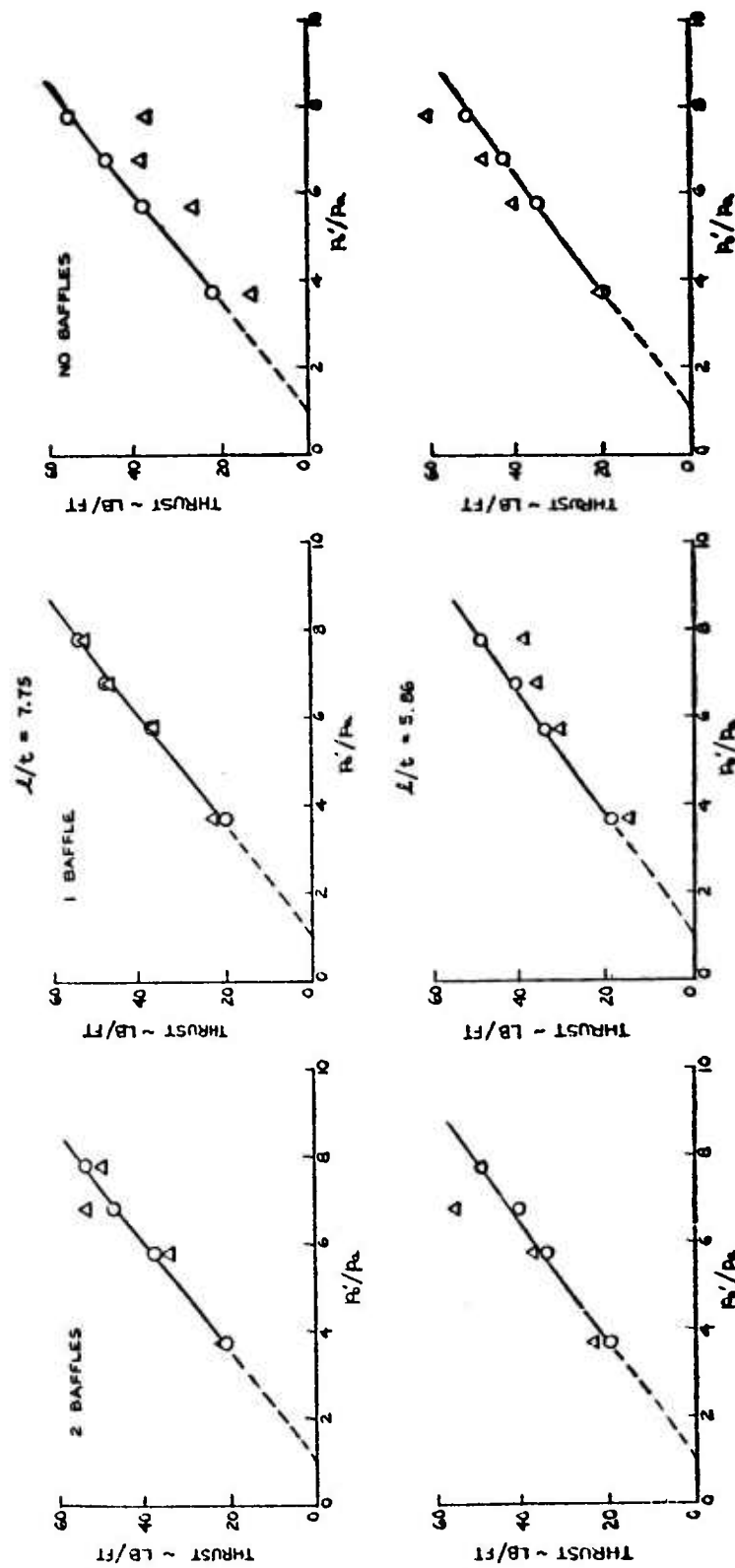


FIGURE 9.1-17 MODEL 3 STRAIGHT EJECTOR TOTAL THRUST



INTEGRATION OF STATIC PRESSURES IN THRUST DIRECTION PLUS PRIMARY NOZZLE THRUST

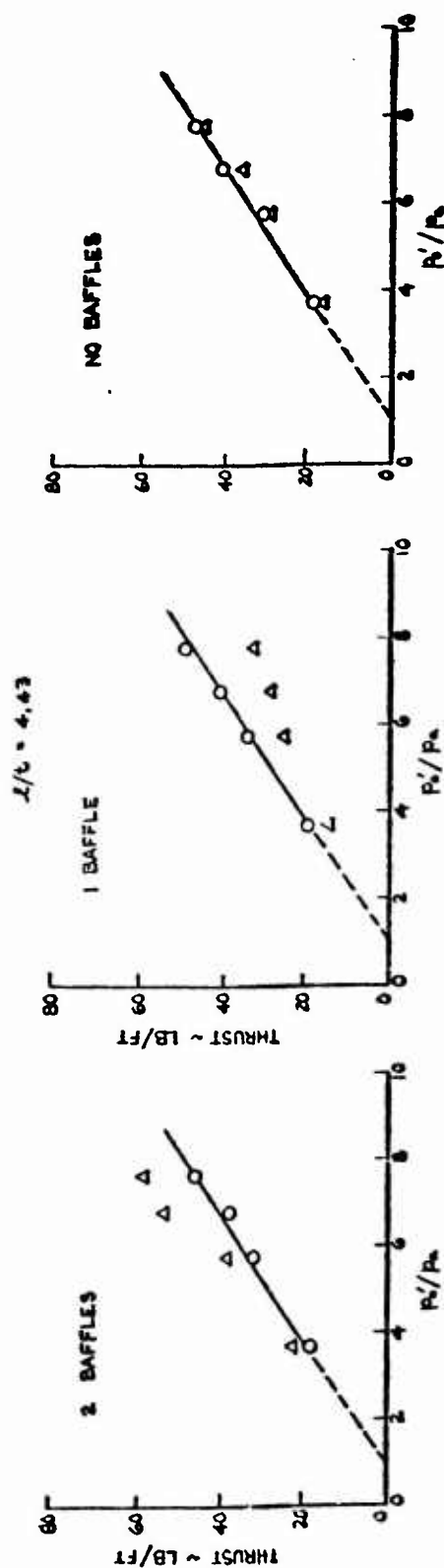
FIGURE 9.1-17 (CONT'D) MODEL 3 STRAIGHT EJECTOR TOTAL THRUST



O INTEGRATION OF STATIC PRESSURES IN THRUST
 Δ DIRECTION PLUS PRIMARY NOZZLE THRUST

$$T_{TOT} = \rho_3 \frac{1}{2} \int V_3^2 dt + \frac{1}{2} \int (P_1 - P_2) dt$$

FIGURE 9.1-18 MODEL 4 STRAIGHT EJECTOR TOTAL THRUST



○ INTEGRATION OF STATIC PRESSURES IN THRUST DIRECTION PLUS PRIMARY NOZZLE THRUST

△ $T_{tot} = \rho_3 \frac{1}{t_3} \int v_3^2 dt + \frac{1}{t_3} \int (p_3 - p_a) dt$

FIGURE 9.1-18 (CONT'D) MODEL 4 STRIGHT EJECTOR TOTAL THRUST

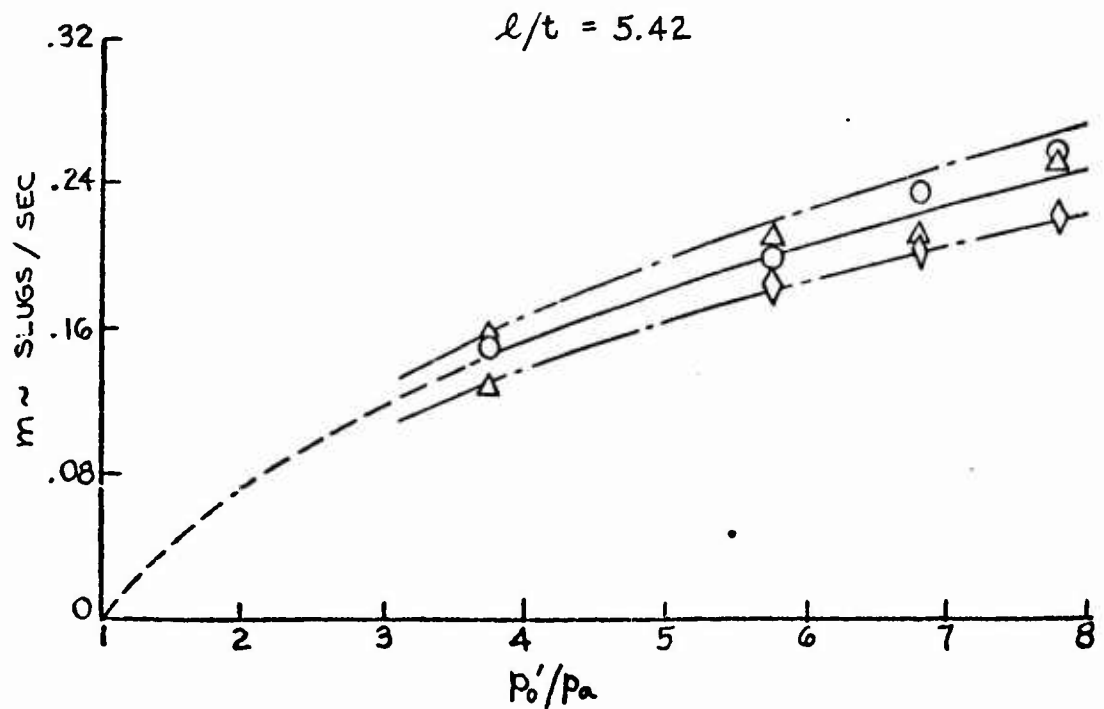
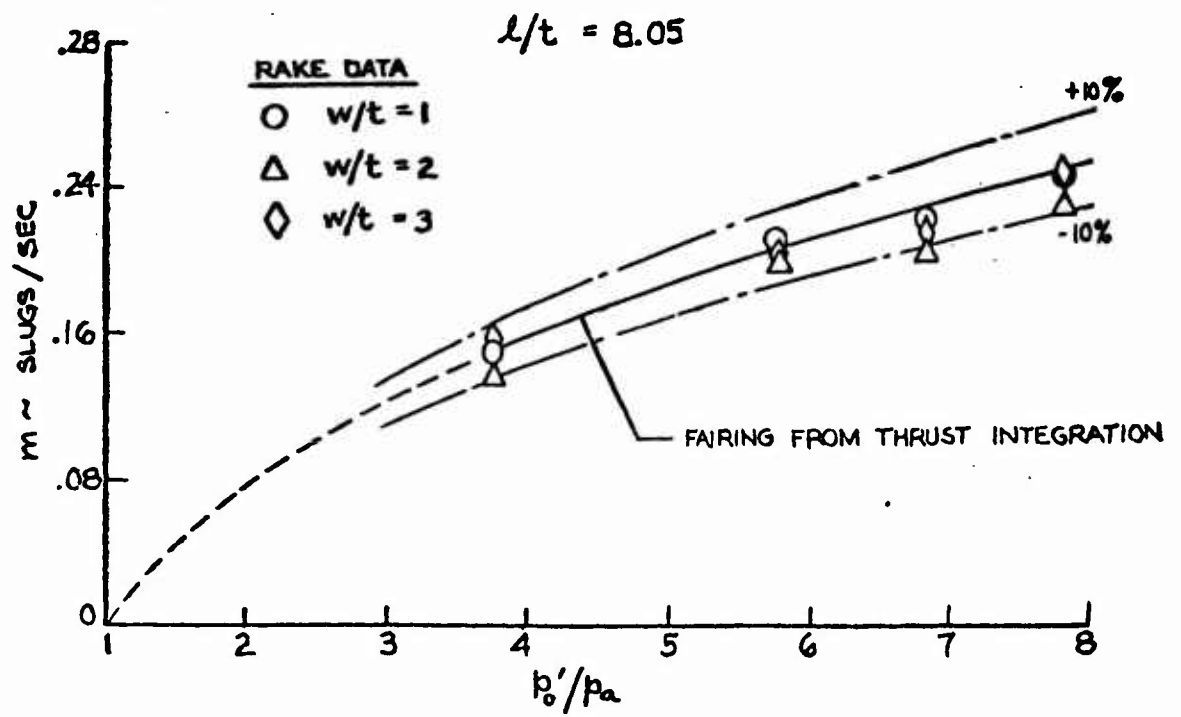


FIGURE 9.1-19 EXPERIMENTAL STRAIGHT EJECTOR TERTIARY MASS FLOW - MODEL 2

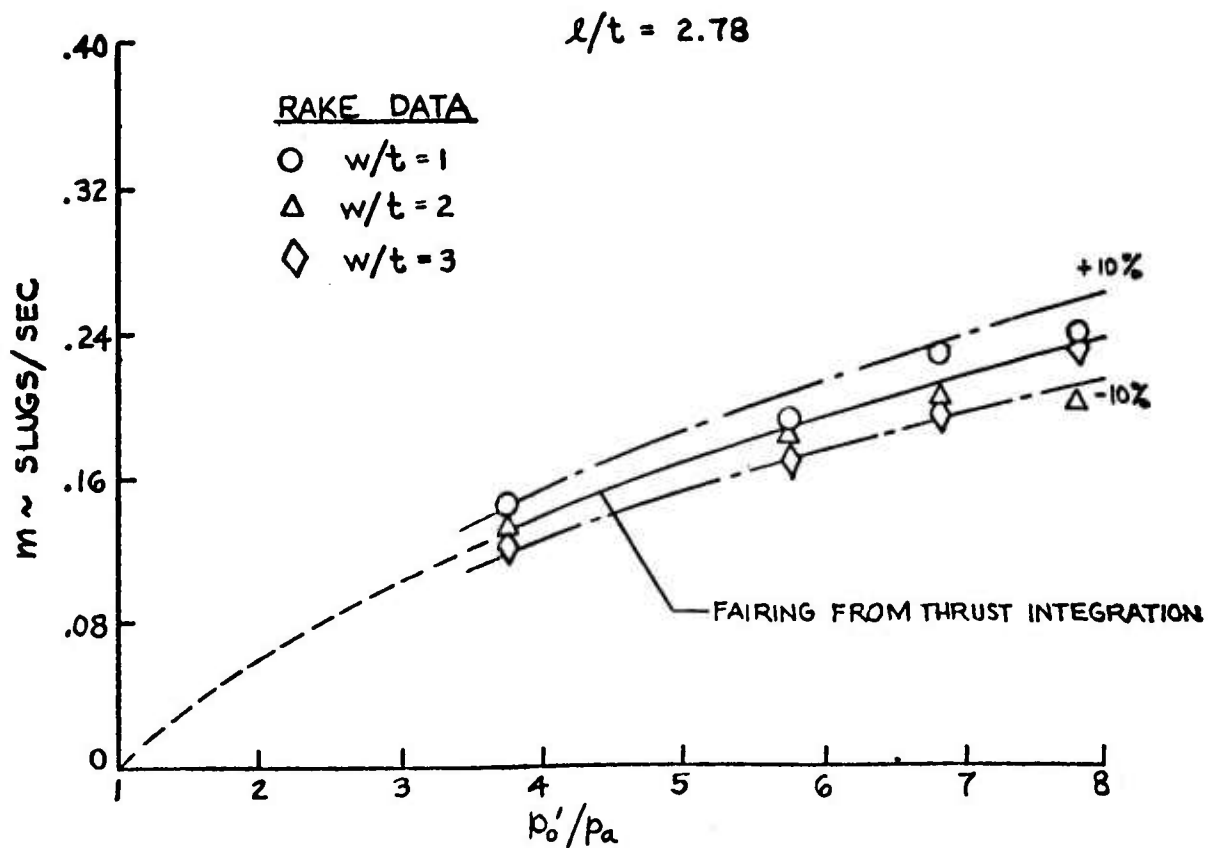


FIGURE 9.1-19 (CONT'D) EXPERIMENTAL STRAIGHT EJECTOR TERTIARY MASS FLOW - MODEL 2

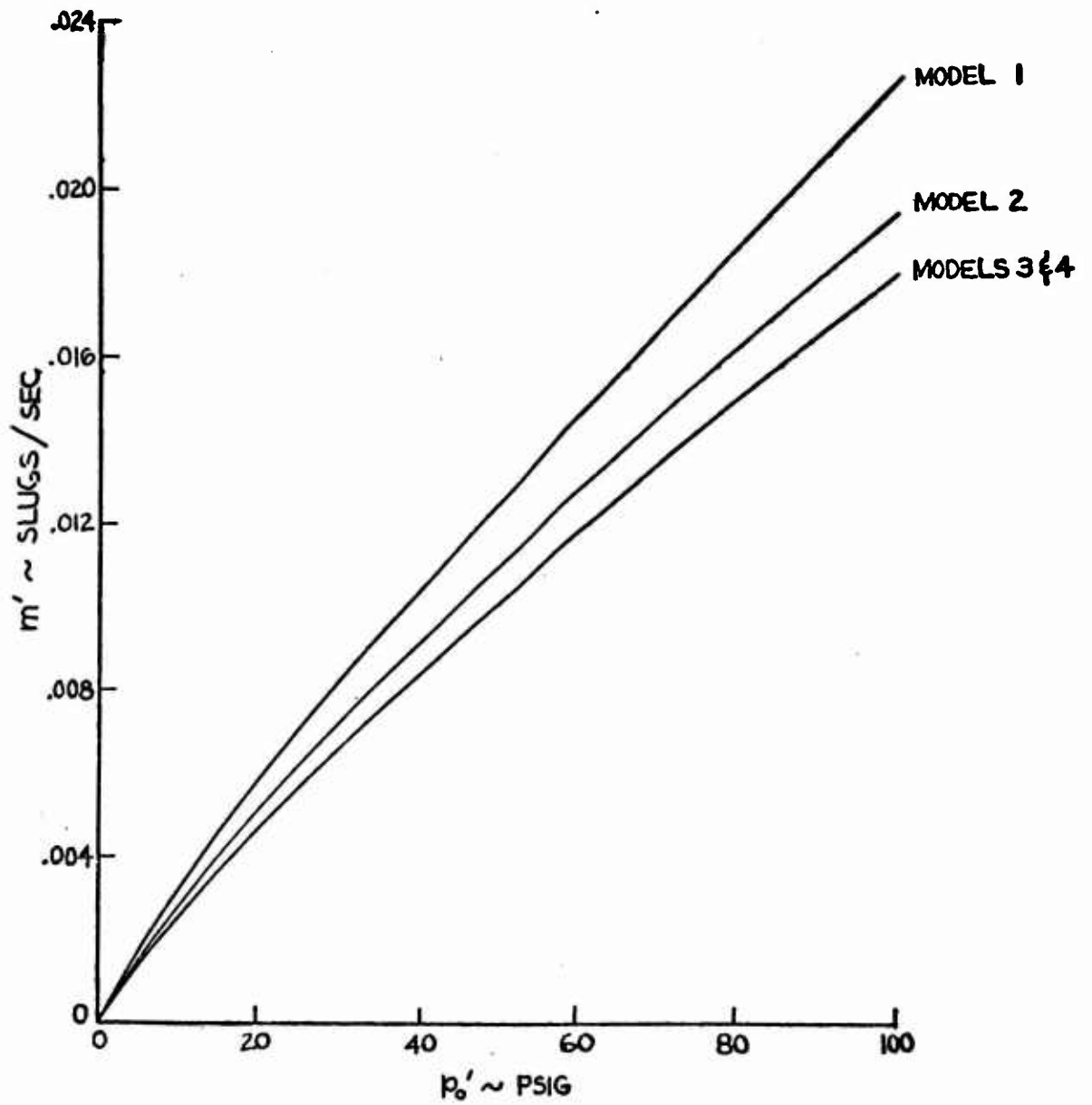


FIGURE 9.1-20 STRAIGHT EJECTOR PRIMARY MASS FLOW - EXPERIMENTAL RESULTS

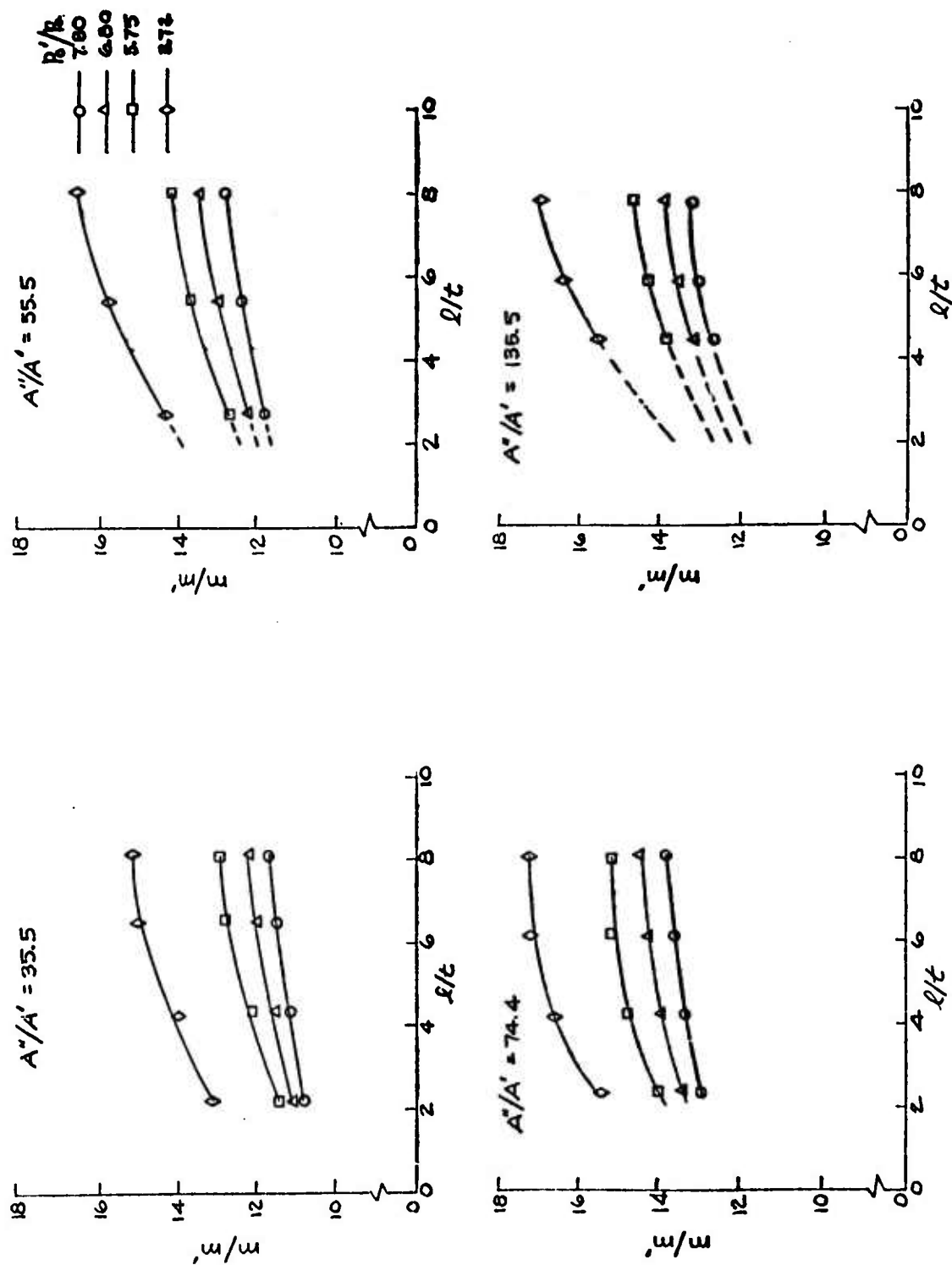


FIGURE 9.1-21 EFFECT OF MIXING SECTION LENGTH ON STRAIGHT EJECTOR MASS AUGMENTATION - EXPERIMENTAL RESULTS

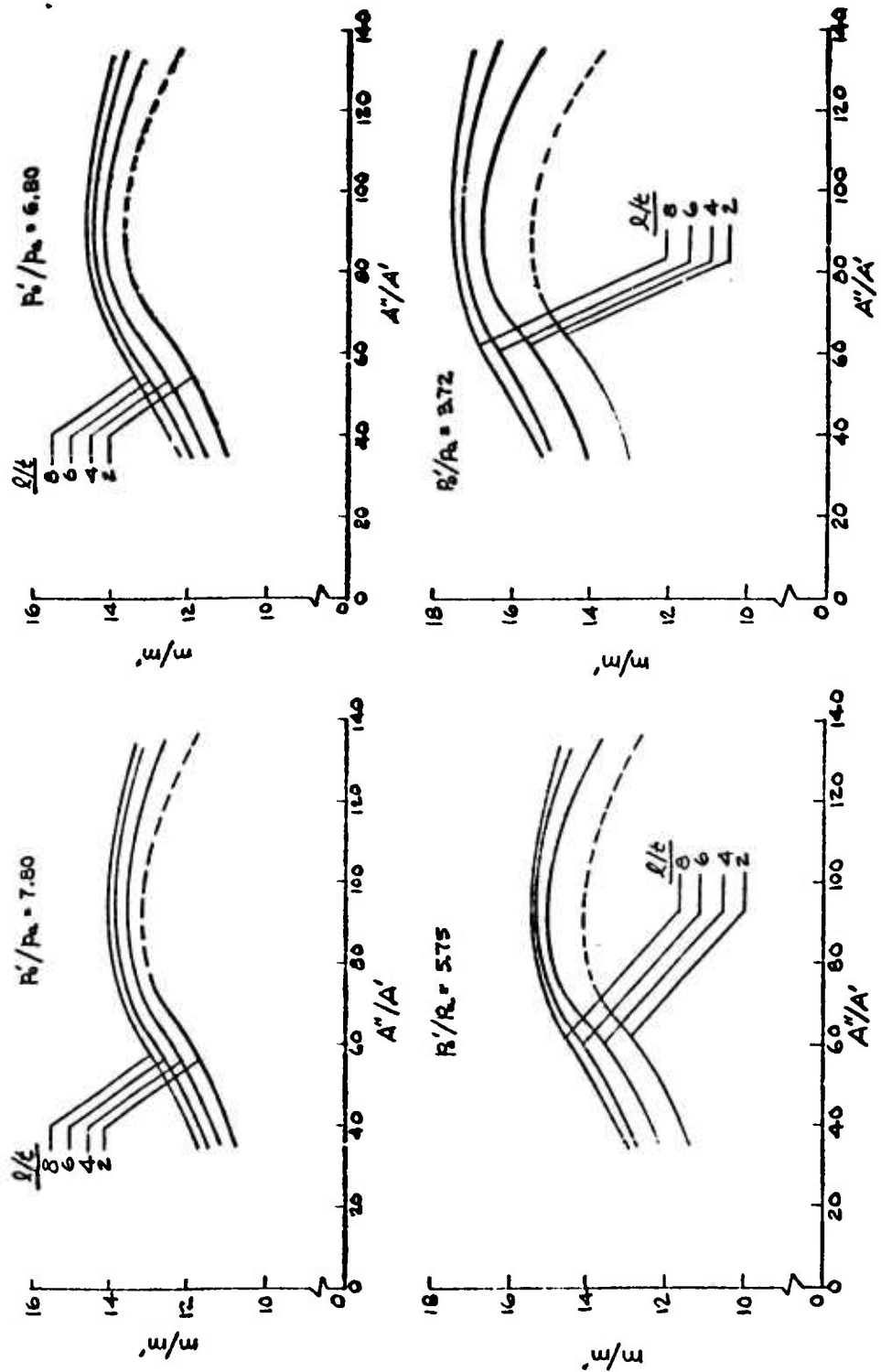


FIGURE 9.1-22 EFFECT OF AREA RATIO ON STRAIGHT EJECTOR MASS AUGMENTATION - EXPERIMENTAL RESULTS

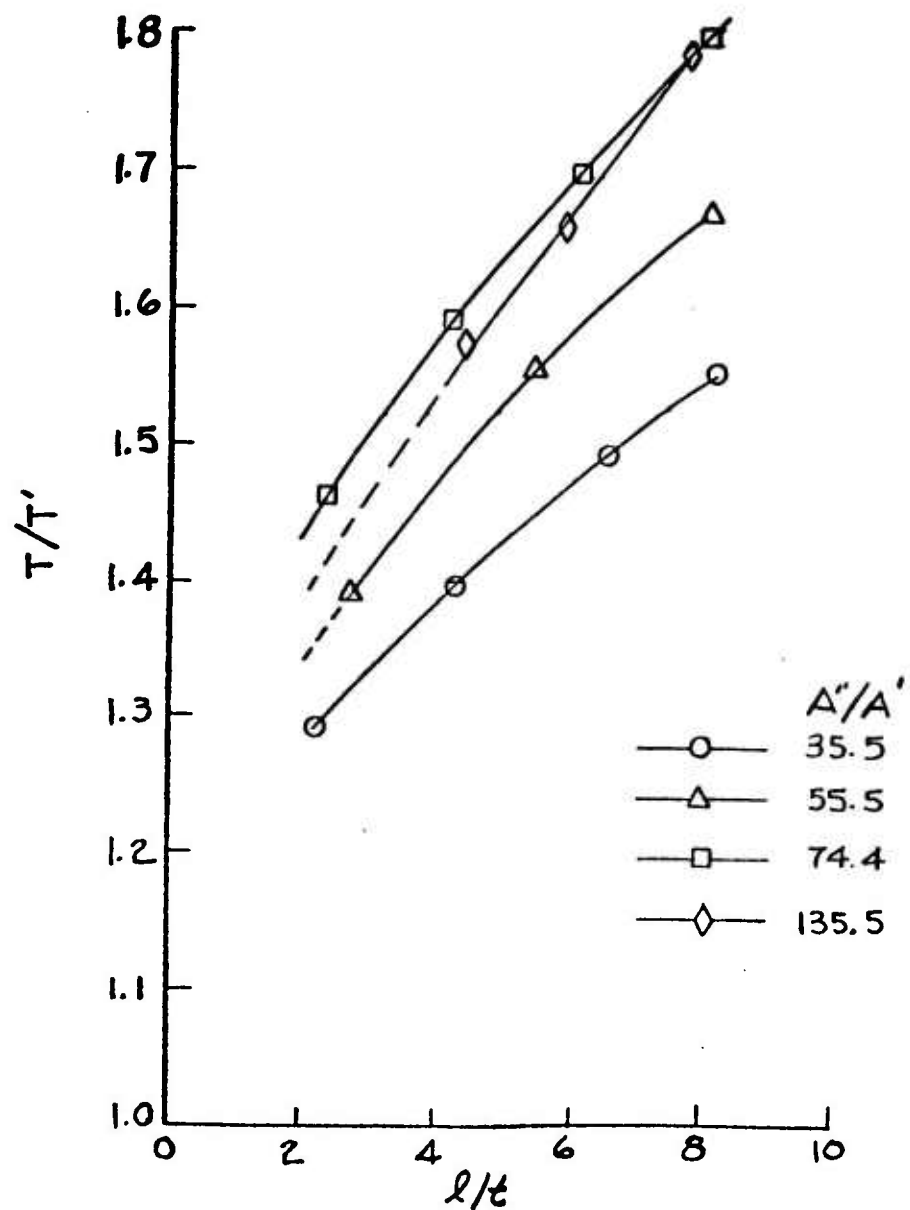


FIGURE 9.1-23 EFFECT OF MIXING SECTION LENGTH ON STRAIGHT EJECTOR THRUST AUGMENTATION (EXPERIMENTAL RESULTS)

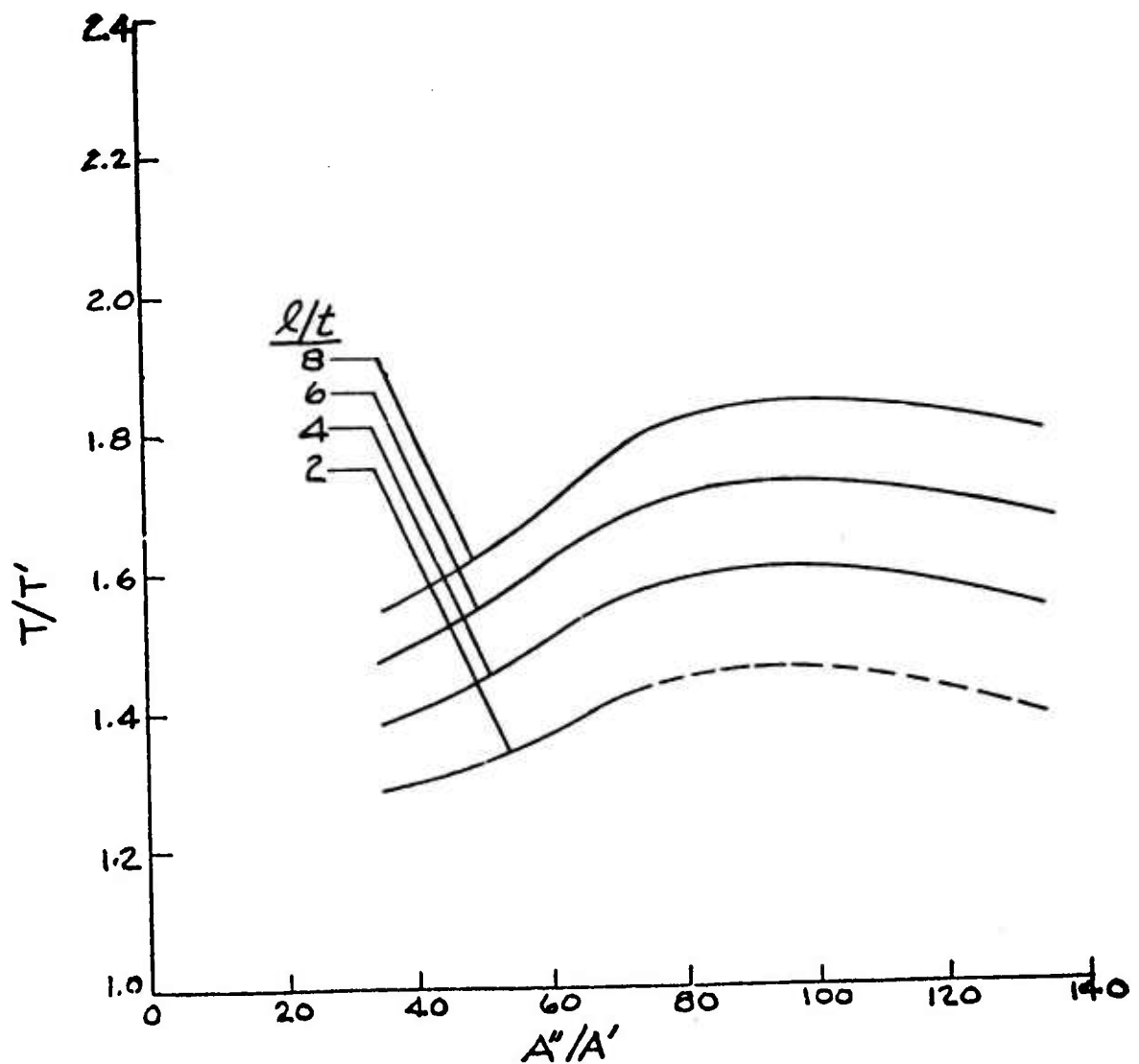


FIGURE 9.1-24 STRAIGHT EJECTOR THRUST AUGMENTATION (EXPERIMENTAL RESULTS)

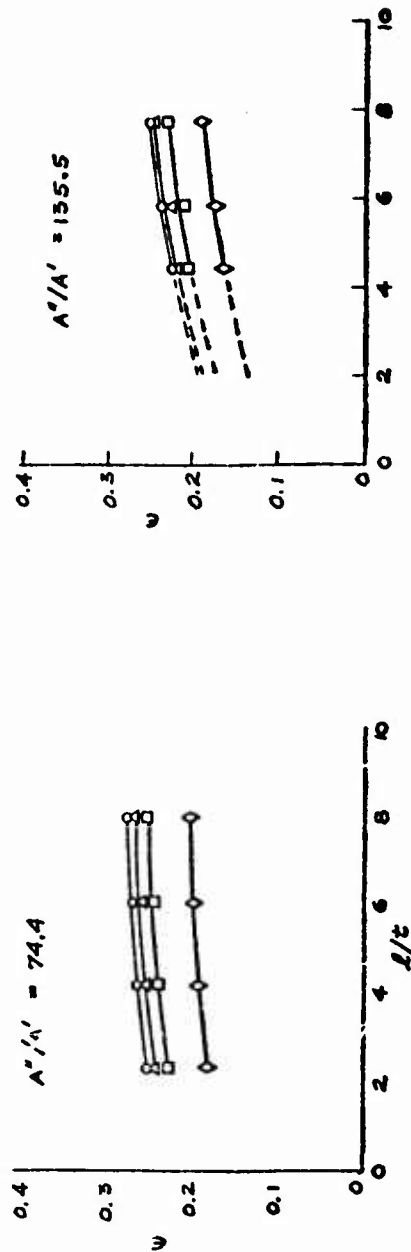
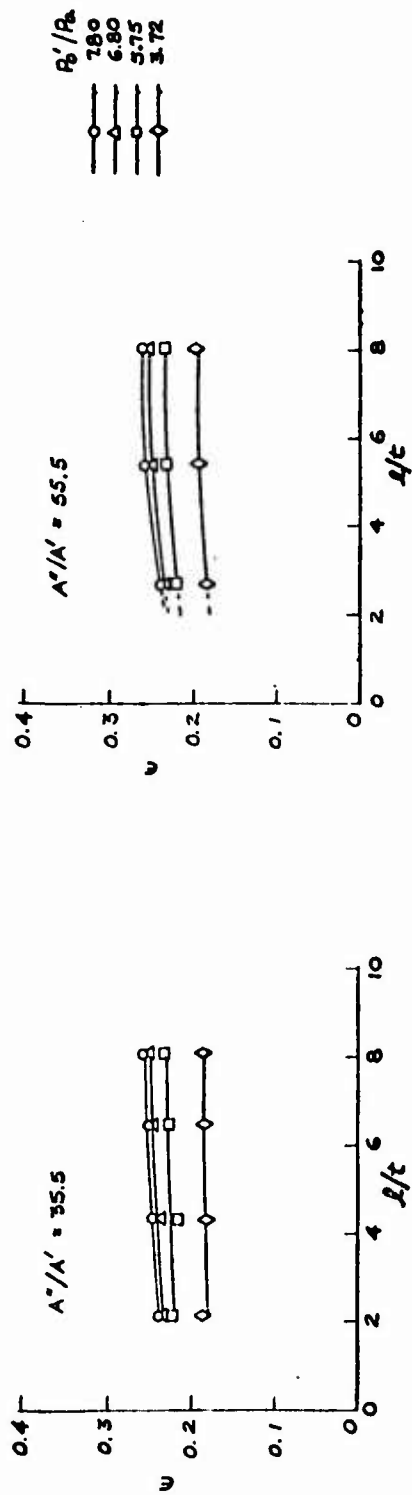


FIGURE 9.1-25 EFFECT OF MIXING SECTION LENGTH ON STRAIGHT EJECTOR EFFICIENCY. EXPERIMENTAL RESULTS

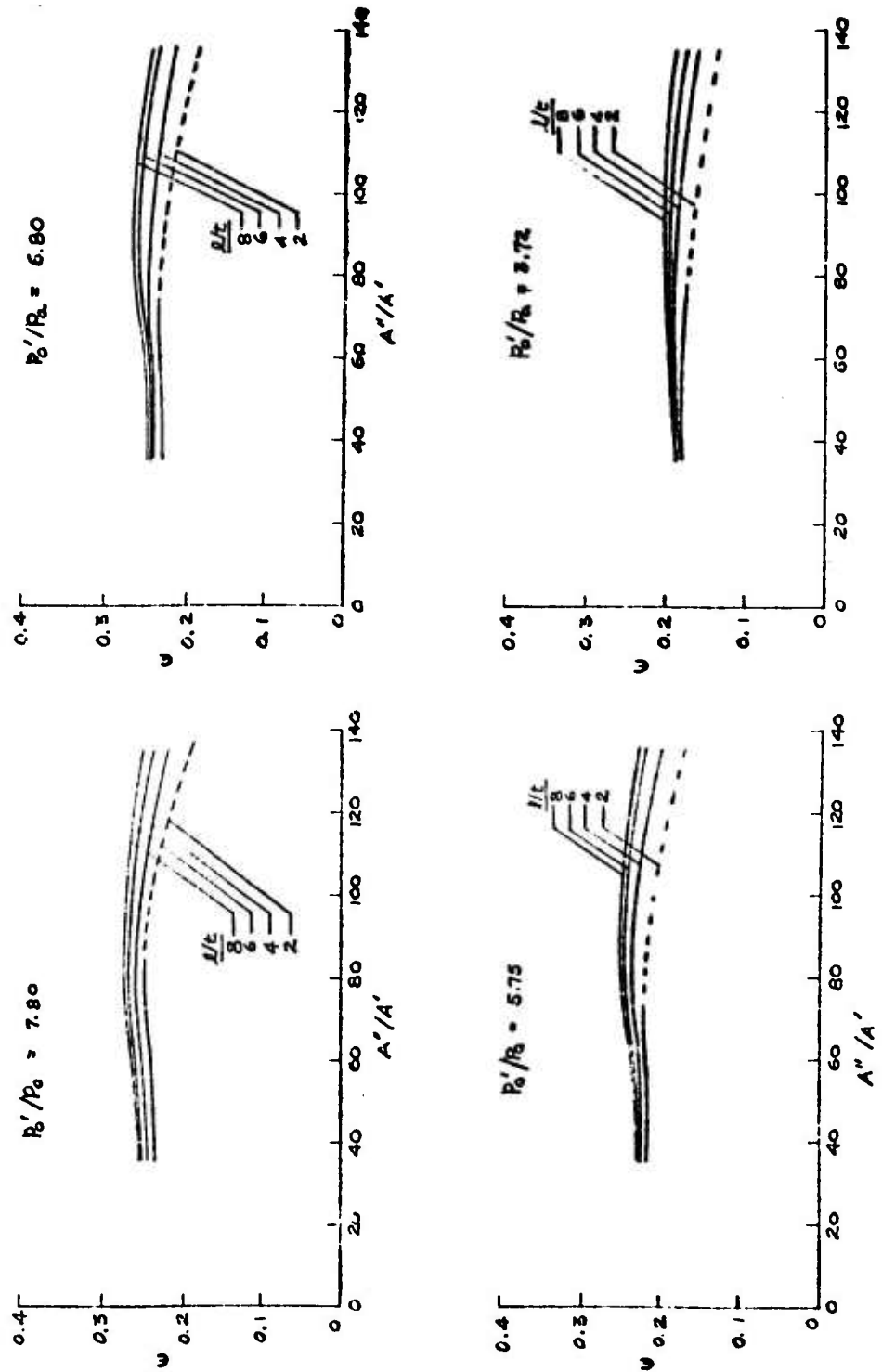


FIGURE 9.1-26 EFFECT OF AREA RATIO ON STRAIGHT EJECTOR EFFICIENCY - EXPERIMENTAL RESULTS

V_i = VELOCITY AT $p'_0/p_a = 7.80$

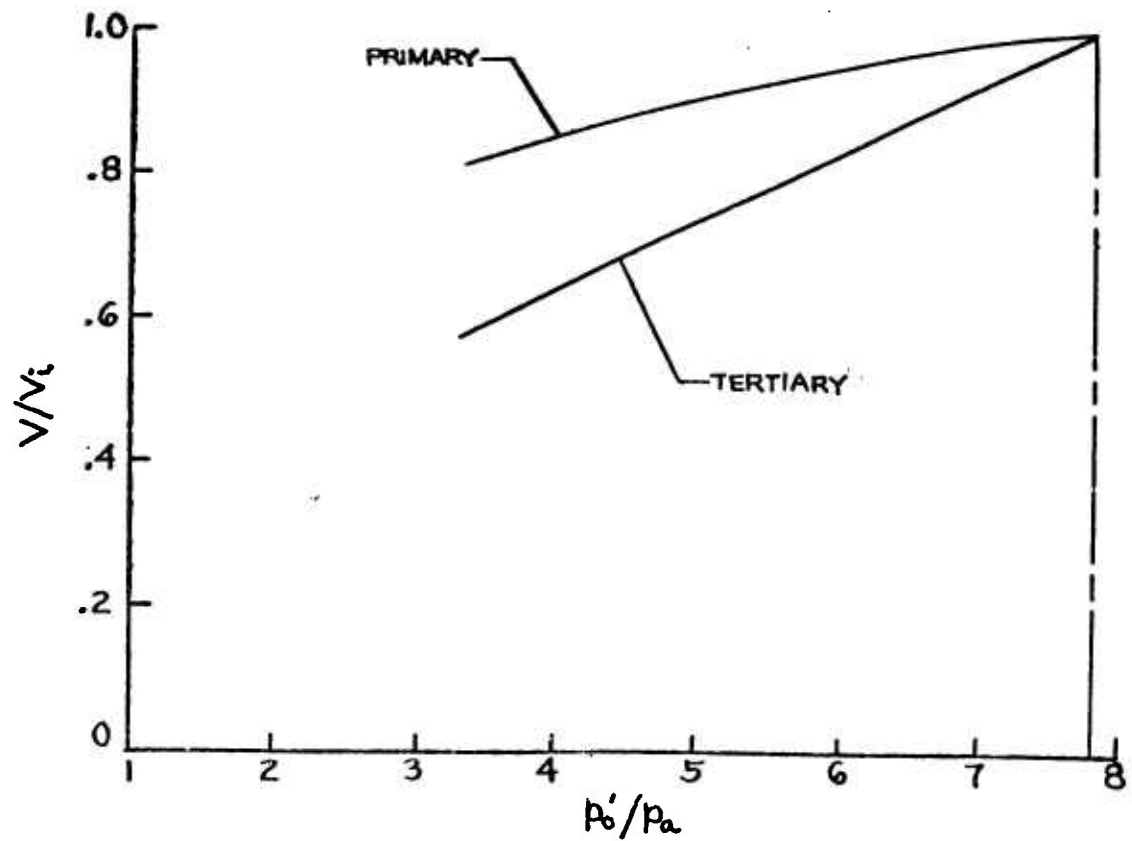


FIGURE 9.1-27 EFFECT OF PRIMARY TOTAL PRESSURE RATIO ON TERTIARY AND PRIMARY VELOCITY - MODEL 3 STRAIGHT EJECTOR

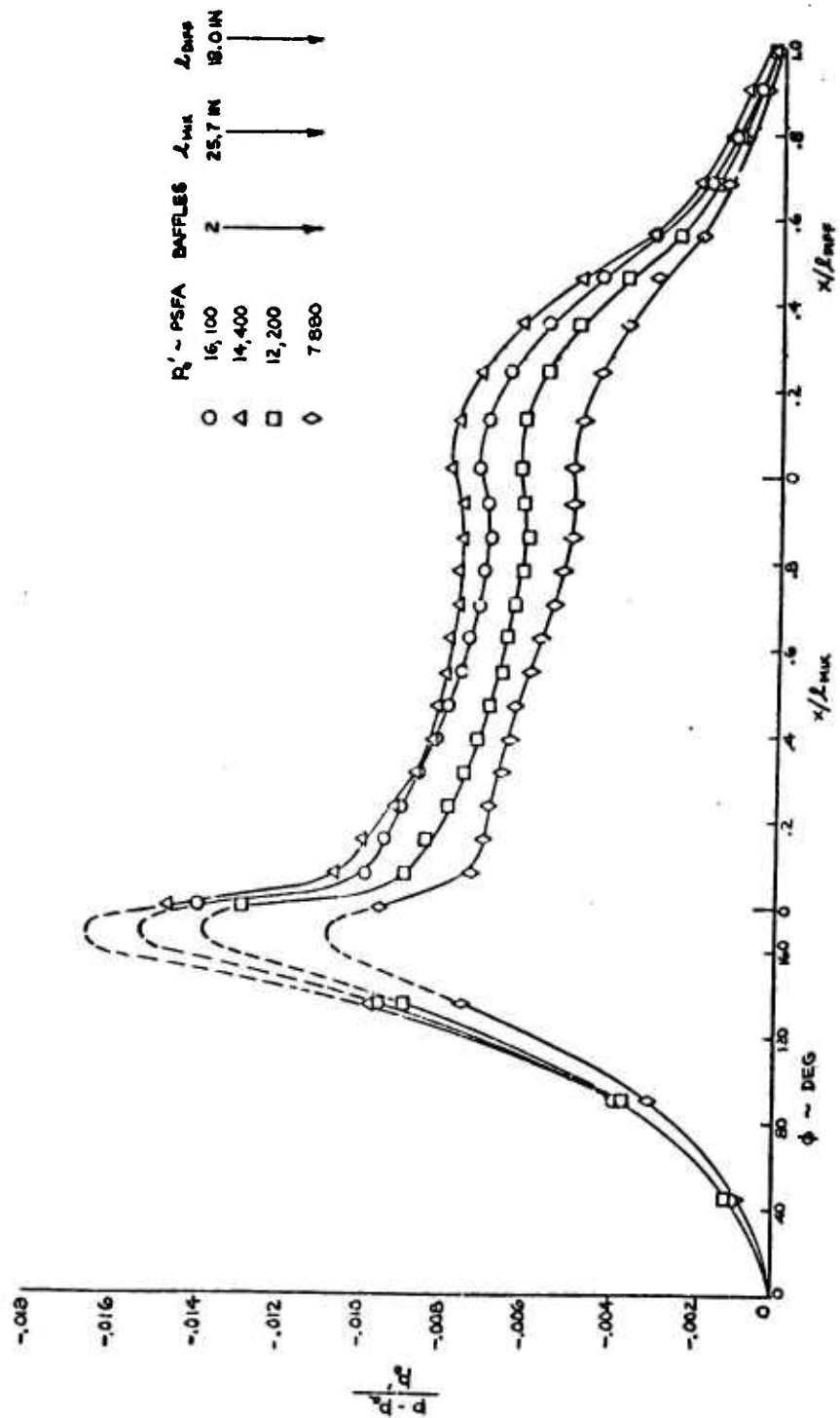


FIGURE 9.1-28 MODEL 3 STRAIGHT EJECTOR LONGITUDINAL STATIC PRESSURE DISTRIBUTIONS - $L/t = 8.09$

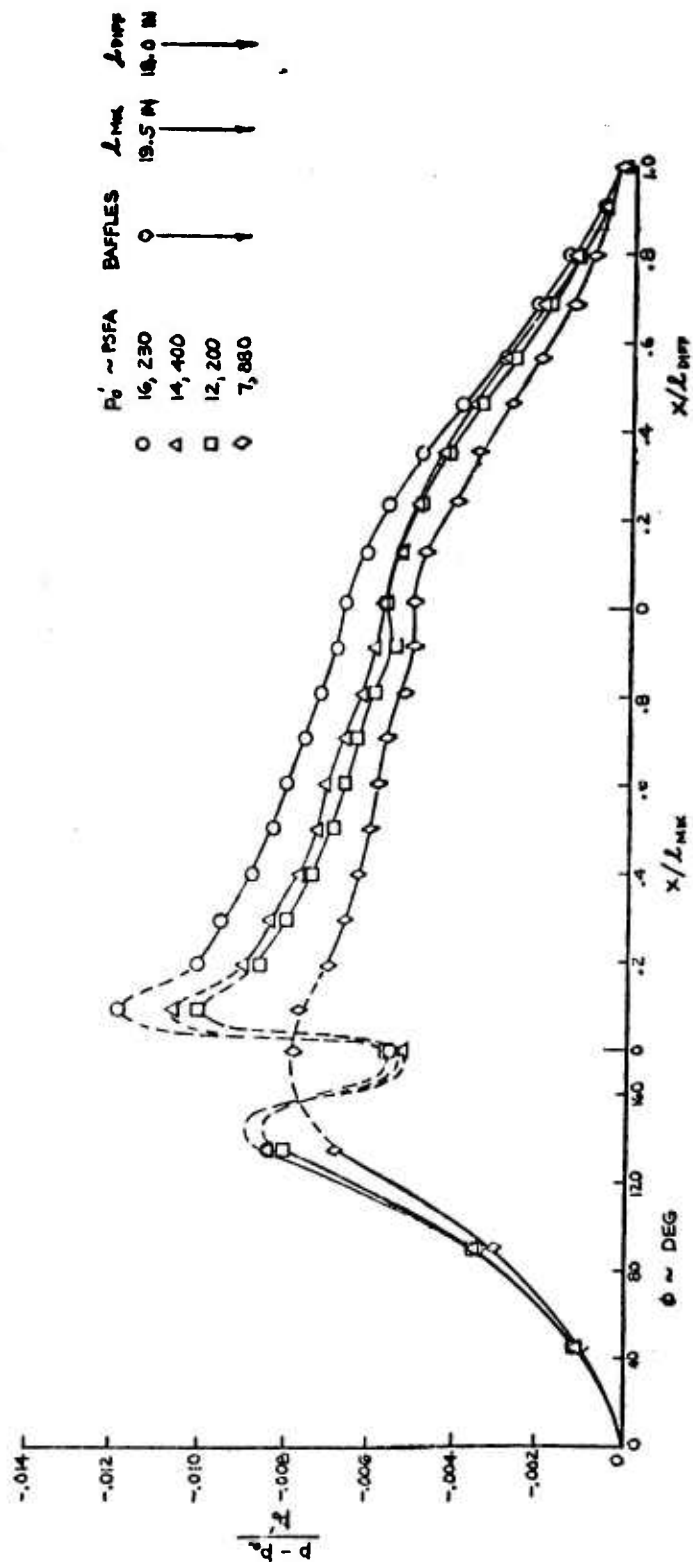


FIGURE 9.1-29 MODEL 3 STRAIGHT EJECTOR LONGITUDINAL STATIC PRESSURE DISTRIBUTIONS - $L/b = 6.1$

9.2 RECIRCULATING EJECTOR TESTS

9.2.1 SMALL SCALE TWO-DIMENSIONAL TESTS

Small two-dimensional Ejectijet pilot models were fabricated before the large models and tested in the assembly shown in Figures 9.2-1 and 9.2-2. The purpose of these models was to determine the basic feasibility of various configurations and to establish the effect of various center block shapes on the base pressure generated. In this manner, several configurations could be checked out before the large scale models were constructed and tested. It was not practical to attempt to obtain highly accurate data from these small scale models because of the difficulty in miniaturizing the instrumentation and determining the scale effect and correcting the data.

Of the configurations tested, three are shown in Figures 9.2-3 through 9.2-5. These models give representative results for the other models tested. In all cases, the same set of primary nozzles was used. The location of the primary nozzles was varied both in angle and position along the center line of the ejector mixing section.

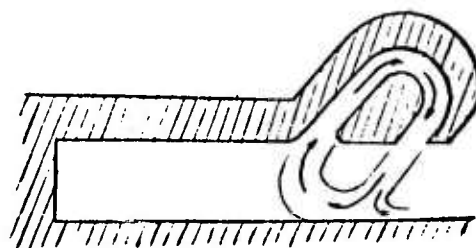
The results of these tests are as follows:

1. Primary nozzle location: The base pressure obtained varied according to both nozzle location and nozzle inclination. Maximum base pressure was obtained in all configurations when the exit of the primary nozzle was located near the entrance to the mixing section and the nozzles were aligned with the ejector center line.
2. Base pressure: All configurations functioned with the base pressure ranging from 9 to 14 pounds per square foot. Configuration B provided the highest base pressure at any height, where the height

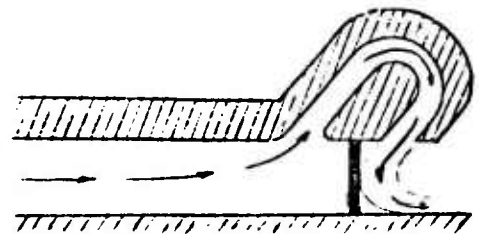
was measured from the model base to the ground board, but was undesirable since the clearance height was much less than the model base height. Configuration C was then tested and performed approximately 90 percent as well as Configuration B and 30 percent better than Configuration A without the penalty in reduced height of B.

3. Coanda spoilers: Initial tests on Configuration A showed that the flow was attaching to the underside of the center block. Installation of the coanda spoilers shown in Figure 9.2-3 prevented the flow from attaching to the bottom surface, and raised the base pressure from 2 psf to 10 psf at a height of 3 inches. The shape of the undersurface of the center block Configuration C in Figure 9.1-5 acted as a coanda spoiler and the flow did not attach on this model.

4. Inlet pressure recovery: Several additional center blocks were built to investigate the effects of varying the inlet shape of the mixing section. No significant improvement in overall ejector performance was obtained. Subsequently, a test was run comparing the mass augmentation obtained while running the ejectors as shown in the following sketch:



RECIRCULATING CONFIGURATION



NON - RECIRCULATING CONFIGURATION

The mass augmentation obtained in the recirculating configuration was 17.6 compared to 16.7 in the non-recirculating configuration. This indicates that the small scale tests could only be used for comparative results and to predict basic trends.

5. Over-water tests: The models tested over water provided approximately the same base pressure, at equal heights, as they did on a firm surface. Figure 9.2-6 shows Configuration A, with coanda spoiler, in operation over water. The displaced surface of the water under the base of the model represents a pressure of approximately 10 psf.

One additional configuration is shown operating over water in Figure 9.2-7. This model represents an attempt to reduce the area ratio and overhang dimensions, while increasing the tertiary exit velocity. The base pressure obtained while operating over water was approximately 13 psf.

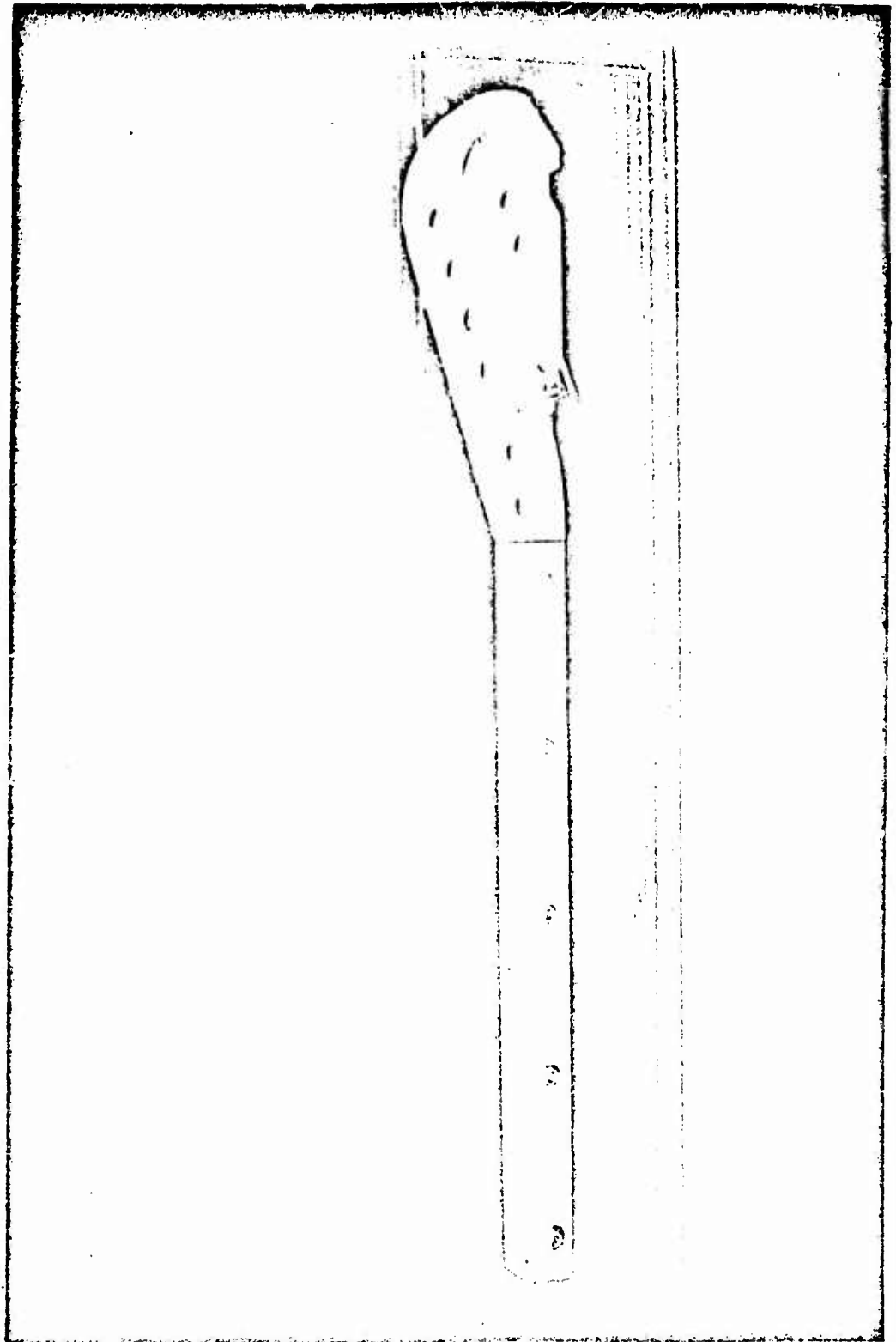


Figure 9.2-1 Small-Scale Recirculating Ejector

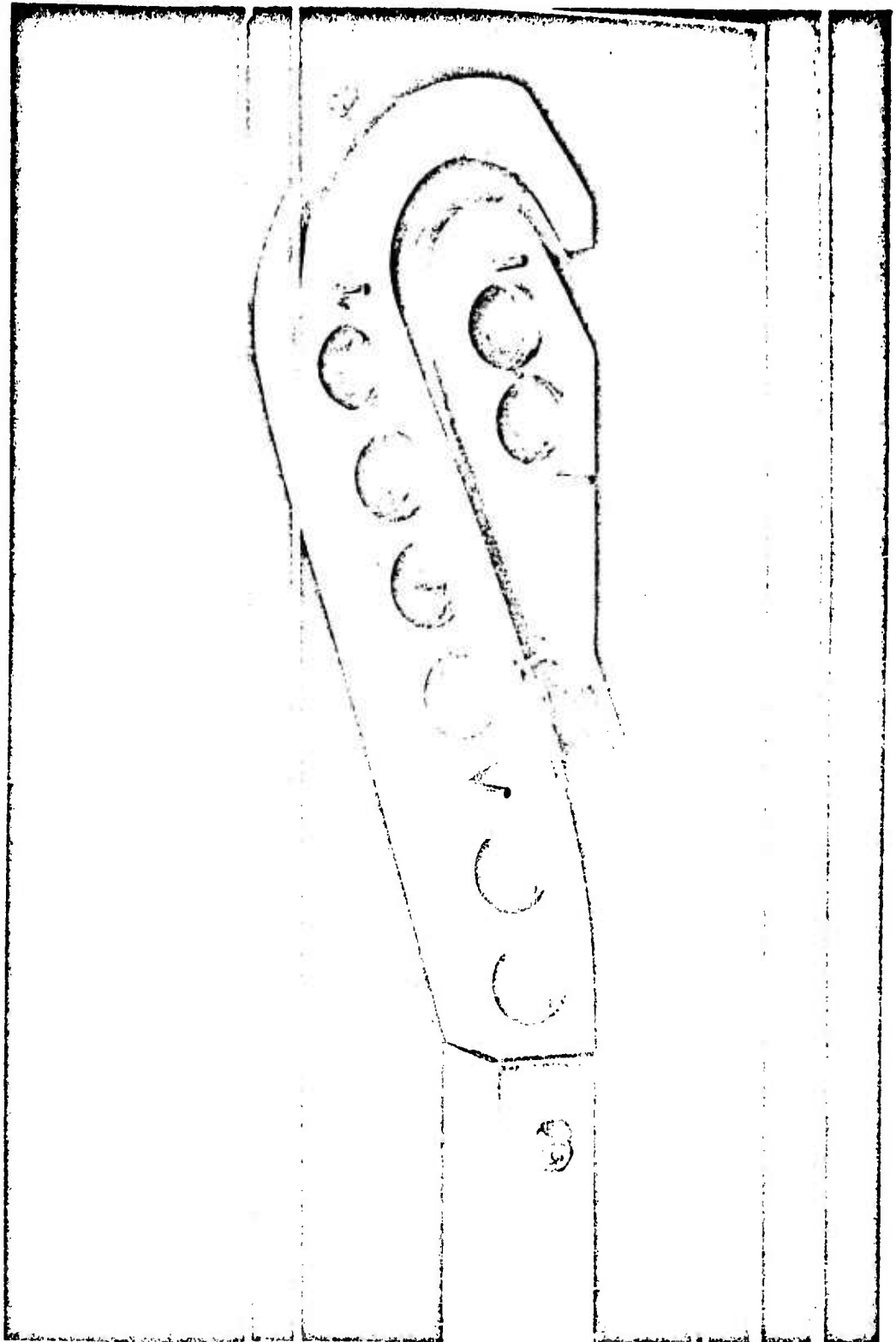


Figure 9.2-2 Close-up of Small-Scale Recirculating Ejector

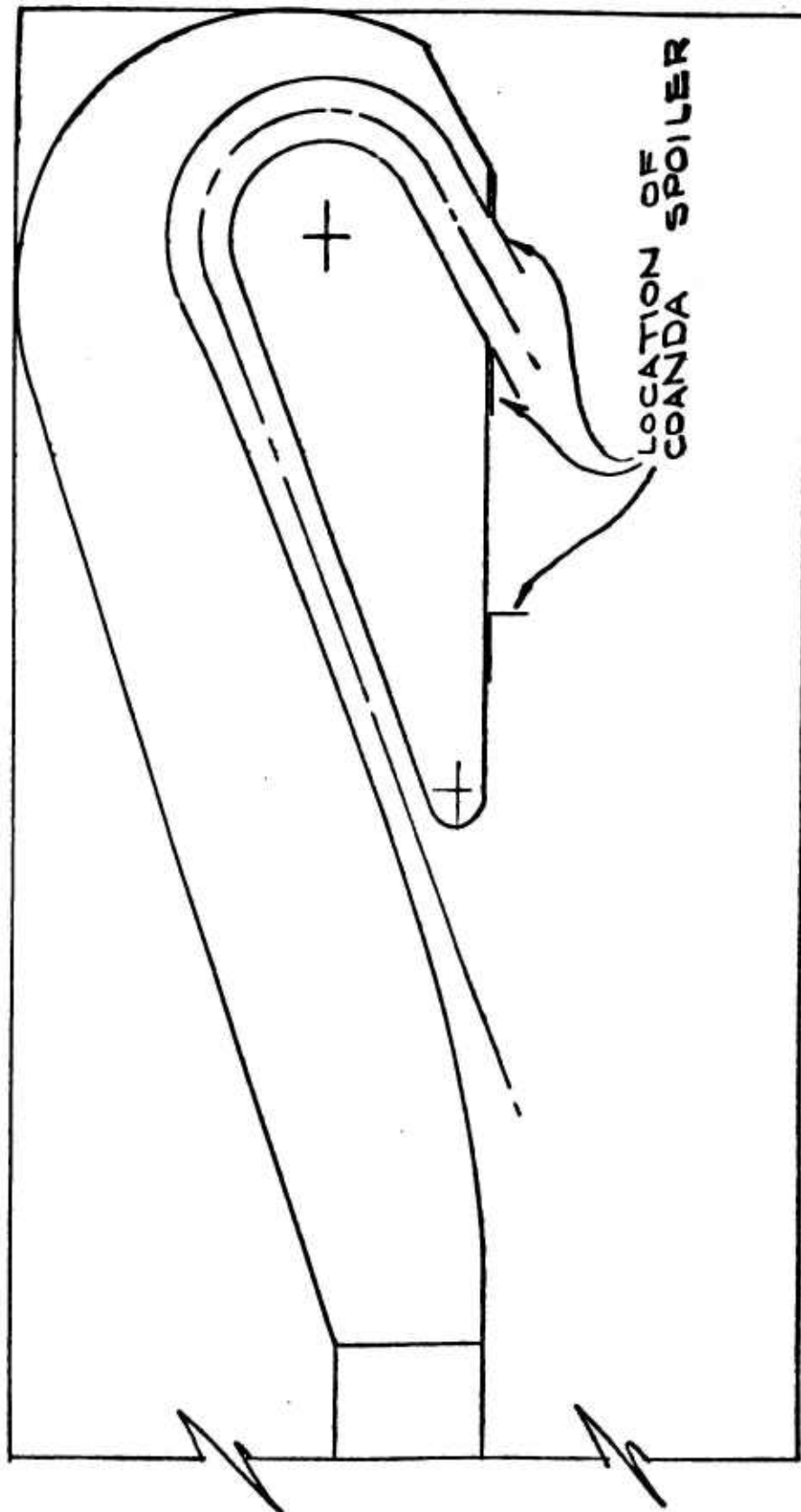
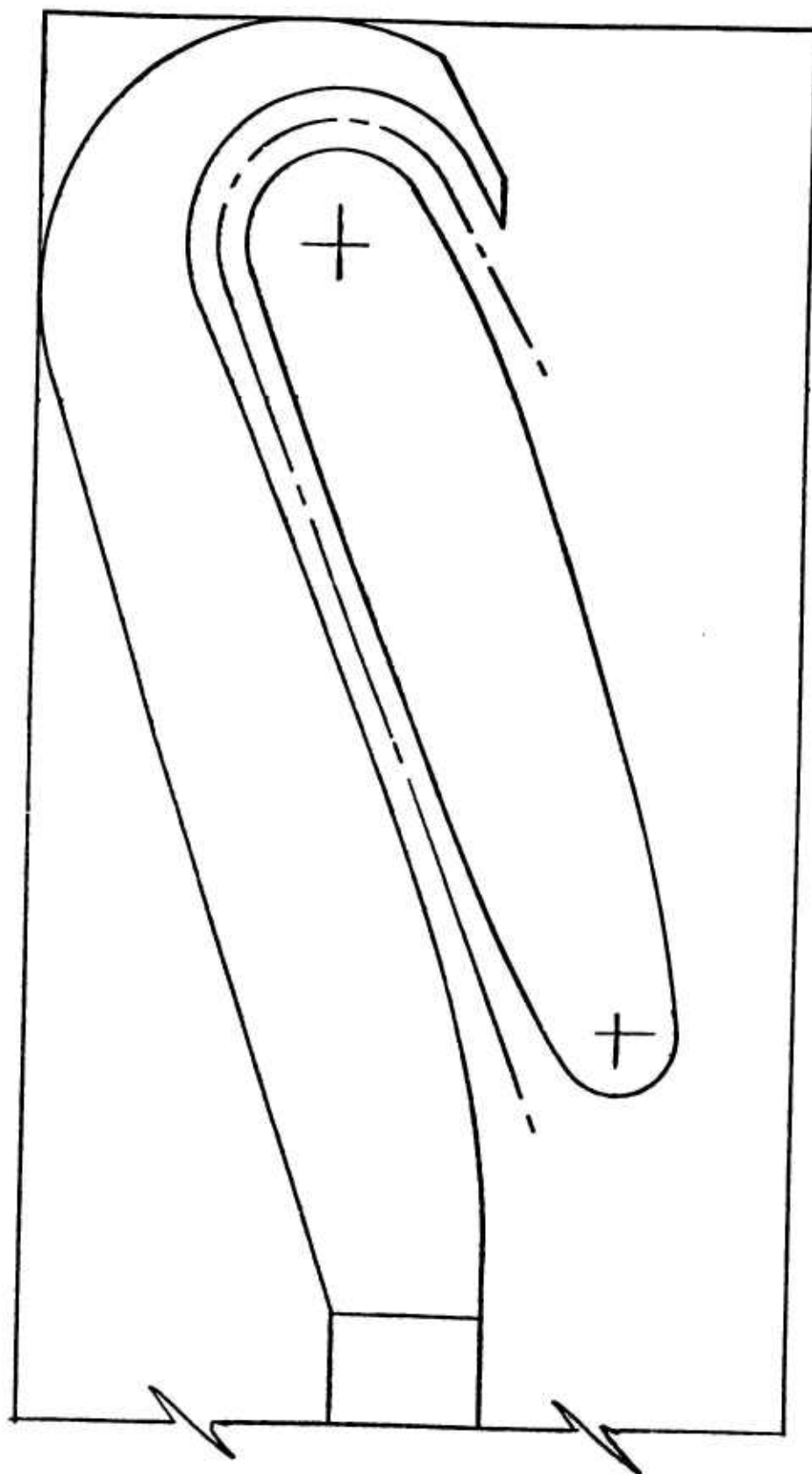


FIGURE 9.2-3 CONFIGURATION A - SMALL SCALE RECIRCULATING EJECTOR



9.2-7

FIGURE 9.2-4 CONFIGURATION B - SMALL SCALE RECIRCULATING EJECTOR

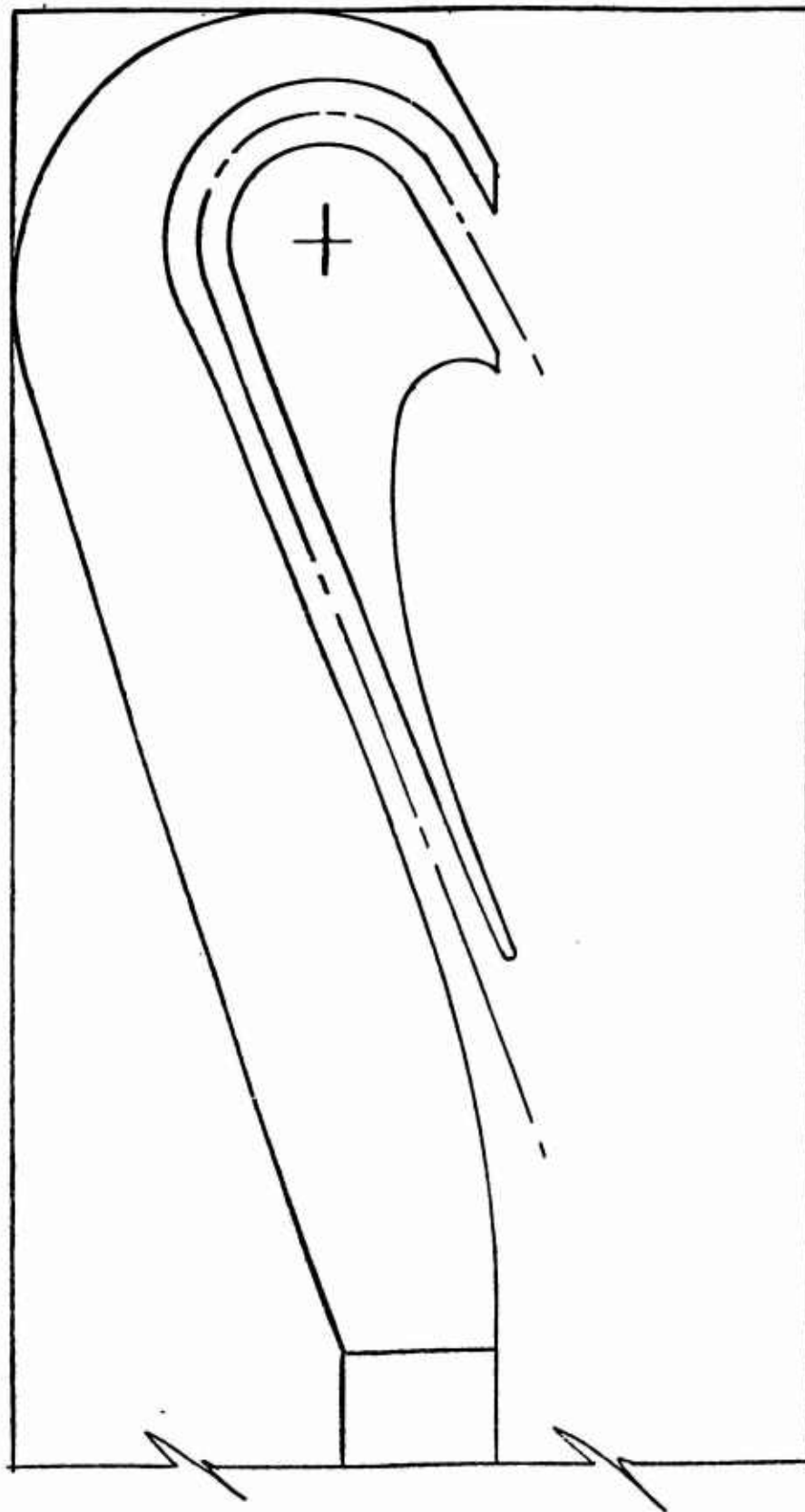


FIGURE 9.2-5 CONFIGURATION C - SMALL SCALE RECIRCULATING EJECTOR

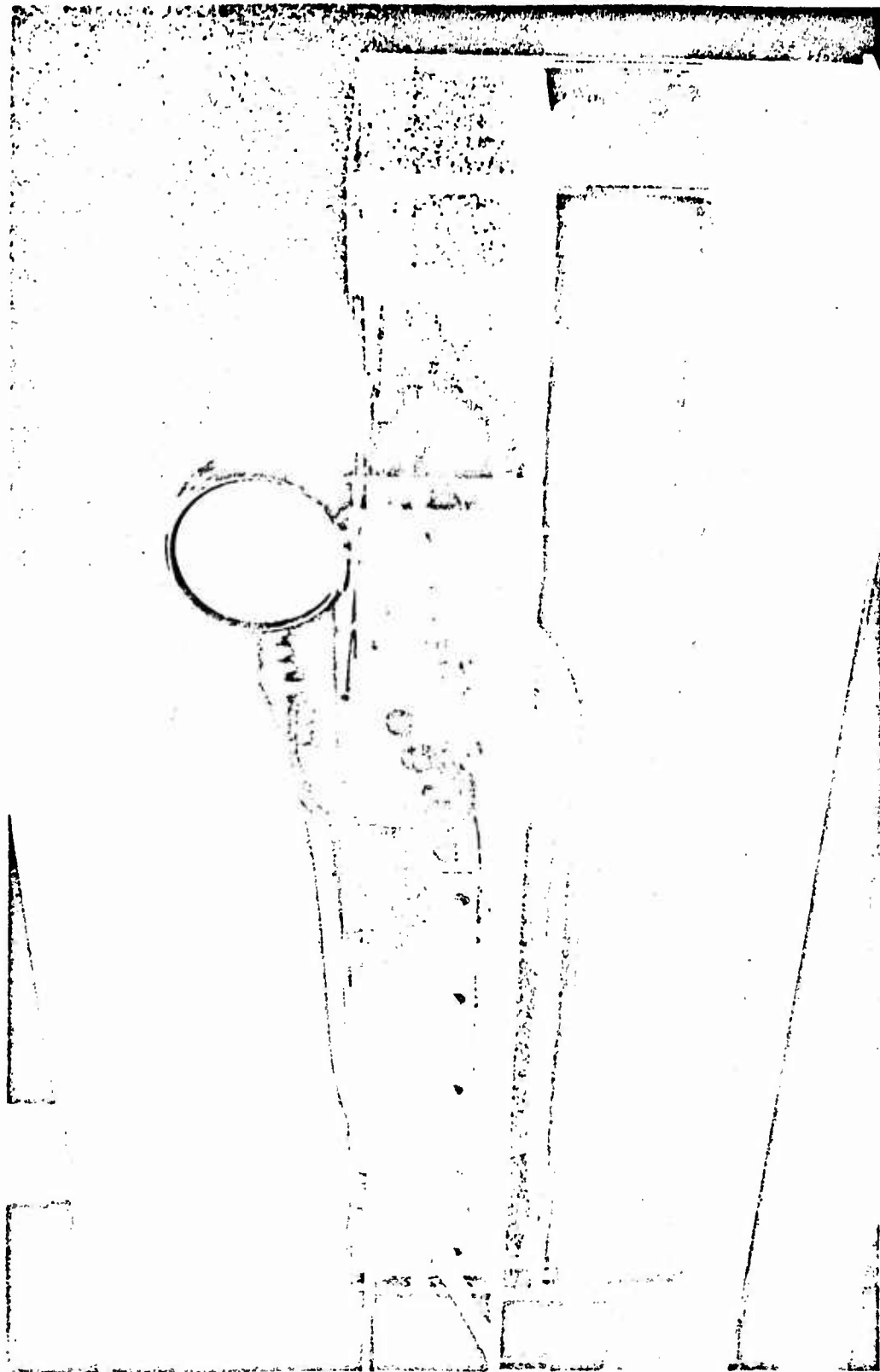


Figure 9.2-6 Water Test of Small-scale Recirculating Ejector - Configuration A



Figure 9.2-7 Water Test of Small Scale Recirculating Ejector

9.2.2 Large-Scale Two-Dimensional Tests

9.2.2.1 Description of Test Item

An overall view of the ejector test facility used in the large scale tests is given in Figure 9.1-1. Figure 9.2-8 is an isometric drawing of the two-dimensional ground board-model base set-up. One side-wall was fabricated of $3/4$ inch plywood and the other of $3/8$ inch plexiglass, which provided visual observation of the flow. It also aided in locating and aligning the various components and instrumentation. The vertical position of the ground board could be raised or lowered over a range from 4 to 36 inches.

The recirculating ejectors were generally fabricated of $1/8$ inch sheet aluminum formed to the desired contour. The formed aluminum sheets were then attached to an external frame which had been precision-cut and shaped to the correct contour. Highly curved contours, such as inlet lips, were formed of wood.

The primary manifolds and nozzles used in the recirculating ejector tests are shown in Figure 9.2-9. The manifolds and nozzles, shown dimensionally in Figures 9.2-10 through 9.2-12, were similar in construction to those employed in the straight ejector tests with the exception of the manifolds which were one-piece. The primary air system remained unchanged from the previous straight ejector test program.

9.2.2.2 Instrumentation

Instrumentation of the recirculating ejector facility consisted of

- a. Primary mass flow meter
- b. Pitot-static rake at tertiary exit
- c. Traversing single total-head probe at secondary inlet
- d. Static pressure taps on ground board, model base, plus inside and outside walls of the recirculating ejector.

The primary mass-flow meter has been previously discussed in Section 9.1.2.1.

The pitot-static rake used at the tertiary exit is shown in Figure 9.2-13. The spacing of the individual probes is 0.5 inches. The mounting attachments used in conjunction with this rake were of such a design that the rake could be positioned to fit all ejector configurations.

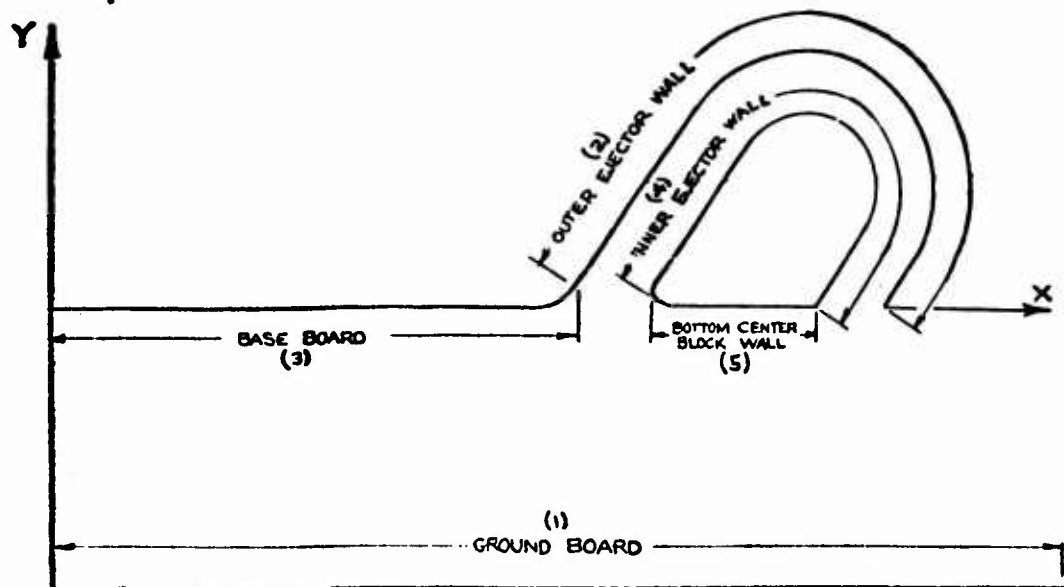
A large number of static pressure taps (approximately 175) was employed in order to make the linear integration data reduction technique, discussed later, as accurate as possible.

A single total head probe was traversed across the thickness of the secondary inlet between the primary nozzles in the exit plane of the primary nozzle to measure secondary total pressure recovery.

9.2.2.3 Data Reduction

In the analysis of the experimental data on the recirculating ejector models, an IBM program was used to circumvent the large amount of hand labor that otherwise would be required. The load and moment integrations on all models were broken into five regions. These regions are listed and diagramed next.

1. Ground board
2. Outer ejector wall
3. Base board
4. Inner ejector wall
5. Bottom center block wall.



The spacing used on the static pressure taps was small enough to allow the assumption of a linear variation in pressure between taps to be used. Matrix techniques were used to convert the initial manometer board readings, in inches of water, to forces and moments.

The data input to the program was:

- a. $\{h_1\}$ - a column matrix of pressure readings in inches of water
- b. $\{x_1\}$ - a column matrix of x locations in feet
- c. $\{y_1\}$ - a column matrix of y locations in feet
- d. $\{K_1\}$ - a column matrix of constants used to convert the pressure readings from inches of water to lb/ft^2

Force Integration

The first operation performed on the input data was the conversion of the pressure readings from inches of water to lb/ft^2 . This was accomplished by a diagonal matrix, $[K]$, with the correcting constants along the diagonal.

$$[K] \begin{Bmatrix} h_1 \\ h_2 \\ h_3 \\ \vdots \\ h_n \end{Bmatrix} = \begin{Bmatrix} p_1 \\ p_2 \\ p_3 \\ \vdots \\ p_n \end{Bmatrix}$$

$\begin{bmatrix} K_1 & & & & \\ & K_2 & & & \\ & & K_3 & & \\ & & & \ddots & \\ & & & & K_n \end{bmatrix}$

where p_i denotes the value of gage pressure at the appropriate pressure tap.

A matrix was required to integrate the pressures. The assumption of linear pressure variation between taps was used here. The incremental load between any two points, X_j and X_{j+1} , is

$$\Delta L = (p_j + p_{j+1}) \left(\frac{x_{j+1} - x_j}{2} \right)$$

The incremental loads between all the given points was then evaluated by constructing the previously mentioned integration matrix with the coefficients of the ΔL equation.

This matrix, $[INT_L]$, is

$$[INT_L] = \begin{bmatrix} -\frac{x_1}{2} & \frac{x_1}{2} & 0 & \cdots & 0 \\ 0 & -\frac{x_2}{2} & \frac{x_2}{2} & 0 & \cdots & 0 \\ \vdots & \vdots & \vdots & \ddots & \vdots & \vdots \\ 0 & \cdots & 0 & -\frac{x_{n-1}}{2} & \frac{x_{n-1}}{2} \end{bmatrix}$$

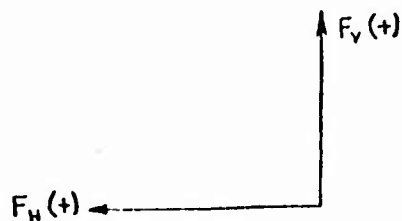
A summing matrix, S , was used to add up the appropriate incremental loads so that the loads applied to the five regions could be determined. This matrix is

$$[S] = \begin{bmatrix} 1 & 1 & 1 & 1 & 1 & 0 & 0 & 0 & 0 & 0 \\ 0 & 0 & 0 & 0 & 0 & 1 & 1 & 1 & 1 & 0 \\ 0 & 0 & 0 & 0 & 0 & 0 & 0 & 0 & 0 & 0 \\ 0 & 0 & 0 & 0 & 0 & 0 & 0 & 0 & 0 & 0 \\ 0 & 0 & 0 & 0 & 0 & 0 & 0 & 0 & 0 & 1 \end{bmatrix}$$

The complete integration procedure for evaluating the vertical loads, $L_1 - - - L_5$, applied to the five regions is

$$\begin{Bmatrix} L_1 \\ L_2 \\ L_3 \\ L_4 \\ L_5 \end{Bmatrix} = [S][INT_L][K]\{h_i\}$$

The horizontal loads were then evaluated in the same manner by substituting the y locations in the integration matrix, $[INT_L]$, for the corresponding x values. The matrix $[K]$ was input only once in the IBM procedure and for this reason the following sign conventions were used.



FOR REGIONS 2, 3, 4, AND 5



FOR REGION 1
 $F_H = 0$

Moment Integration

In the procedure for integrating the moments, the only necessary change in the previous loads procedure was in the integrating matrix $[INT_L]$.

In this case, again assuming a linear variation in pressure between the pressure taps, the incremental moment about the reference axis due to the pressure acting between any two points, x_j and x_{j+1} , is

$$\Delta M = (p_j) \left(\frac{x_{j+1} - x_j}{2} \right) (x_{j+1} + x_j) \\ - (p_j - p_{j+1}) \left(\frac{x_{j+1} - x_j}{2} \right) \left(x_j + \frac{2}{3} [x_{j+1} - x_j] \right)$$

or

$$\Delta M = p_j \left(\frac{x_{j+1} - x_j}{2} \right) \left(\frac{2}{3} x_j + \frac{1}{3} x_{j+1} \right) \\ + p_{j+1} \left(\frac{x_{j+1} - x_j}{2} \right) \left(\frac{2}{3} x_{j+1} + \frac{1}{3} x_j \right)$$

The integration matrix for moments, $[INT_M]$, was then constructed.

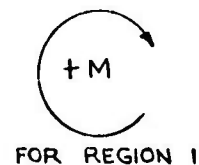
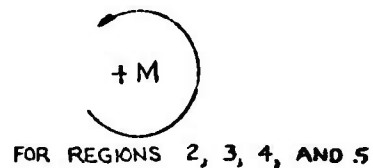
$$[INT_M] = \begin{bmatrix} \left(\frac{x_{j+1} - x_j}{2} \right) \left(\frac{2}{3} x_j + \frac{1}{3} x_{j+1} \right) & \left(\frac{x_{j+1} - x_j}{2} \right) \left(\frac{2}{3} x_{j+1} + \frac{1}{3} x_j \right) & 0 & \dots & 0 \\ \vdots & \vdots & \vdots & \ddots & \vdots \\ 0 & \dots & 0 & \left(\frac{x_n - x_{n-1}}{2} \right) \left(\frac{2}{3} x_n + \frac{1}{3} x_{n-1} \right) \end{bmatrix}$$

The complete integration procedure for integrating the five moments, $M_1 - -M_5$, due to the vertical loads in the five regions is

$$\begin{Bmatrix} M_1 \\ M_2 \\ M_3 \\ M_4 \\ M_5 \end{Bmatrix} = [S][INT_M][K]\{h_i\}$$

The procedure for evaluating the moments due to the horizontal loads is the same as for the vertical loads with the y coordinates replacing the x coordinates in the integration matrix, $[INT_M]$.

The sign convention for all models is



Tertiary Flow Calculations

Measurements of total and static pressure were made at the exit of the recirculating ejector in order to determine the properties of the jet. Small spacing between the probes was again used so that a linear pressure variation between probes could be used.

The desired output from the tertiary data is

a. Mass flow = $w \int_0^{t_e} \rho V dt$

b. Tertiary momentum = $\int_0^{t_e} \rho V^2 dt$

c. $\bar{V} = \frac{1}{t_e} \int_0^{t_e} V dt$

d. $\bar{V^3} = \frac{1}{t_e} \int_0^{t_e} V^3 dt$

e. Mass ratio = $\frac{w \int_0^{t_e} \rho V dt}{m'}$

where

w	= width of ejector	ft
ρ	= density	slugs/ft ³
t_e	= thickness of ejector exit	ft
V	= velocity	ft/sec
m'	= primary mass flow	slugs/sec

The velocities were calculated using the Bernoulli equation and the required integrations were handled in the same manner as the load and moment integrations assuming linear variations in all variables between probes. These calculated velocities were also included in the printout.

9.2.2.4 Model 1 Recirculating Ejector

9.2.2.4.1 Design Philosophy

The first recirculating ejector configuration shown in Figures 9.2-14 and 9.2-15 was derived from the following considerations:

- a. To reduce the fabrication time and cost, it was decided to use the three primary nozzles from Model 2 straight ejector. These nozzles were designed for a primary total pressure ratio of 6.8 which then became the design value for Model 1 recirculating ejector.

Since the ground-board model-base portion of the test rig was 18 inches wide, the primary nozzle spacing was necessarily required to be 6 inches, and the thickness in the exit plane of the primary nozzles was also required to be 6 inches for symmetry. This resulted in an area ratio, A''/A' , of 231.

Solutions for several values of mixing section pressure and secondary pressure recovery were determined for a tertiary velocity of 200 fps, until a solution was obtained which yielded the required primary and secondary areas. The theory was used in its basic format at this stage and did not include turn or diffuser losses. Figure 9.2-16 shows the mass augmentation obtained from these solutions plotted as a function of area ratio and total pressure recovery. The design point for Model 1 is indicated on this figure and corresponds to a mass augmentation of 22 and a pressure recovery of 25 percent. Although these flow conditions chosen for the first recirculating ejector are far from any theoretical maximum, they were judged to be a good starting point for this test program.

- b. The straight ejector experimental results indicated that a mixing section length-thickness ratio of 4 can be employed with only a small penalty in performance. This value was used here to provide reasonable overall dimensions.

- c. Diffusion of the mixed tertiary flow occurred in the 180° turn. At the time it was felt that a straight diffuser was not necessary since the flow would be distorted in the turn anyway due to centrifugal force, and diffusion in the turn would not aggravate this condition significantly.
- d. The entrance and exit angles, along with the distance between the entrance and exit, were determined from the initial lift studies discussed in Section 7.3.1. In this study, the distance between the entrance and exit are functions of model base height above the ground and the mass augmentation. The mass augmentation determines the angle at which the tertiary flow impinges on the ground and therefore affects the length between the ejector entrance and exhaust. The value of 60° for the entrance and exit angles was a compromise value derived from the lift optimization studies of Section 7.3.1 which theoretically resulted in a reasonable predicted base pressure, momentum lift, and overall dimensions.

9.2.2.4.2 Tests and Basic Results

Tests of Model 1 were conducted at primary total pressures of 100, 85.3, 70, 60, and 40 psig for heights of 34.7, 25.4, and 15.2 inches. In order to determine the factors which affect the flow under the ejector, tests were also made with and without coanda spoilers at the tertiary exit.

The effect of primary total pressure on base pressure for a fixed height is shown in Figure 9.2-17. The outline of the ejector in the upper portion of the figure is drawn to scale as is the location of the ground plane. This aids in determining the relationship between the ground board pressure distribution and the recirculating ejector and model base.

If the centerline of the tertiary exit is extended to the ground board plane, it appears that the tertiary jet impinges on the ground board at an angle equal to the exit angle. However, the negative pressure region under the

secondary inlet shows that the jet actually curves inward as predicted. This can be explained from the fact that the peak in the pressure distribution caused by the jet impinging on the ground board is a stagnation point, and the stagnation streamline is situated near the outside wall of the exit, as indicated by the mass augmentation (Table 9.2-1) and the exit total pressure distribution (Figure 9.2-18).

It should be pointed out that the negative pressure region on the ground board under the ejector does not reflect the true negative pressure that exists between the tertiary exit flow and the secondary inlet flow. The ground board pressure distribution also includes the pressures internal to the ejector, since all pressures acting on a body necessarily act on the ground in an equilibrium condition.

Figure 9.2-19 shows the variation in ground board pressure distribution with height at a constant primary total pressure of 85.3 psig. It is noted that the effect of increasing height is manifested in a thickening of the tertiary jet and a progressively poorer turning process from the ground board into the secondary inlet. At a height of 15.2 inches, the location of the jet stagnation point on the ground board in relation to the tertiary exit, indicates that the tertiary jet radius of curvature has decreased markedly. This observation is verified by the sizable increase in negative pressure under the ejector.

Typical total pressure distributions at the tertiary exit and secondary inlet are presented in Figure 9.2-18. The generally triangular shape of these profiles is representative of the first three recirculating ejector models tested. As a result, no additional profiles are presented or discussed although integrated values are presented as a percentage of the tertiary total pressure recovered at the secondary inlet in Table 9.2-1. The distributions of Figure 9.2-18 correspond to pressure recoveries of 16, 29, and 39 percent at heights of 35, 25, and 15 inches respectively.

Comparisons of experimental recirculating ejector performance with theoretical predictions are presented in Section 10.2.

9.2.2.5 Model 2 Recirculating Ejector

9.2.2.5.1 Design Philosophy

Model 2, shown in Figures 9.2-20 and 9.2-21, was designed as a full scale section of the ejector system for a manned test vehicle. A close-up view of the primary nozzle installation is shown in Figure 9.2-22. The total head probe used to measure secondary pressure recovery can be plainly discerned.

The primary flow parameters were calculated assuming a turbine mass flow of 4 pounds per second at a pressure of 39.5 psig for a vehicle perimeter of 46 feet at the primary nozzle location. Tertiary exit conditions were determined assuming a vehicle height above the ground surface of 18 inches, a base pressure of 15 psf, and a thickness/height ratio of 0.25. From these design conditions, a required mass augmentation of 40, and an exit velocity of 150 fps, were calculated.

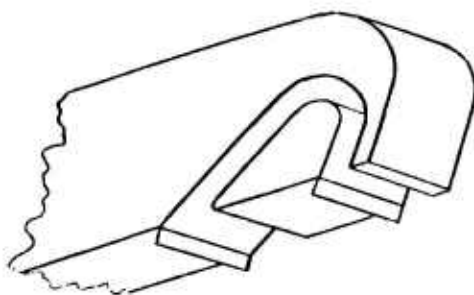
Solutions of the theoretical ejector equations at various values of mixing section pressure and secondary pressure recovery were obtained in the manner of Model 1, until a solution was found which gave the desired mass augmentation. The area ratio associated with this solution defined the basic geometry of the ejector. The theoretical values of mass augmentation obtained from these solutions are plotted in Figure 9.2-23 and the design area ratio of 4.36 is indicated.

An inlet and exit angle of 50° was used on this configuration, since values of this magnitude were shown to be desirable from a control force point of view by the lift optimization equations derived in Section 7.3.1. The benefits of shallow tertiary exit angles did not become apparent until later tests.

It is noted in Figures 9.2-20 and 9.2-21 that the diffuser section is situated upstream of the 180° turn which is a constant area turn. This, of course, resulted in a shorter mixing-section length ($l/t = 2.5$), thus requiring part of the mixing process to take place in the diffuser section.

9.2.2.5.2 Tests and Basic Results

Tests were conducted at the design primary pressure of 40 psig at 7 heights ranging from 5 to 35 inches with and without a spoiler at the tertiary exit. This spoiler was tested to determine its effectiveness in delaying attachment of the tertiary flow to the bottom of the center block at large heights above the ground board. The same spoiler was also mounted on the model base in the vicinity of the secondary inlet in an attempt to improve secondary pressure recovery, and to extend the region of maximum base pressure on the model base. The sketch below shows the two spoiler locations.



The effect of model base height on the ground board pressure distribution is shown in Figure 9.2-24. The negative pressure under the ejector, created by the inward turning of the tertiary exit flow before it impinged on the ground, is again noted at a height of 8.4 inches.

Figure 9.2-25 shows the effect of spoiler location on base pressure. At heights greater than 20 inches, $t_e/h < 0.2$, the spoiler at the tertiary exit (see previous sketch) is effective in delaying attachment of the flow to the center block of the ejector. However, at heights lower than 12 inches, this spoiler configuration results in a rapid deterioration of lift performance. The spoiler, in this location at low heights, disrupts the recirculating flow pattern and causes much of the tertiary flow to be expelled out from under the model in the manner of an annular jet. The recirculating ejector is now operating in the manner of a conventional ejector and pumps air out of the base region.

In Figure 9.2-25 the effect on base pressure of placing a spoiler at the secondary inlet is shown to be small. In the height range $0.2 < t_e/h < 0.3$ this spoiler configuration does generate some additional lift thus indicating a slight reduction in the effect of the ejector inlet on the model base pressure distribution.

A summary of the performance of Model 2 is contained in Table 9.2-1 for all tests in which secondary pressure recovery was measured.

9.2.2.6 Model 3 Recirculating Ejector

9.2.2.6.1 Design Philosophy

At this stage of the program, data analysis of Models 1 and 2 had proceeded sufficiently far that the importance of reducing the negative pressure in the core of the recirculating flow under the ejector became apparent. As a result, Model 3 recirculating ejector was designed to determine the effect of tertiary exit angle on ejector performance and the external pressure distribution.

Model 3 was designed to have the same performance as Model 2, hence the same value of area ratio (436) and essentially the same mixing section and diffuser design were employed. In addition, Model 3 used the same primary nozzle-header combination as Model 2. The only significant change was in the inlet and exit angles. The inlet angle was reduced from 50° to 30° . The tertiary exit was constructed of removable sections which provided exit angles of 30° , 45° , and 60° . This variable exit angle feature is illustrated schematically in Figure 9.2-26. An insight into how the exit angle was physically changed is provided by Figure 9.2-27. On this configuration the primary header was relocated exterior to the outside wall of the ejector to reduce blockage of the entrained secondary air.

9.2.2.6.2 Tests and Basic Results

Figures 9.2-28 through 9.2-30 show the effect of tertiary exit angle and height on the ground board pressure distributions for Model 3. A marked change in the pressure distribution is noted as the exit angle is reduced from 60° to 30° .

The negative pressure region under the ejector is quite prominent for an exit angle of 60° at all heights. Reducing the exit angle to 45° results in nearly zero pressure in this region, and the 30° exit angle actually produces positive pressure along the entire model length to the left of the jet impingement point. These pressure distributions prove rather conclusively the dependence of the cavity pressure (pressure under the ejector) on tertiary exit angle, and also show that the distance between the ejector inlet and tertiary exit are of lesser importance. Section 10.2.2, which presents a comparison of theoretical cavity pressure with experimental results, shows that the mass augmentation is the prime factor in determining the optimum exit angle as originally predicted by the theoretical analysis of Reference 6 and the current analysis of Section 7.2.3.

9.2.2.7 Tandem Straight Ejector Tests

The ejector theory, as evolved in Section 7, indicates the effect of pressure recovery on the ejector performance parameters; efficiency and mass augmentation. The magnitude of performance improvement which can be attained by increasing the pressure recovery is well depicted in Figures 8.3-1 through 8.3-3.

Systematic empirical investigation of pressure recovery was not possible with the recirculating ejector models which were tested. Pressure recovery was a dependent test variable and could not be controlled during the test program. Consequently, the effect of pressure recovery on the performance of each ejector configuration could only be studied in a limited range.

A study to determine the effect of pressure recovery on ejector performance was accomplished by operating two straight ejectors in tandem. The tertiary flow of the upstream ejector was directed into the inlet of the downstream ejector. By proper regulation of the tertiary flow of the upstream ejector, the downstream ejector could be tested under a wide range of pressure recovery values.

The ejectors were arranged along a common centerline with the end of the diffuser of the upstream ejector placed approximately one foot from the inlet

of the downstream ejector. The primary total pressure could be regulated on either ejector from 0 to 100 psig. The tertiary flow of the downstream ejector was measured by a pitot-static rake mounted longitudinally at the diffuser lateral centerline. The inlet total pressure was measured by a total pressure rake mounted in the exit plane of the primary nozzles. The rake was mounted laterally between the ejector side wall and the first nozzle. Primary flow of the downstream ejector was measured by the orifice flowmeter and a Bourdon pressure gage. The primary pressure of the upstream ejector was also measured by a Bourdon gage.

The effect of pressure recovery on the performance of the downstream ejector was measured by operating the downstream ejector at a constant primary flow condition and varying the flow of the upstream ejector. This flow was varied by running the primary total pressure of the upstream ejector in increments from 0 to 100 psig. The inlet and tertiary flow of the downstream ejector was measured at each operating point. The run conditions are summarized below.

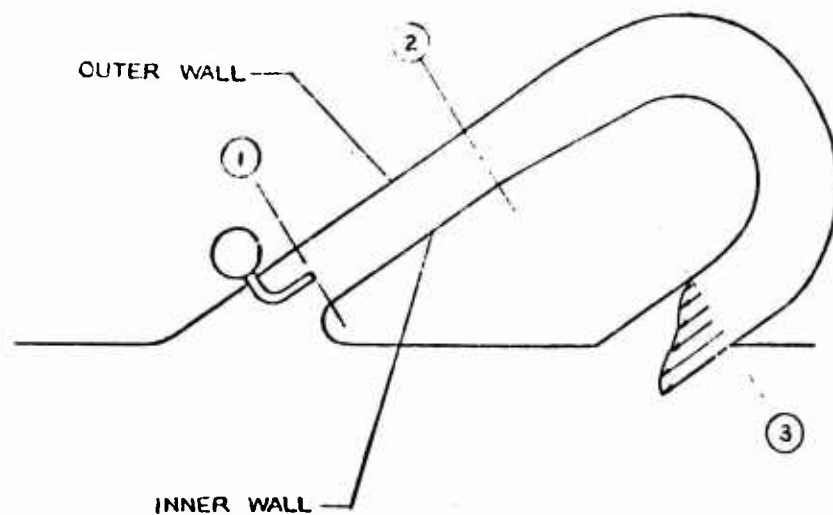
RUN	Primary Pressure of Downstream Ejector	Primary Pressure of Upstream Ejector
1-6	20 psig	0, 20, 40, 60, 80, 100 psig
7-12	40 psig	"
13-18	60 psig	"

The performance of the downstream ejector is shown in Figure 9.2-31 with mass augmentation and efficiency plotted against pressure recovery for each primary flow condition. The limitations of the test set-up are seen at the higher downstream primary pressure. Since the tertiary flow of the upstream ejector is not forced to flow into the downstream ejector, the separation of the two ejectors and mismatch of the upstream diffuser and downstream inlet results in spillage, thus limiting the pressure recovery obtained to about 30% at $P_0' = 60$ psig. Also the area ratio of the downstream ejector was probably too small when both ejectors were operated at the higher primary pressures.

This simple test demonstrates the gain in performance resulting from the recovery of tertiary total pressure as predicted by the theory. The test also indicates that very high mechanical efficiencies are practically possible when the ability to recovery tertiary total pressure is present. The upper limit of efficiency has apparently not been reached by the limited amount of recirculating ejector testing accomplished to date.

9.2.2.8 Model 4 Recirculating Ejector

The results of the tests of Models 2 and 3 showed lower than predicted performance with respect to tertiary momentum and base pressure. For this reason flow surveys were made to evaluate the characteristics of the flow internal to the recirculating ejector. The first test was made on Model 3 with velocity surveys made at stations 1, 2, and 3 as shown in the figure below.



The velocity distribution at Station (1) - the secondary inlet - was found to be uniform in the lateral and vertical directions. The velocity distribution at station (2) - the end of the mixing section - was extremely irregular with the maximum value occurring at the outer wall. In the lateral direction, five velocity peaks were detected indicating that the flow from the five primary nozzles had not completely mixed with the secondary flow at this station. The usual triangular velocity distribution occurred at Station (3) - the tertiary exhaust - with the maximum value at the outside wall.

In order to make an initial investigation of the effect of this irregular velocity distribution on internal losses, Model No. 4 of Figures 9.2-32 and 9.2-33 was constructed. This model incorporated a plenum chamber to reduce the flow velocity through the turn plus two sets of turning vanes to further alleviate turning losses.

Velocity surveys were then made on this model. The irregularities in the velocity distribution at the end of the mixing section were still present although not as pronounced as in Model 3. The velocity distribution was found to be rectangular at the tertiary exhaust.

The results of this test showed approximately a 10 percent decrease in exit momentum and base pressure compared to the comparable run on Model 3. Thus, the extra sophistication introduced by the addition of the plenum and turning vanes did not afford any additional performance.

9.2.2.9 Modified Model 1 Recirculating Ejector

9.2.2.9.1 Design Philosophy

The ejector theory of Section 7, when only mixing section friction losses are considered, indicates that high recirculating ejector performance (efficiency and mass augmentation) is obtained at high values of secondary pressure recovery and correspondingly high area ratios, A''/A' , as demonstrated by Figures 7.2-1 and 7.2-2. However, a comparison of the experimental performance results given in Table 9.2-1 for Models 2 and 3 recirculating ejectors with the theoretically predicted performance of Figure 9.2-23 shows that the large area ratio (436) does not provide the expected performance even though in some cases the design secondary pressure recovery was very nearly attained. It was necessary to introduce additional factors such as diffuser and turn losses into the ejector theory in order to obtain satisfactory correlation between theory and experiment. When the modified theory was used in an optimization or parametric study as exemplified by Figures 8.3-1 and 8.3-6, ejector performance improved with decreasing primary total pressure and correspondingly decreasing area ratio.

In order to experimentally verify these theoretical implications, Model 1 recirculating ejector was modified as shown in Figure 9.2-34. The tertiary exit angle was reduced from 60° to 30° to eliminate the negative cavity pressure common to the original configuration. The area ratio was reduced by increasing the primary nozzle area. Three area ratios were tested in this manner; 73, 122, and 231 which was the original area ratio. Each area ratio was tested over the available range of primary pressures at an optimum height for this configuration of 15 inches between ground board and model base.

The efficiency values obtained from these tests are plotted in Figure 9.2-35 as a function of primary pressure and area ratio. It is noted that maximum efficiency increases from 40 percent with an area ratio of 231 to 70 percent with an area ratio of 73. These results are presented in a more meaningful manner in Figure 9.2-36 in which base pressure is plotted as a function of primary horsepower and area ratio. At constant primary horsepower a marked increase in base pressure is observed as area ratio is reduced. For example at a primary horsepower of 30 per foot the base pressure is increased 40 percent by reducing the area ratio from 231 to 73.

This upward trend in ejector efficiency with decreasing area ratio should continue so long as secondary pressure recovery is maintained and mass augmentation does not drop off rapidly to its minimum value of 1. An examination of mass augmentation values in Table 9.2-2, which is a summary of experimental results from this ejector, shows that mass augmentation decreases somewhat with decreasing area ratio; however, at $A''/A' = 73$ mass augmentation values greater than 10 are still obtained.

Since secondary pressure recovery was measured only at $A''/A' = 122$, the effect of reduced area ratio on pressure recovery can not be determined. However, it is interesting to note in Table 9.2-2 that the pressure recovery is approximately 50 percent for $A''/A' = 122$ compared to 40 percent for the original Model 1 configuration (Table 9.2-1).

TABLE 9.2-1

Summary of Recirculating Ejector Experimental Results

Model	A ² /A ¹	θ ₁ Deg	θ ₂ Deg	Run	h Inches	P ₀ PSIG	m/m'	Press Recov Percent	P _b max PSF	P _b PSF	P ₀₄ PSF	V ₄ FPS	P _b /P ₀₄
1	231	60	60	101	34.7	100	13.9	15.0	11.71	2.24	26.85	144.5	.083
				102		85.3	14.9	16.0	10.15	1.81	22.00	133.3	.082
				103		70	15.8	19.9	8.07	3.01	15.80	112.7	.190
				104		40	19.8	23.4	5.20	2.39	10.02	93.4	.238
				105	25.4	100	15.8	31.4	21.34	16.20	32.25	168.6	.503
				106		85.3	17.0	29.2	18.21	14.30	27.80	152.2	.515
				107		70	20.0	30.3	15.09	12.30	23.60	144.8	.520
				108		40	22.7	31.8	8.33	7.30	12.88	106.8	.566
				110	15.2	85.3	23.3	39.2	26.54	25.00	37.30	200.7	.670
				112	15.2	40	27.2	44.5	10.15	9.60	14.80	128.0	.650
				114	25.4	85.3	16.4	24.1	15.61	11.50	24.30	141.7	.473
				120		85.3	19.5	31.8	16.91	14.60	24.55	150.5	.590
				122		40	22.3	36.8	7.29	6.40	10.72	99.8	.596
2	436	50	50	202	25.4	40	22.4	24.0	1.04	.42	7.50	87.5	.056
				203	17.2		20.8	48.2	5.98	5.55	7.50	80.9	.740
				204	12.4		25.6	56.4	8.85	8.58	10.40	99.3	.825
				205	8.4		27.2	65.8	9.63	9.38	11.20	105.7	.838
				206	6.4		27.7	60.0	8.85	8.49	11.00	108.1	.772
				207	4.8		27.6	55.0	7.81	7.35	10.70	107.9	.687
				209	25.4		17.5	17.1	3.12	2.04	5.55	68.4	.368
				210	17.2		22.1	48.0	6.50	6.12	8.20	86.4	.746
				211	12.4		25.4	49.0	8.59	8.26	11.24	98.7	.735
				212	8.4		25.0	56.3	6.77	6.60	9.86	96.9	.670
				220	17.2		21.0	34.2	6.50	6.32	8.66	84.2	.730
				221	12.4		24.9	50.7	9.11	8.62	12.59	100.0	.685
				222	8.6		26.6	41.8	8.59	8.09	11.75	105.4	.690

TABLE 9.2-1 Continued

Model	A"/A'	θ_1	θ_2	Run	h Inches	p_o' PSIG	m/m'	Press Recov Percent	p_b max PSF	r_b PSF	p_{o4} PSF	V_4 FPS	$\overline{p_b/p_{o4}}$
3	436	30	60	310	17.2	40	24.3	35.0	5.20	5.05	10.00	94.3	.505
				311	12.4		25.7	40.8	6.24	6.15	10.40	99.8	.591
			45	312	8.4		27.5	36.2	6.24	6.05	10.50	102.2	.576
				326	17.2		25.5	38.1	6.77	6.60	11.60	97.7	.569
				327	12.4		26.4	46.2	8.59	8.24	12.40	102.7	.665
				328	8.4		27.4	52.3	9.89	9.75	13.90	109.2	.701
			30	330	17.2		24.4	49.5	8.07	7.47	11.20	97.2	.667
				331	12.4		25.3	56.7	8.33	8.07	11.80	100.7	.684
				332	8.4		29.6	59.5	13.53	13.30	15.70	118.0	.847
				334	4.8		27.7	68.6	14.31	14.15	14.00	112.8	1.010

TABLE 9.2-2

Summary of Modified Model 1 Recirculating
Ejector Experimental Results

A"/A'	θ_1 Deg	θ_2 Deg	h Inches	P_o' PSIG	m/m'	Press Recov Percent	$\overline{P_b}$ PSF	$\overline{P_{o4}}$ PSF	V_4 FPS	$\overline{P_b/P_{o4}}$
231	60	30	15.2	80	21.8	.400	42.9	-	188.3	.932
231				91	20.1	.398	48.9	-	199.1	.960
122				30	17.5	.466	39.0	41.78	187.0	.942
				40	16.3	.504	53.1	55.28	212.0	.940
				50	15.5	.533	63.6	67.49	237.2	.905
				60	15.3	.594	77.5	82.55	264.0	.913
				70	14.5	.620	87.0	96.08	284.0	
				80	13.4	.610	97.4	106.82	296.0	
73				9.2	12.8	.562	33.0	-	163.0	-
				16.4	12.5	.562	55.0	-	203.0	-
				21.9	12.2	.620	67.0	-	235.0	-
				29.3	11.2	.610	84.0	-	261.0	-
				35.6	10.6	.640	100.3	-	285.0	-
				44.6	10.6	.684	118.0	-	311.0	-

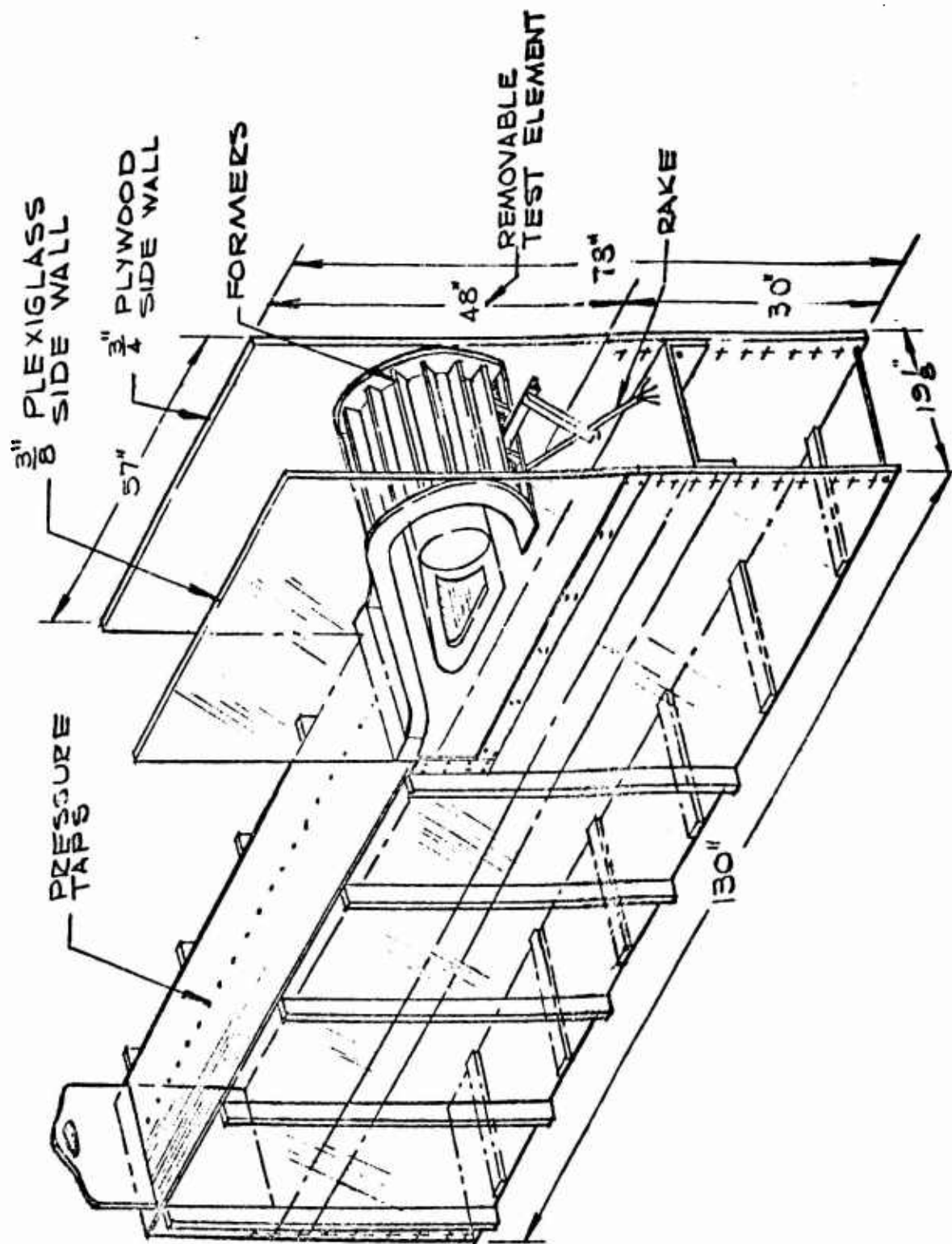


FIGURE 9.2-8 LARGE-SCALE RECIRCULATING EJECTOR TEST SET-UP

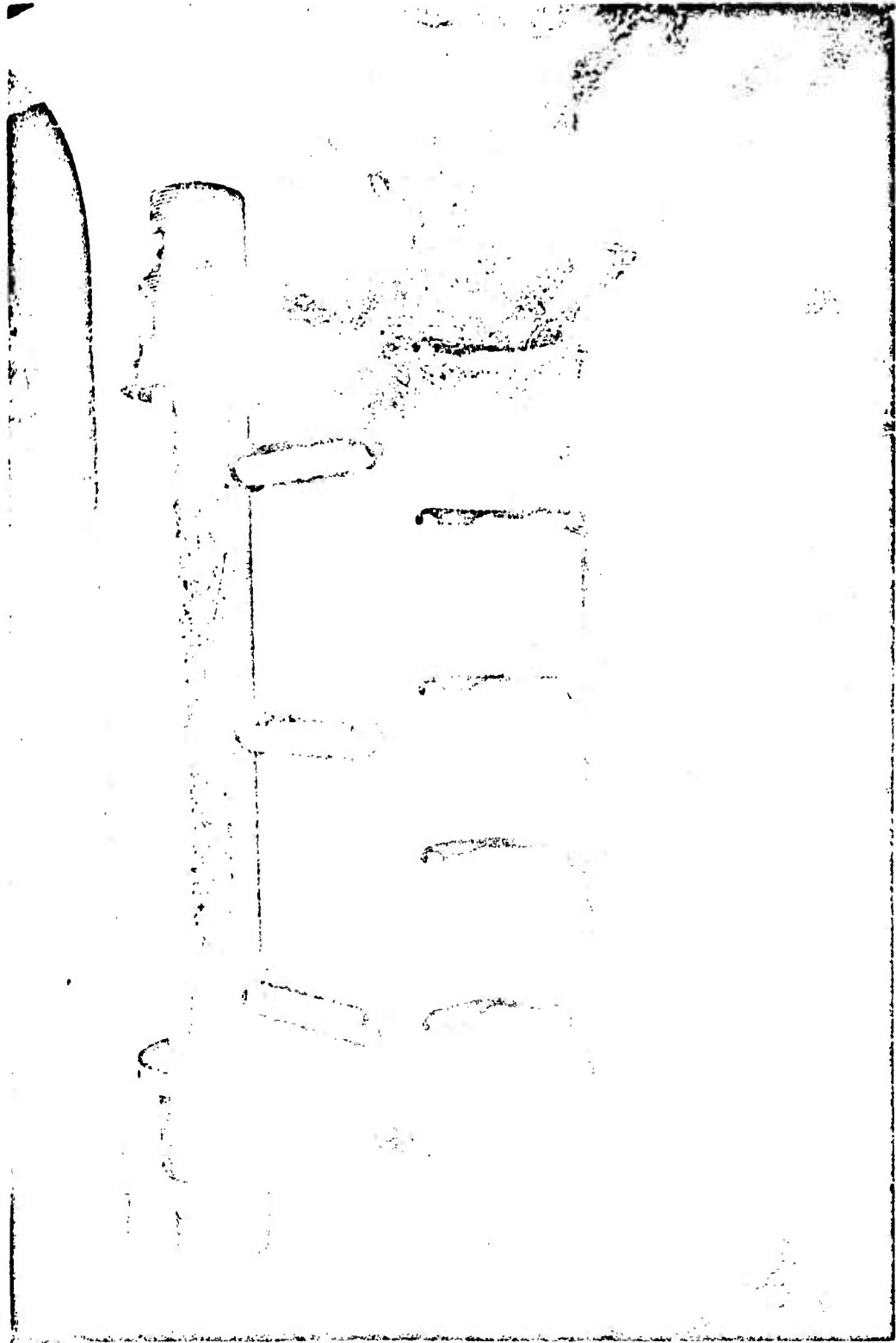
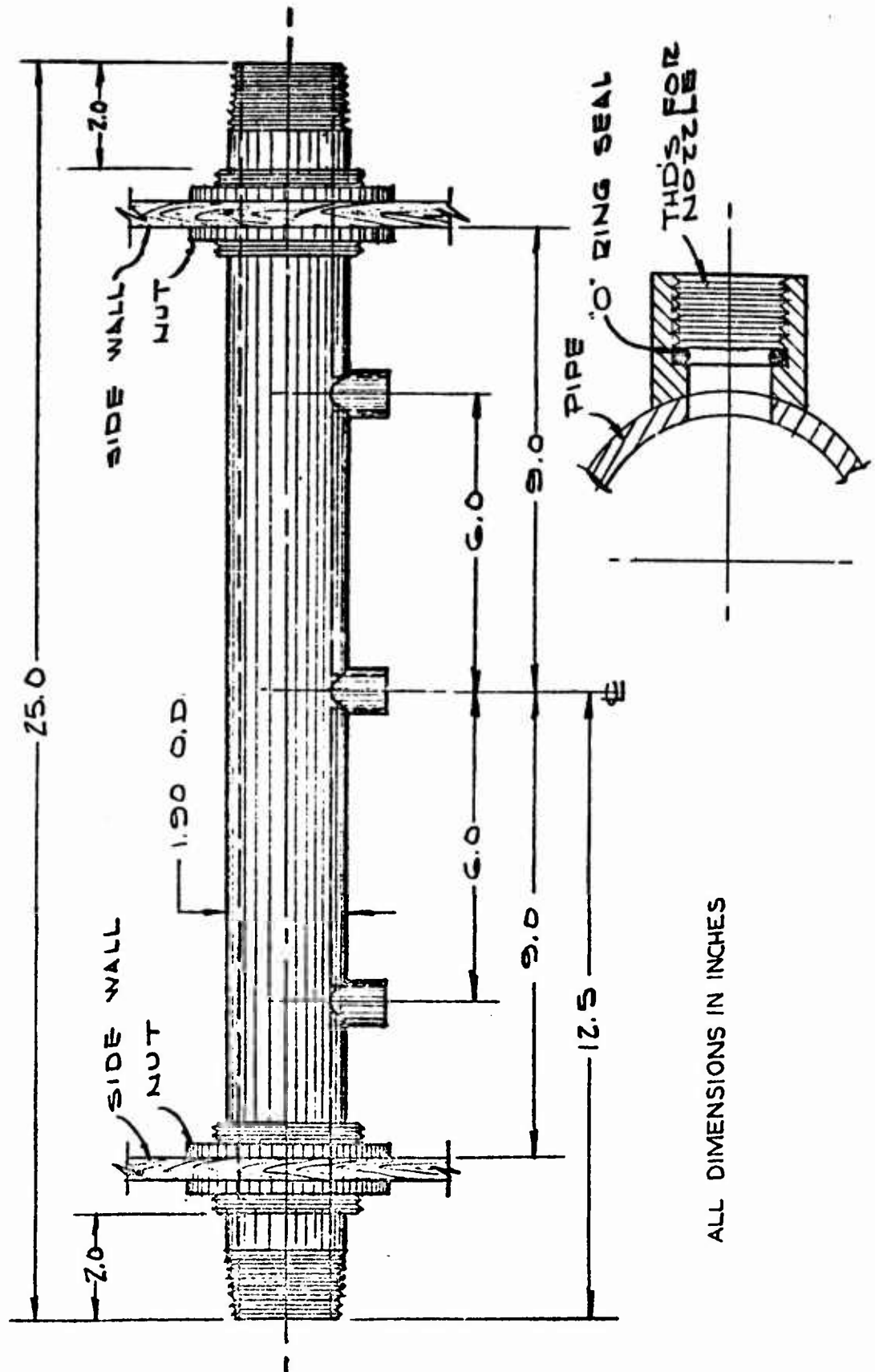
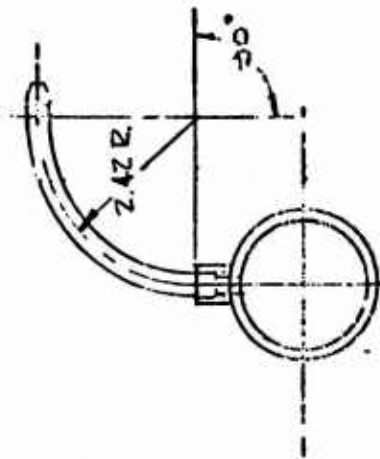
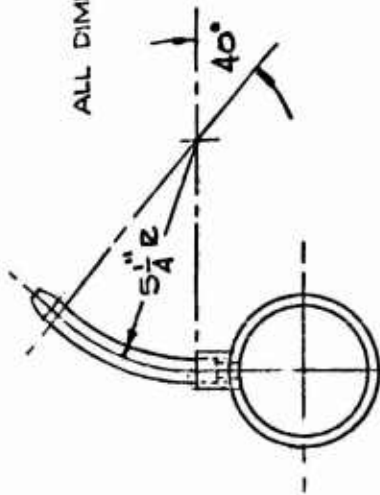
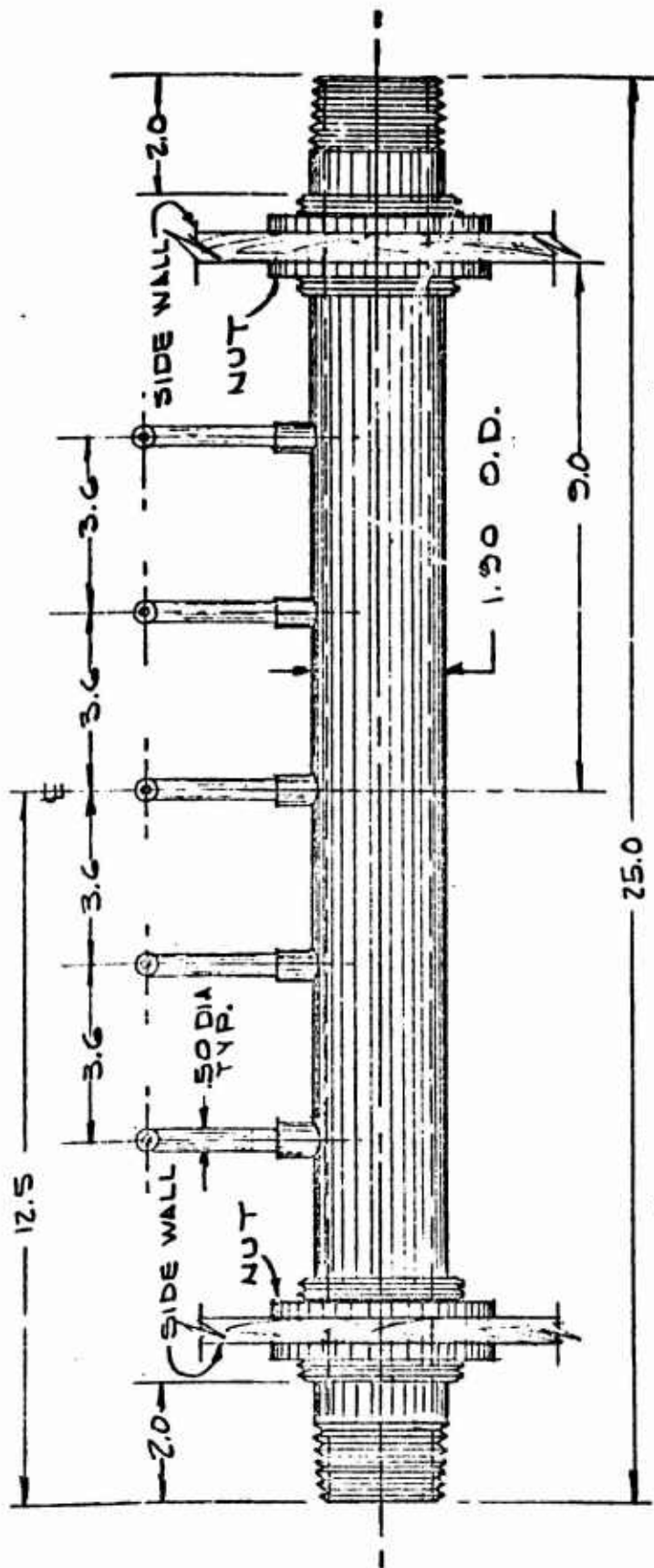


Figure 9.2-9 Primary Nozzle-Header Combinations for Recirculating Ejectors



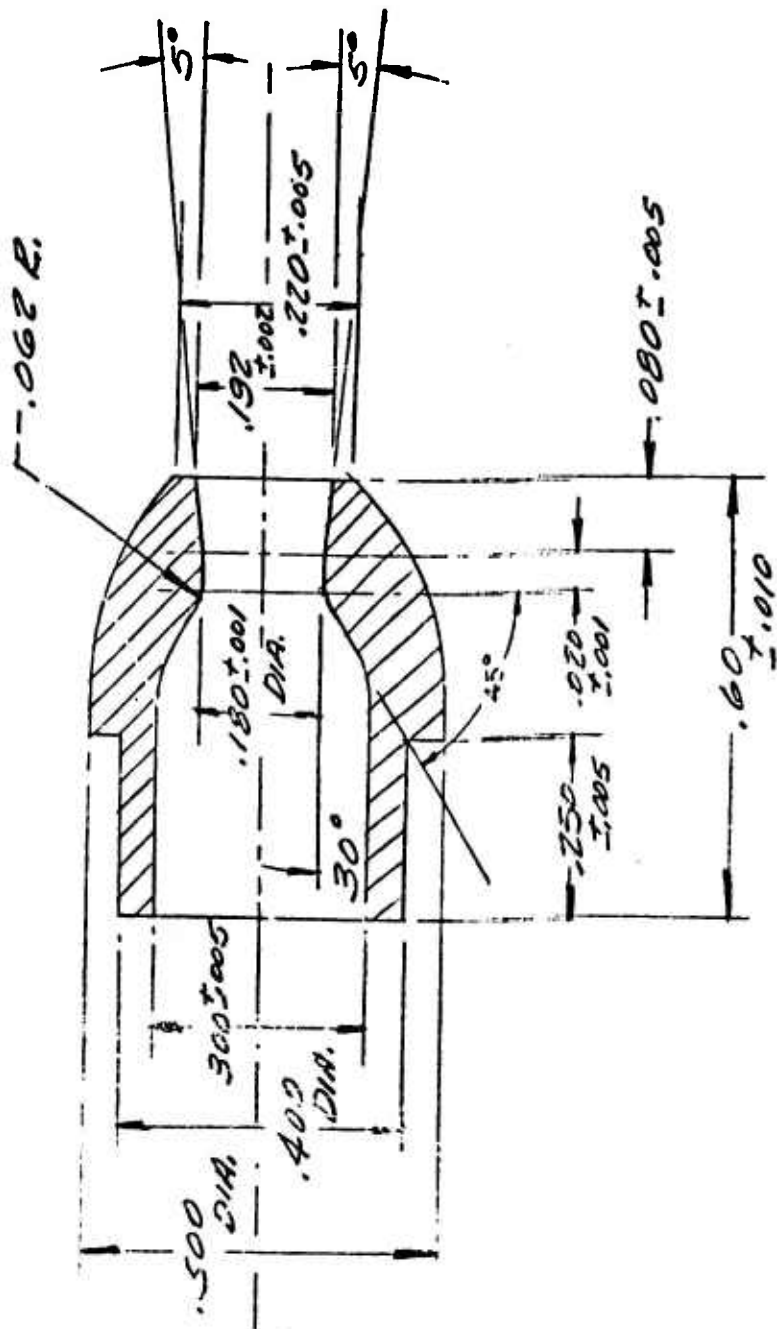
ALL DIMENSIONS IN INCHES

FIGURE 9.2-10 MODEL 1 RECIRCULATING EJECTOR PRIMARY MANIFOLD



ALL DIMENSIONS IN INCHES

FIGURE 9.2-11 MODEL 2 AND 3 RECIRCULATING EJECTOR PRIMARY MANIFOLD



SCALE 4 X SIZE

FIGURE 9.2-12 NOZZLE FOR MODEL 2 AND 3 RECIRCULATING EJECTOR

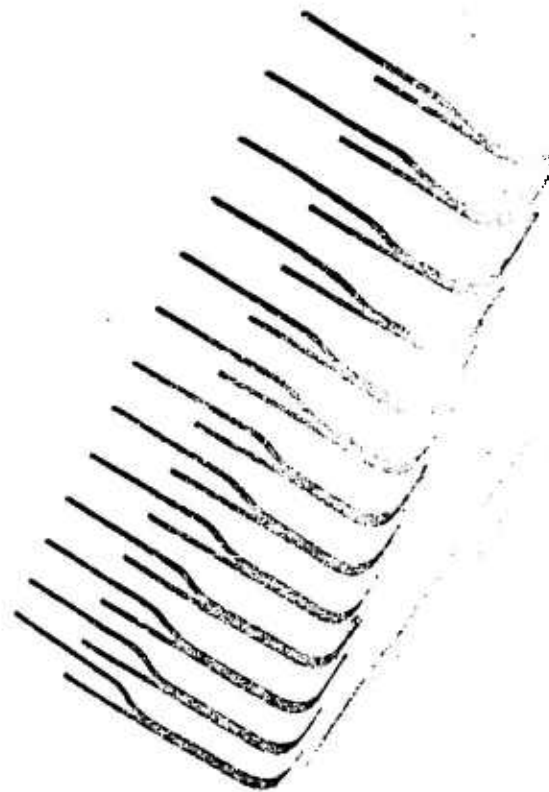


Figure 9.2-13 Recirculation Ejector Exit Pitot-Static Rake

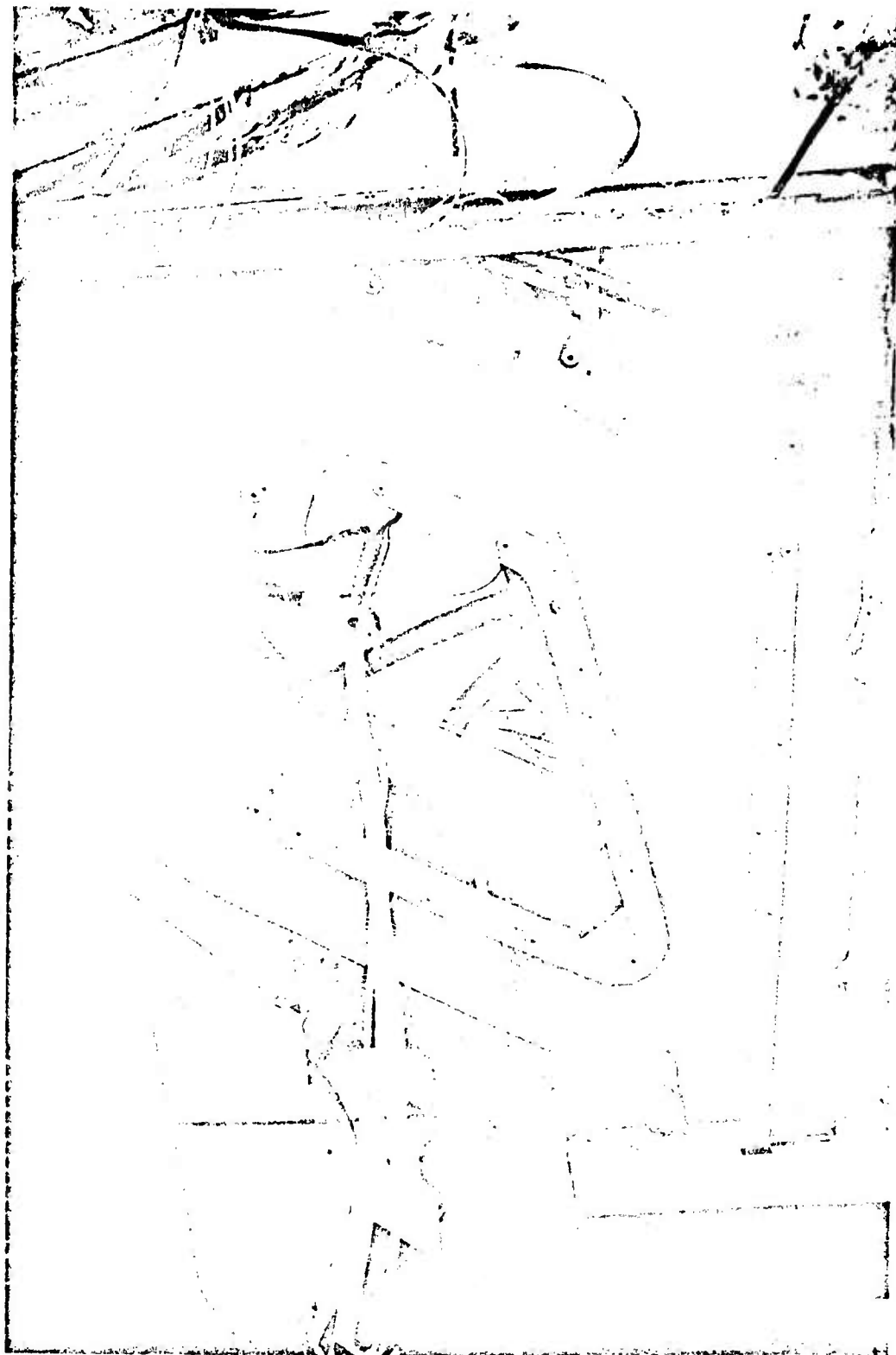
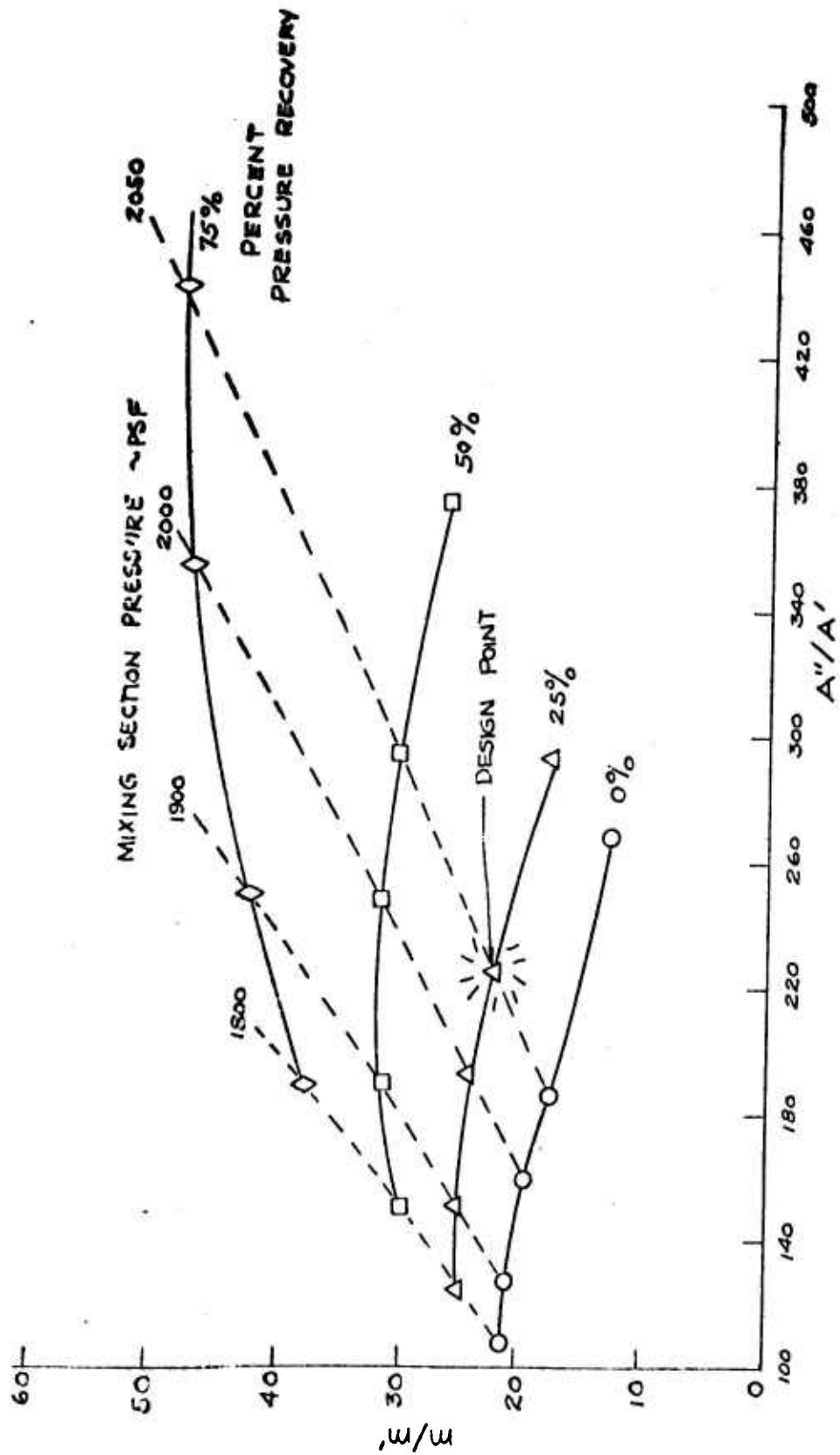


Figure 9.2-14 Model 1 Recirculating Ejector



9.2-12

FIGURE 9.2-16 MODEL I RECIRCULATING EJECTOR THEORETICAL MASS AUGMENTATION

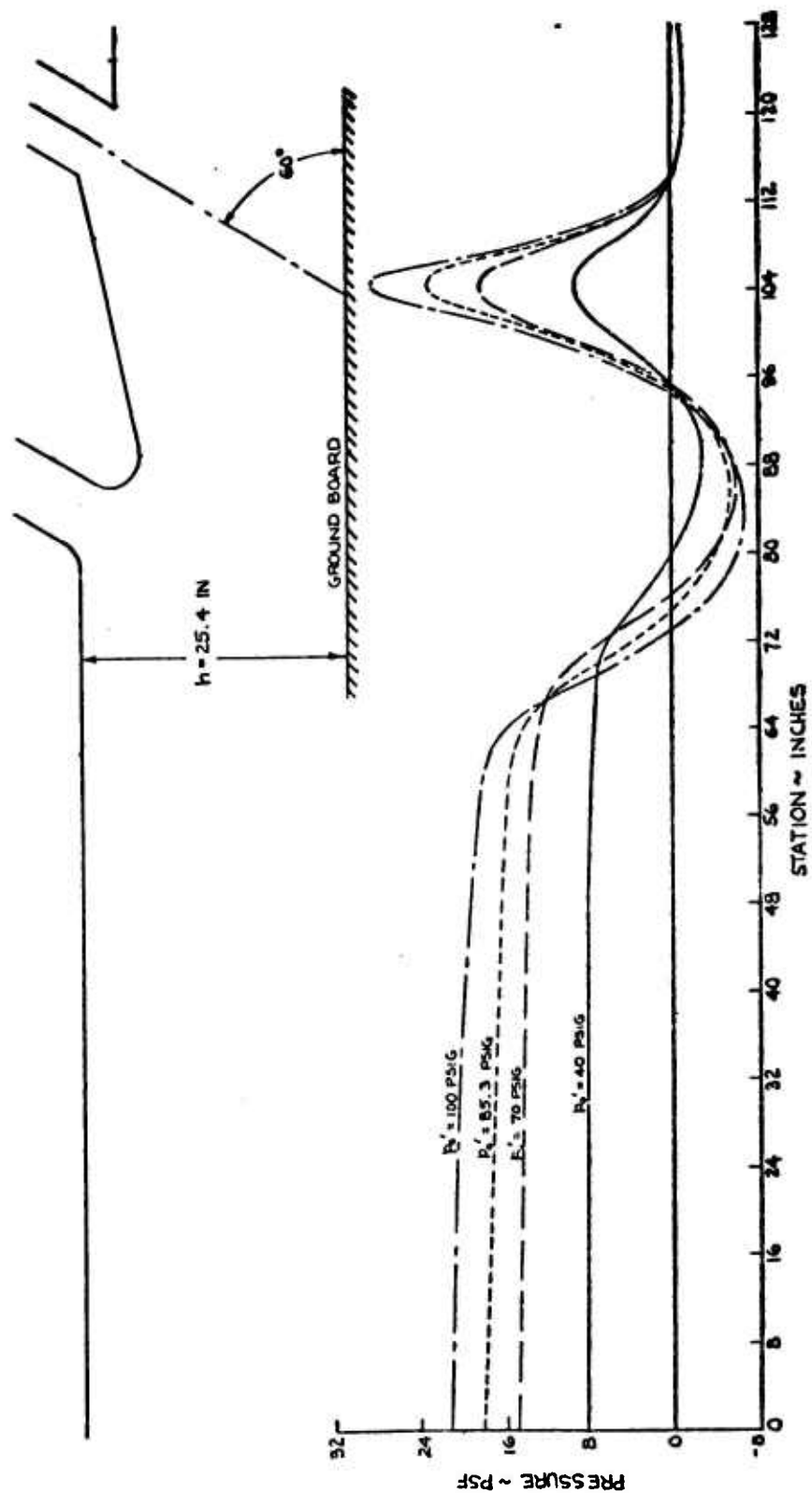


FIGURE 9.2-17 EFFECT OF PRIMARY TOTAL PRESSURE ON THE GROUND BOARD PRESSURE DISTRIBUTION OF MODEL I RECIRCULATING EJECTOR

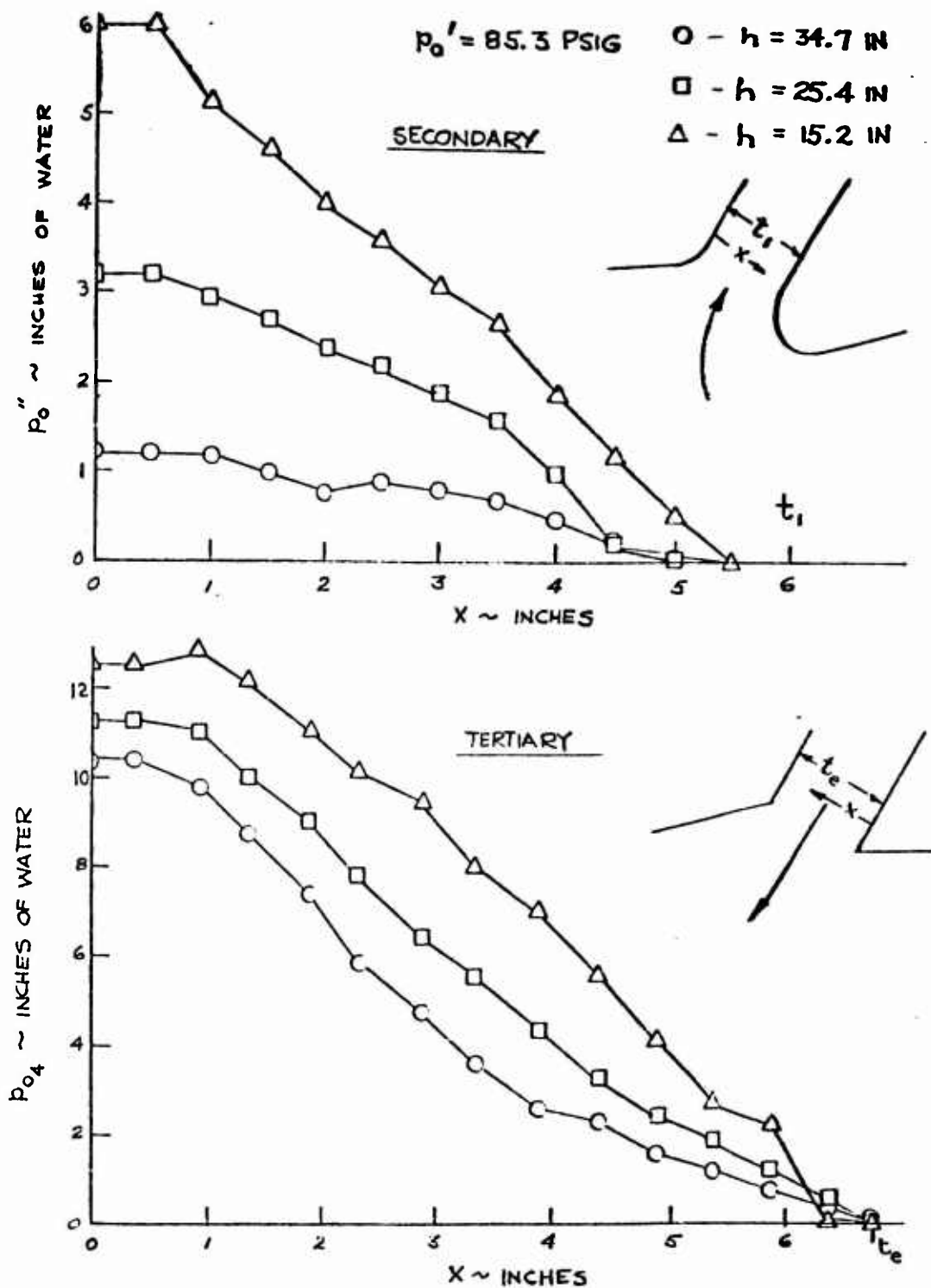


FIGURE 9.2-18 MODEL 1 RECIRCULATING EJECTOR SECONDARY AND TERTIARY TOTAL PRESSURE DISTRIBUTIONS

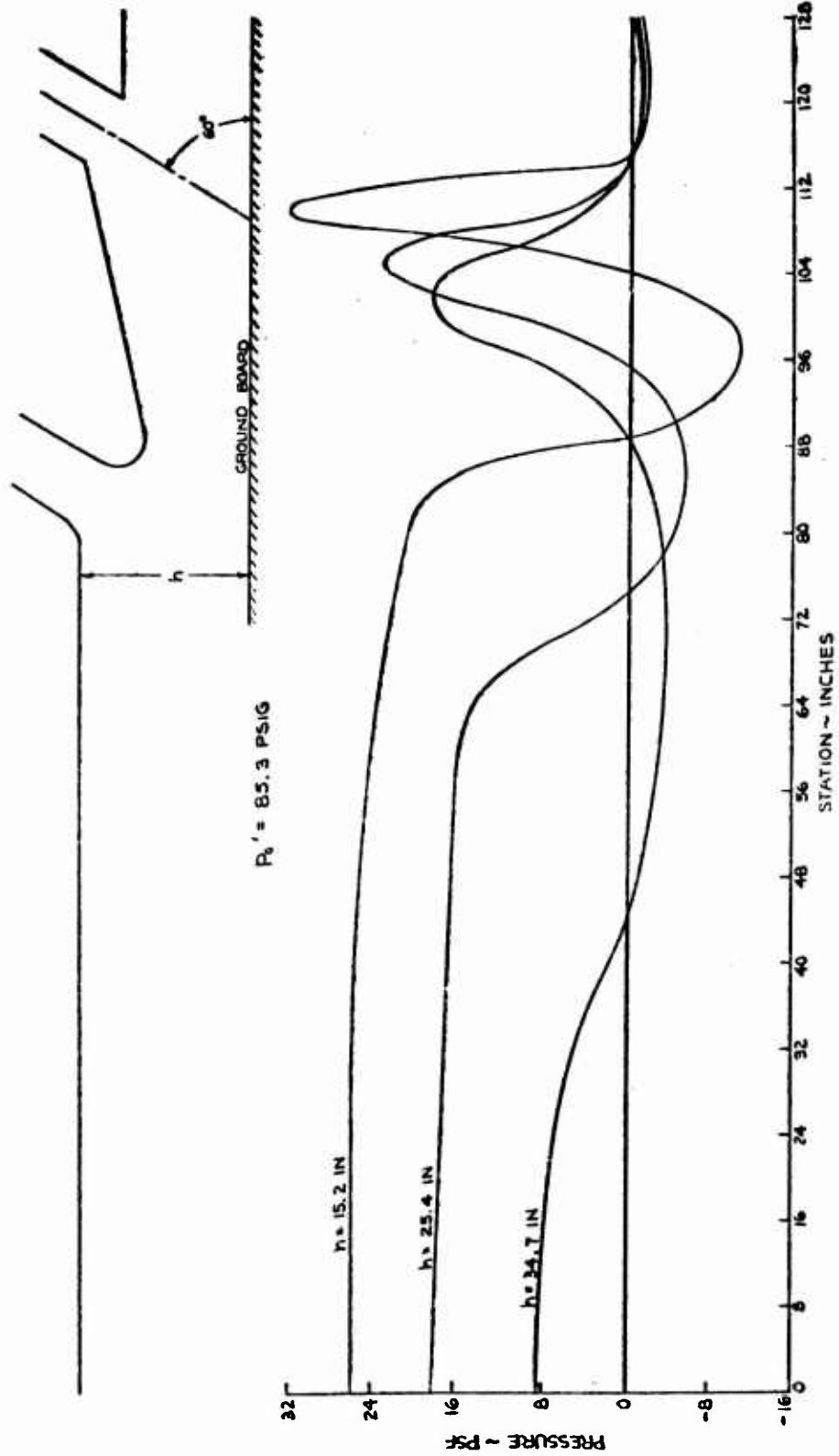


FIGURE 9.2-19 EFFECT OF HEIGHT ON THE GROUND BOARD PRESSURE DISTRIBUTION OF MODEL 1 RECIRCULATING EJECTOR

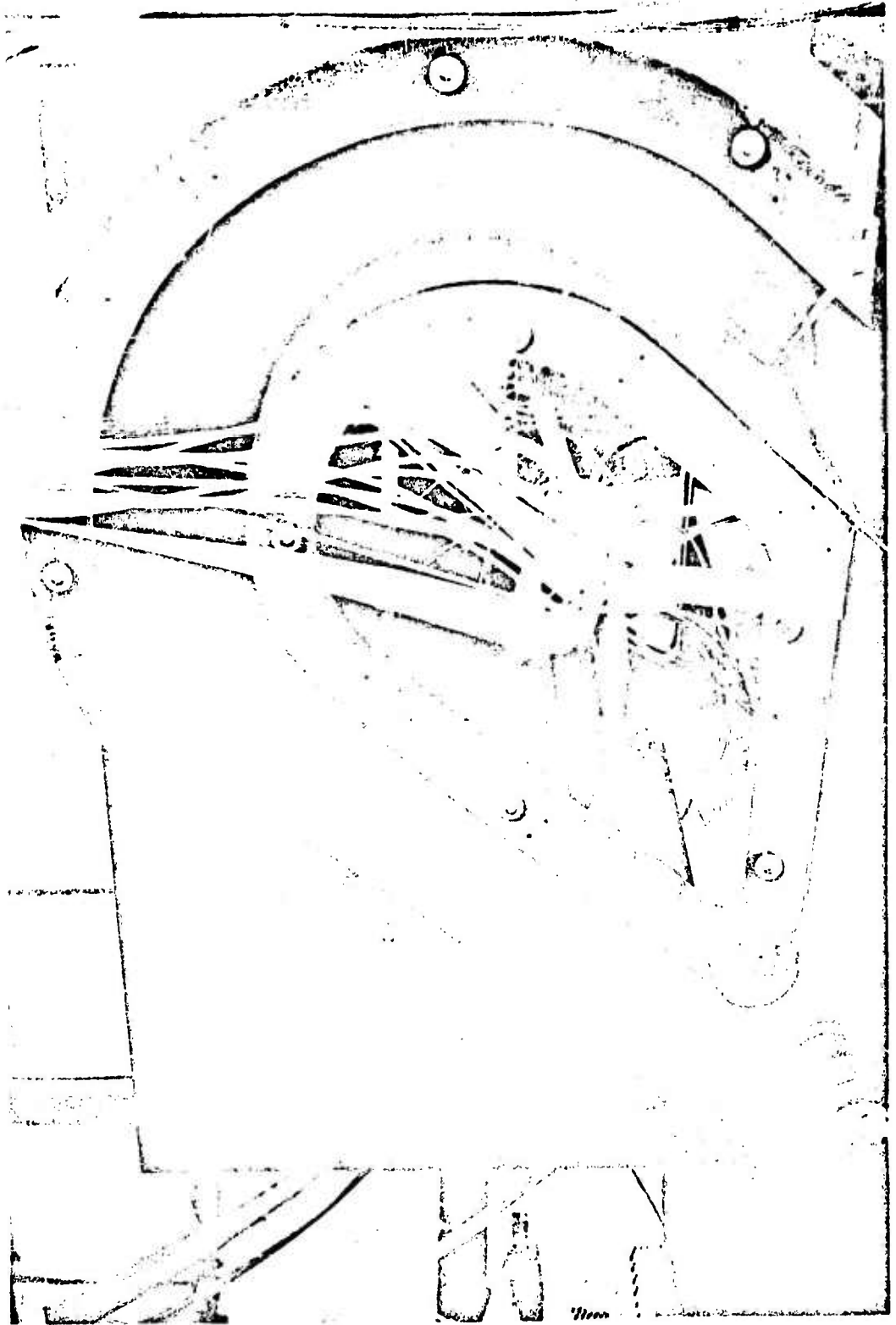


Figure 9.2-20 Model 2 Recirculating Ejector

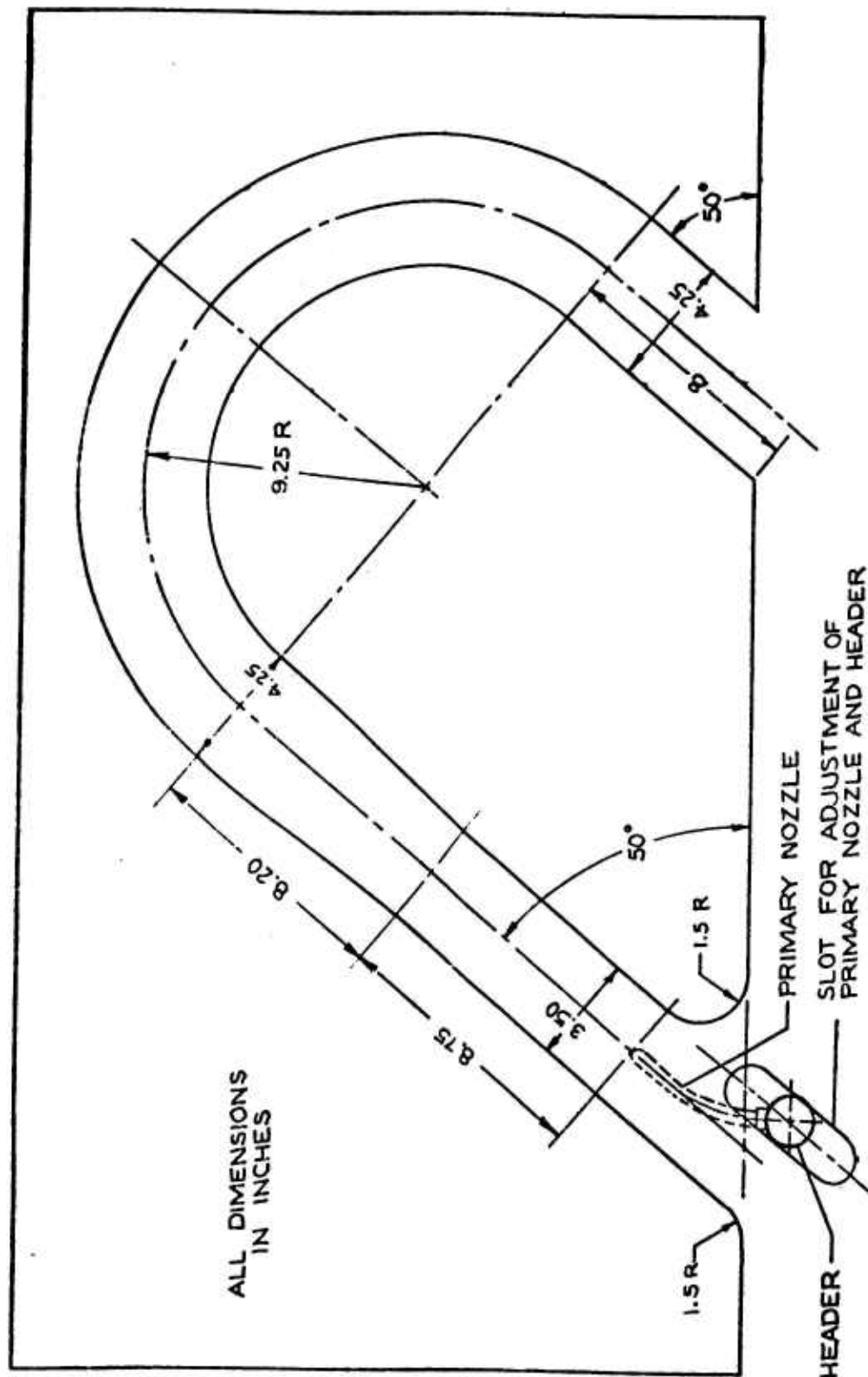


FIGURE 9.2-21 MODEL 2 RECIRCULATING EJECTOR - DIMENSIONAL DRAWING

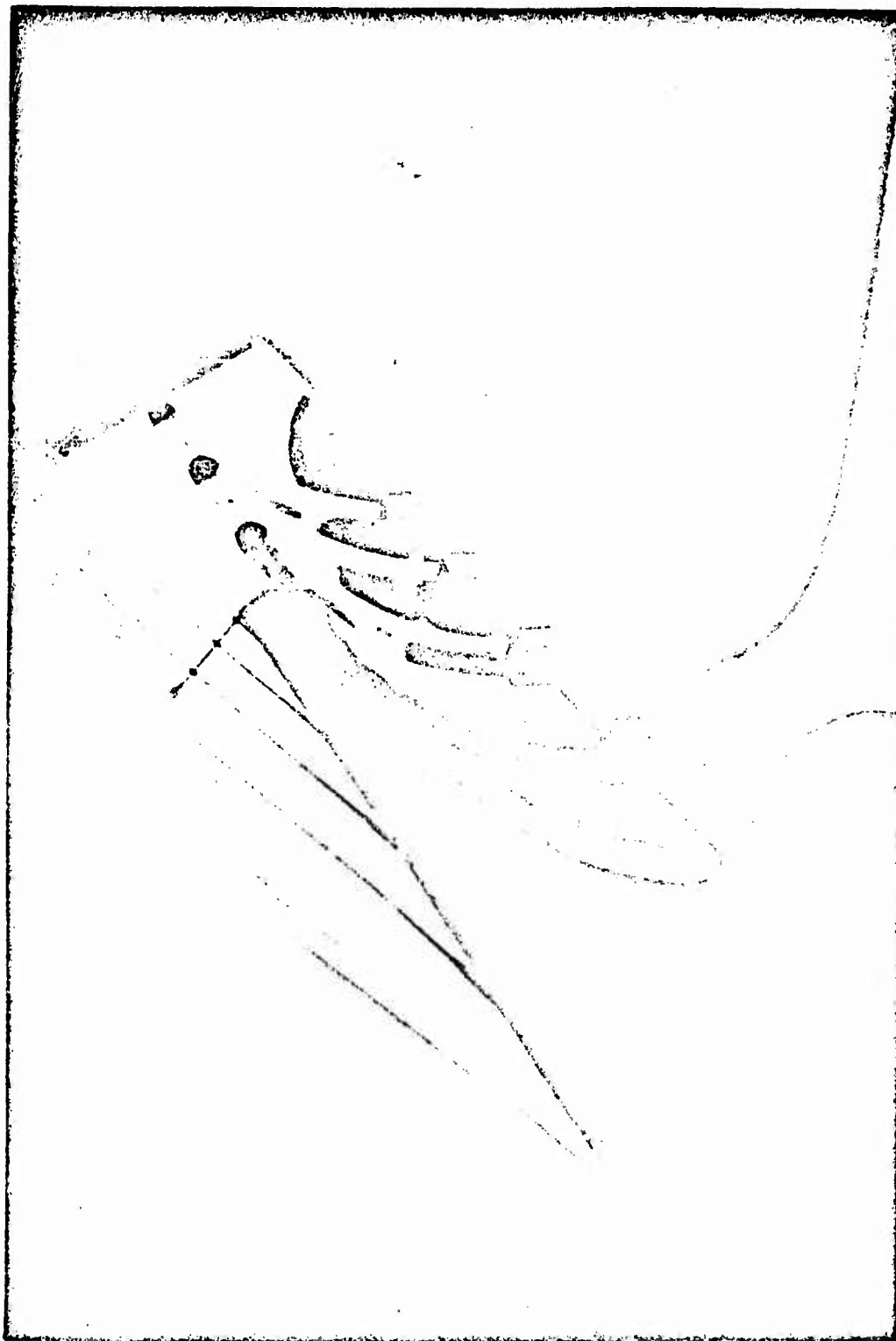


Figure 9.2-22 Model 2 Primary Nozzle-Header Installation

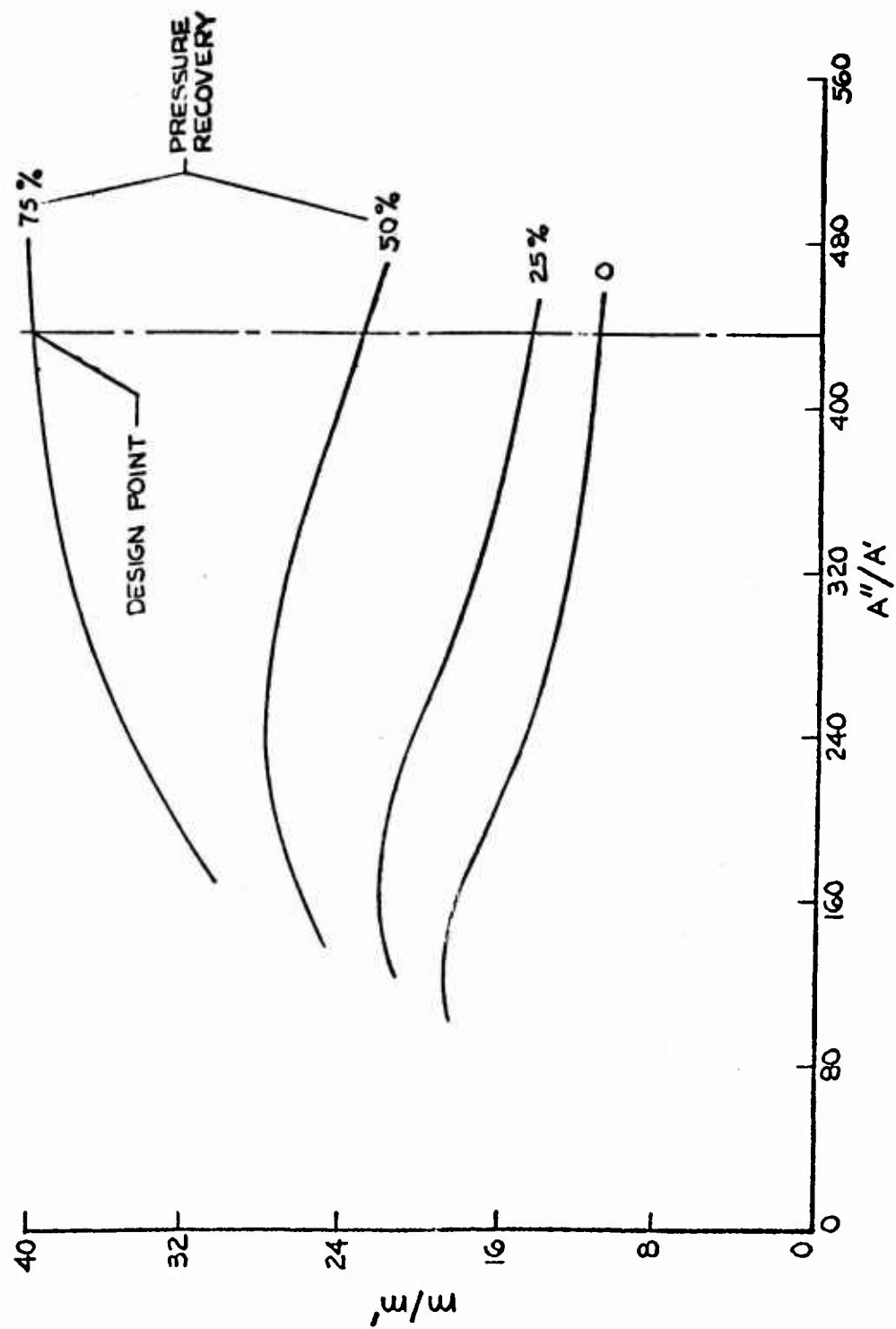


FIGURE 9.2-23 THEORETICAL MASS AUGMENTATION FOR MODEL 2 RECIRCULATING EJECTOR

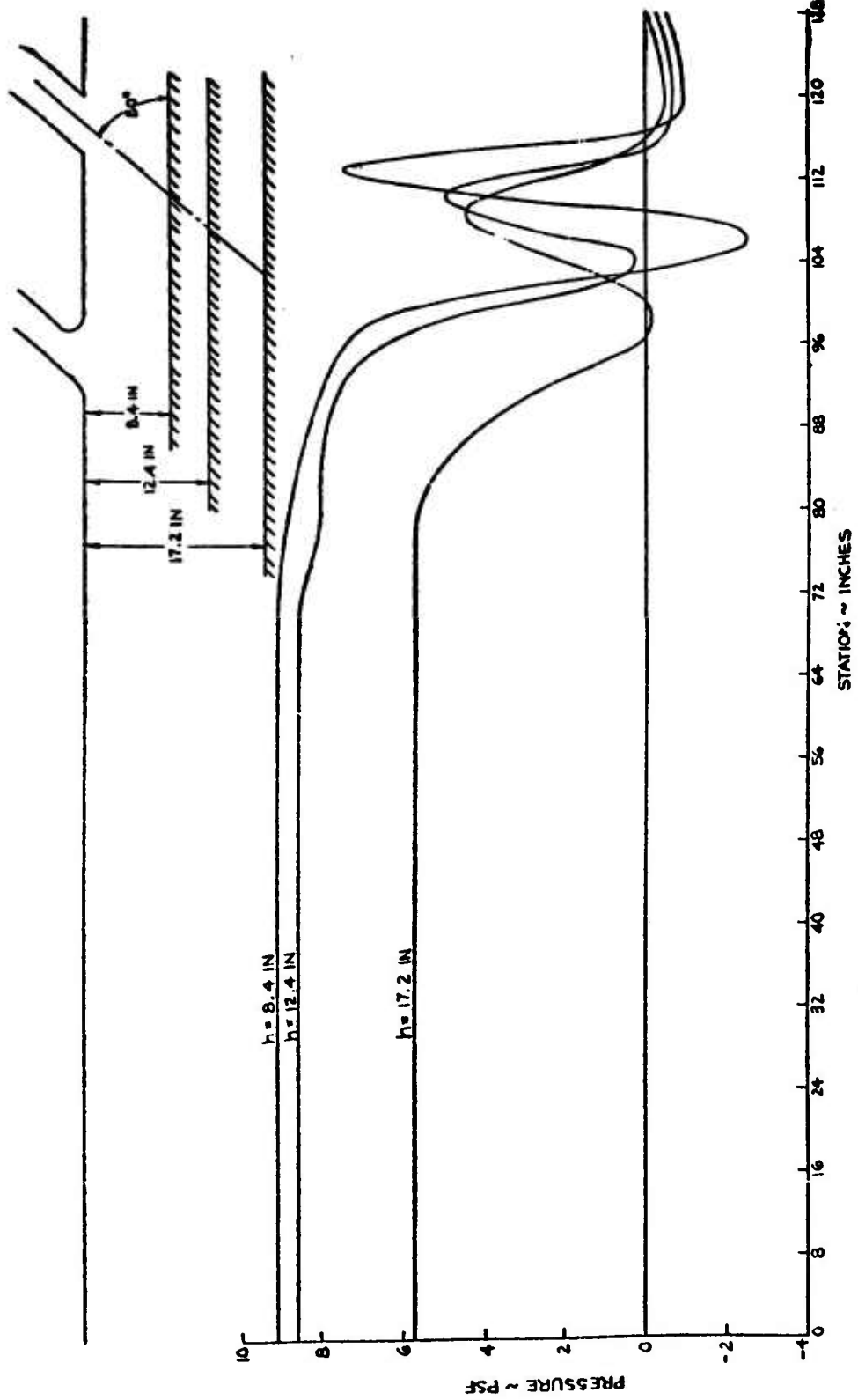


FIGURE 9.2-24 EFFECT OF HEIGHT ON THE GROUND BOARD PRESSURE. DISTRIBUTION OF MODEL 2 RECIRCULATING EJECTOR

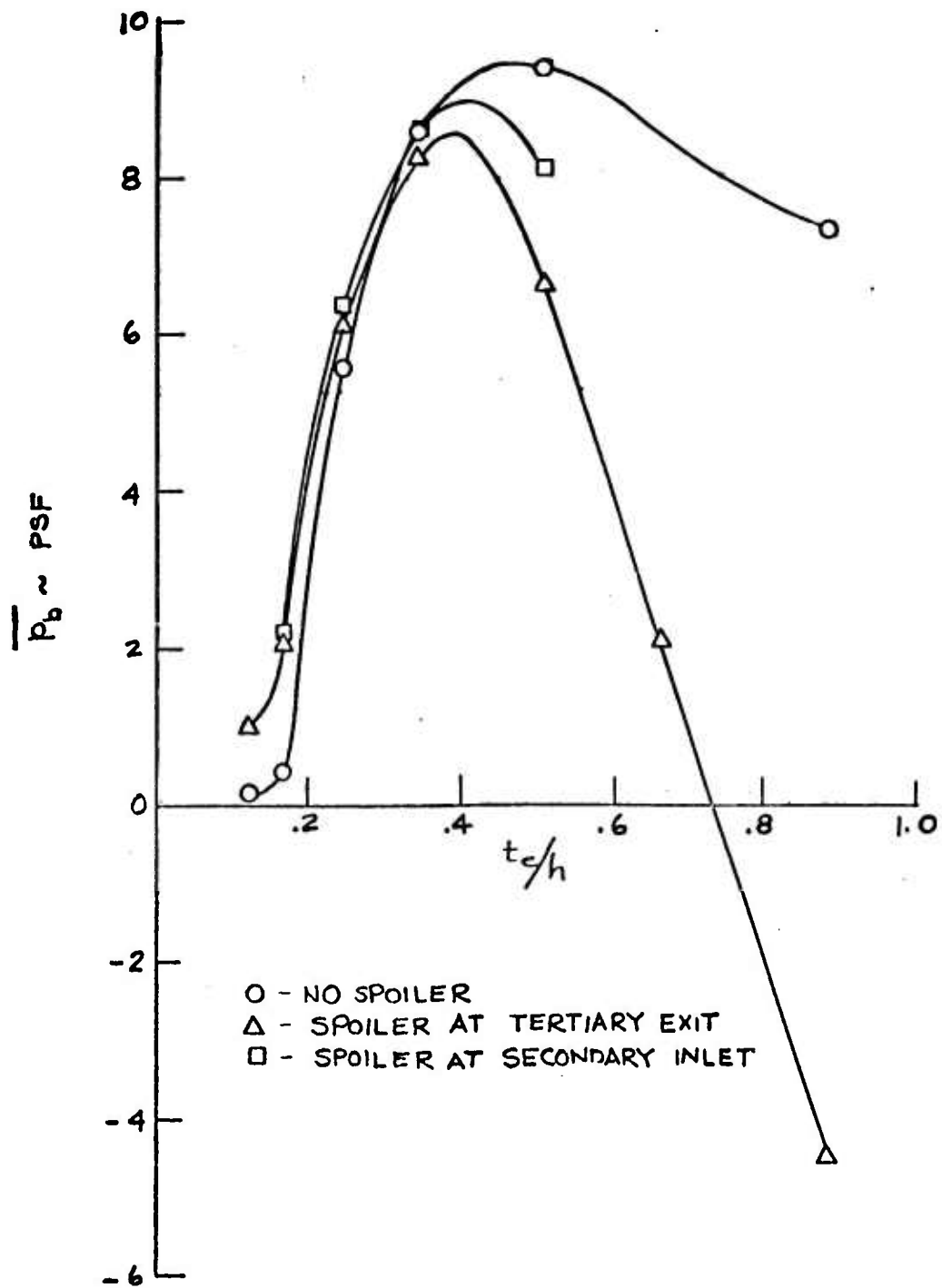
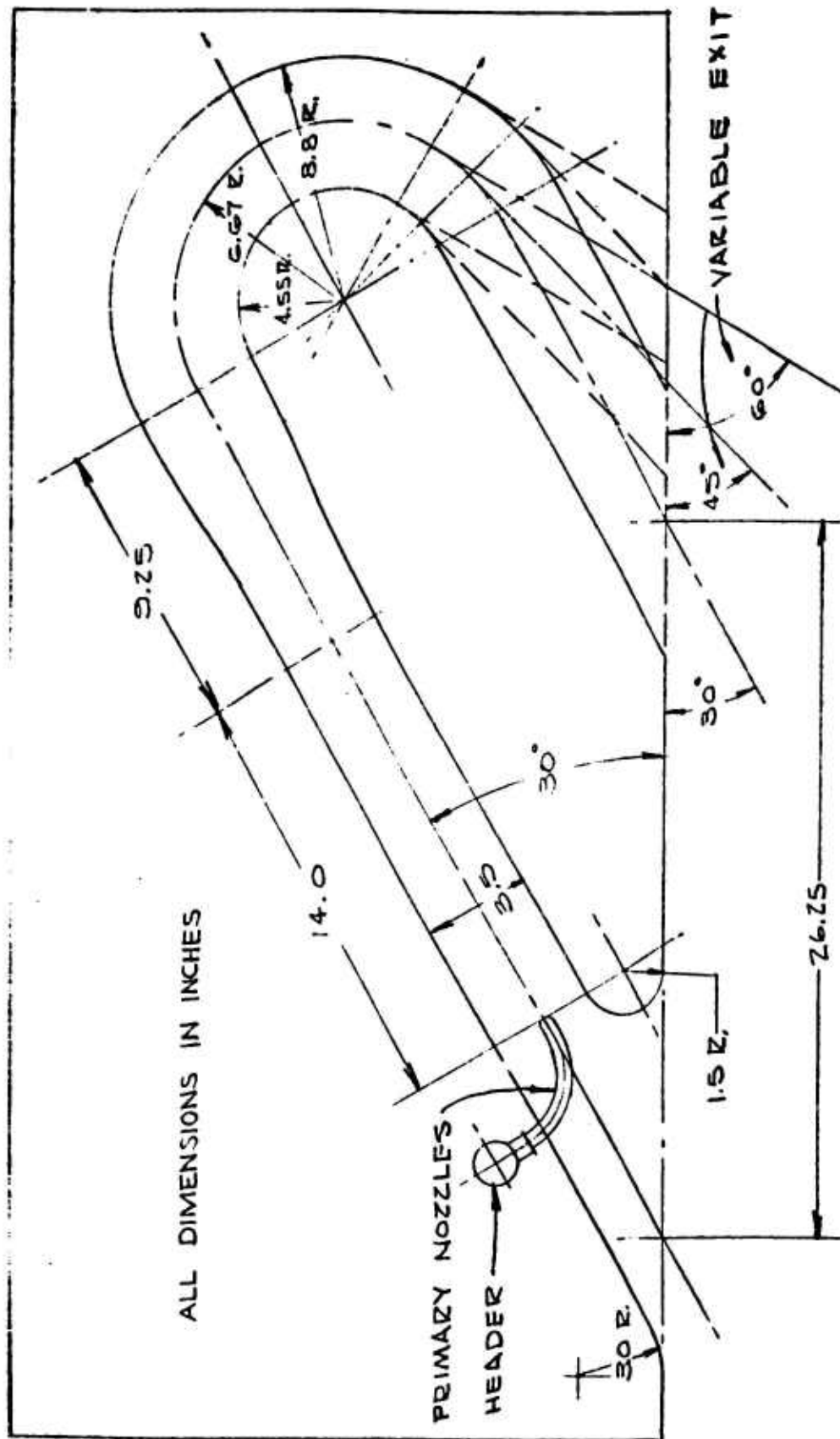


FIGURE 9.2-25 EFFECT OF SPOILER LOCATION ON BASE PRESSURE - MODEL 2 RECIRCULATING EJECTOR



9.2-52

FIGURE 9.2 -26 MODEL 3 RECIRCULATING EJECTOR - DIMENSIONAL DRAWING

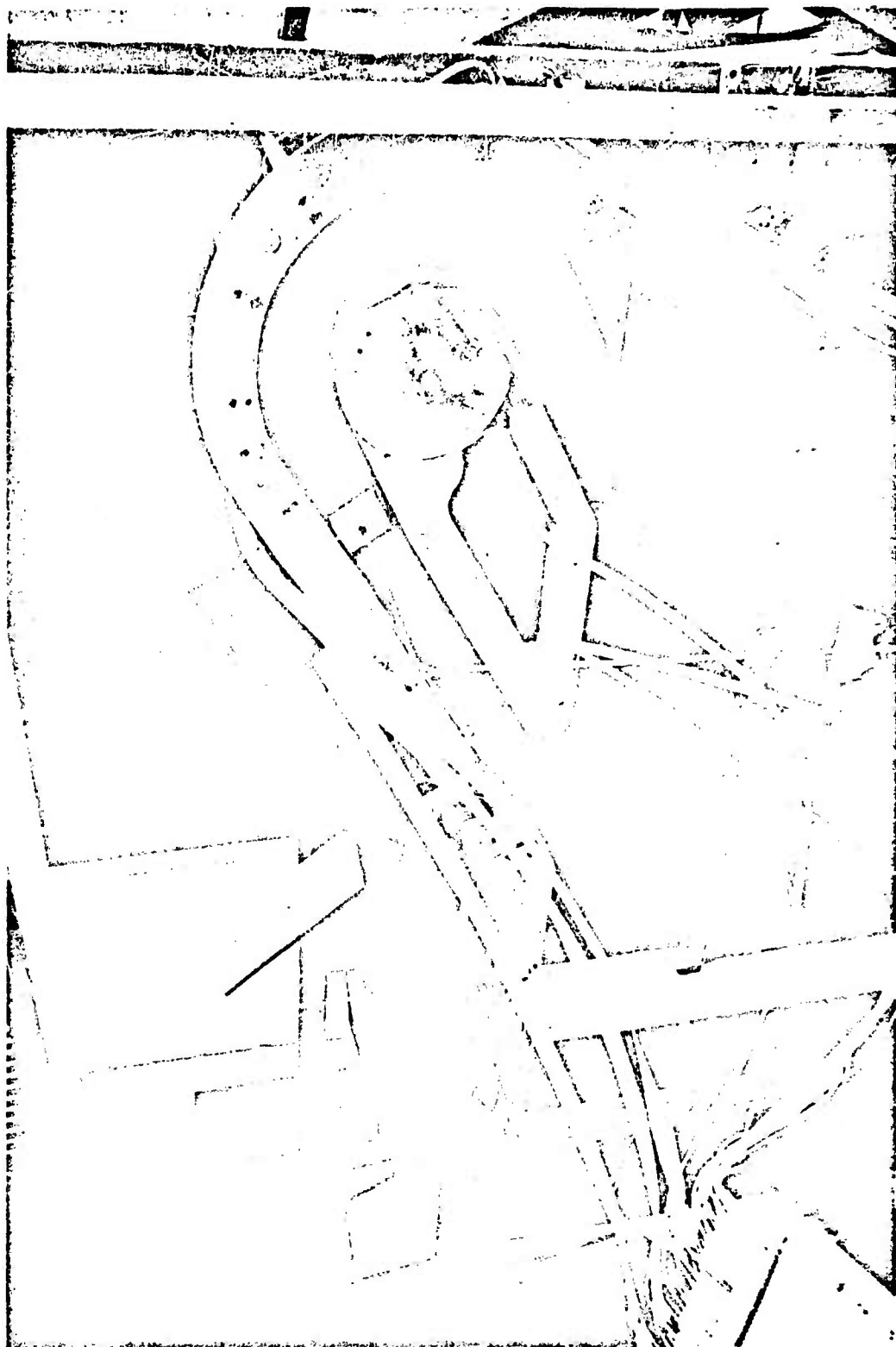


Figure 9.2-27 Model 3 Recirculating Ejector $\theta_1 = \theta_2 = 30^\circ$

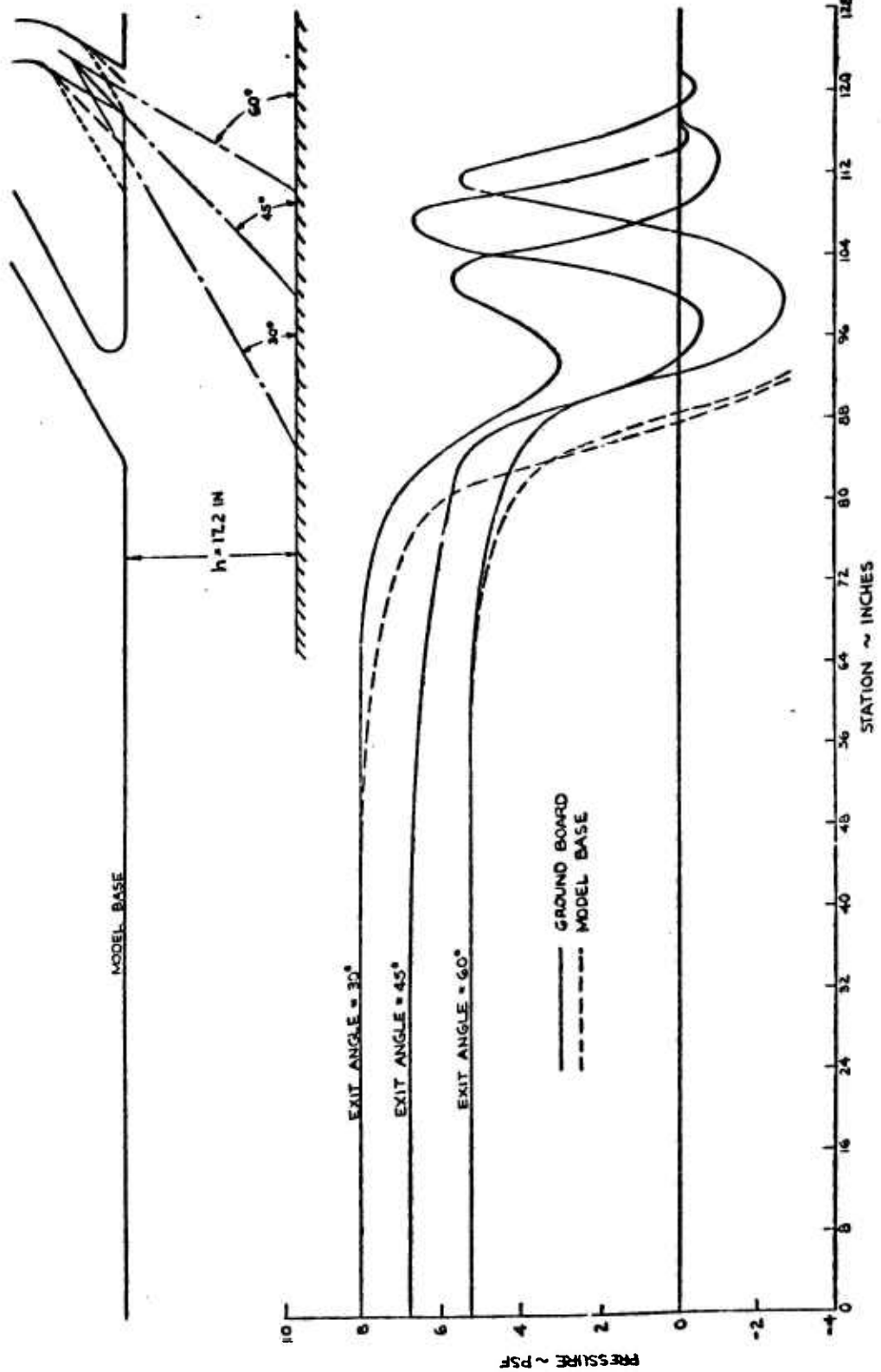


FIGURE 9.2-28 EFFECT OF TERTIARY EXIT ANGLE ON THE MODEL BASE AND GROUND BOARD PRESSURE DISTRIBUTIONS OF MODEL 3 RECIRCULATING EJECTOR - $h = 17.2 \text{ IN}$

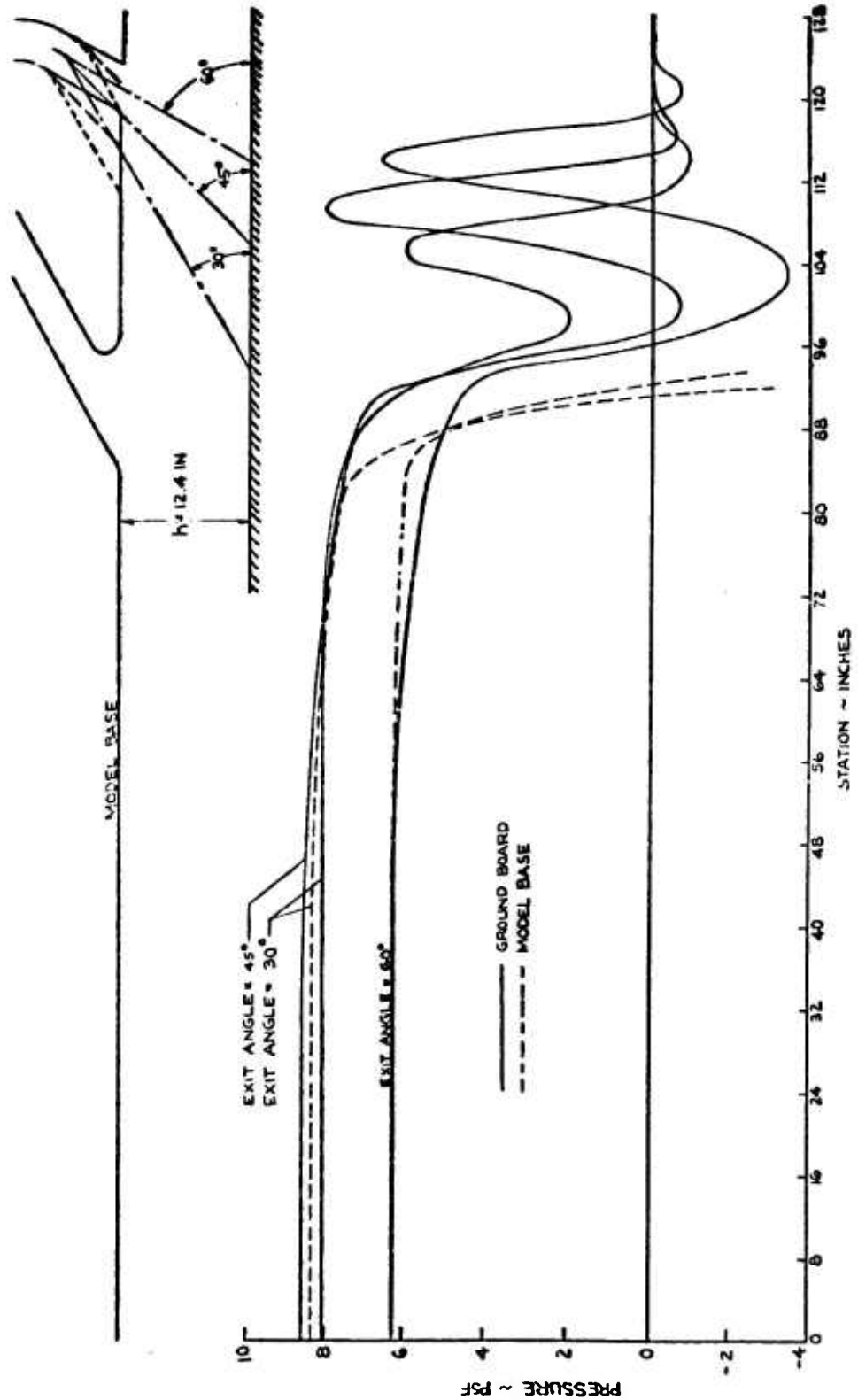


FIGURE 9.2-29 EFFECT OF TERTIARY EXIT ANGLE ON THE MODEL BASE AND GROUND BOARD PRESSURE DISTRIBUTIONS OF MODEL 3 RECIRCULATING EJECTOR - $h = 12.4 \text{ IN.}$

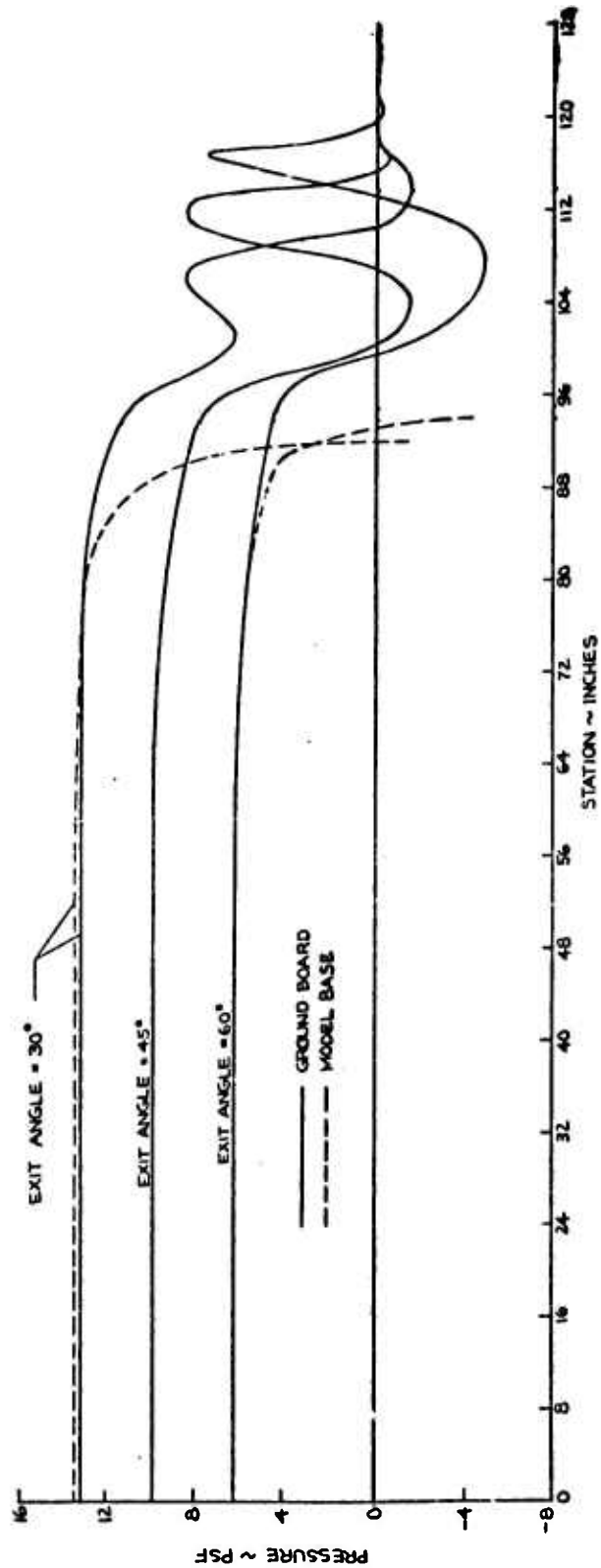


FIGURE 9.2-30 EFFECT OF TERTIARY EXIT ANGLE, ON MODEL BASE AND GROUND BOARD PRESSURE DISTRIBUTIONS OF MODEL 3 RECIRCULATING EJECTOR - $h = 8.4$ IN

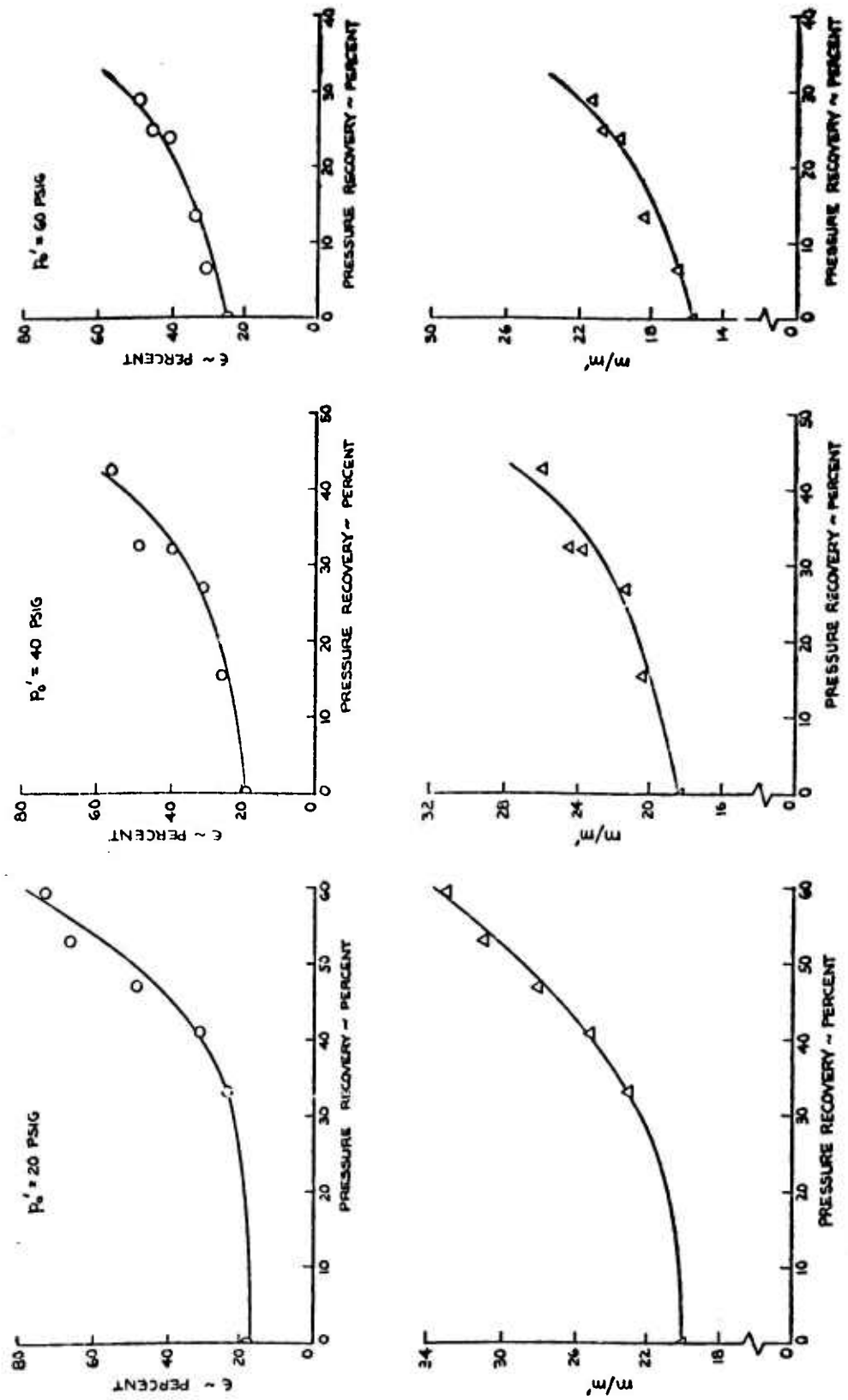


FIGURE 9.2-31 PERFORMANCE OF DOWNSTREAM EJECTOR IN TANDEM STRAIGHT EJECTOR TESTS

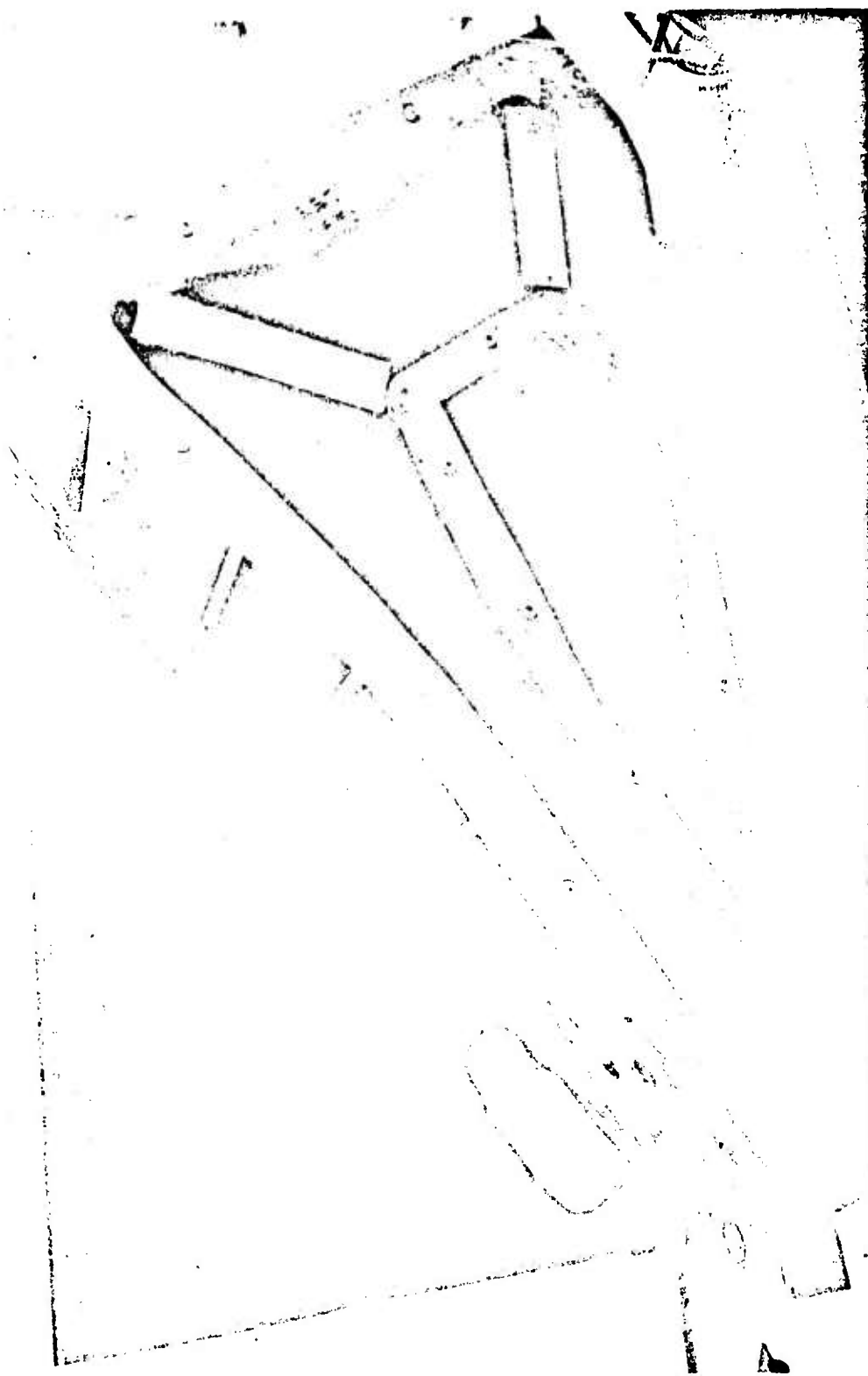


Figure 9.2-32 Model 4 Recirculating Ejector

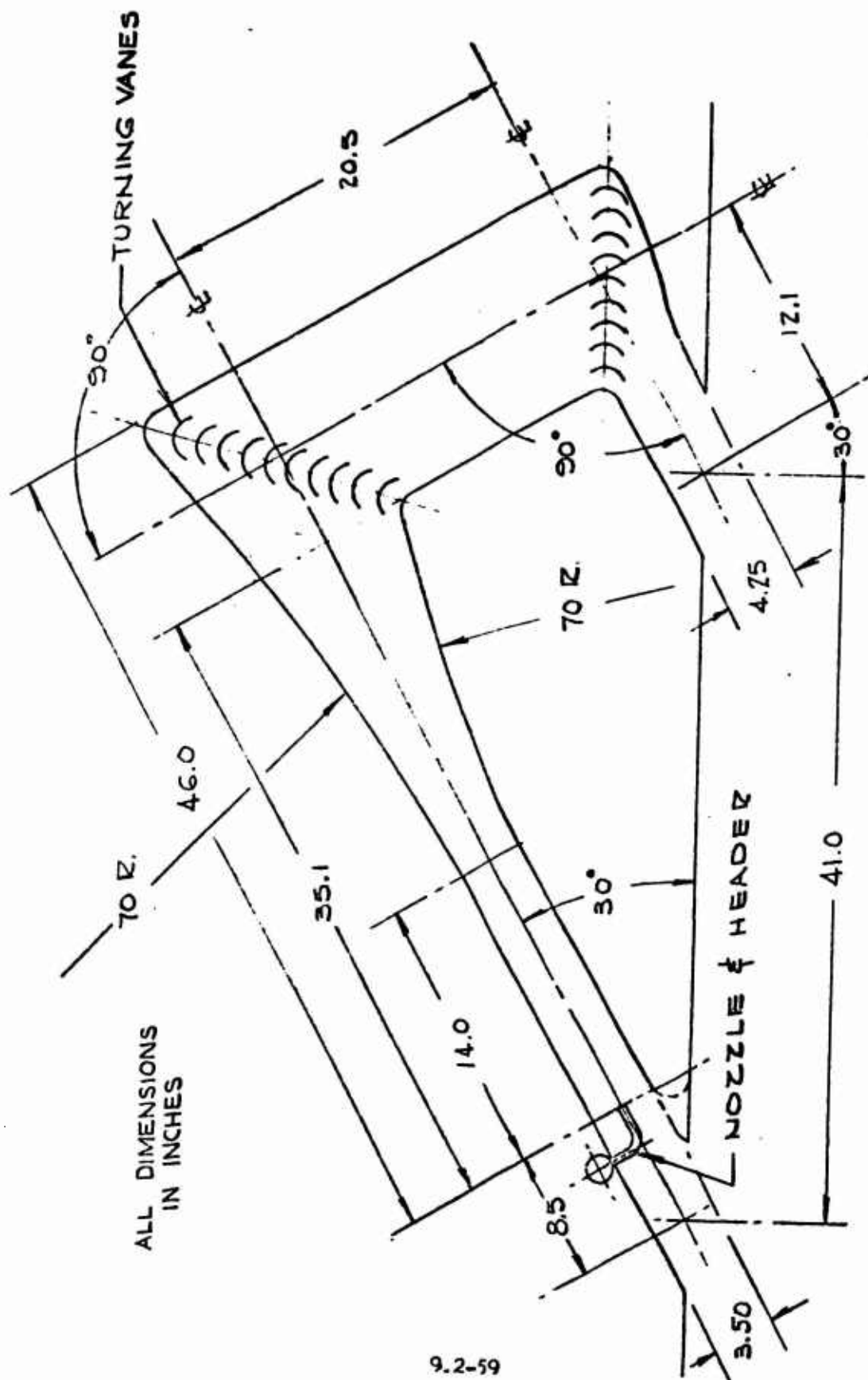
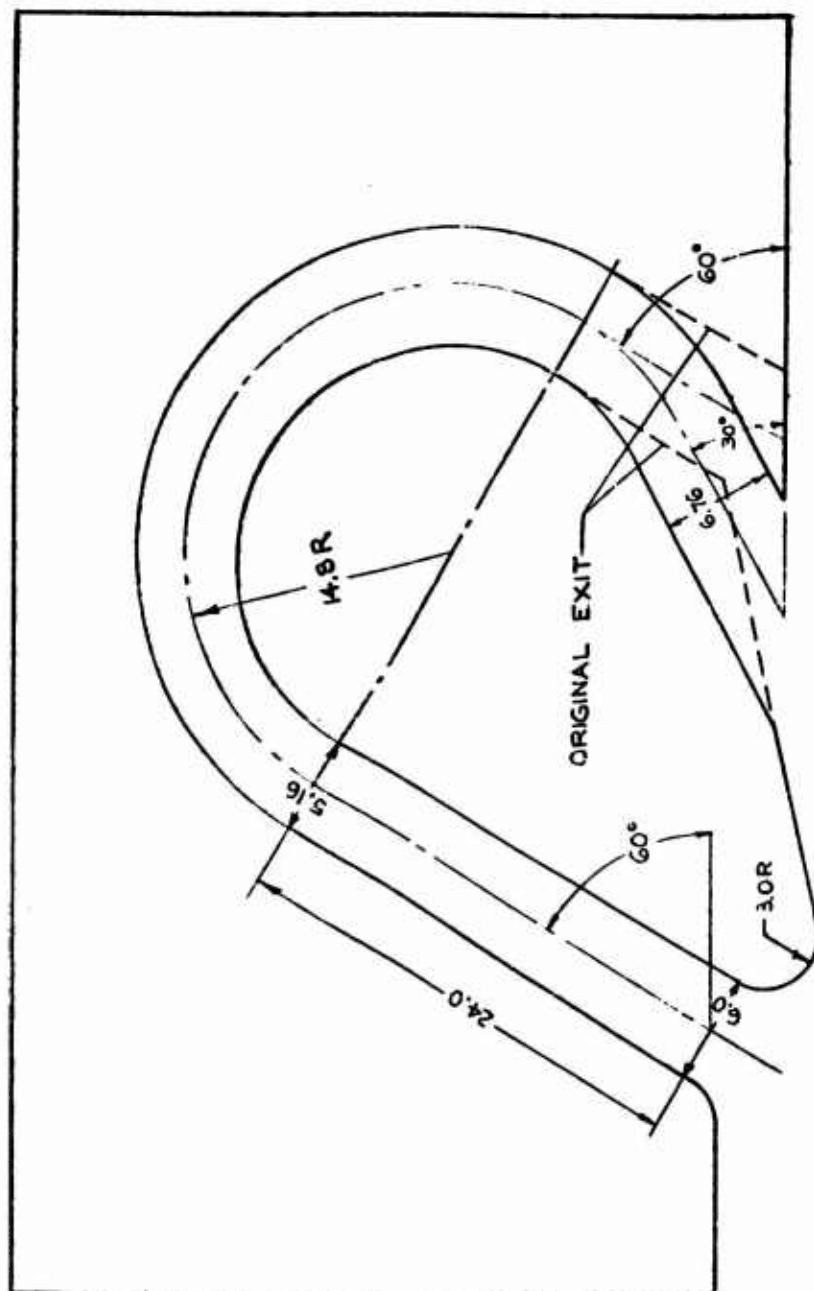


FIGURE 9.2-33 MODEL 4 RECIRCULATING EJECTOR - DIMENSIONAL DRAWING



ALL DIMENSIONS IN INCHES

FIGURE 9.2 - 34 MODIFIED MODEL 1 RECIRCULATING EJECTOR

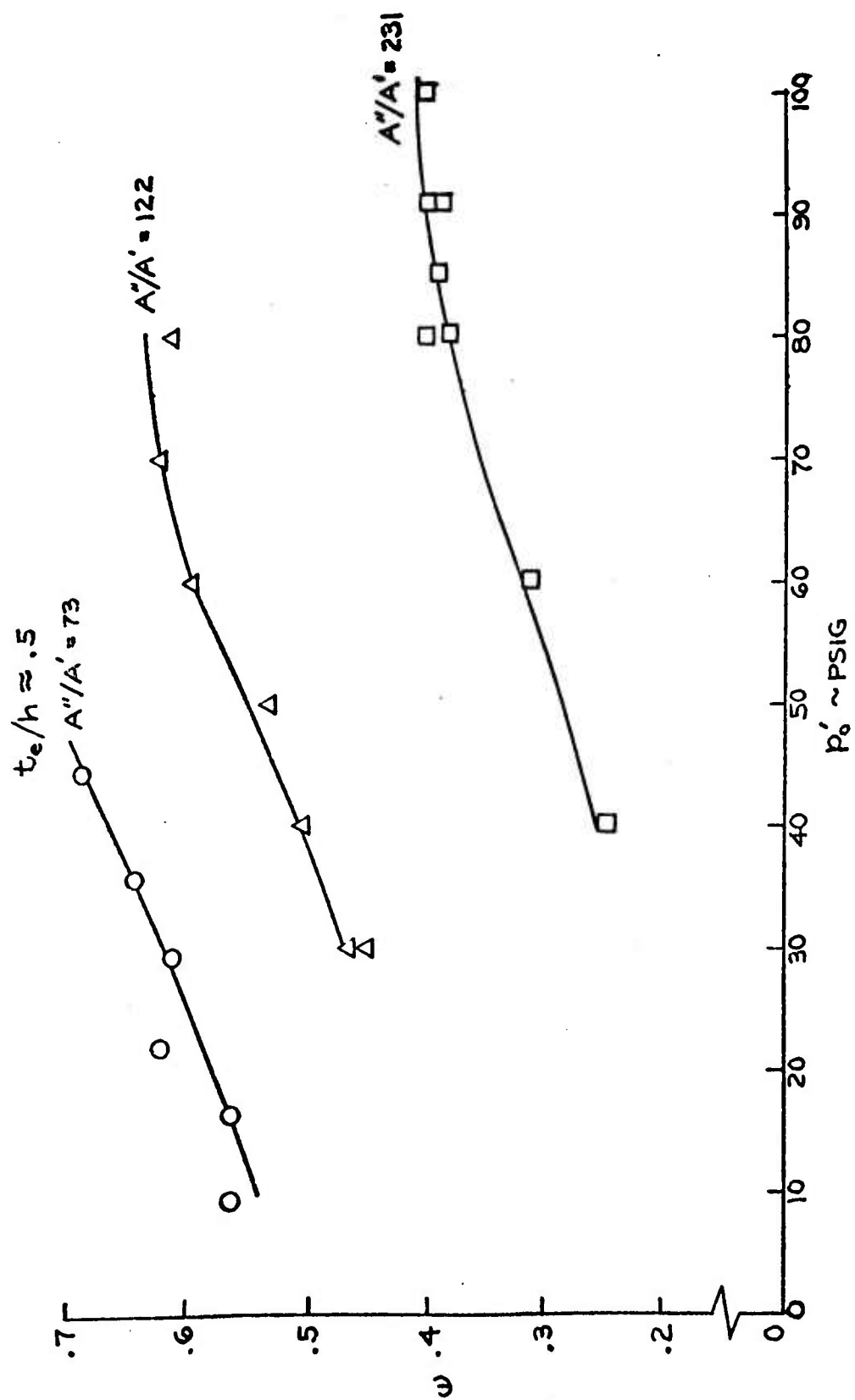


FIGURE 9.2-35 RECIRCULATING EJECTOR EFFICIENCY (EXPERIMENTAL RESULTS)
MODIFIED MODEL 1 RECIRCULATING EJECTOR

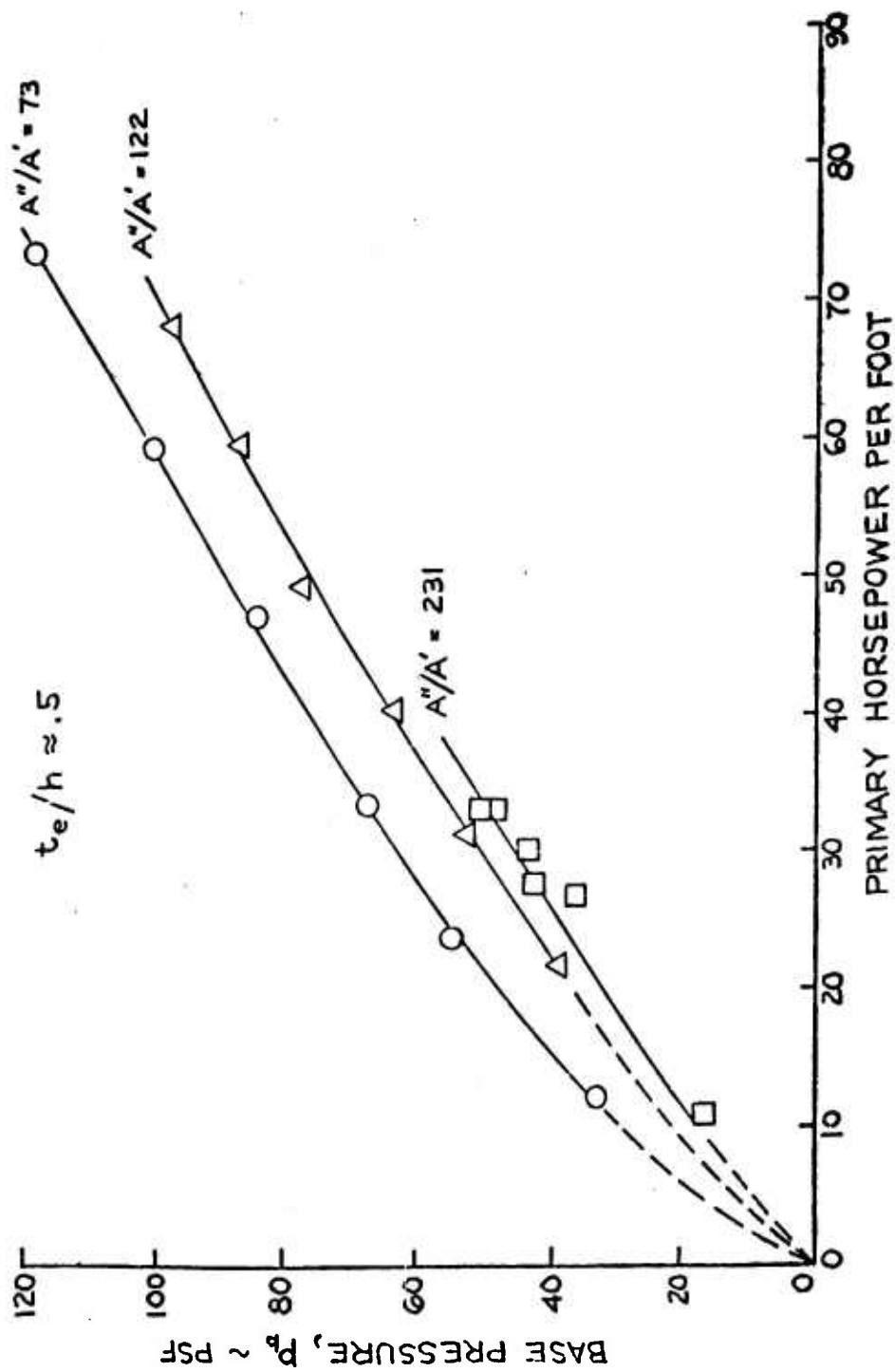


FIGURE 9.2-36 EFFECT OF AREA RATIO ON BASE PRESSURE AND PRIMARY HORSEPOWER - MODIFIED MODEL 1 RECIRCULATING EJECTOR

10.0 COMPARISON OF THEORY WITH EXPERIMENT

10.1 STRAIGHT EJECTOR

The straight ejector test program was conducted primarily to substantiate the ejector theory for zero secondary total pressure recovery. Also, since the program was quite systematic in nature, empirical corrections might evolve, which could increase the accuracy and reliability of the theory. A comparison of experimental values of mass augmentation, thrust augmentation, and efficiency, with theoretical predictions for the ejector configurations tested, is presented in Figures 10.1-1 through 10.1-4.

The theoretical curves were obtained in the following manner. Experimental values for primary total pressure, average mixing section pressure, and tertiary total pressure were substituted into the digital program which solves the ejector equations of Section 7.1. A diffuser loss (total pressure drop) was included by using the empirical loss factors given in Reference 31 for the particular diffuser design used in these tests. This loss was introduced into the digital program by increasing the tertiary total pressure at the end of mixing, p_{o_2} , by the amount of the pressure drop, and increasing the exit static pressure by the same amount. This technique effectively simulated the conditions of an ejector operating against a back pressure equal to the diffuser loss. In this manner, exit flow parameters, such as mass flow or velocity, were not changed from the experimental values.

Solutions were obtained by substituting several values of tertiary mass flow and exit velocities, which were close to the experimental values of the particular tested configuration, into the program while holding

exit area constant. The tertiary total pressure, p_{o_2} , was also varied in proportion to velocity. This was repeated until a solution was obtained which matched the experimental primary mass flow. The resulting values for mass augmentation, thrust augmentation, efficiency, and area ratio were then compared to the experimental values.

Figure 10.1-1 compares the effect of mixing section length, primary pressure ratio, and area ratio on mass augmentation. The agreement in magnitude and trend is generally good. It is noted that theoretical mass augmentation increases with decreasing mixing-section length whereas the reverse is true for the experimental case. This is due to the fact that the theory assumes complete mixing regardless of the mixing length hence, as the mixing section is shortened, the frictional force is reduced and the mass augmentation naturally increases. Figure 10.1-1 shows that both theory and experiment indicate very nearly the same optimum area ratios. The values of theoretical mass augmentation are slightly higher than the test results, and it is thought that diffuser losses were probably higher than predicted.

Theoretical thrust augmentation presented in Figure 10.1-2 is also seen to increase with decreasing mixing section length. The assumption of complete mixing in the theoretical analysis, regardless of mixing length, is again responsible for this trend. Figure 10.1-3 compares the effect of area ratio on thrust augmentation with the theory and experiment. The curves are quite similar in shape; however, the agreement in magnitude is not particularly good. It is interesting to note that the theoretical simulations also showed thrust augmentation to be, for all practical purposes, independent of

primary pressure.

Good correlation between the pressure measurements of the current tests, and the force measurements of Reference 30 is shown in Figure 10.1-3.

The same comparisons of theory with experiment for ejector efficiency are given in Figure 10.1-4. For the case of efficiency as a function of area ratio, excellent agreement was obtained at each primary pressure ratio for a mixing section length of 8.

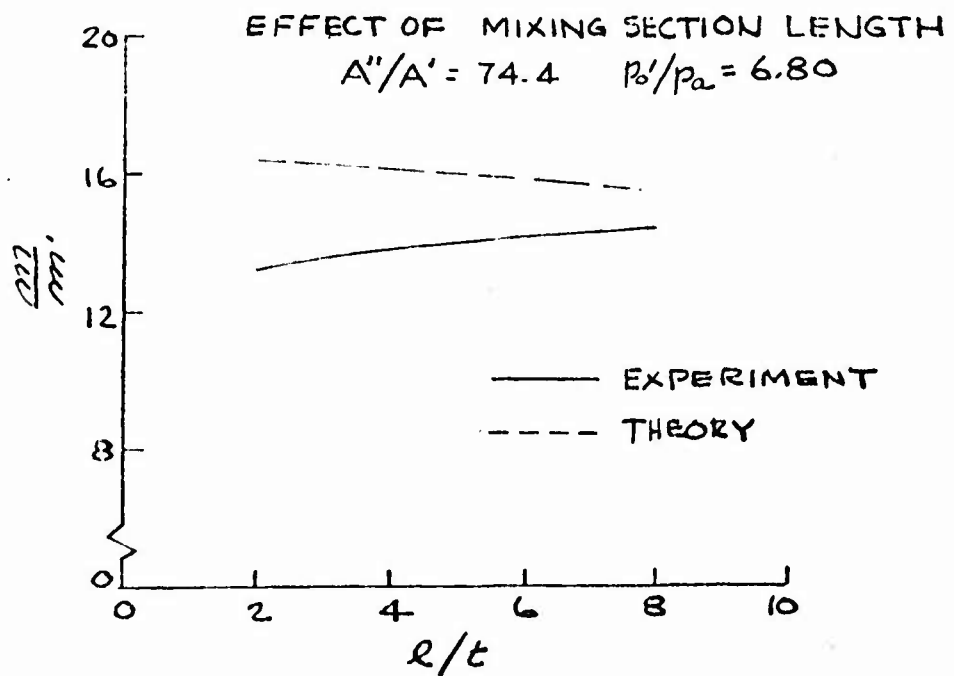
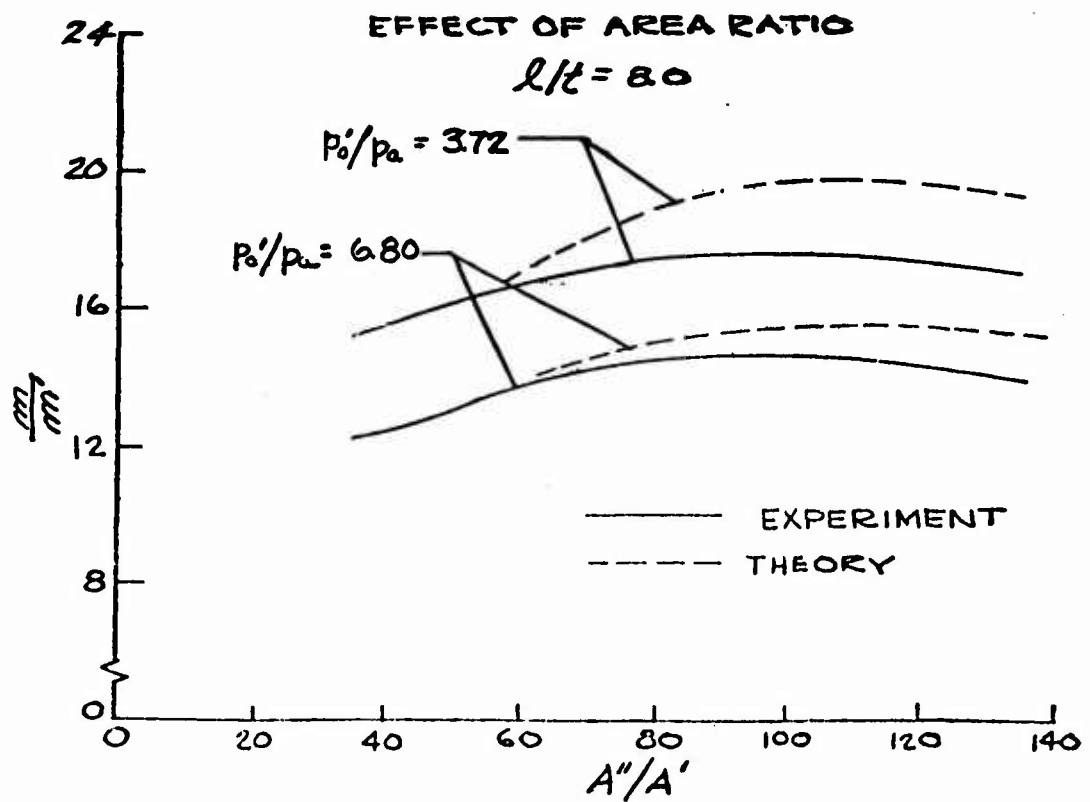


FIGURE 10.1-1 STRAIGHT EJECTOR MASS AUGMENTATION
COMPARISON OF THEORY WITH
EXPERIMENT

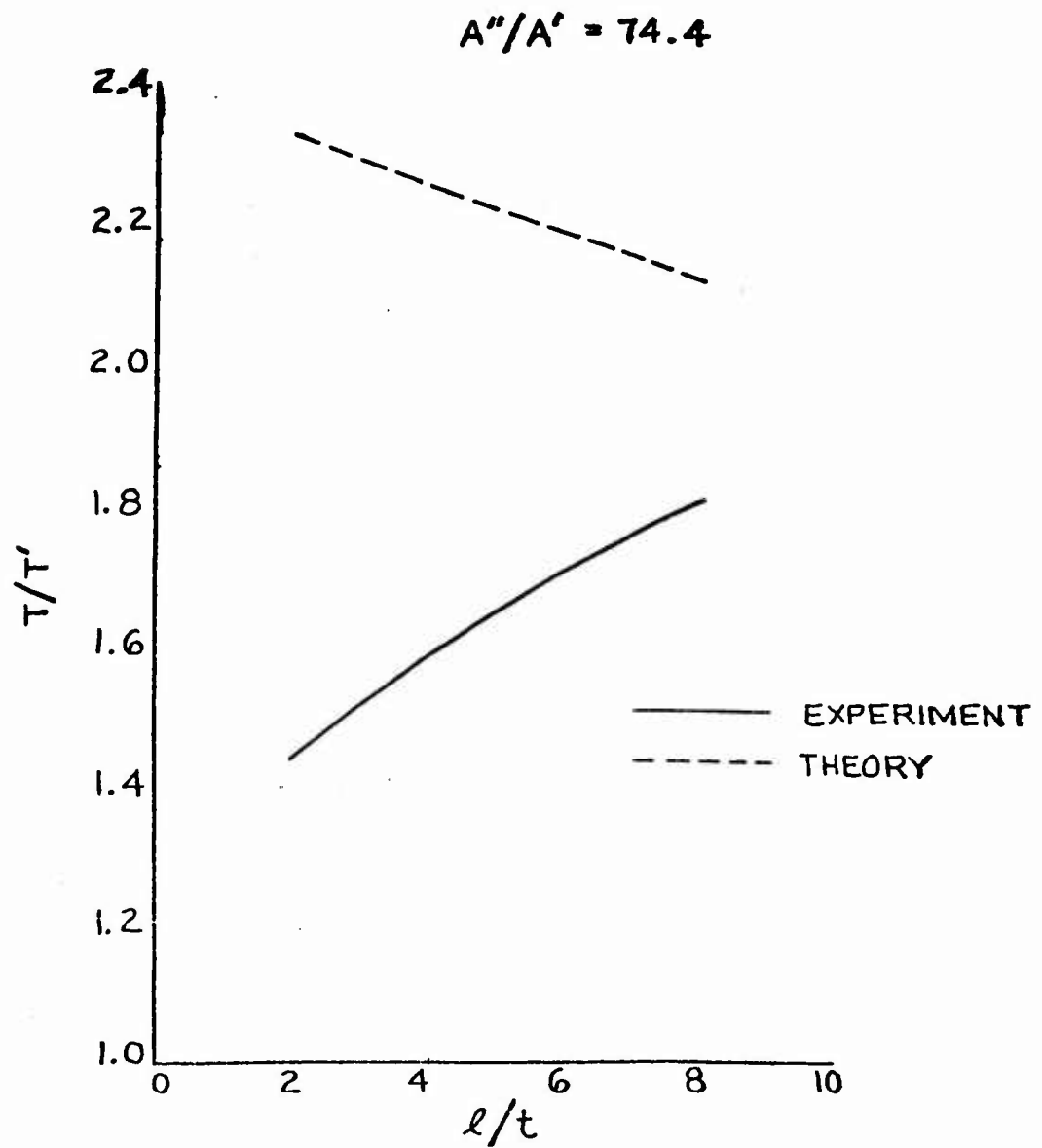


FIGURE 10.1-2 STRAIGHT EJECTOR THRUST AUGMENTATION—COMPARISON OF THEORY WITH EXPERIMENT—EFFECT OF MIXING SECTION LENGTH

$$l/t = 8.0$$

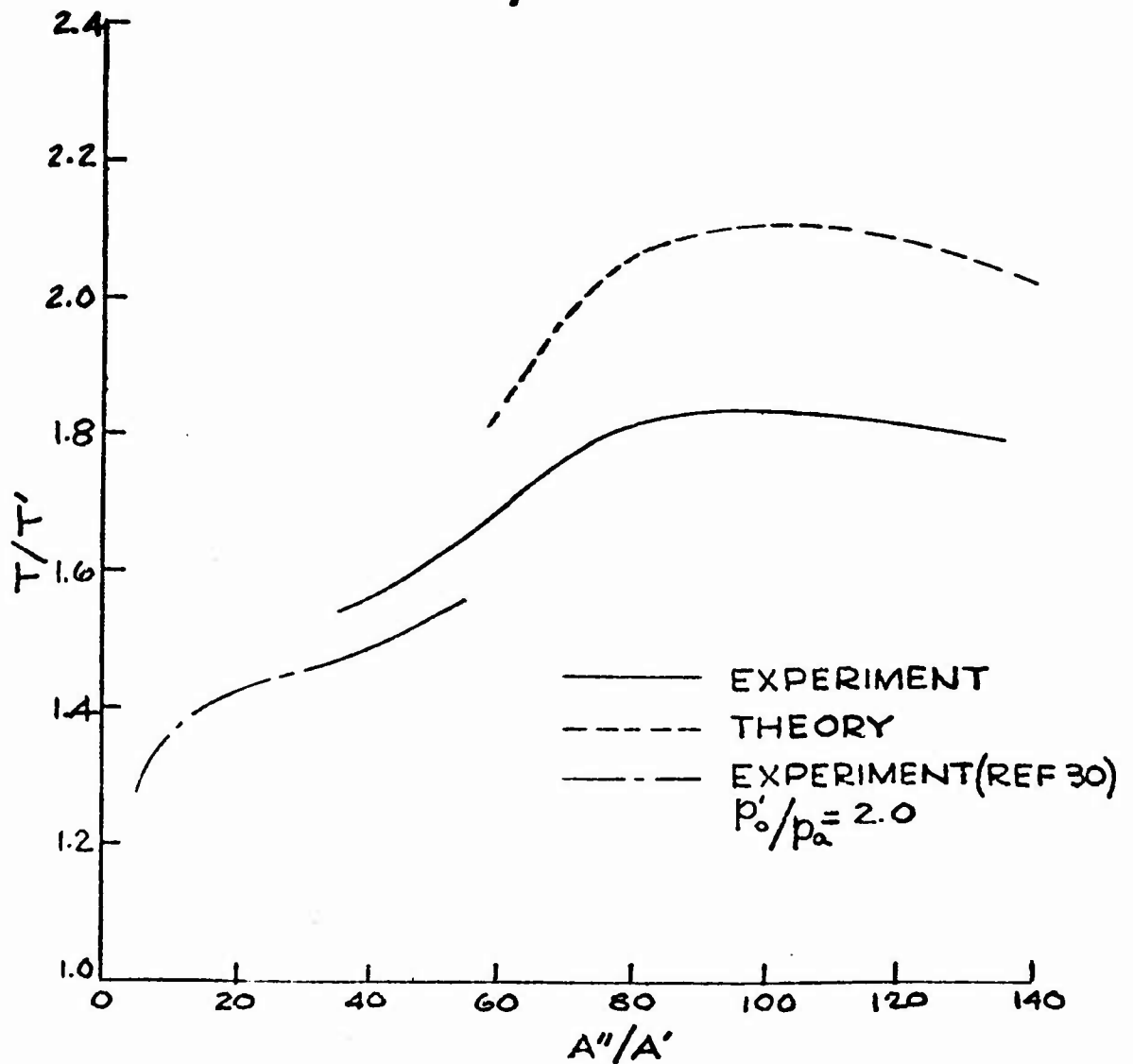
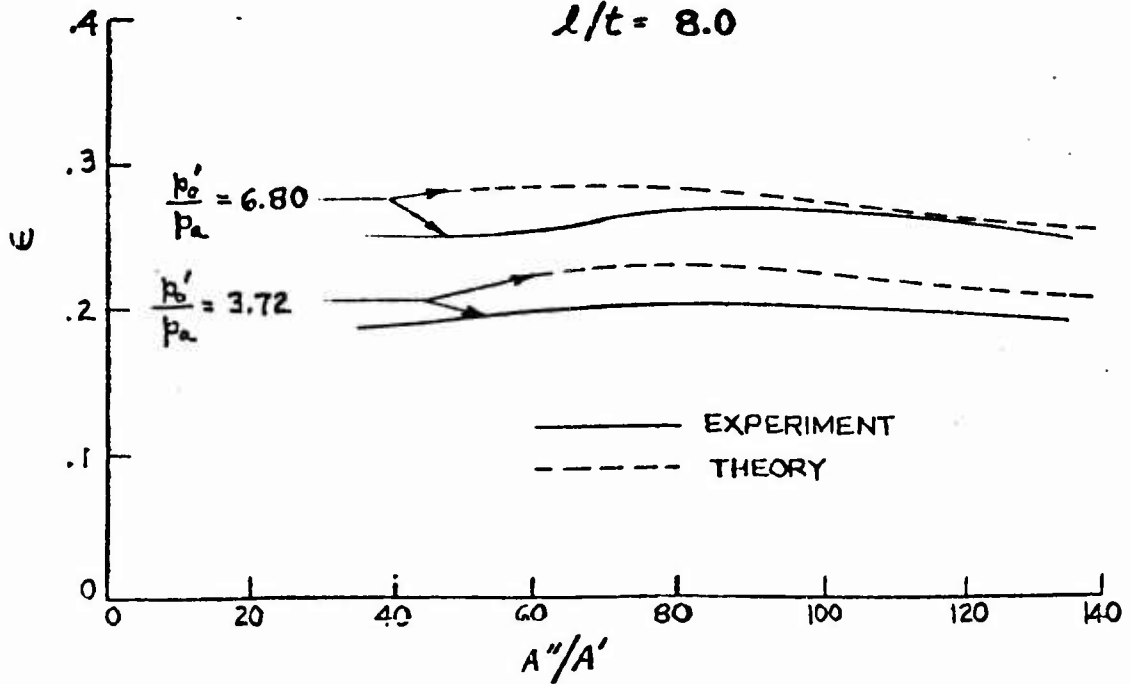


FIGURE 10.1-3 STRAIGHT EJECTOR THRUST AUGMENTATION—COMPARISON OF THEORY WITH EXPERIMENT—EFFECT OF AREA RATIO

EFFECT OF AREA RATIO

$$l/t = 8.0$$



EFFECT OF MIXING SECTION LENGTH

$$A''/A' = 74.4$$

$$p_0'/p_a = 6.80$$

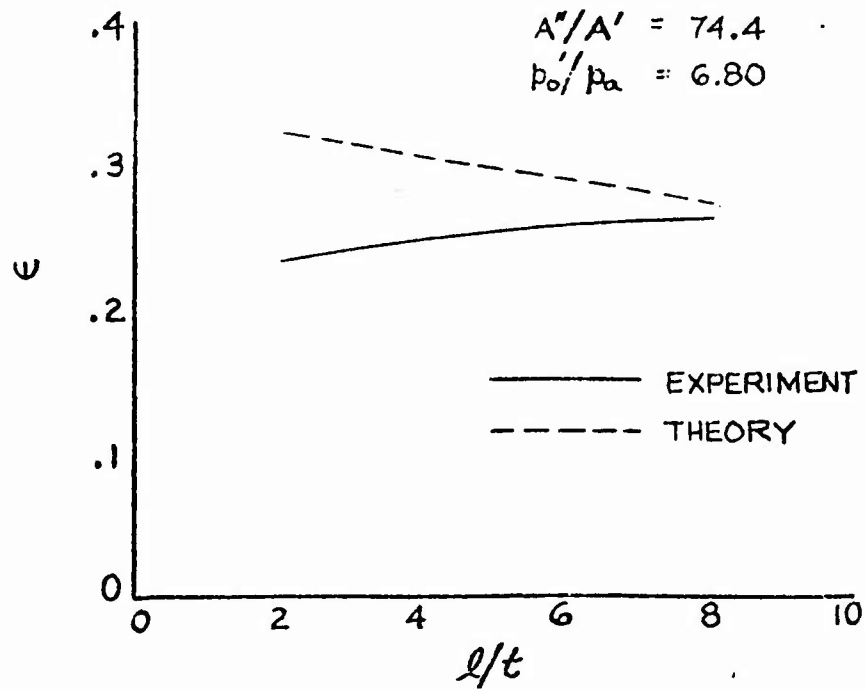


FIGURE 10.1-4 STRAIGHT EJECTOR EFFICIENCY—COMPARISON OF THEORY WITH EXPERIMENT

10.2 RECIRCULATING EJECTOR

10.2.1 Internal Flow of the Ejector

It has been demonstrated in Section 10.1 that performance of the straight ejector (zero secondary pressure recovery) can be predicted provided diffuser losses, or any other additional losses, are properly introduced into the theoretical ejector analysis and provided the mixing process has been completed. The same approach is now applied to the recirculating ejector to determine if the performance obtained experimentally can be reasonably duplicated by the ejector theory.

To accomplish this, the diffuser and turn geometry of the test model was analyzed by the empirical methods of Reference 9 to determine the total pressure loss coefficients in these regions. In the manner of the straight ejector simulation, the experimental value of the exit total pressure was increased by the amount of the diffuser-turn loss and substituted into the ejector theory for the tertiary total pressure at the end of mixing. Once the test value for pressure recovery was introduced, the remainder of the recirculating ejector simulation process was identical to that of the straight ejector for the case of constant mixing section pressure.

If primary and secondary total temperatures are the same, the graphical method of Section 7.1.3 can be used effectively to obtain solutions for the case of non-constant mixing section pressure. In this method the iteration on the velocity at the end of mixing, v_2 , is avoided, and the force due to non-uniform mixing-section pressure can be introduced directly into Equation (7.2-39).

On the other hand, if primary and secondary total temperatures are vastly different, the digital program which was specifically designed to solve the iterative form of the problem is best used. For this case another means of including the mixing-section pressure force must be devised. This is done by adjusting the mixing-section wetted area and length parameters, a and b , to give a retarding force equal to the sum of the frictional and pressure forces.

These techniques for matching theoretical ejector performance to experimented results were extensively applied to Models 1 and 3 recirculating ejectors. The results are presented in Figures 10.2-1 and 10.2-2 by comparing the theoretical values of mass augmentation and efficiency with the experimental values. It is seen that agreement with experiment within ± 10 percent can generally be achieved. A comparison between predicted and actual area ratios is not necessary, since the primary and secondary areas are direct functions of primary and tertiary mass flow, consequently, area ratios compare in the same manner as the mass augmentation.

10.2.2 External

Comparisons between experiment and theory are given in Figures 10.2-3 through 10.2-5 for three recirculating ejector configurations. The theoretical values were obtained by the methods presented in Section 7.2.3. Plots are given of p_b and p_c versus height and, to demonstrate the comparison of the jump across the recirculated stream, a plot of $(p_b - p_c)$ versus height is included for each model. It is seen that the comparison between theory and experiment is good. In all cases average pressures in the cavity and base regions were used. It should be noted that the location of the peak point of p_b is predicted by this method and the predicted base pressures are on the conservative side of experimental values.

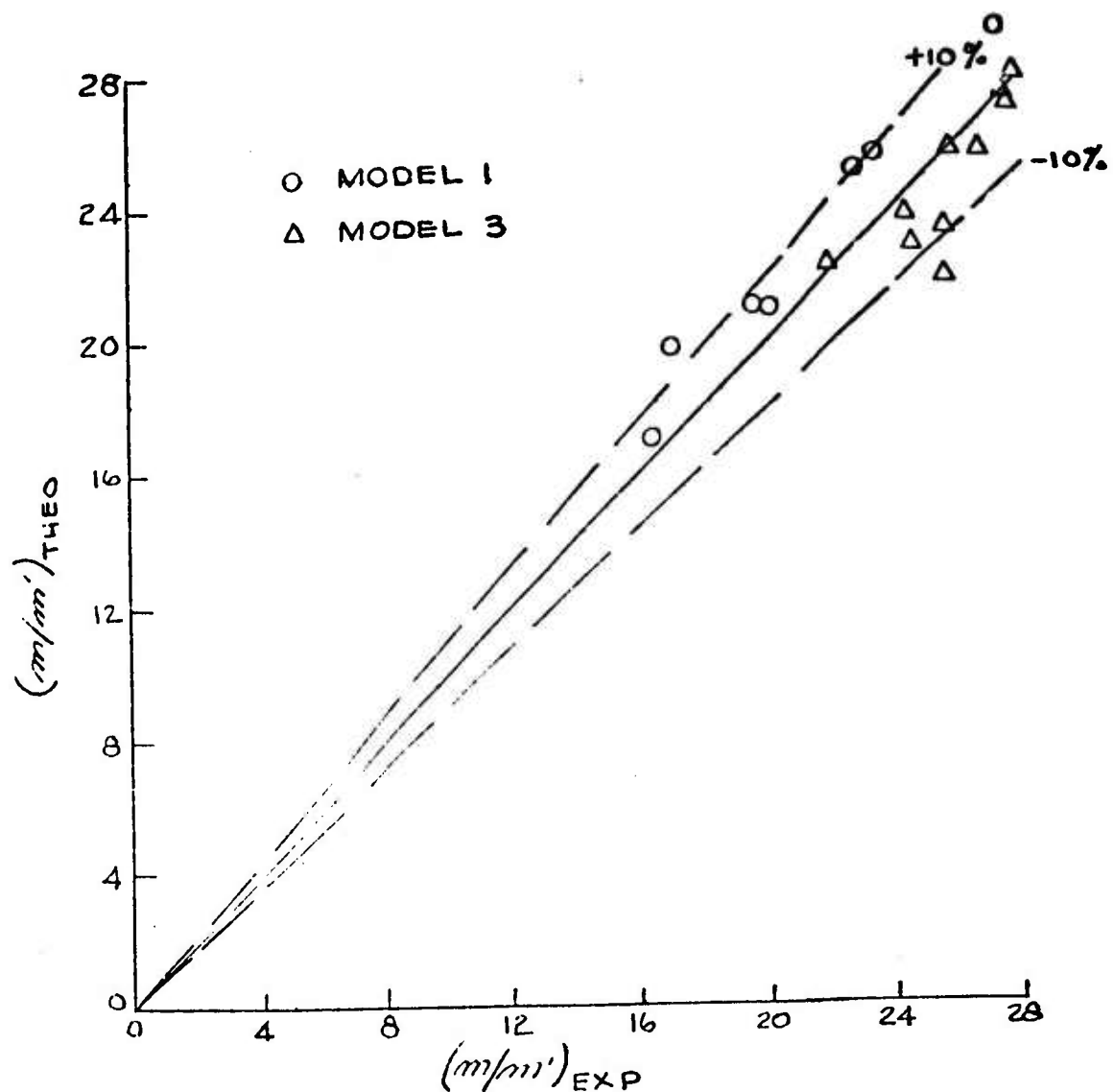


FIGURE 10.2-1 COMPARISON OF THEORETICAL AND EXPERIMENTAL VALUES OF MASS AUGMENTATION - MODELS 1 & 3 RECIRCULATING EJECTORS

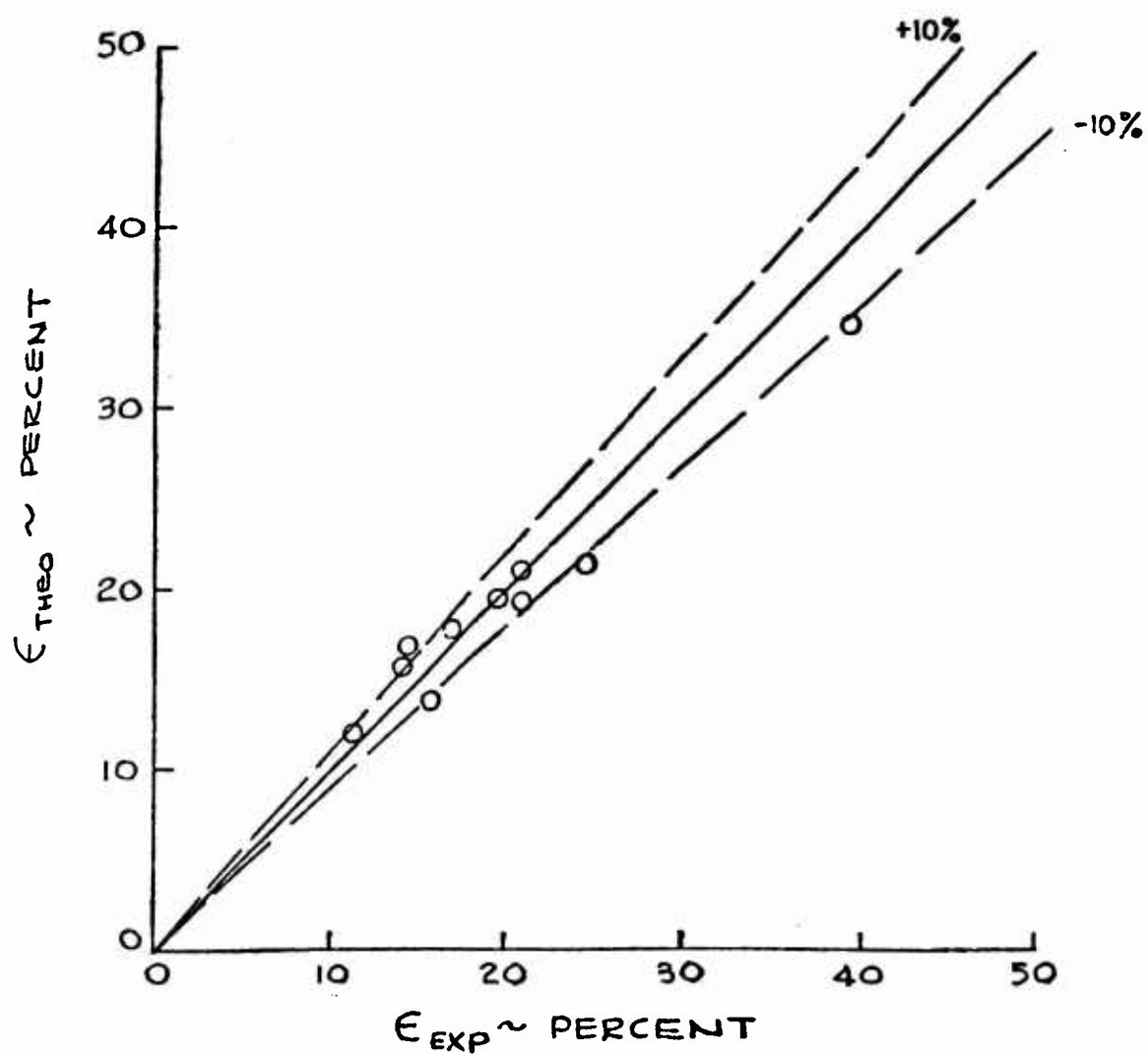


FIGURE 10.2-2 COMPARISON OF THEORETICAL AND EXPERIMENTAL VALUES OF EFFICIENCY - MODEL I RECIRCULATING EJECTOR

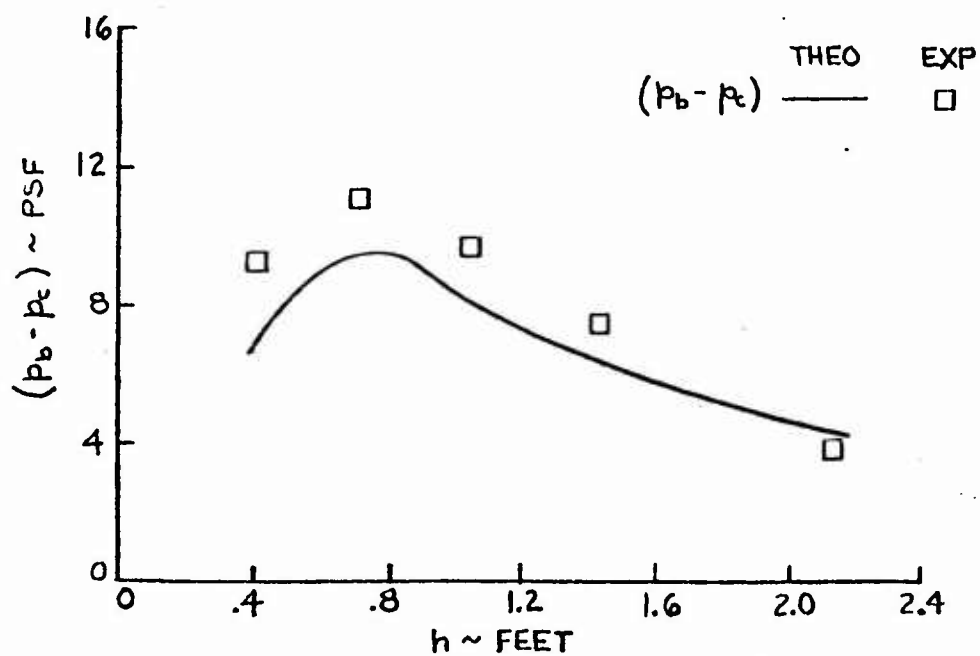
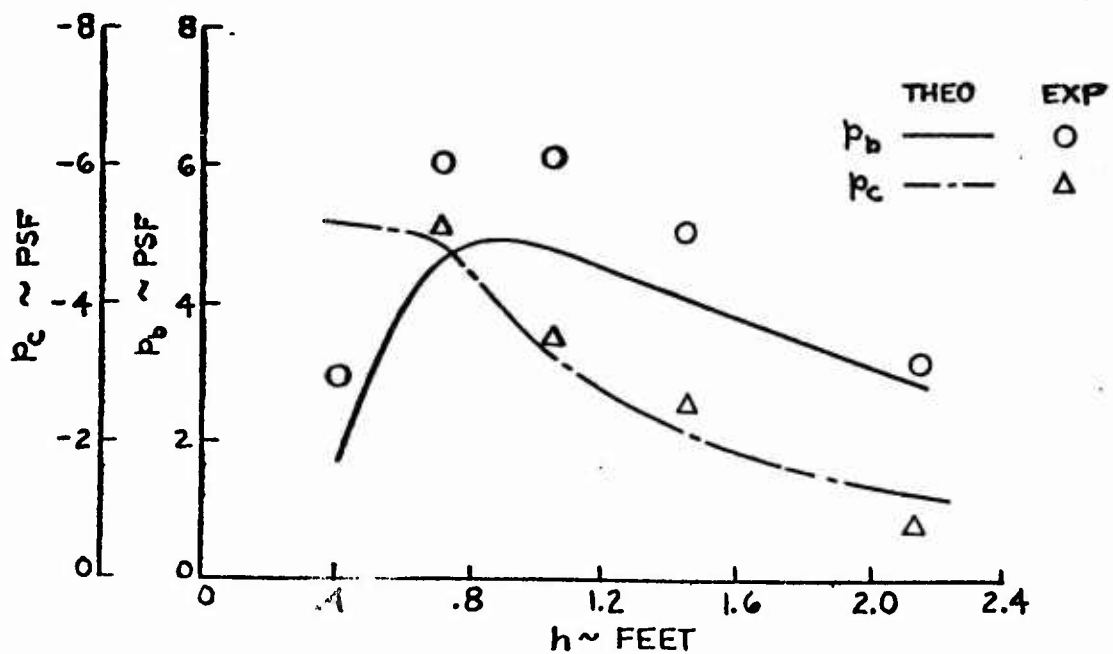


FIGURE 10.2-3 COMPARISON OF THEORY WITH EXPERIMENT FOR BASE PRESSURE AND CAVITY PRESSURE - MODEL 3 RECIRCULATING EJECTOR - $\theta_1 = 30^\circ$, $\theta_2 = 60^\circ$

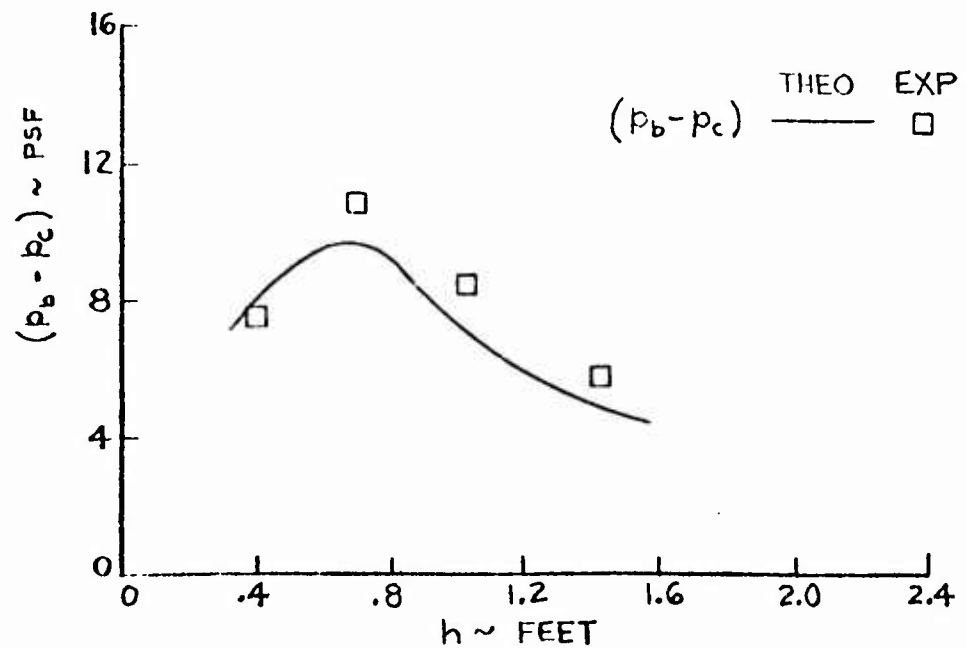
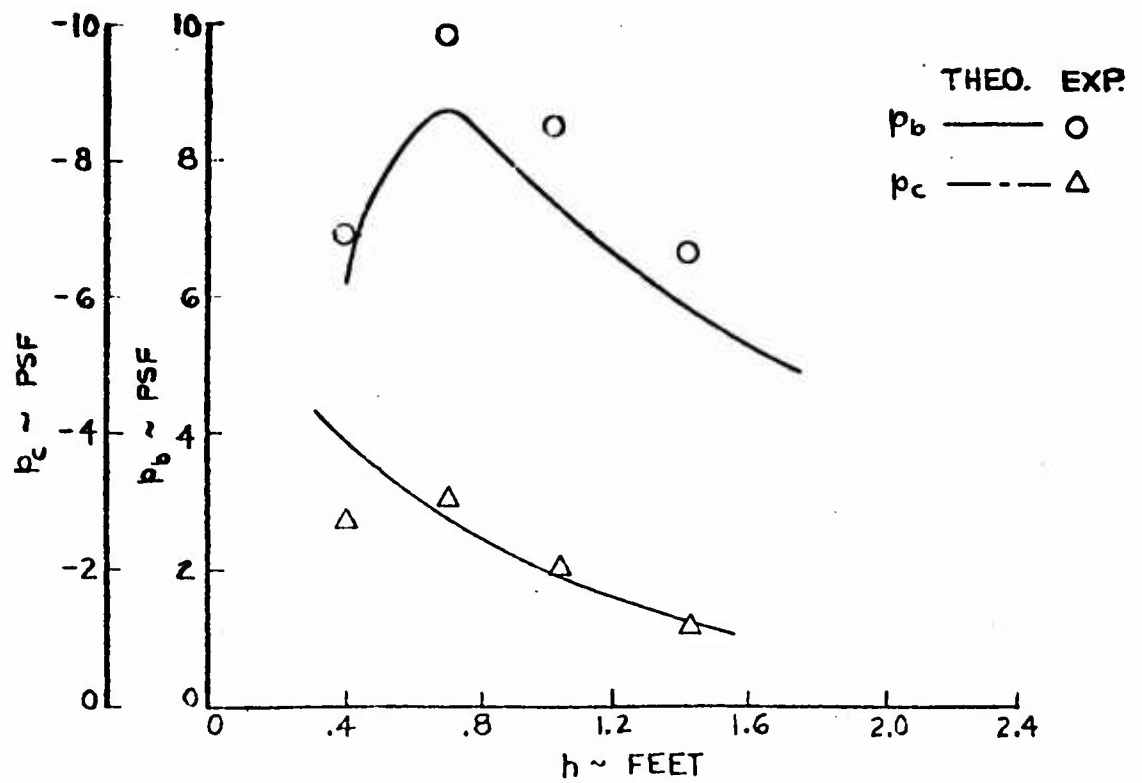


FIGURE 10.2-4 COMPARISON OF THEORY WITH EXPERIMENT FOR BASE PRESSURE AND CAVITY PRESSURE - MODEL 3 RECIRCULATING EJECTOR - $\theta_1 = 30^\circ$, $\theta_2 = 45^\circ$

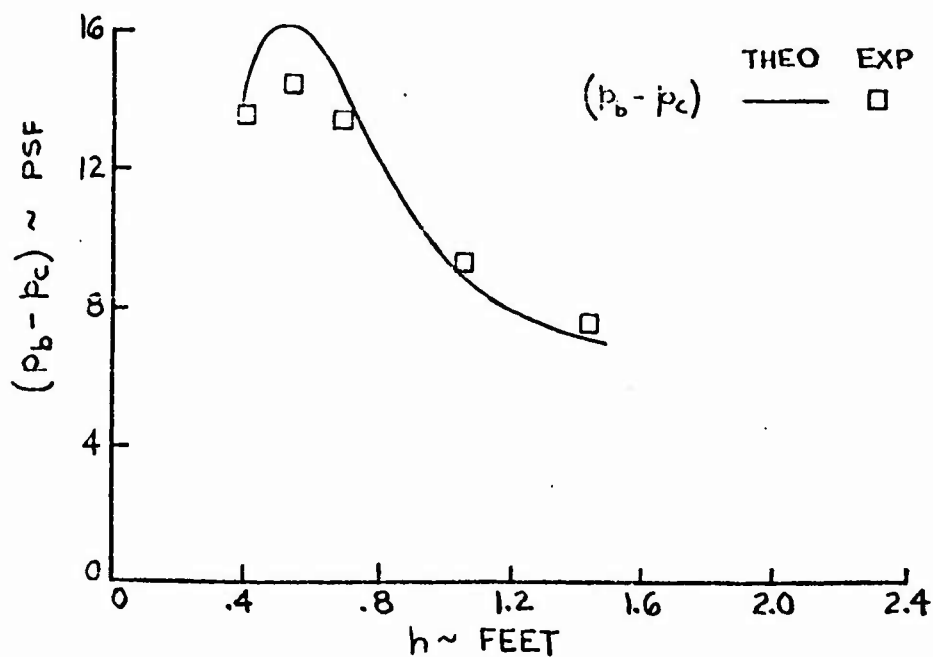
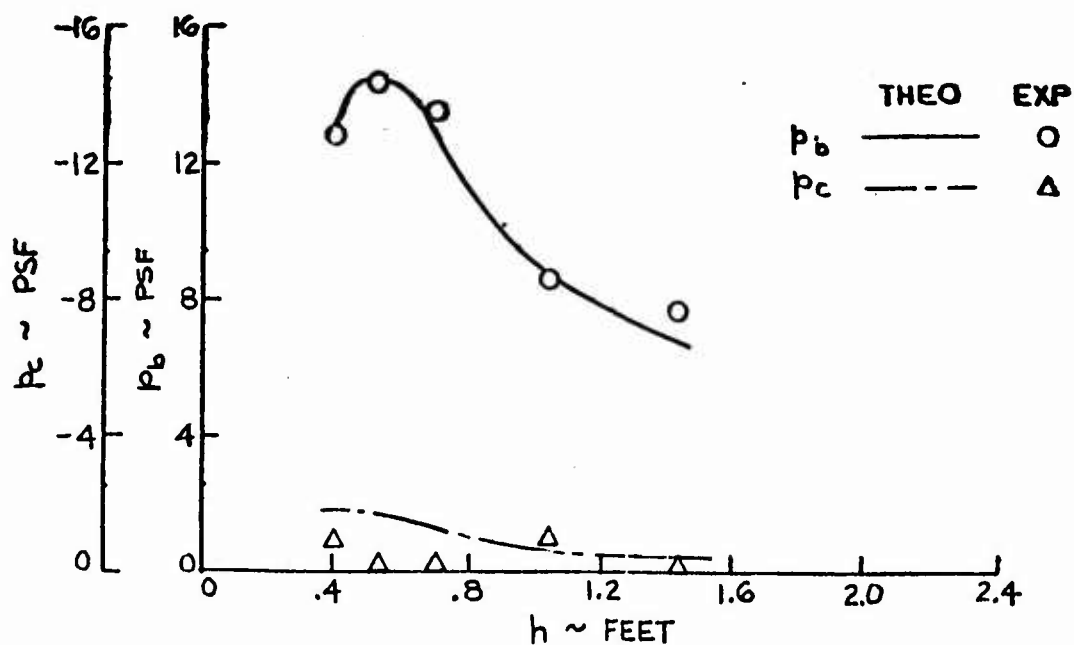


FIGURE 10.2-5 COMPARISON OF THEORY WITH EXPERIMENT FOR BASE PRESSURE AND CAVITY PRESSURE - MODEL 3 RECIRCULATING EJECTOR - $\theta_1 = 30^\circ$, $\theta_2 = 60^\circ$

11.0 REFERENCES

1. Gates, M. F., and Cochran, C. L., "Investigation of Special Ground Effect Machine Configurations", ARD-284, Hiller Aircraft Corporation, Palo Alto, California, December 1960.
2. Weiland, C., "Labyrinth Seals", Symposium on Ground Effect Phenomena, Princeton University, October 1959.
3. Schneider, Allen J., and Rosenberg, Murray H., "Tests of Power Seal Configurations For Ground Effect Machines", Research Memorandum RM-186, Grumman Aircraft Engineering Corporation, Bethpage, Long Island, New York, March 1961.
4. Cockerell, C. S., "Some Possible Developments in the Hovercraft Field", Report Number HDL/61/2, Hovercraft Development Limited, 1961.
5. Eames, Michael C., "Fundamentals of the Stability of Pheripheral Jet Vehicles", Volume 1, Pneumodynamics Corporation, Bethesda, Maryland, November 1960.
6. Martin OR 1275, "Recirculation as a GEM Lift System", October 1960.
7. Montague, Hugh B., "Report on Analytical Study of Ejectors", The Martin Company, Orlando, Florida, Report 1360, December 1960.
8. Schlichting, H., Boundary Layer Theory, McGraw-Hill Book Co. Inc., New York, 1955.
9. "Aero-Space Applied Thermodynamics Manual", Society of Automotive Engineers, Inc., New York, February 1960.
10. Chaplin, Harvey R., "Theory of the Annular Nozzle in Proximity to the Ground", David Taylor Model Basin Aero Report 923, July 1957.
11. Stanton-Jones, R., "Some Design Problems of Hovercraft", Institute of the Aerospace Sciences, Paper No. 61-45, January 1961.
12. Ehrich, F. F., "The Curtain Jet", Journal of Aero-Space Sciences, Vol. 28, No. 11, November 1961.
13. Strand, T., "Exact Inviscid Incompressible Flow Theory of Static Peripheral Jets in Proximity to the Ground", Convair Aero Report No. ERR-SD-002, November 1959.
14. Chaplin, H. R., "A Preliminary Design Technique for Annular-Jet Ground Effect Machine", Department of the Navy DTMB Aero Report 966, September 1959.
15. Webster, W. C., "Static Stability of GEM - Thin Jet Theory", Hydronautics Tech Report 011-1, December 1960.

16. Feng, T. Y. "Hovering and Longitudinal Dynamics of the Ground Effect Machine with Derivation of the Stability Derivatives for Vertical Motion" IAS National Specialists Meeting, May 1960.
17. "Unpublished Results of the Recirculation Model Tested at DTMB Wind Tunnel", December 1961.
18. Chaplin, H. R., "Preliminary Correlation with Theory of Data from Wind Tunnel Test of DTMB GEM Model 448", DTMB Unnumbered Report, June 1960.
19. Chaplin, H. R., "Design Study of a 29-Foot GEM", Department of the Navy DTMB Aero Report 999.
20. Walker, N. K., "Unpublished Analysis of Some Recent U. S. Wind Tunnel Investigation", Letter dated 24 November 1961.
21. Johnson and Chaplin, "Results of GEM III Tethered Tests", Department of Navy, DTMB, Aero Report 1012, August 1961.
22. Gas Turbine Specifications - 1961
Gas Turbine, January-February, 1961
23. Gas Turbines-Propulsion - 1961
Automotive Industries, March 15, 1961
24. Wosser and Van Tuyl, "A GEM for Amphibious Support", Office of Naval Research, 9 January 1961.
25. Lighthill, M. J., "On Sound Generated Aerodynamically", Proceedings of the Royal Society, Part J-A211, 564 (1952), Part II 222, 1. (1954)
26. Ghebotov, V., and Farvell, A., "On the Prediction of Acoustic Environments From Rockets", Ramo-Wooldridge Corporation, Report GM-TR-190, June 1957.
27. Martin OR 850-1, "Preliminary Results of Two-Dimensional Tests of Several Annular Nozzles in Proximity to the Ground", March 1960.
28. Henry, John R., "Design of Power-Plant Installation Pressure - Loss Characteristics of Duct Components", NACA L4F26, June 1944.
29. Johnson, Jr., J. K., Shumpert, P. K., Sutton, J. F., "Steady Flow Ejector Research Program", Lockheed - Georgia Company, ER-5332, September 1961.
30. Rabeneck, G. L., Shumpert, P. K., and Sutton, J. F., "Steady Flow Ejector Research Program", Report ER-4708, Lockheed Aircraft Corporation, Georgia Division, December 1960.
31. Henry, John R., Wood, Charles C., and Wilbur, Stafford W., "Summary of Subsonic-Diffuser Data", NACA RM L56F05, October 1956.

32. "Power Test Codes - Flow Measurement", Chapter 4, Part 5, American Society of Mechanical Engineers, 1960.
33. Pope Alan, Wind-Tunnel Testing, 2nd Edition, John Wiley and Sons, New York 1954.
34. Zucrow, M. J., Aircraft and Missile Propulsion, Volume 1, pp 117-121, John Wiley and Sons, Inc., New York, 1958.
35. McCullough, George B., "The Effect of Reynolds Number on the Stalling Characteristics and Pressure Distributions on Four Moderately Thin Airfoil Sections", NACA Technical Note 3524, Washington, November 1955.

DISTRIBUTION

USAWC	1
USATMC(FTZAT), ATO	1
USAPRDC	1
DCSLOG	1
Rsch Anal Corp	1
ARO, Durham	2
OCRD, DA	2
Ofc of Maint Engr, ODDR&E, OSD	1
NATC	1
ARO, OCRD	1
DCSOPS	1
USAERDL	2
USAOTAC, Center Line	2
OrdBd	1
QMRECOMD	1
CoIT	3
USATCDG	1
USATMC	19
USATSCH	4
USATRECOM	77
TCLO, USAERDL	1
TCLO, USAABELCTBD	1
USATRECOM LO, USARDG (EUR)	3
CNO	1
CNR	3
BUWEPS, DN	1
BUWEPS, DN	1
ACRD(OW), DN	1
USNSRDF	1
USNPGSCH	1
BUSHP, DN	1
USNOTS	1
Dav Tay Mod Bas	1
MCLFDC	1
MCEC	1
USASGCA	1
Canadian LO, USATSCH	3
BRAS, DAQMG(Mov & Tn)	4
USASG, UK	1
Langley Rsch Cen, NASA	2

NASA, Wash., D.C.	6
Ames Rsch Cen, NASA	2
Lewis Rsch Cen, NASA	1
USGPO	1
ASTIA	10
USAMRDC	1
HUMRRO	2
Ofc Sec Def, Dir Def R&E	1
Maritime Admin	1

Martin Company, Orlando Division,
Orlando, Florida

1. Fluid Dynamics

2. Aerodynamics

RECIRCULATION PRINCIPLE FOR GROUND
EFFECT MACHINE TWO-DIMENSIONAL TESTS,
by A. Ortell, Rept. OR 2073, Contract
DA 44-177-TC-710, Task 9R99-01-005-04,
Jun 62, 262 p. incl. illus. tables
(TCREC technical rept. 62-66)
Unclassified report

The report presents the results of a
theoretical and experimental investi-
gation of the recirculation principle
for ground-effect-machine lifting
(over)

Martin Company, Orlando Division,
Orlando, Florida

1. Fluid Dynamics

2. Aerodynamics

RECIRCULATION PRINCIPLE FOR GROUND
EFFECT MACHINE TWO-DIMENSIONAL TESTS,
by A. Ortell, Rept. OR 2073, Contract
DA 44-177-TC-710, Task 9R99-01-005-04,
Jun 62, 262 p. incl. illus. tables
(TCREC technical rept. 62-66)
Unclassified report

The report presents the results of a
theoretical and experimental investi-
gation of the recirculation principle
for ground-effect-machine lifting
(over)

Martin Company, Orlando Division,
Orlando, Florida

1. Fluid Dynamics

2. Aerodynamics

RECIRCULATION PRINCIPLE FOR GROUND
EFFECT MACHINE TWO-DIMENSIONAL TESTS,
by A. Ortell, Rept. OR 2073, Contract
DA 44-177-TC-710, Task 9R99-01-005-04,
Jun 62, 262 p. incl. illus. tables
(TCREC technical rept. 62-66)
Unclassified report

The report presents the results of a
theoretical and experimental investi-
gation of the recirculation principle
for ground-effect-machine lifting
(over)

Martin Company, Orlando Division,
Orlando, Florida

1. Fluid Dynamics

2. Aerodynamics

RECIRCULATION PRINCIPLE FOR GROUND
EFFECT MACHINE TWO-DIMENSIONAL TESTS,
by A. Ortell, Rept. OR 2073, Contract
DA 44-177-TC-710, Task 9R99-01-005-04,
Jun 62, 262 p. incl. illus. tables
(TCREC technical rept. 62-66)
Unclassified report

The report presents the results of a
theoretical and experimental investi-
gation of the recirculation principle
for ground-effect-machine lifting
(over)

systems. The various recirculation concepts are reviewed and evaluated, and one system is explored in detail. This system, using ejectors to pump the required air, was selected primarily because of the severe ingestion problem inherent in the recirculation principle as conceived for GEM.

The use of ejectors necessitated some preliminary investigation of ejectors per se, and the results of this effort are included. A basic data report, No. OR-2496, presenting test data on various straight and recirculating ejector configurations, is available on loan from the USATRECOM Library, Fort Eustis, Virginia.

systems. The various recirculation concepts are reviewed and evaluated, and one system is explored in detail. This system, using ejectors to pump the required air, was selected primarily because of the severe ingestion problem inherent in the recirculation principle as conceived for GEM.

The use of ejectors necessitated some preliminary investigation of ejectors per se, and the results of this effort are included. A basic data report, No. OR-2496, presenting test data on various straight and recirculating ejector configurations, is available on loan from the USATRECOM Library, Fort Eustis, Virginia.

systems. The various recirculation concepts are reviewed and evaluated, and one system is explored in detail. This system, using ejectors to pump the required air, was selected primarily because of the severe ingestion problem inherent in the recirculation principle as conceived for GEM.

The use of ejectors necessitated some preliminary investigation of ejectors per se, and the results of this effort are included. A basic data report, No. OR-2496, presenting test data on various straight and recirculating ejector configurations, is available on loan from the USATRECOM Library, Fort Eustis, Virginia.

systems. The various recirculation concepts are reviewed and evaluated, and one system is explored in detail. This system, using ejectors to pump the required air, was selected primarily because of the severe ingestion problem inherent in the recirculation principle as conceived for GEM.

The use of ejectors necessitated some preliminary investigation of ejectors per se, and the results of this effort are included. A basic data report, No. OR-2496, presenting test data on various straight and recirculating ejector configurations, is available on loan from the USATRECOM Library, Fort Eustis, Virginia.

Martin Company, Orlando Division,
Orlando, Florida
RECIRCULATION PRINCIPLE FOR GROUND
EFFECT MACHINE TWO-DIMENSIONAL TESTS,
by A. Ortell, Rept. OR 2073, Contract
DA 44-177-TC-710, Task 9R99-01-005-04,
Jun 62, 262 p. incl. illus. tables
(TCREC technical rept. 62-66)

Unclassified report

The report presents the results of a
theoretical and experimental investi-
gation of the recirculation principle
for ground-effect-machine lifting

(over)

1. Fluid Dynamics
2. Aerodynamics

1. Fluid Dynamics
2. Aerodynamics

Martin Company, Orlando Division,
Orlando, Florida
RECIRCULATION PRINCIPLE FOR GROUND
EFFECT MACHINE TWO-DIMENSIONAL TESTS,
by A. Ortell, Rept. OR 2073, Contract
DA 44-177-TC-710, Task 9R99-01-005-04,
Jun 62, 262 p. incl. illus. tables
(TCREC technical rept. 62-66)

Unclassified report

The report presents the results of a
theoretical and experimental investi-
gation of the recirculation principle
for ground-effect-machine lifting

(over)

Martin Company, Orlando Division,
Orlando, Florida
RECIRCULATION PRINCIPLE FOR GROUND
EFFECT MACHINE TWO-DIMENSIONAL TESTS,
by A. Ortell, Rept. OR 2073, Contract
DA 44-177-TC-710, Task 9R99-01-005-04,
Jun 62, 262 p. incl. illus. tables
(TCREC technical rept. 62-66)

Unclassified report

The report presents the results of a
theoretical and experimental investi-
gation of the recirculation principle
for ground-effect-machine lifting

(over)

1. Fluid Dynamics
2. Aerodynamics

1. Fluid Dynamics
2. Aerodynamics

Martin Company, Orlando Division,
Orlando, Florida
RECIRCULATION PRINCIPLE FOR GROUND
EFFECT MACHINE TWO-DIMENSIONAL TESTS,
by A. Ortell, Rept. OR 2073, Contract
DA 44-177-TC-710, Task 9R99-01-005-04,
Jun 62, 262 p. incl. illus. tables
(TCREC technical rept. 62-66)

Unclassified report

The report presents the results of a
theoretical and experimental investi-
gation of the recirculation principle
for ground-effect-machine lifting

(over)

systems. The various recirculation concepts are reviewed and evaluated, and one system is explored in detail. This system, using ejectors to pump the required air, was selected primarily because of the severe ingestion problem inherent in the recirculation principle as conceived for GEM.

The use of ejectors necessitated some preliminary investigation of ejectors per se, and the results of this effort are included. A basic data report, No. OR 2496, presenting test data on various straight and recirculating ejector configurations, is available on loan from the USATRECOM Library, Fort Eustis, Virginia.

systems. The various recirculation concepts are reviewed and evaluated, and one system is explored in detail. This system, using ejectors to pump the required air, was selected primarily because of the severe ingestion problem inherent in the recirculation principle as conceived for GEM.

The use of ejectors necessitated some preliminary investigation of ejectors per se, and the results of this effort are included. A basic data report, No. OR-2496, presenting test data on various straight and recirculating ejector configurations, is available on loan from the USATRECOM Library, Fort Eustis, Virginia.

systems. The various recirculation concepts are reviewed and evaluated, and one system is explored in detail. This system, using ejectors to pump the required air, was selected primarily because of the severe ingestion problem inherent in the recirculation principle as conceived for GEM.

The use of ejectors necessitated some preliminary investigation of ejectors per se, and the results of this effort are included. A basic data report, No. OR-2496, presenting test data on various straight and recirculating ejector configurations, is available on loan from the USATRECOM Library, Fort Eustis, Virginia.

systems. The various recirculation concepts are reviewed and evaluated, and one system is explored in detail. This system, using ejectors to pump the required air, was selected primarily because of the severe ingestion problem inherent in the recirculation principle as conceived for GEM.

The use of ejectors necessitated some preliminary investigation of ejectors per se, and the results of this effort are included. A basic data report, No. OR-2496, presenting test data on various straight and recirculating ejector configurations, is available on loan from the USATRECOM Library, Fort Eustis, Virginia.

UNCLASSIFIED

UNCLASSIFIED